The Clinical Impact of Multidetector SPET Technology

by

SHAHID MAHMOOD

Institute of Nuclear Medicine,
University College London Medical School

A thesis submitted to the University of London
for the degree of
Doctor of Philosphy
(1994)

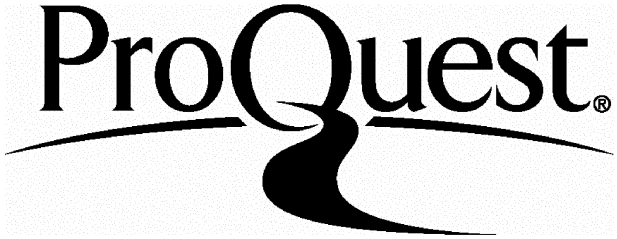

ABSTRACT

Introduction: Single photon emission tomography (SPET) is an established technique in Nuclear Medicine. Recent advances in SPET technology have now permitted the development of multidetector gamma cameras. This thesis evaluates some of these new gamma cameras and their impact on clinical practice.

Aim: (a) To assess four new multidetector SPET gamma cameras (IGE Neurocam, Toshiba GCA-9300A, IGE Optima and Sopha DST).

(b) To establish appropriate acquisition and analytical clinical protocols.

Methodology: For each instrument, the tomographic spatial resolution, contrast and sensitivity were measured. The capability of a new slant hole collimator (IGE Optima) to perform radionuclide ventriculography (RNV) was assessed. To evaluate the utility of these systems, a total of 1215 patient studies were performed (1007 cardiac, 85 skeletal, 73 renal and 50 brain studies). The effect of 8, 16 and 32 minutes data acquisition on image quality and clinical relevance was evaluated. In addition, a new cardiac SPET protocol for rest/stress myocardial perfusion scintigraphy (thallium-201/Tc-99m tetrofosmin) was tested.

Results: Tomographic spatial resolution of the order of 10 mm FWHM was achieved by all four systems. System sensitivity was related to the number of detectors and ranged between 9.2 - 11.2 Kcps/(MBq/ml)/cm per detector. The slant hole collimator with cephalic tilt gave highly reproducible results ($r=0.98, SEE=\pm 2$) for ejection fraction measurements in 75 patients. There was no significant difference in the clinical information obtained using 8 min, 16 min and 32 min acquisitions. Based on patient studies and experience with these multidetector SPET systems, optimum acquisition and analysis protocols for commonly performed SPET studies were documented for routine clinical use. Artefacts due to patient movement during Tl-201 myocardial SPET studies were less frequent on a dual-detector system compared with a

single detector system (0.7% and 4% respectively); while artefacts due to poor positioning or shift in centre of rotation were more. The rest/stress thallium-201/Tc-99m tetrofosmin study protocol (acquisition and analysis) was completed in 90 min. This protocol gave a sensitivity of 80% and specificity of 70% for the detection of coronary artery disease.

Conclusion: For the first time a comprehensive comparison of multidetector SPET systems has been documented. Optimum acquisition and analysis protocols have been identified. The study also shows that the new generation of multidetector SPET systems offer adequate resolution and sensitivity for routine clinical imaging. Increased sensitivity can be translated into an increased patient throughput. This can increase the cost-effectiveness of this new technology.

ACKNOWLEDGEMENTS

I would like to thank Professor Peter J. Ell, who not only supervised this project but also stimulated me, by his dynamic and kind personality and provided the opportunities to conduct the research.

I wish to thank many others by name as they have taught me much over the last few years. I am especially grateful to Dr. P. H. Jarritt, who gave me encouragement and helped me with many technical problems during this project. Dr. K. Kouris, a modest man of integrity, who provided the basis for this project; even away from the Institute he always gave me guidance, encouragement and support.

My special thanks to Miss Gill Clarke, I feel that this work would have been difficult to accomplish, if not impossible without her help. I am also grateful to Dr. Ian Cullum for his useful thought provoking discussions and constructive comments. Special thanks to Sister S. Yepes-Mora, for her assistance throughout the clinical part of this project.

I must take this opportunity to thank colleagues outside the department, especially to Dr. P. O. Kotzki, at the Department of Nuclear Medicine, Laperyonie Hospital, Montpellier, Cedex, France, for his hospitality and allowing me to work on Sopha DST SPET system. I am grateful to Dr. M Buxton-Thomas, for permitting me to work at Kings College Hospital and her cooperation and encouragement during that time.

I would like to acknowledge the help of Mr. Dominic Lui, for helping me with the supply of radiopharmaceuticals, even at odd times. My thanks to all the radiographers of the department for their assistance, especially Miss C. Townsend.

Lastly, I would like to thank all my clinical colleagues, particularly Dr. J. B. Bomanji, Dr. J Buscombe, Dr. D.C. Costa, Dr. G Clunie, Dr. M Gunning and Dr. N Gupta for their support and cooperation, during this study.

CONTENTS

CLAIMS OF ORIGINALITY

This work consists of :

1. A comprehensive comparison of four different multidetector instruments from three different manufacturers.

2. Specific testing of protocols for a new dedicated cardiac single photon emission tomographic (SPET) system

3. Evaluation of a new rest/stress, Thallium-201/Tc-99m tetrofosmin protocol for myocardial perfusion scintigraphy

4. Personal supervision and analysis of 1215 patient studies.

LIST OF EXPERIMENTS

LIST OF FIGURES

CHAPTER 3

CHAPTER 4

CHAPTER 5

CHAPTER 6

LIST OF TABLES

CHAPTER 4

CHAPTER 5

CHAPTER 6

CHAPTER 7

Introduction

Instrumentation in nuclear medicine represents a sophisticated blend of electronics, computers and mechanical devices. Prodigious breakthrough in single photon emission tomography (SPET) imaging has occurred in the last few years. The introduction of a recent generation of multidetector technology for single photon emission tomography (SPET) has extended the boundaries of Nuclear Medicine applications. A detailed assessment of these new instruments is now necessary. Such an assessment should focus on the biological and technical problems that remain to be solved.

The ***aims*** of this thesis were as follows:

a) **The evaluation of four new multidetector SPET gamma cameras**:

1. A three-detector brain dedicated SPET system (*IGE Neurocam*)
2. A three-detector whole body/brain SPET system (*Toshiba GCA-9300A*)
3. A two-detector cardiac dedicated SPET system, with fixed detector geometry (*IGE Optima*)
4. A two-detector cardiac and whole body SPET system, with variable detector geometry (*Sopha DST*)

b) **The establishment of appropriate clinical imaging protocols** for the more relevant and also frequent nuclear medicine procedures such as Tc-99m hexamethylpropyleneamineoxime (HMPAO) brain perfusion SPET, thallium-201 myocardial perfusion SPET, Tc-99m tetrofosmin myocardial perfusion SPET, Tc-99m methylene diphosphonate (MDP) bone SPET and renal Tc-99m dimercaptosuccinic acid (DMSA) SPET studies.

c) The **investigation of short acquisition protocols** for SPET, whilst maintaining image quality.

In this thesis, two approaches have been taken in the evaluation of the new multidetector SPET systems.

The first approach was a tomographic assessment of these systems in order to assess relative merits. The second approach was to assess the clinical applications of these systems in a routine clinical/research setting.

The thesis is divided into three sections:

Section A: explores the use of SPET technology.

Section B: deals with the assessment of the four new multidetector systems.

Section C: deals with the a generalised outcome of the work performed.

Chapter 1 reviews the development of SPET technology and its clinical applications.

Chapter 2 outlines the general methodology for tomographic evaluation of the systems. The detailed acquisition/processing parameters and clinical utility are discussed in each chapter, specific to the system.

Chapter 3 deals with the tomographic assessment as well as the clinical utility of a brain dedicated three-detector SPET system (IGE Neurocam).

Chapter 4 is about the physical and clinical performance of a three-detector whole body / brain SPET system (Toshiba GCA-9300A).

Chapter 5 details the assessment a cardiac dedicated dual-detector system (IGE Optima). Beside the tomographic assessment, the camera feasibility for utilisation of brain SPET has been addressed using 3-D Hoffman brain phantom. Similarly, using a cardiac phantom, the question of 180° vs 360° SPET has been addressed for technetium-99m compounds. Under clinical situations, the relative merits of new slant-hole collimators for radionuclide ventriculography have been assessed. Using repeated SPET acquisitions, the imaging time were optimised for Tc-99m tetrofosmin. Furthermore, to achieve increased throughput feasibility of a combined resting thallium-201 / stress Tc-99m tetrofosmin imaging protocol was evaluated.

Chapter 6 is a brief assessment of a dual- detector SPET system, with variable geometry (Sopha DST). The system is installed in France, where the assessment was done.

Chapter 7 gives the final discussion. The clinical advantages of multidetector system are discussed with reference to the experience gained from such systems. The question of cost-effectiveness is also addressed.

Chapter 8 summarises the conclusions derived from this work.

Chapter 9 (last chapter) gives a brief account of the work in progress and a set of recommendations is enumerated.

SECTION A

Single Photon Emission Tomography (SPET)

Chapter 1

SPET- a review of technology

Nuclear Medicine is defined as a branch of medicine that employs radioisotopes in the diagnosis and treatment of disease (Young et al., 1972). Today an increasing number of Nuclear Medicine procedures are being used not only in the diagnostic work up of patients but also to help in decisions regarding prognosis, risk stratification, choice and follow up of therapy.

1.1. Historical Background

Fundamental to Nuclear Medicine is the tracer principle, as described by George V Hevesy and for which he received a Nobel prize in 1944. Historically there is no clear cut starting date for Nuclear Medicine. If one thinks of the use of either natural or artificial radioactive tracers, its beginning can be linked to 1901 when French physicians Henry Alexander Danlos (1844-1912) and Eugene Block (1878-1950) placed radium in contact with a tuberculous skin lesion. In terms of the use of artificial radioisotopes, Nuclear Medicine started only after 1934 when the French radiochemist Jean Frederick Joliot Curie (1900-1959) and his wife Irene Slodovska Joliot Curie (1897-1956) first produced artificial radioactivity particularly, radiophosphorous P-30 with a half life of 2 minutes. George V Hevesy (1935) successfully used radiophosphorous for metabolic studies in animals and the American neurologist Joseph Gilbert Hamilton (1936) used radiosodium (Na-24) in a leukaemic patient.

The earliest detector in nuclear medicine was the Geiger Müller (G M) tube, used by Hevesy (Hevesy G, 1923) to study calcium metabolism in plants. In 1948, Moore GE studied the localization of brain tumours utilizing I-131

labelled dioiodofluorescein (Moore GE, 1948). Bendick Cassen, in 1951 used a crudely collimated tube to compare the function of thyroid nodules to normal thyroid tissue (Cassen et al., 1951). He introduced the concept of scintigraphy by imaging the distribution of I-131 in the gland. He developed a moving detector utilising a calcium-tungstate crystal coupled to a photomultiplier tube (PMT). Using a single hole lead collimator, he was able to obtain images with a spatial resolution of 1/4 inch. His second generation instrument moved automatically, and became the first rectilinear scanner. Refinements were rapidly introduced to this basic system by Allen and co-workers (Allen et al., 1954) who introduced pulse height analysis and Newell and his colleagues who introduced the focused multichannel collimator (Newell et al., 1952). The Harshaw company began production of thallium activated sodium iodide crystals. To increase the spatial resolution Brownell and Sweet built a positron scanner, since the detection of the annihilation photons by coincidence counting offered better spatial localization of a radioactive source (Brownell et al., 1953). Kuhl and Edwards introduced the concept of section scanning using a dual-probe system, data storage on perforated paper tape and time compressed image display (Kuhl et al., 1964).

1.2. Modern Nuclear Medicine

Modern Nuclear Medicine started with the development of the first scintillation camera by Hal Anger (Anger HO, 1958). It had a 4 inch diameter and 0.25 inch thick crystal, with only seven 1.5 inch diameter photomultiplier tubes. Following the introduction of technetium-99m, (Tc-99m) as a radiopharmaceutical in 1964 by Harper and colleagues (Harper et al., 1962,1964), the Anger gamma camera rapidly became the new device of modern nuclear medicine imaging . In 1968 Anger was also first to report how a gamma camera could be used in a rectilinear scanning mode to perform multiplane longitudinal tomography. The Anger camera continued to evolve: spatial resolution, uniformity and count rate capabilities have improved significantly during the last few years, largely because of extensive digital processing of the signals from the analog detector electronics.

Now the modern gamma camera is not only available for static planar imaging, but also for whole body imaging, for emission tomography using single, dual or triple detector arrangements and in mobile form, allowing bed-side nuclear medicine imaging to be performed on critically ill patients. The images obtained by conventional radiology, x-ray tomography, ultrasonography and magnetic resonance imaging (MRI) are essentially based on structure (anatomy), whereas images obtained by nuclear medicine techniques are principally based on organ function. Hence, the information available is complementary, synergistic, confirmatory and not competitive.

1.3. The Gamma Camera-Basic Principals and Physics

Figure 1.1 illustrates the basic principles of the Anger gamma camera.

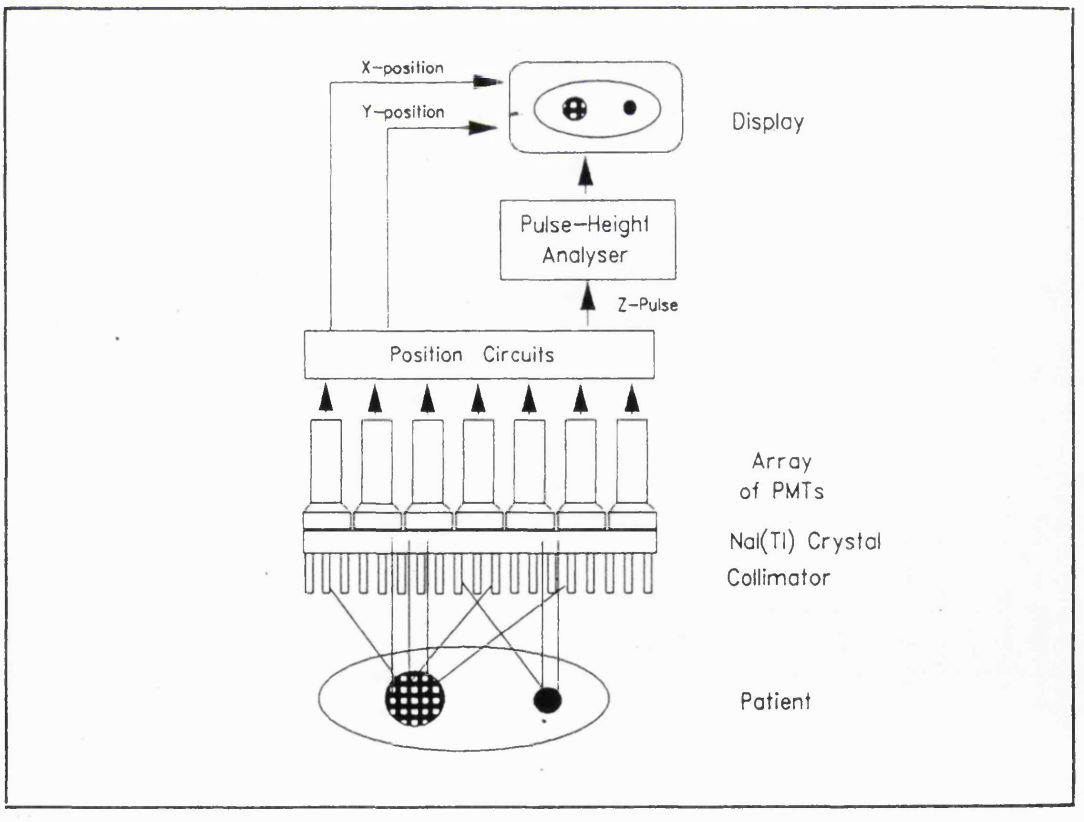

Figure 1.1. : Block diagram of the Anger scintillation camera

Gamma rays from the patient are collimated by a lead collimator and interact with a scintillation crystal producing light photons, which are detected and

amplified by an array of photomultiplier tubes (PMTs). The output signals from PMTs are analysed by position circuitry, which determines the average spatial position of the interaction of each gamma ray within the crystal. The signals are further analysed to distinguish interactions of unscattered photons from those of photons which have been scattered one or more times within the patient before detection. This technique, called Pulse Height Analysis, relies on the fact that during Compton scattering the photon energy is reduced. In a similar manner the gamma rays from two different radionuclides can be distinguished by the energies of their gamma ray emission.

THE SCINTILLATOR

Thallium activated sodium iodide, NaI (Tl) is universally used as a primary detector for the gamma camera. It has a relatively high density of 3.67 gm cm^{-3}, a high atomic number (53 for iodine) and can be manufactured in several shapes or sizes (Zimmerman RE, 1988). Commercial gamma cameras have crystal thicknesses of 12 mm (1/2 inch), 9 mm (3/8 inch) and 6 mm (1/4 inch). Table 1.1 below lists the average absorption fraction by the photoelectric effect for a number of radionuclides used clinically.

Radionuclide	**Principal Energy (keV)**	**Absorbed Fraction**		
		Thickness		
		12 mm	**9 mm**	**6 mm**
Thallium-201	70-80	1.00	1.00	1.0
Technetium-99m	140	0.92	0.85	0.72
Indium-111	173 247	0.73 0.40	0.62 0.32	0.48 0.22

Table 1.1. : Absorbed fraction for Na(Tl) crystals of different thickness. The absorbed fraction is the fraction of photon incident on the crystals which are absorbed by the photoelectric effect.

Poorer energy resolution, deterioration in spatial resolution and increased absorption in the patient are limiting factors in camera design at low energies. The optimal gamma ray energy is therefore 100-200 keV. The energy resolution is typically 10-11% in most modern cameras for technetium-99m. This unfortunately is not sufficient to entirely remove Compton scattered

photons from the photopeak window of the pulse height analyzer and thus leads to reduced contrast in the images.

PHOTOMULTIPLIER TUBES (PMT)

Scintillation photons produced within the crystal are detected by an array of photomultiplier tubes which are optically coupled to the crystal. The photomultiplier tubes are used to convert the light photons to photoelectrons and then to amplify their number by a factor of about 10^6. It is essential to have an extremely stable high voltage supply. Also the effect of local electromagnetic fields will have an impact on the photoelectrons released from the cathode. This effect is minimized by using μ-metal shields around the base of the PMTs. Due to hygroscopic effect, there is always some glass covering the crystal. Some manufacturers use a light guide between the glass and the PMTs, while others directly couple the PMTs to the glass.

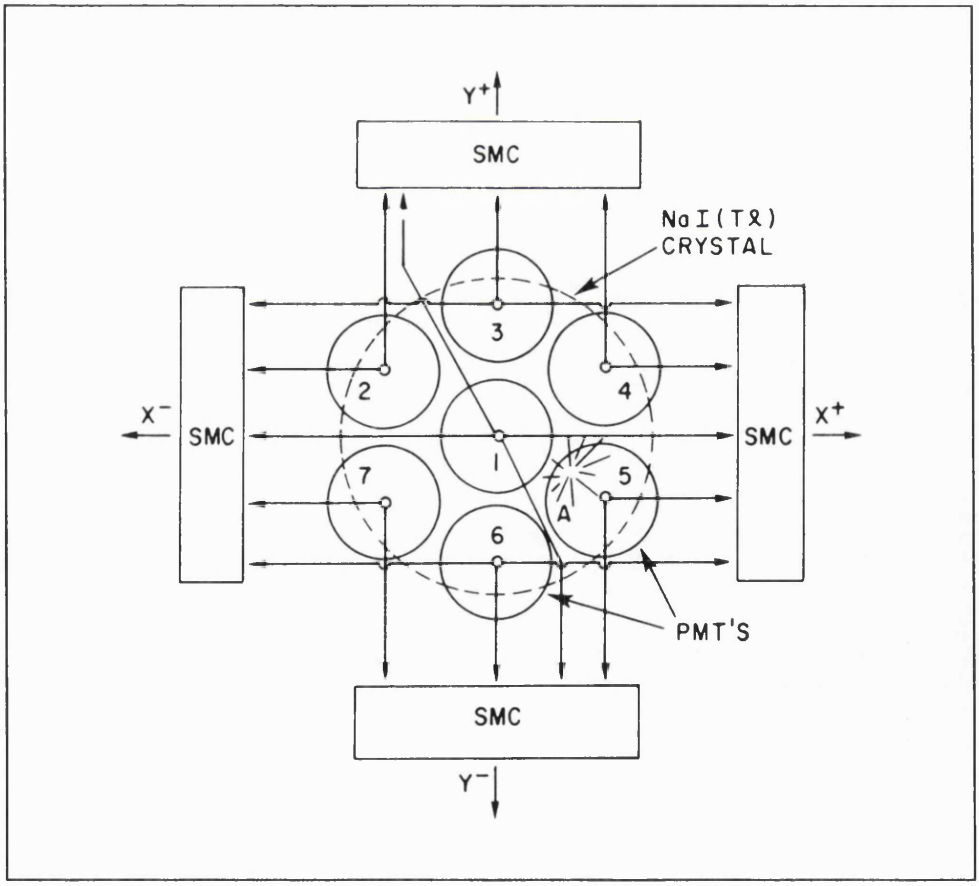

Figure 1.2 : Diagram of a 7 PMT gamma camera
(Adapted from Sorenson JA, Phelps ME. Physics in Nuclear Medicine (2nd ed.): Grune and Stratton, 1987)

The original camera described by Anger (Anger HO, 1958) used an array of 7 PMTs. The early production models used 19 tubes, while cameras with 37 tubes became standard in the 1970s. Most modern cameras assemble 37, 55, 61, 75 or 91 tubes arranged in a hexagonal array. The tubes themselves are usually hexagonal allowing the maximum area of the crystal surface to be covered. The amplitude of the signal from a tube will be a function of the distance of centre of the tube from the location of the interaction in the crystal. The output from each of the PMTs is applied to a resistor matrix to generate four position signals: X+, X-, Y+, and Y- (Figure 1.2). All the signals are summed to form the Z pulse which is proportional to energy absorbed in the crystal.

PULSE HEIGHT ANALYSIS

Pulse Height Analysis enables photoelectric events to be distinguished from the interactions of scattered photons, permitting only photopeak events to be used for image formation. Most gamma cameras provide at least three energy windows, allowing isotopes with two or three primary photons (e.g. Indium-111, Gallium-67, Thallium-201) to be more efficiently imaged and also allowing for dual-isotope imaging. Manufacturers now utilise a multi-channel analyzer for more accurate window placement.

COLLIMATION

A collimator is necessary to obtain an image as gamma rays cannot be focused. The collimator projects an image of the source distribution onto the crystal by absorbing all other gamma rays outside the angle of acceptance. This design of the collimator inherently makes the gamma camera a very insensitive device. Early collimator designs used glued sheets of corrugated lead which were subject to slippage, thereby resulting in variations in sensitivity across the face of the collimator. Most modern collimators are made as a single casting using hexagonal holes. This is a more efficient design than the earlier triangular square or circular holes. Furthermore the casting techniques have greatly improved the uniformity of the collimator, which is particularly important for single photon emission tomography (SPET). Often collimators are designed to improve sensitivity for a given spatial

resolution. Significant gains have been achieved recently.

Collimator type	Relative Sensitivity
Parallel hole	1.0
Fan-beam	1.4-1.6
Cone-beam	2.0-2.5

Table 1.2. : Relative sensitivities for different types of collimators. for brain imaging. It is assumed that all of them would have the same spatial resolution.

Recently International General Electric (IGE) has launched a 15 degree slant hole collimator for radionuclide ventriculography (chapter 5), while many other manufacturers like Toshiba and Sopha have launched cone or fan-beam collimators for brain tomography (chapter 4).

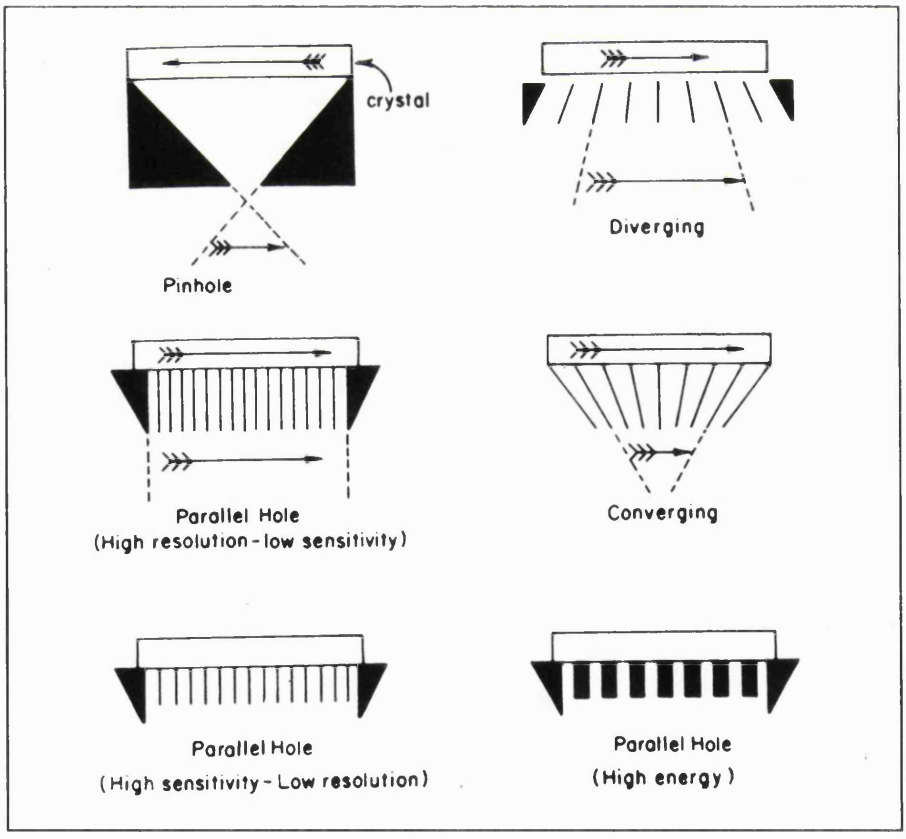

Figure 1.3 : Illustration of some of the collimator types used in Nuclear Medicine.

i) Pinhole Collimator

The first collimator used was a pinhole collimator (Anger H et al., 1959). It consists of a small (2-6 mm diameter) aperture, usually positioned 15-20 cm from crystal. Gamma rays pass through the pinhole to reach the crystal, thereby forming an inverted image (figure 1.3). This collimator only allows a very small fraction of emitted gamma rays to be used to form an image. The image is magnified as the object to pinhole distance is reduced. The magnification effect and the improved resolution give the pinhole collimator unique imaging quality for small organs (such as the thyroid) but this is offset by some image distortion, poorer sensitivity and poor "anatomical" marking facilities.

ii) Parallel Hole Collimators

Although a wide variety of collimators are now available, the parallel hole collimator with the holes perpendicular to the gamma camera crystal remains the most widely used collimator. These collimators have the advantage of not introducing any distortion to the image of the source organs, while both converging and diverging collimators result in the image magnification factor varying with depth. A variation of the parallel hole collimator is the slant hole collimator in which all the holes are parallel but are angled, typically 30° from the perpendicular direction. The purpose of a slant-hole collimator is to get closer to the patient. It is more often used to obtain left anterior oblique (LAO) views of the heart and also in brain tomography.

All the manufacturers offer a wide range of parallel hole collimators covering the low (80-150 keV) medium (150-300 keV) and high (300-400 keV) energy ranges.

Parallel hole collimators are characterised by their sensitivity, resolution and septal penetration for a particular energy range for which they are designed for. Resolution is usually expressed as the Full Width at Half Maximum (FWHM) of the image of a line source, (Wilson RJ, 1988). With reference to figure 1.4 the collimator resolution R_c is approximately given by an equation:

$$R_c = d\ (1+D/L) \quad \ldots\ldots\ldots\ldots\ldots\ldots\ldots \quad (i)$$

where d is the width of each hole, L is the length of the collimator hole and

D is the distance from the surface of the collimator.

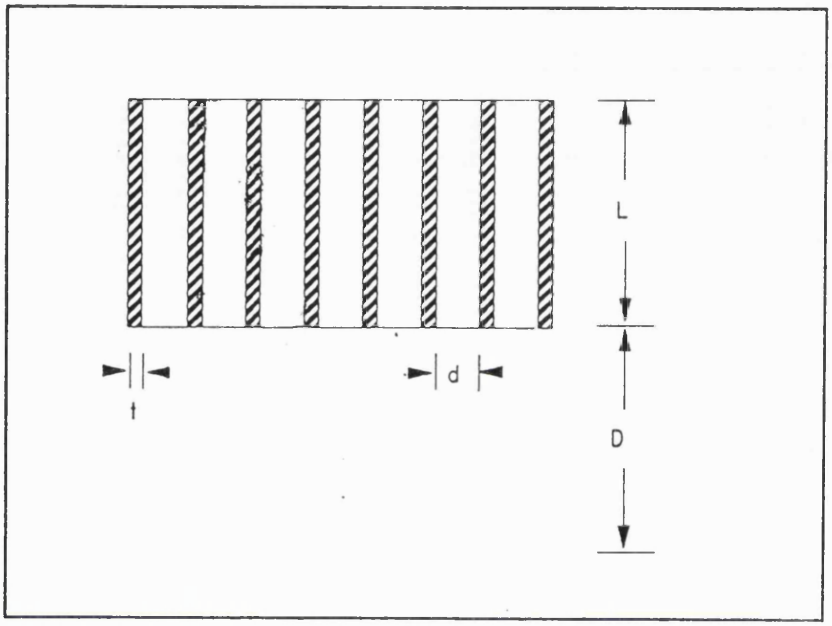

Figure 1.4.: Design characteristics of parallel-hole collimator

The system resolution R_s of the collimator and detector together can be derived from the relationship:

$$R_s = \sqrt{R_i^2 + R_c^2} \quad \text{(ii)}$$

where R_i is the intrinsic resolution of the detector. The efficiency of the collimator is given approximately by:

$$\text{Efficiency } g = d^2/16\ L^2 \quad \text{(iii)}.$$

The resolution can be improved by either reducing the hole size (d) or increasing the hole length (L) (equation i). In either case this will result in a reduction in the efficiency (equation iii) . Due to square terms in equation (iii), a reduction in resolution of a factor of 2, would result in a decrease in efficiency by a factor of 4. A low energy high resolution collimator typically has sensitivity of 5 cpm/kBq for Tc-99m. This is equivalent to an efficiency of 8.3×10^{-5} or that 1 in 12,000 photons emitted by the radionuclide in the patient is detected and used to create the image.

The thickness of septum between the collimator holes is very critical in eliminating the detection of photons reaching the detector obliquely. This is

important not only for the photon energy being used for imaging but also for any low abundance high energy photons that are emitted by a particular radionuclide. Septal penetration results in a broadening of the tail of the line spread function reducing the contrast in the final image. Collimators are usually designed so that the minimum septal path length (W) (Figure1.4) reduces the photon flux to not more than 5% for the specified energy range. Different manufacturers take different approaches to the compromise that must be made between resolution, sensitivity and septal penetration. International General Electric (IGE) uses wider septa enabling the lower energy collimator to be used at energies up to 200 keV. The wider hole size of GE collimators results in a poorer resolution close to the surface of the collimator, but the longer hole length gives improved resolution at depth compared to some other manufacturers e.g., Picker LEHR collimator, but is 22% less sensitive. The Siemens LEHR collimator has better resolution but the final system resolution at 100 mm is no better than the other manufacturers due to poorer intrinsic resolution (Smart RC, 1992).

LIMITATIONS AND CORRECTIONS

Unfortunately the basic Anger camera has a number of imperfections that limit the quality of the final image. Techniques have now developed to correct for energy response, non-linearity and shifts in the gain of the photomultiplier tubes (PMTs).

A number of studies performed in the 1970s demonstrated that major causes of non-uniformity were the variation in the pulse-height spectrum for different PMTs and spatial non-linearities caused by varying light collection efficiency of the PMTs as the interaction in the crystal is moved from the centre of the PMT to its edge (Simmons GH, 1988). All manufacturers now provide on-line digital techniques that will correct the non-uniformities introduced by these effects.

a) Energy Correction:

A high count density flood image is acquired and the pulse height spectrum is recorded for each pixel of a matrix (e.g. 64x64 pixel) over the field of view.

For each pixel the position of the photopeak is determined and the difference in the energy between the photopeak and the mean of all the photopeaks is calculated. A matrix of correction factors is then stored which is used to correct the Energy (Z) pulse on an event by event basis. During acquisition the X and Y location of each interaction is determined and used to read the energy correction value in the appropriate pixel location of a look up table. The Z correction factor is then added to the original Z pulse before pulse height analysis. This technique not only improves the uniformity but also improves the energy resolution as the photopeaks of all the PMTs are now correctly aligned.

b) Linearity Correction:

Linearity correction involves determining the deviation of the observed source position from its correct position on a pixel by pixel basis and storing these deviations in a lookup table.

Manufacturer	Energy Correction	Linearity Correction
Picker	128x128	128x128 interpolated to 4096x4096
General Electric (IGE)	128x128 interpolated to 1024x1024	128x128 interpolated to 1024x1024
Siemens	128x128	64x64 interpolated to 4096x4096

Table 1.3 : The size of the correction matrices used by three manufacturers.

Most manufacturers use spatial sampling of at least 1024x1024, although the correction factors are usually calculated by the linear interpolation from a 64x64 or 128x128 matrix (Table 1.3). The correction is applied "on-the-fly" to each event that is detected. The appropriate X and Y correction values are added to the original X and Y signals before the final image is formed.

c) Automatic Gain Adjustment:

For both energy and linearity corrections to work satisfactorily it is essential

that there is no drift in the gain of the individual PMTs. Manufacturers have developed a number of techniques for automatically monitoring and correcting the PMT gain (Graham LS, 1986).

International General Electric (IGE) uses PMTs which have small light-emitting diodes (LEDs) incorporated into them. The light-emitting diodes are pulsed in synchrony once every millisecond for approximately 3 μ seconds. The gain of the preamp. attached to the PMT is adjusted to maintain this signal at the reference level. As the PMT output from the light-emitting diode is much larger than from an event in the crystal the analysis-electronics can distinguish between them. Elscint use a similar technique, however only one light-emitting diode is used and optical fibres distribute the light output to every PMT.

Siemens have developed a very different technique that uses the radiation from the patient. Two energy windows of 4 keV and 11 keV are positioned on the high side of photopeak, so that they are not affected by scatter. For technetium-99m they are positioned from 140-144 keV and from 144-155 keV. When the PMT gains are correctly balanced then the ratio of the counts in these two windows is 1.0. If the gain drifts this ratio will change and the change in gain necessary to retune the PMT can be calculated. During a patient study, the ratio is calculated each time the counts in any one of the two windows reaches 8,000 counts.

e) Improved Count Rate Performance:

Gamma cameras in the 1970s exhibited dead-times of the order 4 to 8 μ-seconds, giving observed count rates of 22-45 kcps for a 20% count loss. Most manufacturers provided a high count rate mode to enable higher count rates for some dynamic studies to be performed. However this was often achieved by widening the window and bypassing some of correction circuitry. The high count rate was thus achieved at the expense of considerably poorer spatial resolution and uniformity. Furthermore, pulse pile-up at high counting rates lead to mispositioned counts resulting in loss of contrast in the image.

In recent years a number of manufacturers have developed techniques to achieve high count rates while maintaining good image quality. IGE employs

a technique known as "pulse-tail extrapolation" (Lewellen et al., 1989). If a second pulse is received before the first pulse has returned to its base line value, the second pulse is switched to a second amplifier. In addition, an "estimator" circuit estimates the tail of the first pulse which is supplied to the first amplifier, so that the first pulse is amplified without distortion from the second pulse. In addition the estimate of the pulse-tail is subtracted from the second pulse to yield the true second pulse. The IGE system has in fact 5 levels of pulse-tail extrapolation allowing compensation for pile-up of up to 4 pulses. With the system like IGE XR/T, camera has a 20% count rate loss at a count rate of 150 kcps, with minimal deterioration in uniformity and spatial resolution.

Other manufacturers have also introduced pulse pile-up rejection circuitry. Siemens employ a dual integrator and in addition detect pulses which have become piled-up as they appear to decay more slowly.

The above corrections are provided as a standard feature of modern gamma cameras.

IMAGE DISPLAY

Until relatively recently gamma cameras have displayed the images on a cathode ray tube (CRT) using the analogue X and Y signals and employing the Z signal to the image, whenever a photon was detected whose energy fell within the window of the pulse height analyzer. The final hard copy image used for diagnostic interpretation is usually produced in a multiple-formatter camera. These allow multiple images to be produced on a single sheet of x-ray film and enables a series of dynamic images to be displayed together with subsequent static images. Computer images are normally viewed on the video monitor. The vertical resolution of the image is related to the number of raster lines comprising the display. The horizontal resolution is dependent upon the rate of change of the video-signal as the beam is deflected across a line and this is made to be broadly equal to the vertical resolution. High resolution monitors have recently been introduced into Nuclear Medicine. Moreover colour display of the images is now possible. It is pertinent to note that the eye can distinguish around 100 separate grey tones, but 20,000 shades of colour. Another advancement in imaging is the introduction of the laser imager. Laser

imagers have a multiformatting capability and may take both analogue and digital input signal. Direct output from a video monitor is also possible.
Besides Polaroid films, thermal dye and dye-sublimation printers have been developed, offering output of high quality colour images.

1.4. Computers in Nuclear Medicine

Modern Nuclear Medicine has benefitted from the recent development of more powerful and easier to use computer systems. They are not only part of the gamma camera, but other important non imaging applications like patients appointments, booking systems, billing systems and radiopharmaceutical ordering/dispensing systems are also dependent upon the computers.
The central part of the computer system is called the central processing unit (CPU) or microprocessor. It not only performs arithmetic and logic functions but also coordinates the communication of information between the different hardware components and directs the sequence of operations of the entire computer system. The CPU or microprocessor uses a common path called a bus to transfer data from one location to another within the computer. The bus contains a number of electrical lines for addressing (16-32 bits or lines), for data transfer (up to 64 bits or lines) for control signals (varies with CPU), and for electrical power (variable with CPU). The "nuclear medicine computer" may itself vary from a single multi-purpose terminal linked to a specific camera, to a number of acquisition terminals (each attached to a camera system) linked via a "network" to separate dedicated processing and reporting stations. Body contouring, fast dynamic imaging, SPET imaging, image processing and analysis and a wide variety of image displays have been made possible only because of computers. Many common nuclear medicine procedures could not be performed without computer control. The computer is therefore an important part of the gamma camera system, but its ability depends also on the camera hardware to which it is attached and software, both operating system and application software, with which it is programmed.
The figure below (Figure 1.5) shows in a block diagram the functions performed by a basic nuclear medicine computer.

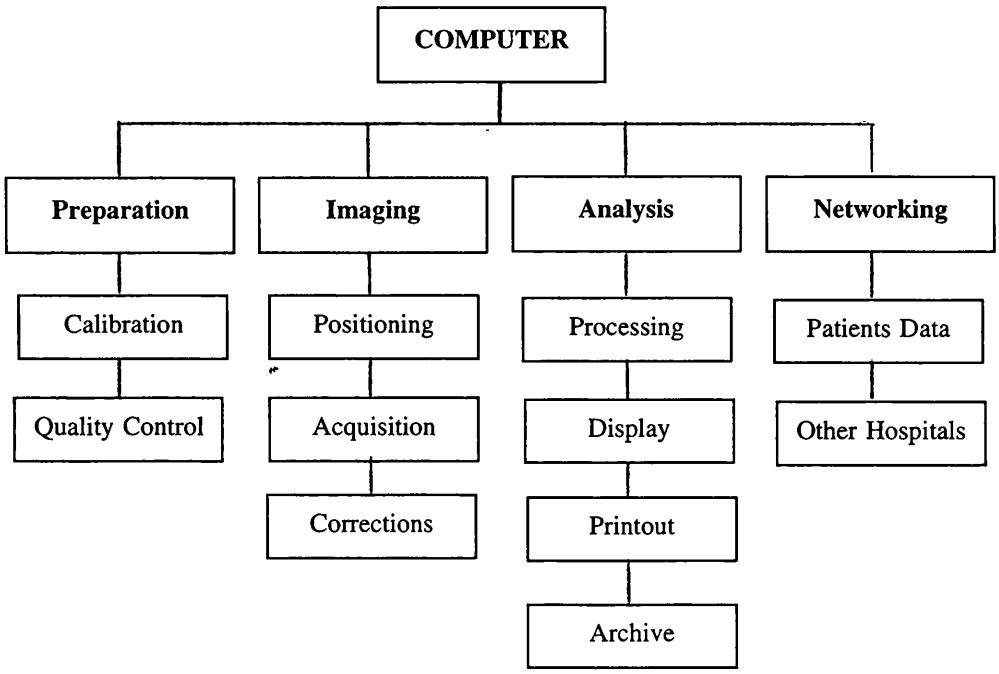

Figure 1.5: The basic functions of a nuclear medicine computer

Computer functions can be divided into four basic categories:

a) Preparation b) Imaging c) Analysis d) Networking.

The preparation, imaging and analysis are most important tasks.

Preparation: Prior to imaging, a computer is used to calibrate the system and to establish routine quality control and correction procedures , for example uniformity energy correction etc.

Imaging: During imaging the computer controls the data acquisition and image display with on line electronic image correction. The acquired image may be in the form of static acquisitions or dynamic studies with a specified framing rate or gated studies.

Anlysis: Post-imaging the computer performs processing and analysis of the patient's data such as SPET reconstruction or dynamic flow analysis. A comprehensive software package should be able to perform a number of image manipulation operations, for example addition, subtraction, division and multiplication of an image by a constant or by another image.

All the major manufacturers supply the computer system, which performs the basic functions needed for nuclear medicine studies. The software available is proprietary and is unique to each manufacturer, but the tasks performed have much in common. Hardware is generally a mixture of both proprietary and commercially available electronics. The final patient image output obtained from commercial systems look very similar. Major computer differences can be found in:

a) How the computer system is implemented in the hardware

b) The ease of data analysis

c) The flexibility of the computer system itself

d) Whether the computer system works with any camera including cameras from other manufacturers

e) Whether the computer system is a commercial product with proprietary software, or an in house product specific to that company only

f) whether the system is "state of the art" and not easily made obsolete by rapidly developing technology.

The users cannot choose the optimum system for their requirements, because major manufacturers offer the gamma camera and the computer system as an integral unit with the intention of providing for an integrated package. Computers which can work with any camera are still limited in some respect by technical incompatibility and proprietary obstacles. The hardware and software technology employed in the commercial computer system by various manufacturers is tabulated below (Table. 1.4)

HARDWARE	CAPABILITIES	USERS
SUN microsystems SPARC workstation, running UNIX	Integrated text and graphics. Vendor customised acquisition and display processing.	**ADAC** (Pegasus) **Toshiba** (GMS-5500A) **Trionix** (Triad) **IGE** (*in development*)
INTEL 486 - microprocessors PC based	Separate text and graphics. Vendor customised acquisition and display processing.	**Elscint** (Apex) **IGE** (Star 4000) **Advanced Nuclear Imaging** (computer only - no camera)
INTEL 486 Multi-bus, IBM 0S/2 (Elscint) INTEL RISC i860 microprocessor	Integrated text and graphics. Vendor customised acquisition and display processing	**Elscint** **IGE** (Star 4000i)
MACINTOSH 68030 / 68040 microprocessor	Macintosh graphics. Vendor customised acquisition and display processing	**Siemens** (ICON) **Scientific Imaging** (Nuclear Mac-computer only. No camera)
MOTOROLA 68040 microprocessor. Flash logic parallel processors. FORTH software.	Command touch screen with separate graphics. Vendor customised acquisition and display processing	**SOPHA** (NXT, DST)
KUBOTA PACIFIC SUPERCOMPUTER (TITAN 750)	Parallel processing. No array processor required. Integrated text and graphics. Vendor customized acquisition and display processing.	**Picker** (Odyssey)

Table 1.4: The hardware technology employed in current commercial computer systems.

It is interesting to note how different companies have implemented their system design from a different technically based hardware platform. Siemens ICON and the Scientific Imaging are based on the Macintosh personal computer. The ADAC system is based on a Sun SparcStation and the Picker

(Odyssey) is based on a Kubota Pacific supercomputer. These systems are based on 32-bit CPU. The Macintosh is based on the Motorola 68030, a CISC (complex instruction set computer) microprocessor. On the other hand, the Sun uses a SPARC microprocessor. These are RISC (reduced instruction set computers). The new systems provide a large memory address space and significantly improved processing power over the previous generations. The Sun-SPARC Station (Pegasus 10) used in ADAC system is rated at 86.1 MIPS (million instructions per second) and 1.7 MFLOPS (million floating point instructions per second), while the Picker (Odyssey) is rated at 89.0 MIPS and 8.5 MFLOPS. A Macintosh IIfx is rated at about 2.6 MIPS and 1.2 MFLOPS. Comparing these figures with previous generation systems in which even large servers such as the VAX-780 used in the Siemens MaxDelta configuration offered about 1 MIPS, while typical minicomputers such as DIGITAL equipment PDP-II and DATA general NOVA had about 0.7 MIPS.

Application software supplied is typically written in C, PASCAL, FORTRAN, FORTH, ASSEMBLER etc.,. Well-written, tested and documented user software may then be used by other centres as relevant to their needs. Software standards, such as ISO 9000, now exist to ensure that minimum quality and reliability standards are complied with and both user and manufacturer software are subject to product liability legislation. The most striking difference of the new software is the windowing environment and graphical user interface. Windowing is a metaphor allowing multiple logical terminals to open at one time. A window is basically a frame for viewing something. The contents are determined by the application. More than one window may open at a time, and they may overlap. This allows the operator to set aside information, yet have easy access to it.

Most current systems provide network hardware and software. The most common standard is Ethernet which was developed by Xerox Corp in the 1970s. It defines the low level physical connections but not higher level programs to facilitate communications protocols. This means that there can be multiple systems using the same Ethernet cable which cannot communicate with each other. Figure 1.6 demonstrate a typical Ethernet configuration.

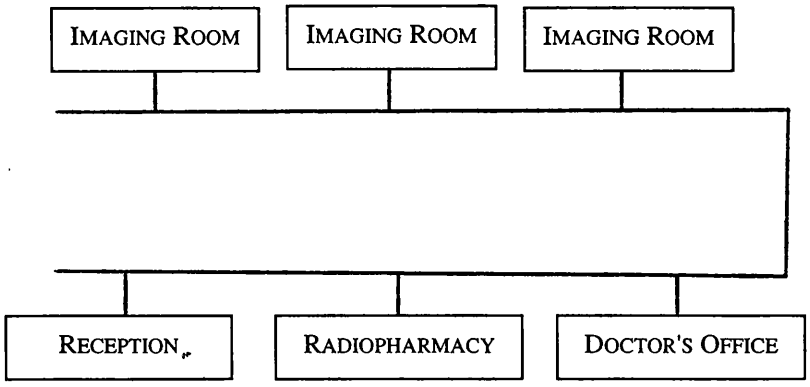

Figure 1.6. : A typical network configuration in a nuclear medicine department

Ethernet is a "backbone" cable running through the department with systems simply tapping into it. Some of these systems could be Macintosh using an Ethertalk protocol to send files back and forth and others could be UNIX based Sun workstations using TCP/IP or VAXes using DecNet. Except for the availability of the backbone these systems would not know of each other's existence. Networks are cost effective because workstations are dedicated to a particular task, yet have access to all the information on other system in the network. This allows the workstations to be configured to perform their specific tasks rather than be loaded with expensive hardware and software to perform any task. For example, the imaging rooms contain acquisition-only stations, the physician offices and reporting rooms contain display-only stations with a few additional processing stations to analyse the studies. In this way the camera time is maximised and the stations for reporting are more available. Networks can extend beyond a department or hospital. Long distance communication relies primarily on telecommunications. Data transfer via the telephone is achieved via modem technology. Modems convert the digital information into analogue frequencies which will pass through the telephone system. High speed 9600 BPS modems are the choice for rapid data transmission. The modems themselves or the communication software can handle data correction and data compression. If higher data rates are needed T1-bridges may be used. These devices use high speed (1.2 million bits per

second/150,000 bytes per second) lines leased from the telephone company to connect two or more local area networks. When they are operational, data from either site may be accessed at close to normal network speeds. There are solutions with even higher data rates, such as direct fibre optic connections, or even microwave transceivers, which are highly reliable and high volume data transmission could be performed.

1.5. Single Photon Emission Tomography

In planar two-dimensional scanning, image information from depth is blurred since it is seen in a single plane. Tomographic imaging adds the missing third dimension. Data which does not arise from the section under study, is selectively removed. Tomographic images offer: improved contrast resolution, 3-D information and improved quantification.

1.5.1. METHODOLOGY

SPET requires a set of multiple views (projections) at many angles around the body. Each projection represents the radionuclide distribution at that angle at which the detector is positioned. Once a sufficient number of projections or profiles are acquired than the original activity distribution can be reconstructed. The gamma camera records multiple profiles at a time, the number being given by matrix size for example 64 or 128.

The method of reconstruction most commonly used today is called "filtered back-projection". It is obvious from the name that this procedure consists of two steps: filtering (or convolution) and back projection.

Let us consider a point source for simplicity (figure 1.6). Back-projection takes the value of a profile element acquired at a particular angle and places that value in each pixel in the reconstruction matrix along the line of that angle. This is done for every element of the profile and at every acquisition angle. Then the back projections are added together. The more angles that are used the better is the estimate of the original distribution. Unfortunately the result of this process is a very blurred reconstruction because equal values are assigned to all points along the matrix line. This is known as the "star effect"

and is unsatisfactory for clinical interpretation and therefore data must be filtered. This leads to the technique of filtered back-projection. The filter applies negative weighting to values of the profile elements surrounding the element of interest before back-projection. This balances the positive and negative values outside the object of interest, which cancel out when back-projected, thus eliminating the "star" artefact.

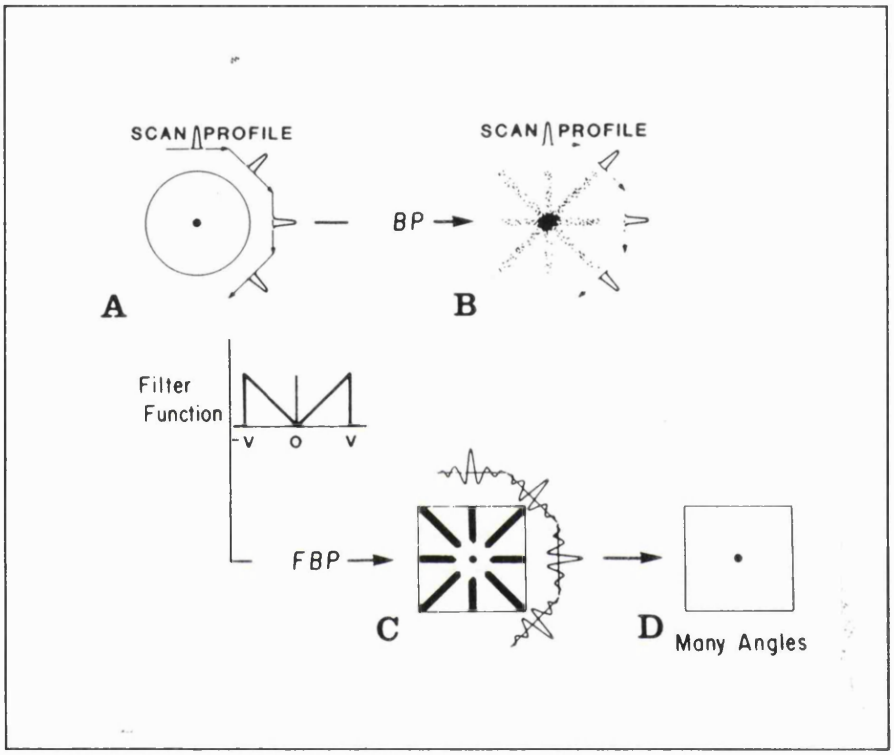

Figure 1.7: Illustration of single photon emission tomography (SPET) data acquisition and image reconstruction. data collection results is a series of projection data represented by profiles (A). Reconstruction consists of a filtered backprojection (FBP). Filtering of the projections results in data set (C), which when bakprojected results in the reconstruction of an image of the original object (D). Simple backprojection (BP) without filtering results in a blurred image (B).

Filters are expressed in terms of their action on spatial frequencies rather than spatial dimensions. The mathematically correct filter to eliminate the star artefact is called a Ramp filter because of its shape in the frequency domain. It gives increasing weight to higher spatial frequencies thus removing the blurring. Unfortunately, noise also occurs at high spatial frequencies and therefore the Ramp filter also amplifies the noise components in the data. That is why the Ramp filter is usually multiplied by a low pass filter to round

off or window the function at high spatial frequency in order to remove noise and to pass true image information dominant at low spatial frequencies. However in reducing noise, resolution may also be degraded and therefore the choice of filter plays a most important role in the production of high quality clinical SPET images. The maximum frequency i.e., the frequency at which a function drops to zero is known as Nyquist frequency and is defined as 1/2 r, (r=system resolution of system, in FWHM).

1.5.2. FILTERS USED IN SPET RECONSTRUCTION

The choice of filter for a particular study depends to some extent on what is available on different commercial systems and is also somewhat subjective. The importance of understanding the function of different filters and their parameters and the effect on the final image of varying these parameters can not be over- emphasized (Gilland et al., 1988).

LOW PASS SMOOTHING FILTERS

These filters can be divided into two groups:

(a) filters only requiring the critical frequency to be specified:

Hanning, Shepp-Logan etc.,

(b) filters requiring the slope or order of the filter along with critical frequency: Butterworth

Critical or cut-off frequency : The critical frequency determines how much smoothing will be applied to the images. The lower the critical frequency the greater the smoothing but loss of resolution will occur. Higher critical frequencies will give noisier images but better resolution. The choice of critical frequency depends upon the count density in the study and the resolution required. The filters used in today's commercial system usually require the operator to enter the critical frequency value. The unit for this critical frequency varies with manufacturers and may be expressed as cycles/field of view or cycles/pixel or cycles/cm. Depending on the units used, a critical frequency may vary with matrix size, zoom and field of view. If expressed as cycles/cm, the value is independent of these parameters. For the Hanning filter, the critical frequency is defined as frequency at which filter rolls off to

zero, whereas for the Butterworth filter a critical frequency may be defined as the point where the gain has dropped to 0.7 of maximum. Table 1.5 lists the units used by different manufacturers.

Manufacturer	Critical Frequency (f_c) units
Siemens	Fraction of f_n
Elscint	Fraction of f_n
IGE	Cycles / cm
Toshiba	Cycles / pixel
Sopha	Cycles / pixel
NucLear Mac	Cycles / pixel

Table 1.5. : Units expressed for critical frequency (f_c) by different manufacturers. (f_n = Nyquist frequency)

To compare the critical frequencies from different manufacturers, it is best to convert these into a convenient unit. The most meaningful unit for critical frequency in terms of cycles / cm, because it has the advantage that it is independent of the matrix size, zoom and field of view (FOV) and resolution. Table 1.6 summaries the formulae to convert the various units from and to units of cycles / cm.

Units	Conversion to cycles/cm	Conversion from cycles/cm
Cycles / FOV	$f_{ccm}=f_{cfov}*1/Mp$	$f_{cfov}=f_{ccm}*Mp$
Fraction of f_n	$f_{ccm}=f_{cfra}*1/2p$	$f_{cfra}=f_{ccm}*2p$
Cycles / pixel	$f_{ccm}=f_{cpix}*1/p$	$f_{cpix}=f_{ccm}*p$

Table 1.6.: Conversion formulae for critical frequencies. (p=size of pixel in cm, M= matrix size, f_{ccm} = critical frequency as cycles/cm, f_{cfov}= critical frequency as cycles/FOV, f_{cfra}= critical frequency as fraction of f_n, f_{cpix}= critical frequency as cycles/pixel

Order or slope : Some filters, Butterworth, for example allow the order or slope of the filter to be varied by the operator. Increasing the order for a given

critical frequency will give a sharper cut-off of high frequency noise but allow more of low frequency image data to be included. The shape of the Butterworth filters differ from the Hanning and Shepp-Logan in the sense that it keeps the value close to 1.0 at low frequency and has a steeper roll off. For the images with high count statistics requiring high resolution, a high order, high critical frequency filter should be used whereas for the noisy low count images it is important to select a low order filter with a low critical frequency.

RESOLUTION RECOVERY FILTERS:

Resolution recovery filters such as Metz and Wiener are basically designed to boost low and middle spatial frequencies in order to recover the resolution lost in the imaging system (King et al 1983,1984, 1987). Modulation transfer function (MTF) describes the instrument's response, as a function of spatial frequency and it is actually the Fourier Transform of the point spread function. These filters are the inverse of the MTF. Ideally the MTF should be determined for each study as it varies with the radionuclide, collimator, radius of rotation, scatter etc., but this is not practical and only some parameters are fed into an idealised equation.

METHODS OF APPLYING THE FILTER

Reconstruction filtering: The purpose of this filtering is to correct for the "star" artefact. It may be the ramp filter or the ramp in combination with a low pass filter such as Shepp-Logan, Hanning, or Butterworth to produce some degree of smoothing. It is applied one dimensionally to each count profile, therefore there is no smoothing across the slices which will affect the coronal and sagittal images which are reconstructed from the transaxial data. Theoretically, all the reconstruction filters pass through the origin i.e., gain = 0, at zero spatial frequency.

2-D PREFILTERING: This filtering is applied to the planar images before reconstruction. It provides smoothing between the slices, as well as in the slice plane but it does not correct for the "star" artefact. Therefore a pre-filter is always used in combination with a ramp reconstruction filter. Pre-filters do not pass through the origin but have a gain = 1, at zero spatial frequency. Pre-filters are also low pass smoothing filters such as Shepp-Logan, Hanning and

the Butterworth, but can also be the resolution recovery filters such as Wiener or Metz filters. It is better to pre-filter a study and then reconstruct with a ramp filter rather than to do reconstruction filtering.

Pre-filtering should be exercised judiciously, but can improve reconstructed image quality when applied correctly. Figure 1.8 demonstrates an example of different filters being applied to the same data.

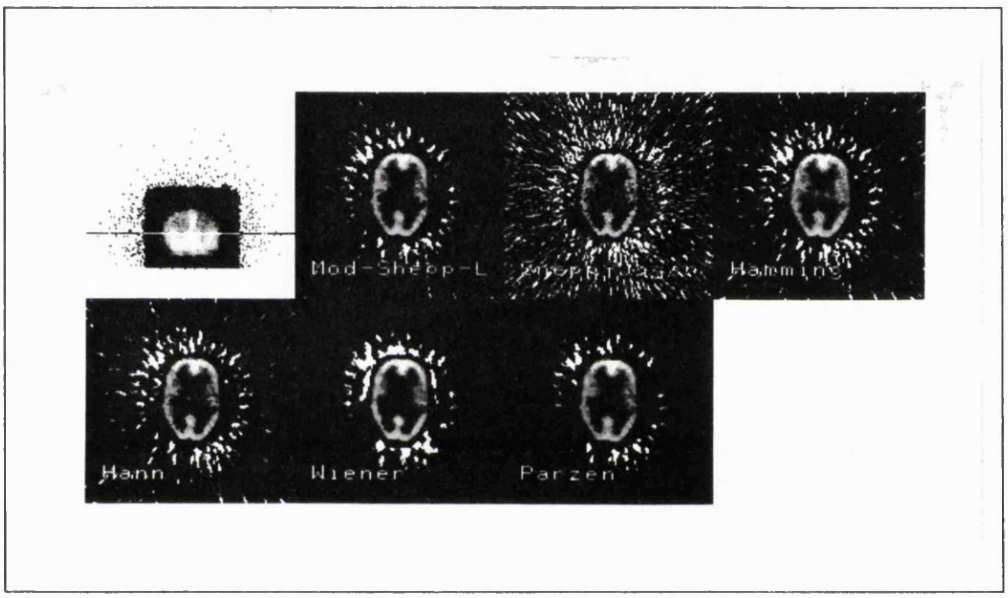

Figure 1.8: Demonstration of the effect of different types of prefilters. Six different filters are applied to a Hoffman brain phantom SPET data. The transverse slices at the level of thalami are displayed. It is important to note that although resolution is much better with Wiener and Parazen filters, there is some loss of activity from the thalami. This is different in the case of the Hamming filter, where in the thalami the activity is still conserved, but the image looks slightly more noisy.

1.5.3. Quality Assurance

Artefacts can be produced if strict quality control is not maintained (Grahm LS 1989, Halma et al., 1989, Murphy PH. ,1987). It is very important that regular and accurate quality assurance is maintained on a SPET camera. The two most important corrections for SPET are uniformity correction and centre of rotation correction.

Uniformity Correction

Non-uniformity in the detector may be caused by several factors e.g., collimator sensitivity variations due to misalignment of collimator holes, poor

tuning of the detector and non uniformity in the crystal itself. If non-uniformity is not corrected adequately then ring artefacts will occur in the reconstructed SPET image (Rogers et al., 1982). Non-uniformity can be corrected for by acquiring a high count extrinsic flood image, which is then used to form a correction matrix to be applied to the acquired data.

Centre of Rotation (COR)

In order to obtain artefact free, high resolution images it is essential that the axis of rotation of the camera is known in relation to the position of the computer matrix. COR calibration measurements must be performed to identify the actual position in the camera image which views the axis of rotation so that a shift can be applied to position this point at a known point in the reconstruction. This shift is performed in the computer software and is referred to as the COR correction. If this is not performed regularly and accurately there will be loss of spatial resolution and contrast in the SPET images. It is important to note:

a) COR error greater than 0.5 pixel causes loss of image resolution

b) The mean COR value should not exceed 2 or 3 pixel from the true centre of computer matrix, otherwise the usable field is reduced.

c) Frequent changes in the COR value may indicate a mechanical problem in the camera gantry

d) SPET studies must be reconstructed with the COR value obtained at the time of acquisition of the study. The frequency of COR measurement depends upon the extent of the stability of the camera.

e) COR values may vary between collimators and therefore must be measured for each collimator used (Cerquiera et al., 1988). COR may also vary across the field of view probably due to non-perpendicular alignment of the collimator holes (Busemann-Sokole, 1987). This should be checked at the time of acceptance testing.

Head Tilt

SPET reconstruction also assumes that data is acquired at angles directly perpendicular to the axis of rotation. The gamma camera head must always be level, otherwise loss of resolution and contrast will occur due to more than

one transaxial plane being viewed in a single projection.

Radius of Rotation

The resolution of a parallel hole collimator decreases with increasing source to detector distance. In SPET studies, therefore, the radius of rotation should be as small as possible. Radius of rotation can be improved by several different hardware means for example, an elliptical orbit facility, a cut-away detector head for brain tomography or a multi-detector gamma camera.

Motion Artefacts

Patient or radioactivity movements are difficult errors to assess and to correct. This is because when SPET acquisition is carried out, it assumes that during the time of acquisition the distribution of the radiotracer in the organ is invariable. Motion artefacts can be assessed by observing the acquisition data in cine mode or as a sinogram. Some manufacturers provide software for patient movement correction between acquisition frames.

1.5.4. Factors Affecting Quantification

Accurate quantification of the radioactivity distribution is the ultimate aim of SPET. (Blockland et al, 1992). The two important factors which affect the quality of the final image and quantitative analysis are attenuation and scatter.

a. Attenuation Correction

Attenuation of photons in the body results in a loss of counts in the reconstructed image which affects the quality of image and ability to obtain quantitative information. Many correction techniques have been developed to correct for attenuation (Blockland et al, 1992). These include:

i) Pre-processing of the projection data: This is the simplest form of attenuation correction and it uses the geometric mean of opposing projections.

ii) Modified back-projection algorithms: The attenuation correction is incorporated into the filter used in image reconstruction. A constant attenuation coefficient is used.

iii) Post reconstruction correction: This computes a correction factor for each pixel of the reconstructed slice based on the mean attenuation for that pixel to all projections. This is known as the first order Chang correction

(Chang, 1978). A second order correction uses the first order corrected reconstructed slice and reprojects it using the same attenuation and these projections are then compared with the original projections of the object. The difference between the two sets of projections is back-projected to form a correction image which is then added to the first order corrected slice. This algorithm also assumes uniform attenuation throughout the image volume.

The post-processing method of Chang is the most popular technique in use by commercial companies. To date the commercial algorithm assumes a constant attenuation coefficient throughout the image volume. This may be applied to body sections such as the head, where the attenuation coefficient distribution is fairly uniform. It is, however, unsatisfactory for areas such as the cardiac or chest region where photon attenuation varies greatly due to different surrounding organs such as the lungs. Methods for correcting for non uniform attenuation such as transmission scanning to determine an actual attenuation coefficient map are the subject of ongoing research (Bailey et al., 1987, Almquist et al., 1990)

b. Scatter Correction

Scatter photons degrades the contrast in the images, and reduce resolution, cause edge blurring and will affect quantitative analysis. Attenuation decreases the number of photons in an image, where scatter adds unwanted photons. One way therefore for correcting for scatter is to under-correct for attenuation by using a reduced value for attenuation coefficient. This may be a reasonable and simple approach for qualitative imaging but is not suitable for quantification. Many methods for scatter correction are continually being reported in literature (Blockland et al., 1992, Gilardi et al., 1988).

i) Dual window substraction: (Jaszczak et al, 1984) In this method a fraction of the image reconstructed from data in a secondary lower energy "scatter" window is subtracted from the image reconstructed from data in the primary photopeak window. A fraction of 0.5 was calculated to be the best value to restore the image contrast (Jaszczak et al, 1984). This method has not been implemented in any commercial system.

ii) Energy weighted acquisition (EWA): (Halama et al, 1988) This method

utilises all photons to form an image weighting their contribution depending on their energy. Photopeak events contribute positively, scatter events negatively. This technique in the commercial system has been pioneered by Siemens. In a conventional gamma camera single window of say 20% is placed over the photopeak. For Tc-99m this covers the energy range of 126-154 keV. EWA recognises that a photon energy of 150 keV is much more likely to be unscattered photon than a photon of energy 126 keV. Therefore using a multi-channel analyzer instead of a single analyzer, the inclusion of photons in the final image is determined by an energy-dependent weighting function, which has negative weights for scatter energies as well as positive weights near the photopeak.

iii) Dual photopeak method: (King et al., 1992) The basis of this recently suggested method for scatter correction is that Compton scattered photons contribute more to the lower energy portion of photopeak than the higher side. Therefore, if the photopeak region is divided into two overlapping energy windows a regression relationship could be obtained between the ratio of the counts within these windows and the scatter fraction for the counts within the total region.

1.6. Clinical Applications of SPET

During the last decade, SPET has grown from a rarely used technique into a routine clinical tool. The potential clinical advantages of SPET over planar imaging are: a) better anatomical resolution of structures, allowing for better localisation of extent and severity of disease b) higher contrast resolution c) 3-D assessment of the distribution of radionuclides, leading o improvement in data quantification.

Here follows a description of typical applications of SPET.

1.6.1. Bone Disease

Skeletal SPET has become increasingly useful in the management of benign bone disease (Collier et al, 1985, Collier et al 1987, Jacobson et al, 1984).

Avascular Necrosis : In the hip, the acetabulum extends downwards behind the

femoral head. Therefore, the photon-deficient defect typical of an avascular necrosis of the femoral head may be obscured in planar imaging by activity originating in the underlying acetabulum. Using SPET, however, it is possible to separate underlying and overlying distributions of activity into sequential tomographic images. For this reason, SPET facilitates detection of disease here (Collier et al., 1985).

Knee joints : Within the knees it has been shown that SPET increases the accuracy of scintigraphy in identifying the cause of acute knee pain (Collier et al., 1985). This is particularly true if it is secondary to a meniscal tear (Murray et al, 1990). Impressive SPET scans can be obtained in these conditions.

Lumbar Spine : There is clear evidence, from a series of 1390 patients, that at least, in the lumbar spine there is an increased sensitivity of up to 35 % using SPET in finding lesions when compared with planar imaging (Kanmaz et al,1992). Gates et al., also reported the usefulness of SPET in patients with lower back pain (Gates et al., 1988). SPET is also of advantage in evaluating persistent low back pain in patients who had undergone surgery of the lumber spine (Lysins et al., 1989, Onsel et al., 1992).

Temporomandibular joint : Clinical experience to date has shown a role for bone SPET in the temporomandibular joint (Collier et al., 1983, Krasnow et al., 1987). Its exact role compared with that of magnetic resonance imaging (MRI) is still to be established. In fact, in at least one publication (Helms et al., 1990) comparing various imaging techniques, SPET was not even included.

Oncological imaging : The potential of bone SPET in oncology is under investigation. Here SPET shows promise not only as a tool, but also because it is being applied in conjunction with an increasing number of specific radiopharmaceuticals (such as monoclonal antibodies, receptors etc.,)

1.6.2. LIVER/ SPLEEN IMAGING

Parenchymal Liver Disease : There has been a marked decline in SPET colloid imaging of liver and/ or spleen, since the introduction of ultrasound and x-ray computed tomography (CT). Some studies have demonstrated that diffuse

non-uniformity of colloid distribution in the liver is a manifestation of hepato-cellular dysfunction and not metastatic disease (Podoloff et al., 1988, 1989). There have been studies showing a superiority of SPET over CT in the detection of diffuse parenchymal hepatic abnormality (Yudd AP et al., 1986, Kodama T et al., 1986).

Haemangiomas : SPET has been very helpful in the differentiation of haemangioma from metastatic disease, suspected on the basis of CT or ultrasound. Birnbaum et al., compared MRI with SPET in 37 patients who had 69 suspected haemangiomas initially detected on CT or ultrasound. They found that MRI had a 20% false positive rate, while SPET study was clearly capable of distinguishing haemangioma from hypervascular metastases. They suggested that MR imaging was superior only for lesions smaller than 2 cm or those close to the heart or major hepatic vessels (Birnbaum et al., 1990).

Lymphoma and Leukaemia : SPET is also helpful in liver and spleen imaging in patients with leukaemia and lymphoma in whom one is trying to differentiate tumour infiltration from hepatotoxicity (Podoloff et al.,1988, 1989). Using a single-detector SPET system, Fawcett and Sayle (1989) suggested that when there is low prevalence of disease (in their study 13%) little is gained by SPET (Fawcett et al., 1989).

1.6.3. TUMOUR LOCALISATION

In tumour imaging, the advantages of SPET are increased accuracy (Deland et al.,1984), improved contrast resolution as a consequence of the tomographic reconstruction technique (Podoloff et al.,1988) and more precise three-dimensional localisation of various lesions by simultaneous display of the transaxial images, not possible with the planar imaging.

Gallium-67 SPET : Hagemeister et al., indicated that gallium-67 (Ga-67) imaging was not adequate in patients with **Hodgkin disease** and **high grade lymphomas** of well defined cellularity, as far as the sensitivity or specificity is concerned (Hagemeister et al., 1990). However, it has been demonstrated that SPET with high dose of gallium-67 was clearly superior to planar imaging in the evaluation of specific areas in the thorax. SPET demonstrated 55 of 57

mediastinal sites, planar imaging 38, chest radiography 30, and CT 47. Most of these sites were in the anterior mediastinum. It was also concluded that SPET was more accurate in depicting foci of gallium-avid lymphoma in the chest and abdomen and excluding the disease when the results of planar imaging were equivocal (Tumeh et al., 1987).

Thallium-201 SPET : were the first to report on The use of thallium-201 for a variety of neoplasm was reported first in 1978 (Hisada et al.,1978). Later the use of SPET with thallium-201 was reported in the central nervous system to study **tumour recurrence versus radiation necrosis** (Ancri D et al.,1987, Schwartz et al., 1992). Hoh and colleagues (1992) evaluated brain tumour recurrence with thallium-201 SPET in correlation with labelled glucose PET studies and histology. Thallium-201 SPET appeared at least as sensitive in detection of tumour recurrence as labelled glucose (Hoh et al., 1992). Extensive preoperative thallium-201 SPET studies in patients with gliomas have shown that by using a "threshold index" the grade of glioma could be predicted with an accuracy of 89% (Kim et al., 1990, Black et al.,1989).

Thallium-201 SPET imaging can be used successfully to investigate a variety of neoplastic diseases including **sarcomas, medullary carcinoma** and **breast** and **lung carcinoma**. The ability to depict precisely in transaxial slices the regional distribution of thallium and compare it directly to CT or MRI images is of great value in mapping the extent of viability and/or blood flow of the tumour seen at thallium SPET to the anatomic changes seen at CT or MRI. This technique has been used in the evaluation of primary foci and in the follow up of the patients after therapeutic intervention.

Another interesting use of thallium-201 SPET is in the evaluation of patients with "**plexopathy**". Most of these patient had either carcinoma of either breast or lung and during therapy developed shoulder pain. The MRI and CT images have demonstrated a variety of findings, most often nodules or masses in the region of the brachial plexus. Evaluation with thallium-201 SPET has led to correct classification of cases as either active tumour infiltration or plexopathy (Podoloff et al., 1992).

Monoclonal Antibody Studies : SPET has potential for imaging with

radiolabelled monoclonal antibodies. Berche et al., (1982) reported that SPET was useful in clinical imaging with I-131 labelled monoclonal antibodies to carcinoembryonic antigen (CEA) in patients with **gastrointestinal tract** and **medullary thyroid cancer**. Another study by Chatal et al (1985), involved the use of SPET in the evaluation of **recurrence of colorectal carcinoma**. SPET depicted only 7 out of 12 liver metastases. They believed that this was due to poor tumour contrast. However, these authors concluded that SPET appeared to be useful in localising **pelvic or abdominal recurrences** in post-operative patients. Delaloye et al (1984) first reported the utility of SPET with I-123 labelled $F(ab')_2$ fragment from monoclonal anti-CEA antibodies used to detect colorectal carcinoma and showed improved accuracy for SPET over planar imaging. Much greater success has been achieved with Tc-99m and In-111 SPET. Lamaki et al (1988) using intact and Fab fragments, reported marked improvement over planar imaging. In particular SPET enabled the localisation of lesions in the **liver** (a site of normal indium accumulation). In another study Lamaki et al (1990) have reported the superiority of In-111 monoclonal antibody imaging over CT and other conventional imaging studies in the diagnosis of **occult lesions**.

In-111 Octreotide SPET: In our experience, using In-111 ocreotide, a somatostatin analogue SPET was helpful in detection of insulinoma.

1.6.4. NEUROLOGY AND PSYCHIATRY

Very substantial progress has been made with SPET and arrival of new radiopharmaceuticals (Ell PJ et al. 1985, Kung HF et al., 1990, Verhoeff et al., 1991). It has been able to study a series of different biological functions (Ell PJ et al., 1992)

Stroke : Stroke is still one of the major causes of mortality. 33% of the patients suffering from transient ischaemic attacks may develop a full vascular accident within 5 years. The diagnosis of stroke has been significantly enhanced by the introduction of x-ray CT and MRI. Now the neurologist is interested in SPET imaging for establishing a prognosis. Potential clinical application for SPET of regional cerebral blood flow in vascular disease

include improved identification of cerebro-vascular disease, in patients with incomplete strokes, the detection of distal effects of vasospasm that often accompanies subarachnoid haemorrhage, and imaging in the subacute phase following cerebrovascular ischaemia, which may be useful in predicting recovery after 90 days (Hellman et al.,1990). An interesting comparison of Tc-99m HMPAO SPET and CT of the brain was performed to assess the prognosis after stroke (Mountz et al.,1990). In this study, there was a clear improvement and better prognosis in patients who had small CT abnormalities and relatively large perfusion deficits. On the other hand, when the deficits at CT and perfusion imaging were equal or when the CT deficit was greater, the clinical outcome was poor.

Head Trauma: Cerebral blood flow studies are more sensitive in the demonstration of the extent and severity of pathology in the brain following head trauma. Roper et al., (1991) performed Tc-99m HMPAO SPET studies in 15 patients with closed head injury. These images revealed focal disturbances of flood flow, not demonstrated on x-ray computed tomography (CT). In another study of 19 patients with closed-head injury by Newton et al.,(1992), they compared Tc-99m HMPAO SPET studies with CT and magnetic resonance imaging (MRI). The distribution of cerebral blood flow abnormalities revealed more lesions than CT or MRI.

Epilepsy : In patients with epilepsy refractory to medical treatment, where surgery is considered a management option, SPET and PET imaging has been used to determine the site of pathology. Rowe et al., (1991) investigated postictal patterns of cerebral blood flow in patients with temporal lobe epilepsy. Tc-99m HMPAO SPET study demonstrated a positive predictive value in correct localization of the focus in 31 out of 32 (97%) cases. Schmitz et al.,(1992) investigated role of ictal and interictal electroencephalography (EEG) with Tc-99m HMPAO SPET studies in 15 patients with focal epilepsy. In 10 out of 11 patients with abnormal EEG recordings were in agreement with cerebral blood flow mapping.

Human Immunodeficiency Virus (HIV) Encephalitis : In this entity of disease, it is still difficult to diagnose early on and the differential diagnosis

often involves depression and psychosis. An early diagnosis may benefit from treatment with zidovudine or azidothymidine. Abnormal patterns of tracer distribution have been reported in such patients on brain perfusion SPET studies, similar to drug abusers (Verma et al., 1992, Masdeu et a.,1991, Holman et al.,1992).

Chronic fatigue syndrome : This is a topic of debate between neurologists and psychiatrists. There is dispute whether there is an organic component and also whether this condition is a specific disease or is only another manifestation of depression. Using Tc-99m HMPO SPET studies, Douli and co-workers (1992) have reported significant hypoperfusion of the brain stem, as a consistent finding in patients with myalgic encephalomyelitis. Simon et al., (1991) have reported temporal blood flow abnormalities in a group of patients with affective disorders, using Tc-99m HMPAO SPET imaging.

Alzheimer's disease : The diagnosis of Alzheimer's disease is clinical. The differential diagnosis is difficult in patients with depression, Parkinson's disease and dementia. There is no effective treatment for this disease, while some other types of dementia may benefit from treatment. Tc-99m HMPAO SPET studies depict characteristic posterior bitemporal parietal perfusion deficits in the majority of the patients (Holman et al.,1992, Butler et al., 1992, Jobst et al.,1992). This pattern can often be distinguished from multi-infarct dementia (Bonte et al., 1991).

Parkinson's disease : Recently the dopamine D_2 receptor system has been studied extensively in patients with Parkinson's disease. A successful D_2 SPET tracer is I-123 iodobenzamide (IBZM). Verhoff NPLG et al (1992) reported usefulness of I-123 IBZM SPET in the differential diagnosis of Parkinsonism and in the selection of dopaminergic therapy. Using I-123 IBZM, Tatsch et al., (1992) have reported a sensitivity of 98% in the differential diagnosis of idiopathic Parkinsonism and other Parkinsonian syndrome.

Schizophrenia : The D_2 receptor blockade hypothesis of schizophrenia and the mechanism of action of clozapine has been investigated. I-123 IBZM SPET studies performed in six patients on typical antipsychotic medication and ten patients on clozapine therapy, Pilowsky et al., (1992) demonstrated that

patients on typical antipsychotic medication had a poor therapeutic response, despite having D_2 receptor blocking. All patients on clozapine showed clinical improvement despite a lower level of D_2 blockade by the drug.

The application of SPET in brain imaging is entering a new era. Utility has now extended from the diagnosis to the investigation of outcome and treatment. Investigations of an increasing number of neuroreceptors and labelling of drugs which are relevant to modern treatment of neurological and psychiatric diseases, are probably the most exciting of these applications.

1.6.5. CARDIOVASCULAR SPET IMAGING

I) GATED BLOOD POOL TOMOGRAPHIC IMAGING

Although planar gated blood pool measurements of ejection fraction have shown excellent agreement with results obtained from contrast ventriculography. The former method requires background subtraction. Secondly, left atrial or right ventricular enlargement may contribute to increased counts in the left ventricular region of interest. Gated blood pool tomography (GBPT) may overcome these problems. (Stadius et al.,1985, Gill et al., 1986, Underwood et al.,1985, Corbett JR et al., 1985). Good correlation has been reported for ES and ED volumes compared to contrast ventriculography (Stadius et al., 1985). No background subtraction is required and even in the absence of attenuation and scatter correction, absolute volumes can be calculated (Underwood SR et al., 1985).

Assessment of regional left ventricular function is important in evaluating the **presence or consequences of CAD**, the **effects of interventions** (like thrombolysis, angioplasty or CAB surgery) or the **efficacy of drug treatment**. Contrast ventriculography has been used to evaluate regional function, but it is limited by an inability to examine the septum and lateral walls without performing multiple contrast injections. Although the true three dimensional acquisition that occurs with GBPT allows optimal evaluation of multiple regions of the ventricle, it could not gain popularity amongst clinicians due to the development of and more interest in the echocardiographic techniques and inherent problem with gating in cases of arrhythmia.

II) MYOCARDIAL PERFUSION SPET

During the last two decades, considerable advances have been made in the application of nuclear imaging to the study of myocardial perfusion (Gould et al., 1978, Iskandrian et al., 1991, Mahmood et al, 1992, Jain D et al., 1993) Thallium-201 has been in use for assessment of myocardial perfusion since 1970 (Kaul S, 1989). The sensitivity of exercise thallium-201 imaging is superior to the sensitivity of exercise ECG in detection of CAD (Botvinick et al., 1978, Corne et al., 1979, Verani et al.,1978). SPET is superior to planar imaging (Table 1.6), because of the lack of superimposition and overlap of normal and abnormal areas (Fintel et al., 1989, Maublant et al., 1982, Richie et al., 1982).

	Type	No. of Pts		Sensitivity		Specificity		Accuracy	
		CAD+	CAD-	Plan.	Tomo	Plan.	Tomo	Plan.	Tomo
Fintel et al., (1989)	Ex	96	39	84	91	90	90	86	91
Maublant et al., (1982)	Rest	64	15	89	98	93	93	90	97
Nohara et al.,(1984)	Ex	48	10	92	96	80	70	90	92
Ritchie et al.,(1982)	Ex	38	15	63	87	93	93	71	87
Schmitt et al.,(1982)	Ex	19	15	66	84	-	93	-	88
Tamaki et al., (1984)	Rest	160	39	78	96	92	92	81	95

Table 1.7 : Comparison of planar and SPET thallium-201 studies. It is obvious that SPET studies have an advantage over planar studies in terms of diagnostic accuracy.(Plan=planar, Tomo=tomography, Pts.=number of patients included in the study).

The main clinical applications of thallium-201 SPET in coronary artery disease are:

i) Diagnosis of presence and extent of CAD : The diagnosis of CAD in most patients can be made by careful clinical assessment; roughly 90% of patients with typical angina pectoris have CAD, whilst 90% of patients with non-anginal chest pains and 50% of patients with atypical angina pectoris have CAD. Treadmill exercise testing yields inconclusive results in 30-40% of patients due to sub maximal stress or baseline electrocardiographic changes.

It has a low sensitivity of 50%-60% and is unable to predict the individual diseased artery or arteries, or to quantify the extent of CAD, and also assess myocardial viability. Major advantages of thallium-201 SPET include a higher sensitivity, an ability to localise the site of the disease and to assess the extent of the CAD and myocardial viability.

ii) Assessment after percutaneous transluminal coronary angioplasty (PTCA): PTCA is now being done even in patients with multi-vessel disease, unstable angina and acute myocardial infarction. The technical advances in the field have been enormous and have included the use of better designed steering wires, balloons, catheters, angioscopy, intracoronary ultrasound, laser, atherectomy and stents. A major problem in PTCA continues to be the high rate of re-stenosis which is estimated to be 30%-50%. In most cases re-stenosis appears within six months, but not all the re-stenoses are associated with the recurrence of symptoms. The main indications of thallium-201 SPET in PTCA are:

a) Assessment of immediate results

b) Assessment of residual coronary artery disease

c) Assessment of re-stenosis

d) Assessment of myocardial viability

Hecht et al.(1990) found the exercise SPET thallium-201 imaging to be almost 90% accurate in predicting re-stenosis or progression of disease in other vessel in 116 patients with previous PTCA.

iii) Applications after coronary artery bypass surgery : In patients under going coronary artery bypass surgery (CABG) there is an initial 10-15% re-occlusion rate of the grafts and after 5 years many patients may have the recurrence of the symptoms, either due to graft closure or progression of the disease in the native arteries. The recurrence of the symptoms in these patients requires the use of perfusion studies to determine the presence, location and the extent of the abnormality.

iv) Applications in acute myocardial infarction : The main reasons for imaging after acute myocardial infarction are: **diagnosis, assessment of risk** and **extent** and **assessment of myocardial salvage** after thrombolytic therapy.

Imaging with Tc-99m pyrophosphate or In-111 antimyosin antibody is more specific for the diagnosis of acute myocardial infarction (MI) than thallium-201.

v) Risk stratification : Stress thallium-201 imaging using a submaximal stress test or pharmacological testing with dipyridamole or adenosine are now being increasingly used for risk stratification. Other techniques for risk assessment include pre-discharge coronary angiography, exercise echocardiography/ radionuclide angiography and echocardiographic testing using dobutamine infusion (Brown et al., 1991).

Lessons learned from thrombolytic therapy suggest that 40% of the patients with acute MI may have sub-critical stenosis in one coronary artery after thrombolysis. The final event in these patients is coronary thrombosis. It is also clear that as high risk patients are identified and considered for surgical or non-surgical revascularisation, the remaining patients have low or intermediate risk. Thallium-201 SPET is helpful in risk stratification of these patients. The different predictors of future cardiac events in medically treated patients with stable symptoms are:

a) Presence of redistribution (reversible defects)

b) Extent of ischaemia

c) Extent of perfusion deficit (reversible or fixed)

d) Severity of perfusion deficit

e) Increased lung uptake

f) Number of vascular territories with abnormal thallium uptake

g) Left ventricular dilatation during exercise.

Tc-99m radiopharmaceuticals : The development of technetium-99m labelled agents is a significant advance in myocardial perfusion imaging. There is a general consensus that new perfusion agents like Tc-99m MIBI compares well with Tl-201, for the detection of CAD. The other two new agents are teboroxime and tetrofosmin. Teboroxime has a very high extraction fraction (more than 90%). The experience with Tc-99m tetrofosmin SPET is still limited (chapter 5). The technetium compounds have the advantage that left ventricular function can be evaluated simultaneously by either first pass

ejection fraction or ECG gated SPET and assessment of regional wall motion abnormalities as well. Tc-99m compounds allow better image quality, as they are more suitable for SPET imaging.

1.7. Multidetector SPET Technology

The realization that any improvement in resolution would have led to a loss in sensitivity led to the development of SPET systems with more than one detector, surrounding the patient's body/head. The improvements that can be achieved are dependent on the configuration of the detectors. The current SPET objective is to achieve the best possible resolution, whilst improving the sensitivity of the instrumentation.

By the late 1970s, many manufacturers had developed commercial SPET systems, generally by adding detector rotation to the existing gantries (Jaszcak, 1982). However a fundamental design flaw existed in early SPET systems i.e., the image resolution suffered due to mechanical arm flex at each angle. This resulted in the development of angle dependent, centre of rotation correction. Throughout the 1980s, refinement to SPET systems, including COR correction and removal of the magnetic field effect through PMT μ-metal shielding, significantly improved the SPET image quality. The overall improvement in single detector SPET systems naturally pointed to the development of multi detector SPET systems as a way to increase the sensitivity and hence resolution and clinical efficacy.

In the early 1980s, commercial dual-detector systems were developed by Siemens (ROTA camera), Picker (Dyna Scan), and Toshiba. The system designs were poor and it was virtually impossible to create a high resolution SPET image from the acquired projection data. As more systems underwent clinical trials, a general misconception developed that multi detector SPET systems did not work. Since the manufacturers did not try to improve the design, this generation of multi detector system gradually vanished.

The evolution started, in 1988 when Trionix launched their first three detector SPET system (Triad, *Trionix research Laboratory Inc. USA*). This sooner compelled other manufacturers to develop a new generation of multidetector

SPET systems. The first of these was Picker, who launched their three detector SPET system, shortly followed by Toshiba GCA-9300A, in 1989. At the same time other manufacturers also started looking into possibility of dual-detector systems. Meanwhile, the physicians perceived the number one factor in choice of equipment to be "design appropriate for applications". This encouraged development of organ dedicated SPET systems for brain and heart. Today multi-detector SPET systems are available as 2 , 3 and 4 detector systems (table 1.8). The common geometric configurations are a) two detectors at 90 degrees b) two opposed detectors c) three detectors d) four detectors (figure 1.9). Some manufacturers have also launched two detectors with variable geometric configuration as well (table 1.8).

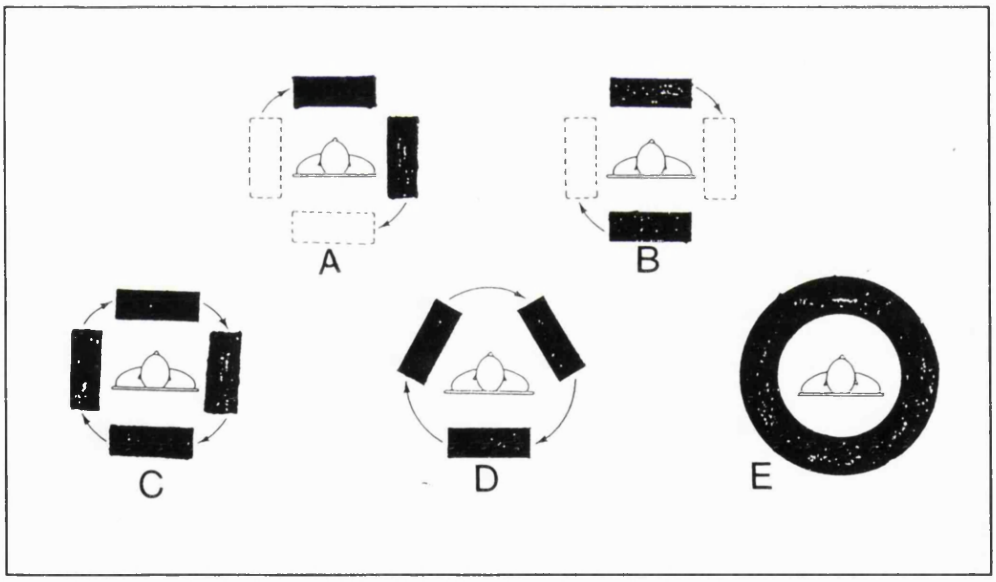

Figure 1.9: Different possible configurations of multi-detector SPET systems:
A) two detectors at 90 degrees B) two opposed detectors C) four detectors D) three detectors E) ring geometry

Manufacturer	Model	No. of detectors	Organ
ADAC	VERTEX	2 opposed	Brain / body
	GENESYS	2 detectors (variable geometry)	Brain / body
	CERESPECT	Annular crystal	Brain
ELSCINT	APEX HELIX	2 opposed	Brain / body
	CARDIAL	2 detectors at 90°	Heart
IGE	MAXUS	2 opposed	Brain / body
	NEUROCAM	3 detectors	Brain
	OPTIMA	2 detectors at 90°	Heart
HITACHI	SPECT 2000	4 detectors	Brain
MEDIMATIC	TOMOMATIC	4x16 detectors	Brain
PICKER	PRISM	3 detectors	Brain / body
SHIMADZU	SET-031	3 rings	Brain
SIEMENS	MULTISPECT 2	2 opposed	Brain / body
	MUTISPECT 3	3 detectors	Brain / body
SME	810	12 detectors	Brain
SOPHA	DST	2 detectors (variable geometry)	Brain / body
TOSHIBA	GCA-9300A	3 detectors	Brain / body
		2 opposed	Brain / body
TRIONIX	TRIAD	3 detectors	Brain / body
	BIAD	2 detectors	Brain / body

Table 1.8 : List of the some of the commercially available multi-detector SPET systems

SME 810

This SPET system was developed in the late 1970s (Jarritt PH et al., 1979). The gantry assembly contains 12 scanning detectors on radial slide rails arranged in a clockwise fashion at 30° intervals. Each detector consists of a highly focused collimator (focal length 15 cm), a 20 x 13 x 2.5 cm NaI(Tl)

crystal, light guide, photomultiplier tube, amplifier and pulse height analyzer. These detectors scan simultaneously. Each detector scans half the region imaged to provide six pairs of data. The system, by concentrating on a single plane, offers considerable gains in sensitivity. The instrument is capable of imaging energies upto 300 keV. Full 3-D reconstruction programs have been developed which allows for high resolution images with decreased cross-talk from the adjacent slices due to the improved axial resolution.

TOMOMATIC

The instrument was developed by Medimatic (Stokely et al., 1980). It uses four banks of 16 crystals arranged in a rectangular array. The sensitivity is optimized, through collimator choice, to permit measurement of cerebral blood flow using dynamic measurements of xenon-133 washout. This level of sensitivity is achieved by a loss of significant resolution.

IGE NEUROCAM

The Neurocam is a brain dedicated three-detector SPET system. The three detectors form almost an equilateral triangular aperture, within which the patient's head is positioned. The details about the system are discussed in chapter 3.

IGE OPTIMA

The camera is primarily designed for 180° cardiac SPET studies. Its variable radius of rotation means that the system could also be used for brain and small organ SPET studies. (chapter 5).

TOSHIBA GCA-9300A

This is a three-detector system for both brain and body SPET imaging. The radius of rotation is variable. (chapter 4)

HITACHI SPECT 2000

The four-detector Osaka/Hitachi SPECT 2000 is a brain dedicated system (Kimura et al., 1990). It utilises four compact gamma cameras rigidly fixed in a square arrangement. The data acquisition is possible both in "step and shoot" and "continuous" modes. The distance between the collimator surfaces of opposed detectors is 260 mm, hence 130 mm radius of rotation (compared to 123 mm for the Neurocam.

CERESPECT

This annular single crystal brain dedicated system (Cerespect) consists of a stationary annular NaI(Tl) crystal and a rotating collimator system (Genna et al., 1988, Smith et al., 1989). The internal diameter of the crystal is 310 mm and it has a thickness of 8 mm. It is viewed by 63 PMTs arranged in three rings. The concentric collimator comprises of three parallel hole collimators viewing the head from three angles simultaneously. Using Tc-99m, the tomographic spatial resolution for the high resolution collimators is 7.5 mm at the centre in air. The tomographic volume sensitivity is 27.0 kcps/(MBq/ml)/cm. The system is shielded up to 275 keV. The system is capable of static and dynamic SPET.

TRIONIX TRIAD

The Trionix Triad SPET system comprises three rectangular detectors arranged in a triangular fashion (Lim et al.,1986). The detectors can be moved radially between 125 mm and 280 mm, allowing both high resolution brain and body imaging. A 9.5 mm thick NaI(Tl) crystal is used with adequate shielding, permitting imaging over the range 50-400 keV. A full 360° acquisition is possible in 5 seconds. The system is provided with high resolution fan beam collimators as well. An automatic patient contouring feature has recently been introduced on the system.

TRIONIX BIAD

The system has same similar detectors as the Triad system, except that they are arranged opposite to each other, permitting not only SPET acquisitions but also simultaneous anterior and posterior whole body imaging.

PICKER PRISM

Like the Toshiba GCA-9300A and Trionix Triad, the Prism SPET system comprises of three detectors, with a 9 mm thick NaI(Tl) crystal. The useful field of view for each detector is 400 mm x 240 mm. These detectors are in an open ring configuration, rather than a tunnel gantry. A range of parallel hole collimation is available for imaging up to 400 keV. Fan beam collimators are also available.

SIEMENS MULTISPECT 3

This system has three large field of view of detectors, allowing acquisitions up to 400 keV. It has a minimum sampling time of 15 seconds for 360° rotation. The system also uses a series of infra-red beams to aid the set-up of patient body contouring. This feature may be helpful for implementation of attenuation correction procedures in the future.

ELSCINT CARDIA-L

This is another recent addition to the multidetector SPET systems. Two detectors are configured in a "L" geometry at 90° to each other (similar to the IGE Optima). The field of view is 400 mm x 250 mm. Its design enables swivelling of the detectors to a vertical position. This unique feature facilitates transition from tomographic myocardial perfusion to upright bi-plane functional imaging procedures. The gantry may also swivel about vertical axis, enabling swift interpositional change between the bicycle ergometer and the SPET position. It allows acquisitions up to 240 keV.

ELSCINT HELIX

This is a two-detector SPET system. It has unique feature of a "slip ring" allowing dynamic SPET. The camera is also supplied with ultra-flared fan beam collimators for brain SPET studies.

ADAC VERTEX / SOPHA DST

Both of these systems from two different manufacturers comprise of two-detectors SPET systems. The detectors can be positioned at 90° to each other for optimum 180o SPET acquisition or they can be positioned opposed to each other allowing 360° SPET / whole body planar acquisitions. (details of Sopha DST in chapter 6).

SECTION B

Assessment of Multidetector SPET Systems

Chapter 2

Materials and Methods

2.1. Hardware

The following multidetector single photon emission tomography systems have been investigated:

1. **IGE Neurocam**: a three detector brain dedicated SPET system.(Chapter 3)
2. **Toshiba GCA-9300A**: a three detector whole body/brain SPET system. (Chapter 4)
3. **IGE Optima**: a two detector cardiac dedicated SPET system, with fixed detector geometry. (Chapter 5)
4. **Sopha DST**: a two detector cardiac and whole body SPET system, with variable detector geometry. (Chapter 6)

2.2. Physical Assessment of the Systems

The two main parameters assessed were tomographic volume sensitivity and spatial resolution.

2.2.1 Tomographic Volume Sensitivity

Tomographic volume sensitivity is variously defined in the literature. Any measurement is dependent upon the object imaged, its radius and length relative to the detector field of view, the energy window used and the energy resolution of the system. The measurement further requires the method for the determination of data acquisition time to be closely defined.

Data Acquisition : A cylinder (200 mm dia. x 300 mm) was filled with an accurately measured amount of Tc-99m, (300 MBq.) uniformly mixed in water. The cylinder was placed in the centre of field of view, parallel to the axis of rotation. Tomographic acquisitions were performed in step and shoot mode for 64 projection over 360° degrees. A matrix size of 64x64 was used. Data were

acquired using different types of collimators depending upon each individual system. A 20% energy window at 140 keV with 3% offset was used.

Data Processing/Analysis : The exact time of start and finishing of each acquisition was noted. Using the total counts acquired within the length of the field of view (FOV), the actual time of the data acquisition (i.e., excluding the time of rotation) and the activity used (decay corrected), the tomographic volume sensitivity was expressed as kcps/(MBq/ml)/cm.

2.2.2. TOMOGRAPHIC SPATIAL RESOLUTION

SPET systems have a characteristic resolution volume, determined by in-plane and axial resolution. This volume is approximately cylindrical, of height 2 x Full Width at Half Maximum (FWHM) (axial) and diameter 2xFWHM (in plane). Reconstructed images of these objects will reflect both the size and radioactive concentration f the object. However, for objects smaller than this the signal is blurred so as to occupy the entire resolution volume. This is known as the partial volume effect. The total counts in the object will still be conserved, even though the activity per pixel is decreased. It is a resolution rather than a sensitivity problem. This problem is particularly marked in the brain where the grey and white matter are convoluted at a scale less than the resolving power of the system. This makes accurate determination of radioactivity in each tissue type independently impossible. Therefore, average values are always taken into account.

Data Acquisition : Measurements of the reconstructed spatial resolution were made using Tc-99m capillary line sources in air using different collimator sets and a wide variety of acquisition conditions, wherever permitted. Three line sources were placed in an acrylic jug such that they were horizontal and radially spaced at 0, 40 and 80 mm from the centre of the FOV. The data were normally acquired in step and shoot mode but in two systems data were also acquired in continuous mode. A matrix size of 128x128 was used, with 20% energy window and 3% offset. The minimum radius of rotation was used for each system. The data were acquired separately for each detector and for all detectors simultaneously.

Data Processing/Analysis : All reconstructions were performed using no prefilter, ramp backprojection filter and no attentuation correction. For IGE SPET systems, the calculations were done using IGE software, whilst for Toshiba-GCA 9300A and Sopha DST, after horizontal and vertical profiles were analysed, a personal computer was used for the other calculations. The spatial resolution was expressed as the Full Width at Half Maximum (FWHM) and Full width at Tenth Maximum (FWTM) of the line spread function.

2.2.3. HOFFMAN PHANTOM STUDIES

Data Spectrum's three dimensional Hoffman phantom provides the first truly three-dimensional simulation of the radioisotope distribution for the blood flow found in the normal brain (Hoffman et al., 1990). The phantom allows quantitative and qualitative analysis of radioactivity, as they would appear with Tc-99m HMPAO single photon emission tomography.

The phantom is constructed from Lucite, a substance similar to perspex. It is basically composed of 19 stacked slices and a chamber which is filled with radionuclide solution. Some portions of the brain slices have been designed to fill in more relative radioactivity than others (grey and white matters). Each slice of the phantom is made of 5 thinner sub-slices; 2 slices of 0.76 mm interleaved with 3 slices of 1.52 mm forming the composite thickness of 6.1 mm. Each slice is differentiated into grey matter, white matter and ventricles. The boundaries for these regions were derived from a set of 19 T1 weighed spin echo MRI scans taken over a normal brain at 7 mm intervals.

The phantom simulates the 4:1 blood flow ratio in the grey and white matter respectively. The ventricles are void of any radioactivity (figure 2.1).

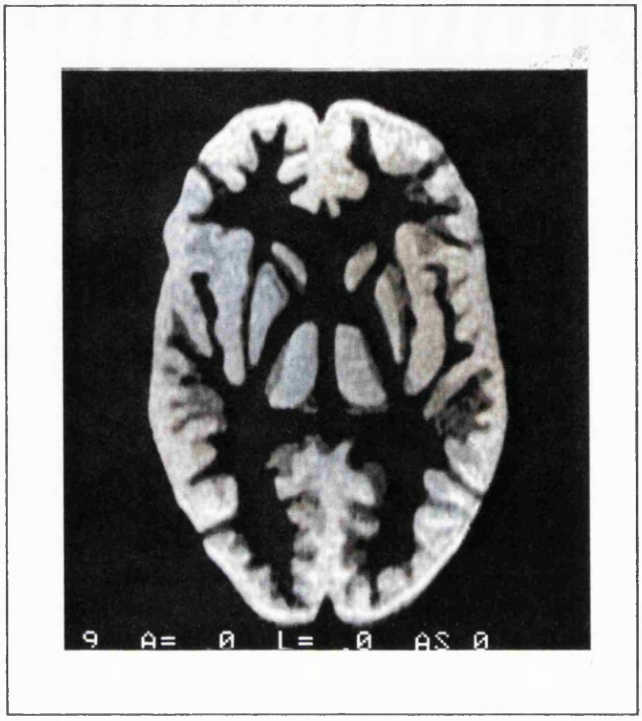

Figure 2.1. : Transverse slice of the Hoffman brain phantom, with magnetic resonance imaging (MRI) at the level of thalami. The structures markedly resemble the human brain.

Data Acquisition **:** The phantom was placed in the appropriate cylinder and filled with uniformly mixed Tc-99m (approximately 400 MBq.) as pertechnetate, in distilled water to which a small quantity of a detergent (*Decon*) was added. The filling was done extremely carefully to ensure that no significant air bubbles remained trapped. The addition of detergent reduces the surface tension between the liquid and phantom helping to fill the smaller convolutions.

The acquisitions were performed using high resolution collimators. A matrix size of 128x128 was used. A 20% energy window with 3% offset was used. The data were acquired for approximately 4 million counts, which is near to a clinical situation for a brain SPET using Tc-99m HMPAO. The data reconstruction and filters used are mentioned in the relevant chapters. Attenuation correction was used whenever possible.

Data Processing/Analysis **:** Regions of interest (ROIs) of 4x4 pixel were used to obtain grey to white matter ratio in the transverse slices. Several samples were obtained from the basal ganglia, the thalamus, visual cortex, cerebellum,

frontal-parietal, temporal cortex and white matter separately for each hemisphere (Figure 2.2). The average counts obtained from the grey matter were then divided by the average counts recorded from the white matter.

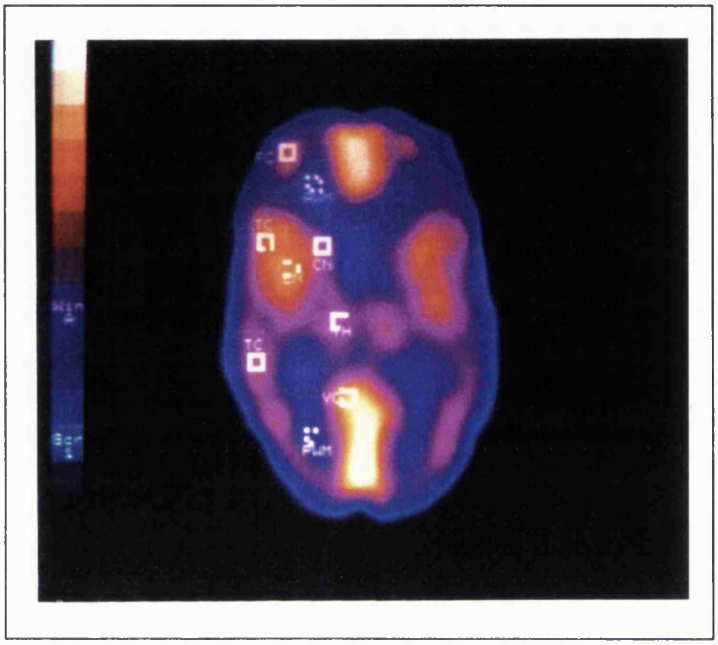

Figure 2.2. : Transverse slice of Hoffman phantom, demonstrating different regions of interest (ROI) used for semiquantitative analysis. (FC=fontal cortex, TC= temporal cortex, VC= visual cortex, AWM=anterior white matter, PWM=posterior white matter, CN=caudate nucleus, LN= lentiform nucleus, TH=thalamus)

2.2.4. CARDIAC PHANTOM STUDIES

A specially designed heart-lung phantom was used to investigate change in the geometrical shape and image contrast in 180° and 360° single photon emission tomography. The phantom consists of a two chambered ventricle. The inner chamber is used to model the left ventricular cavity and the space between the inner and outer chambers models the "ventricular wall/myocardium". The phantom also has a thoracic spine made of Teflon. The various parts of the phantom i.e., ventricular wall lungs and spine are contained in a perspex cylinder. The non uniform attenuations present in the phantom closely match those in the real clinical situation. An activity of 32 MBq of Tc-99m was uniformly distributed in the ventricle wall (myocardium). The remaining space of the phantom was filled with water and a uniform distribution of 8 MBq of Tc-99m as background (table 2.1).

Chamber	Volume ml +/- 2ml	Activity MBq. +/- 0.5 MBq	Concentration MBq /ml
LV Cavity	117	0.0	0.00
Ventricle wall	61	32.0	0.53
Body	6692	8.0	$1.20E^{-3}$

Table 2.1: Details of volumes and activities used in chambers of cardiac phantom

Data Acquisition : Acquisitions were made on IGE dual-detector gamma camera (Optima) and Sopha dual-detector SPET system (DST) with high resolution parallel hole collimators. On the IGE Optima, data were acquired both in "step and shoot" and "continuous" mode, whilst on the Sopha-DST acquisitions were made only in "step and shoot" mode. The data were acquired for 180° and 360° on both systems.

Data Processing/Analysis : The data were prefiltered using a Hanning filter with a cut-off frequency of 0.8 cycles/cm. A ramp filter was used during back-projection. No attenuation or scatter correction was applied. The reconstructed transaxial slices were then reorientated into vertical long axis (VLA), horizontal long axis (HLA) and short axis (SA). Using midventricular VLA, HLA and SA, regions of interest (ROI) of 4x4 pixel were placed over the anterior wall, lateral wall, inferior wall, septum, apex and left ventricular cavity.

The image contrast was calculated using standard formula:

$$I = (C1 - C2)/(C1 + C2)$$

where C1 is total number of counts in first ROI, C2 is the total number of counts in the second ROI. The image contrast between the apex and left ventricle cavity (LVC), the lateral, anterior and inferior walls and LVC, and septum and LVC was calculated.

2.3. Clinical Experience

The systems were used under a wide variety of clinical and research protocols. The main aim of the clinical studies were to determine whether high resolution images could be obtained, using shorter acquisition times. Wherever permitted the studies were compared utilising different acquisition times and modes. Since each system was assessed according to its design and capabilities, it was not possible to use the same predefined protocols for clinical studies e., IGE Neurocam is a brain dedicated system, therefore only brain SPET studies could be carried out, whilst IGE Optima is a cardiac dedicated system for not only SPET studies, but also with capability to perform planar (gated) radionuclide ventriculographic studies. The details concerning the clinical studies are discussed in the relevant sections of each chapter for each camera.

Chapter 3

IGE Neurocam- a brain dedicated three-detector SPET system

3.1. Description

The IGE Neurocam was the first three-detector Anger type, brain-dedicated SPET system installed at the Institute of Nuclear Medicine, The Middlesex Hospital, London. The camera consists of three detectors with a field of view of 200 mm x 176 mm. The small field of view of the detectors in an almost equilateral triangle form, gives aperture being as close as possible to an adult head. The radius of rotation is 12.25 cm. Each detector has 27 photomultiplier tubes attached to the back of 6.5 mm thick NaI(Tl) scintillation crystal. The patient couch is attached to the gantry. The height of the head-rest is fixed, which allows easy and reproducible positioning of the patient for repeated studies.

The system is provided with a set of low energy general purpose and another set of low energy high resolution collimators. The collimators are adequate for gamma rays of energy up to 170 keV. Data acquisition is controlled by an IBM compatible personal computer (PC). Data are energy-corrected on an event by event basis as they are acquired; uniformity corrections are applied at the end of data acquisition. The acquired data are then transferred from PC to an IGE Star-3000 computer (S3000), for reconstruction and display of the images. The centre of rotation (COR) corrections are applied on the S3000 computer at the time of tomographic reconstruction.

3.2. Tomographic Assessment

The detailed physical assessment of the system has been reported by Kouris K et al., (1992).

3.2.1. AIMS

The aims of this study were:

a.) to perform a tomographic assessment of the system for comparison with other systems.

b.) to define the optimum acquisition parameters for clinical studies

3.2.2. METHODS

Tomographic Volume Sensitivity : The tomographic volume sensitivity was measured using a 20-cm diameter cylinder as described in chapter 2. Data were acquired using both general purpose and high resolution collimators. Data were also acquired on a single detector gamma camera (IGE 400XCT), for comparison.

Tomographic Spatial Resolution : Measurements of reconstructed tomographic spatial resolution were made using Tc-99m capillary line sources using both general purpose and high resolution collimators as described in chapter 2. Measurements were made for each detector and for the summed configuration of the three detectors.

Hoffman Brain Phantom studies : a.) Data acquisition on IGE Neurocam: The tomographic acquisitions were made using the Hoffman brain phantom (chapter 2). The acquisitions were made for each detector separately and also a single data acquisition for all three together. The acquisitions were made using 64 x 64 W matrix and 128 x 128 W matrix. The number of projections was 128 for all acquisitions. Repeated acquisitions were made five times, a few weeks apart. Approximately 4 million counts (MCnts.) were acquired for each acquisition. The data were prefiltered using a Hanning filter, with a cutoff frequency of 1.0 cycles/cm. A ramp filter was applied during backprojection. 1 pixel (4 mm) thick slices were generated for the data acquired by 64 x 64 W matrix size. Slice thickness was 2 pixel (4 mm) for 128 x 128 W matrix data acquisition. Attenuation correction was applied. The edge of the slice was determined by using 10% threshold and the attenuation coefficient was 0.12 cm^{-1}. Regions of interest of 16 x 16 mm size were used to obtain regional cerebrum/cerebellum activity ratios (Chapter 2, Figure 2.2). At least four regions were placed for each area of the brain, for each acquisition. The

average counts obtained from the grey matter were then divided by the average counts recorded from white matter.

b.) Data Acquisition on SME 810: Three different acquisitions were also made on SME 810. It has high sensitivity and resolution in the transverse plane but poorer resolution between the slices. After positioning the phantom, single slices of different levels, from cerebellum to upper parietal region were obtained sequentially by moving the phantom through the gantry in steps of 10 mm. Ten slices of 300 seconds duration were obtained using an energy window of 115-170 keV and 128 x 128 matrix size. The acquired data were then processed on a personal computer, Macintosh IIx. Transverse, sagittal and oblique planes were derived using dedicated software (Strichman Medical Equipment Inc., version 2.66). A linear attenuation correction was applied. Regional cerebrum/cerebellum ratios were obtained for different areas of brain.

Statistical Analysis: The mean radioactivity ratio for each region was calculated as a mean+/-sd The mean ratios between the two systems (IGE Neurocam and SME 810) were compared using students' *t test.*

3.2.3. RESULTS

Tomographic Volume Sensitivity **:** The results of tomographic volume sensitivity are tabulated in table 3.1.

Collimator	**IGE Neurocam** (kcps/(MBq/ml)/cm)	**IGE 400XCT** (kcps/(MBq/ml)/cm)
Low energy, general purpose	47.4	11.1
Low energy, high resolution	28.1	6.6

Table 3.1: Comparison of tomographic volume sensitivity between two systems and different collimators, using 20% window with 3% offset at 140keV.

Tomographic Spatial Resolution: The tomographic spatial resolution was expressed as FWHM (full width at half maximum) and FWTM (full width at tenth maximum). The results are tabulated in table 3.2.

Detector	Radial Distance 0 mm.		Radial Distance. 40 mm.		Radial Distance 80 mm.	
	FWHM	FWTM	FWHM	FWTM	FWHM	FWTM
Det. 1	8.8	15.8	8.4	15.8	8.1	15.5
Det. 2	8.3	15.6	8.2	15.7	8.3	15.8
Det. 3	8.8	15.7	8.2	15.8	8.0	15.6
All	9.0	16.5	8.4	16.2	8.0	16.0

Table 3.2: Tomographic spatial resolution expressed as FWHM and FWTM for all the detectors using high resolution collimators. (Data were acquired at 140keV, using 20% window and 3% offset)

Hoffman Brain Phantom: Figure 3.1 displays the excellent image quality achieved with Neurocam. Using the square regions of interests of 16 x 16 mm size the average grey/white matter ratios were similar for all the three detectors. (Table 3.3. and 3.4.)

Brain regions	IGE Neurocam (mean±sd)	SME 810 (mean±sd)
Visual cortex	0.94 ± 0.010	0.93 ± 0.013
Right visual cortex	0.96 ± 0.015	0.83 ± 0.029
Left visual cortex	0.95 ± 0.011	0.81 ± 0.021
Brain stem	0.86 ± 0.050	0.88 ± 0.027
Right frontal cortex	0.78 ± 0.017	0.96 ± 0.012
Left frontal cortex	0.74 ± 0.010	0.87 ± 0.059
Right parietal cortex	0.69 ± 0.015	0.84 ± 0.027
Left parietal cortex	0.77 ± 0.017	0.75 ± 0.034
Right temporal cortex (lateral)	0.83 ± 0.036	0.91 ± 0.062
Right temporal cortex (medial)	0.71 ± 0.020	0.66 ± 0.015
Left temporal cortex (medial)	0.70 ± 0.019	0.68 ± 0.013
Left temporal cortex (lateral)	0.79 ± 0.051	0.84 ± 0.029
Right thalamus	0.82 ± 0.019	0.84 ± 0.041
Left thalamus	0.82 ± 0.028	0.83 ± 0.017
Right caudate nucleus	0.87 ± 0.032	0.80 ± 0.021
Left caudate nucleus	0.76 ± 0.017	0.75 ± 0.100
Right putamen	0.94 ± 0.032	0.94 ± 0.041
Left putamen	0.91 ± 0.029	0.88 ± 0.018
Right white matter	0.48 ± 0.019	0.41 ± 0.036
Left white matter	0.47 ± 0.031	0.39 ± 0.032

Table 3.3: Comparison of the ratios of radioactivity in Hoffman phantom, corrected for cerebellum. No significant difference between the two systems is observed.

Detector		Grey/White matter ratio
Detector 1	(64 x 64 W matrix)	2.09 ± 0.027
Detector 2	(64 x 64 W matrix)	2.07 ± 0.081
Detector 3	(64 x 64 W matrix)	2.17 ± 0.019
All three together	(64 x 64 W matrix)	2.03 ± 0.031
All three together	(128 x 128 W matrix)	2.14 ± 0.016

Table 3.4: Grey/white matter ratios calculated for each detector data separately and for the combined data as well. The number of projections was 128 for all the acquisitions.

3.2.4. DISCUSSION

The results of tomographic volume sensitivity show that Neurocam has more than 3 times the sensitivity of the single detector gamma camera, from the same manufacturer, i.e. IGE 400XCT (table 3.1). The increased tomographic volume sensitivity is a benefit of a multidetector system. This enhances the signal/noise ratio and therefore results in better image quality.

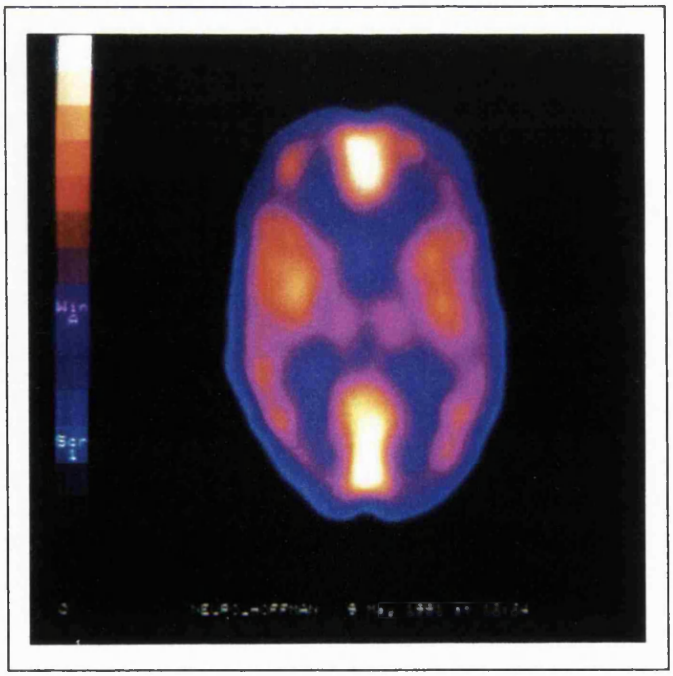

Figure 3.1: Hoffman brain phantom (Transaxial slice at the level of thalami)

Another way to increase signal/noise ratio is to improve spatial resolution. The tomographic resolution of Neurocam for reconstructed line sources in air is 9.0

mm at FWHM (table 3.2). These results are similar to those reported by Kouris et al., (1992). However, the results of each detector individually were slightly better than the combined data. This could be partly due to the fact that although the centre of rotation value is different for each detector, the software on the S3000 only allows one centre of rotation offset value per set of projections. This means that a single value has to be used for the three different detectors. Normally the offset correction value used is mean of the two extreme values for the three detectors. Although, a slight discrepancy amongst the three detectors may not cause significant degradation in image quality, it would be advantageous to have reconstruction software that could cope with a different COR offset value for planar images acquired with different detectors. Another solution is to apply COR correction during acquisition, before data are transferred to the S3000 for reconstruction.

The repeated acquisitions gave similar ratios for the distribution of the radioactivity in the different regions of the Hoffman phantom. The mean ratio ($\pm$ sd) for different regions is displayed in table 3.3. In comparison to SME 810, a multidetector system with 12 sodium iodide detectors (5x8x1 inch) gave similar ratios ($p<0.005$). The grey/white matter ratio was 2.14 ± 0.016 for Neurocam and 2.47 ± 0.027 for SME. On SME 810, each detector performs a rectilinear scan and each projection is formed by the combination of the data from opposed detectors, giving a slice thickness of approximately 17 mm. This leads to better resolution in axial plane, whilst poorer resolution between the slices. Other factors which may affect the resolution are the method of reconstruction, filter application and attenuation correction applied. All these parameters are different between two systems. Even within the same system use of different attenuation correction would have resulted in different ratios (figure 3.2).

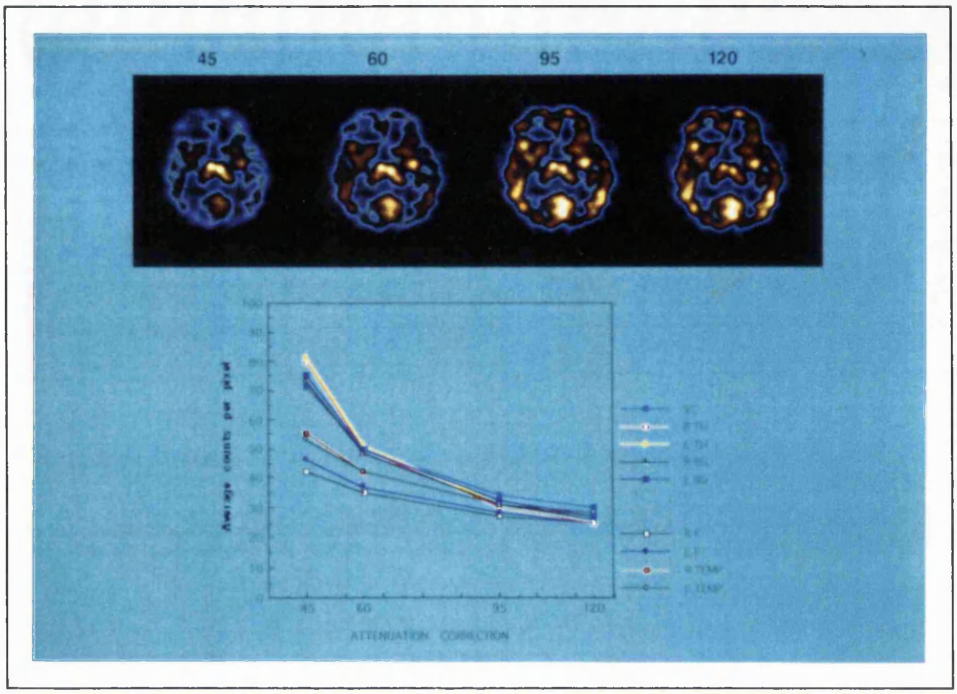

Figure 3.2: Effect of applying different attenuation coefficient to quantitative ratios. (Transaxial slices at the level of thalami are displayed). The wider difference between different regions become narrower by applying increased attenuation correction factor.

The IGE Neurocam provides good spatial resolution for brain single photon emission tomography, with reasonable acquisition time. It was felt that the optimum resolution could be achieved by using 128 x 128 W matrix size and 128 projections (table 3.4). This would require more data to be handled by the computer.

3.2.5. CONCLUSION

The IGE Neurocam is the first brain dedicated Anger type multidetector system offering a profound improvement in resolution, when compared to old multidetector systems (e.g. SME 810) and single detector rotating gamma camera systems. With developments in attenuation and scatter correction such a system may be of great help in obtaining absolute quantification for brain studies.

3.3. Clinical Experience

Although the Institute of Nuclear Medicine has a limited referral for brain SPET studies in the routine clinical setting, most of the studies are being carried out under various research projects. We have been performing approximately 300 Tc-99m HMPAO studies every year. (chapter 7). The main clinical scenario in which the studies are performed are listed below:

1. Multi infarct dementia 2. Alzheimer type dementia 3. Epilepsy
4. Wilson's disease 5. Infantile autism 6. Myalgic Encephalomyelitis
7. Parkinson's disease 8. HIV related Encephalitis
9. Stroke 10. Psychiatric disorders such as schizophrenia, depression
11. Pre and post carotid endarterectomy

I-123 IBZM receptor studies have also been performed as well. The typical data acquisition and processing protocol for Tc-99m HMPAO SPET studies is shown in table 3.5.

Parameter	IGE Neurocam	IGE 400XCT
Collimator	LE HR	LE HR
No. of views	128	64
Matrix size	64	128
Pixel size (mm)	4.0	3.2
Energy window, offset	20%, 3%	20%, 3%
Time per view (seconds)	20	30-40
Total time (minutes)	14	35-45
Counts per view (KCnts)	35	50
Total counts (KCnts)	4,480	3,200

Table 3. 5. : Comparison of acquisition and processing protocol for a multidetector and single detector gamma camera for brain SPET studies. (LE HR= low energy high resolution).

Besides the patients studies, a pool of Tc-99m HMPAO SPET studies from eleven normal volunteers, aged 20-38 years (mean 24.4 years) were quantitatively analysed. This formed a normal data base for quantitative

comparison. The distribution of Tc-99m HMPAO in these volunteers was seen to be symmetrical in both hemispheres with the relative ratios normalised to visual cortex, being greatest in the cerebellum (1.025 $\pm$ 0.034), lentiform nuclei (0.97$\pm$0.102),caudate nuclei (0.80 $\pm$ 0.082) and thalami (0.89 $\pm$ 0.096). The areas corresponding to white matter had lowest HMPAO uptake (0.54 $\pm$ 0.058)(Ourania D, 1993)(Figure 3.2). Patient studies are routinely reported quantitatively in comparison with this data.

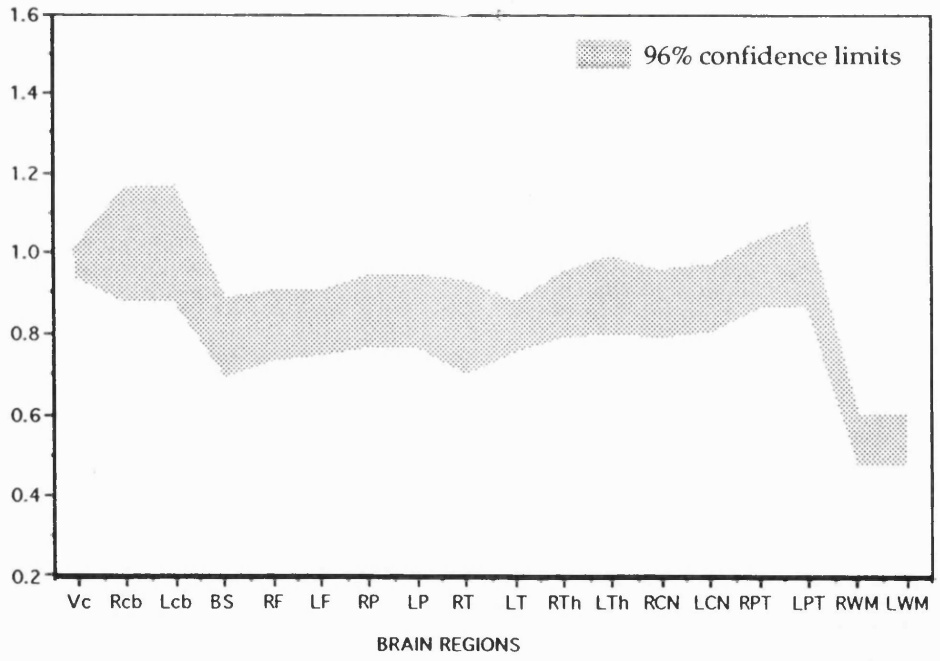

Figure 3.2: Graph demonstrating Tc-99m HMPAO distribution in normal volunteers. The radioactivity ratios are normalised to visual cortex. Rcer (right cerebellum), Lcer (left cerebellum), BS (brain stem), RF (right frontal cortex), LF (left frontal cortex), RT (right temporal cortex), RTh (right thalamus), LTh (left thalamus), RCN (right caudate nucleus), LCN (left caudate nucleus), RPT (right putamen), LPT (left putamen), RWM (right white matter), LWM (left white matter).

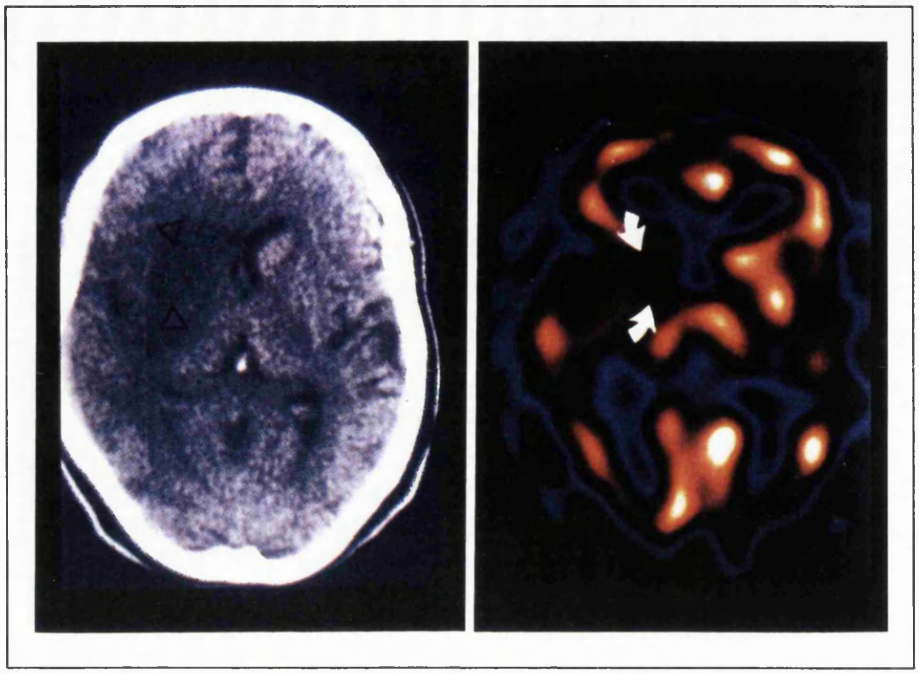

Figure 3.4: X-ray CT scan and Tc-99m HMPAO SPET images in a patient with cerebral infarction of the right internal capsule involving the ispilateral thalamus and head of the caudate nucleus and particularly the complex putamen / globus pallidus.

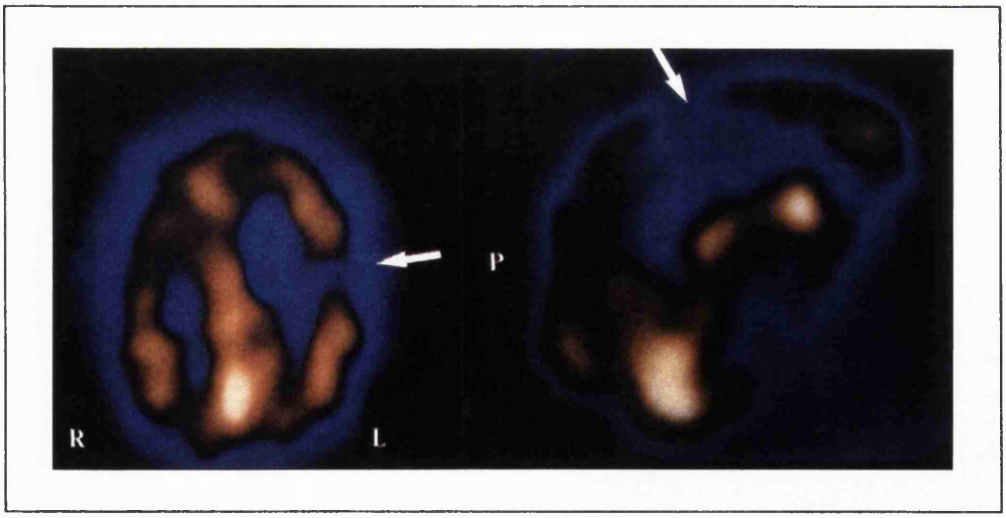

Figure 3.5: Tc-99m HMPAO SPET study displaying transaxial and sagittal slices, in a patient with left parietal infarction (arrows).

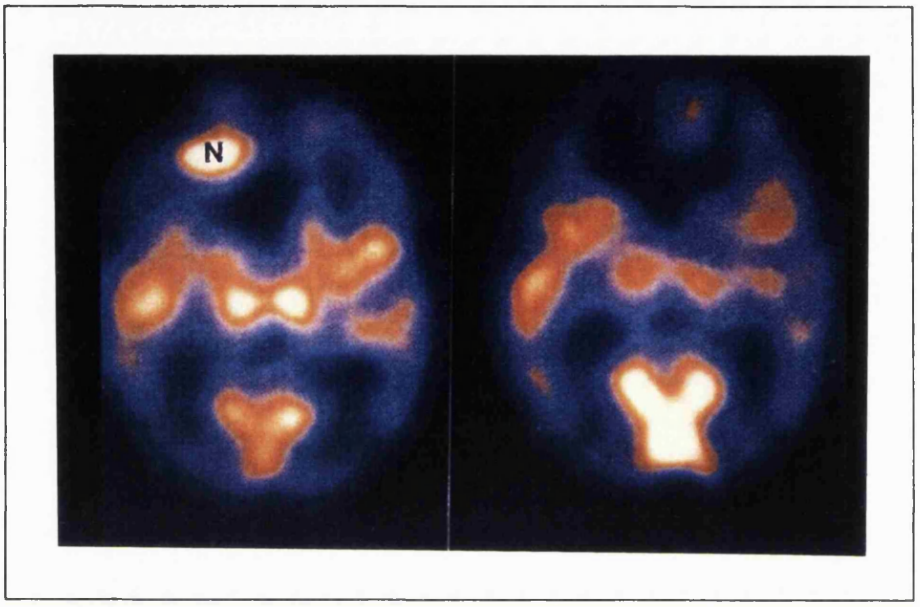

Figure 3.6: Increased concentration of Tc-99m HMPAO in a neuroblastoma (N) of right retro-orbital area, extending into the frontal cortex, before (left) and three months after radiotherapy (right).

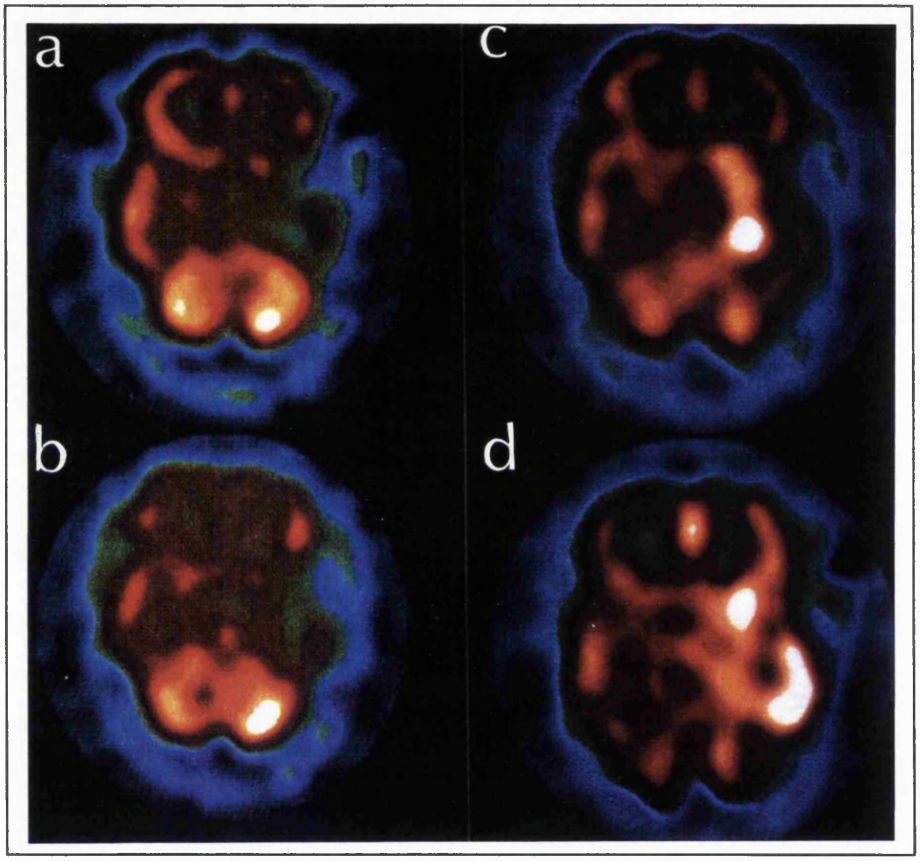

Figure 3.7: A Tc-99m HMPAO SPET study in a patient with epilepsy. Interictal study (**a**) demonstrated hypoperfusion of the left temporal region. Similar finding were seen in study performed immediately after seizure (**b**). On the contrary the study carried out during twilight states of the patient (**c**), showed a marked increase in the mesial aspect of the left temporal lobe (area corresponding to amygdala). This hyperfusion extended further into lateral parts of the left temporal lobe (**d**) in the scan carried out during complex partial seizures.

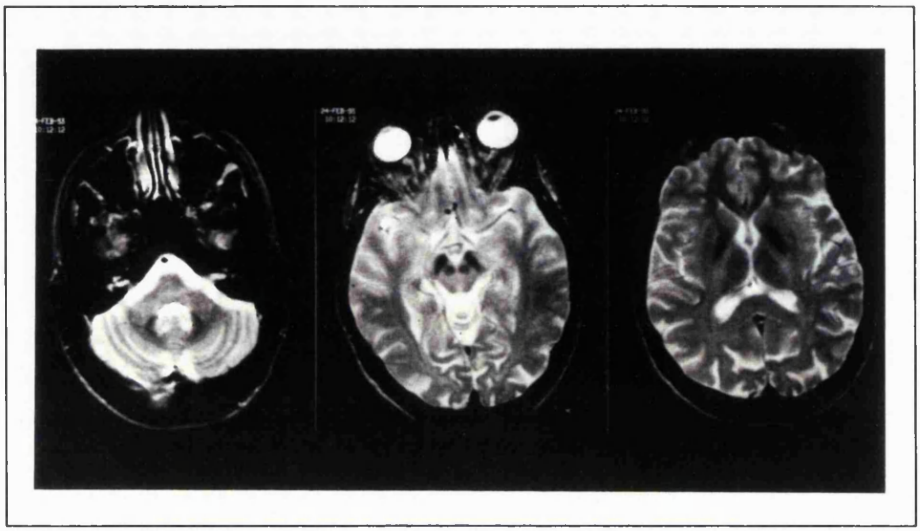

Figure 3.8 a: MRI transverse slices through the cerebellum (left), pons (middle), and basal ganglia (right). Normal study. (clinical diagnosis =Wilson's disease)

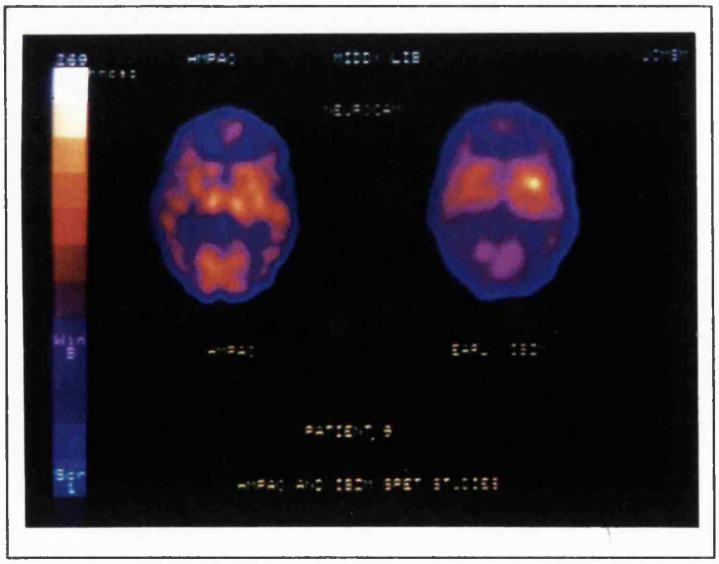

Figure 3.8.b: Study of the same patient as in figure 3.8a with diagnosis of Wilson disease. Left: Tc-99m HMPAO study showing relatively high uptake in the thalami and left putamen. Right: Early IBZM study demonstrating highest activity in the left putamen.

Figures 3.3 -3.8 demonstrate the clinical utility of brain SPET studies, under a variety of conditions. The improved sensitivity allowed a split dose protocol for neuroactivation studies (George MS et al., 1991), to be carried out. The general purpose collimators permitted an evaluation of the kinetics of new receptor ligand e.g., I-123 IBZM.

Using the IGE Neurocam, the positioning of the patient is very easy and reproducible results could be obtained (Kouris K et al., 1992). Because of the ease of operation, ease of patient and data handling and high resolution image quality, it could be easily concluded that the IGE Neurocam has been an efficient and reliable mutidetector brain SPET system.

If multidetector systems are to achieve artefact free images it is important that detector response is similar for all the detectors and that there is no misalignment between the detectors. Uniformity corrections, PMT tuning values, energy corrections and centre of rotation correction should be performed frequently. Figure 3.9 demonstrates the types of artefact possible when using such a system for brain SPET studies.

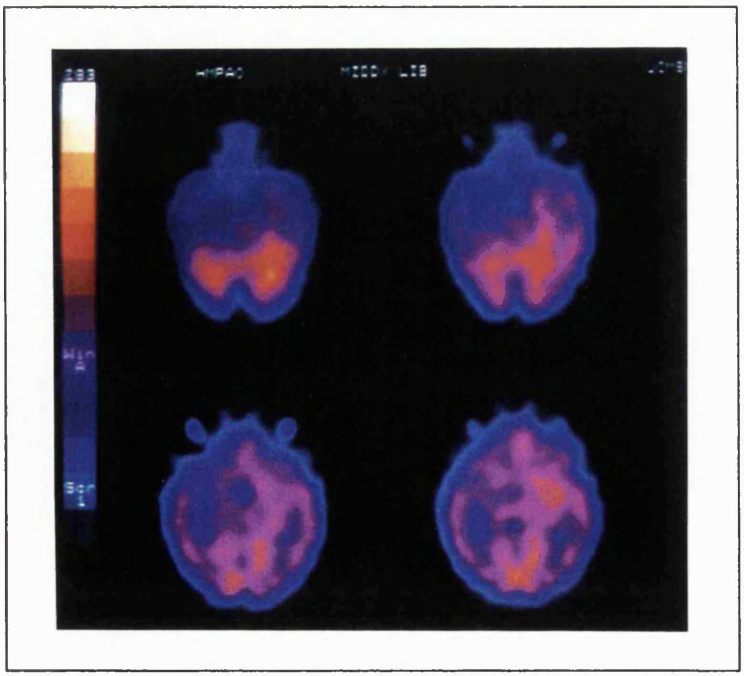

Figure 3.9: Tc-99m HMPAO SPET study : Transverse slices of a normal volunteer demonstrating marked hypoperfusion on right side. This artefact was due to variation in response in one of the detectors. The study could easily lead to a wrong diagnosis.

Conclusion

IGE Neurocam could be an ideal brain dedicated multidetector SPET system, provided its software for SPET reconstruction and method of linearity correction are modified. It results in high resolution and good image quality. The decreased acquisition time, with ease of patient positioning is helpful for clinical studies even in severely ill patients and epileptic studies. The split dose protocols have enhanced new areas of medical research.

Chapter 4

Toshiba GCA-9300A, a three-detector whole-body/brain SPET system

4.1. Description

The GCA-9300A (*Toshiba Corporation Medical Systems, Tokyo, Japan*) was the first three-detector single photon emission tomography system for both brain and body imaging (Ichihara T, 1990; Hisada K, 1991) installed at the Institute of Nuclear Medicine. It was the first such system in the United Kingdom.

The Toshiba GCA-9300A consists of three Anger-type gamma cameras forming a triangular aperture in a rotating gantry. The radius of rotation of each camera can be varied independently between 132 and 307 mm. Each camera has 45 photomultiplier tubes (PMTs) coupled to a 6.5 mm thick sodium iodide (NaI(Tl) crystal and is shielded against gamma and X-rays up to 180 keV. The collimators can be changed using custom trolleys. The collimators available at our institute were the high resolution parallel hole (HR PH) and the super high resolution fan-beam (SHR FB), both cast from lead. The field of view (FOV) is 410 mm x 210 mm (length) with the parallel hole collimators and 220 mm (diameter) x 210 mm (length) with the fanbeam collimators. The fanbeam collimators have a focal length of 397 mm and must be used with the radius of rotation set to 132 mm (the minimum possible value).

Tomographic data can be acquired either in "step and shoot" or "continuous rotation" mode. More than one rotation can be performed in the continuous rotation mode, the data from each rotation being summed for a given angle; the direction of rotation is reversed between rotations. Data are energy and linearity corrected on-line, on an event by event basis. Uniformity correction

of each projection is done prior to tomographic reconstruction. The head rest is attached to the base of the couch. The height of the head rest is fixed but the height of the couch can be adjusted for patient comfort. During a continuous rotation acquisition, the radius of rotation of each camera remains fixed but during a step acquisition the cameras can follow an elliptical path ensuring closer patient proximity.

4.2. Tomographic Assessment

The physical performance of the GCA-9300A was assessed using standard techniques described by, for example, the National Electrical Manufacturers Association (NEMA NU 1, 1986), the American Association of Physicists in Medicine (AAPM, 1987) and various publications (Kouris K et al., 1992). The full results have been reported elsewhere (Kouris K et al., 1993).

4.2.1. AIM

The aim of this study was to assess:

a.) tomographic volume sensitivity

b.) tomographic spatial resolution

c.) response to the 3-D Hoffman brain phantom

4.2.2. METHODS

Tomographic Volume Sensitivity **:** The tomographic volume sensitivity was measured using a cylinder containing an accurately measured amount of Tc-99m uniformly mixed in water (chapter 2). Tomographic acquisitions were performed using the "step and shoot" and "continuous rotation" modes, noting the exact time each acquisition started and finished, for both parallel and fanbeam collimators. Using the total counts acquired within the central 102 mm length of the FOV, the actual time of data acquisition (i.e. for 60 projections: 20 x time per step, whether step or continuous mode) and the activity used (decay corrected), the tomographic volume sensitivity was expressed as kcps/(MBq/ml)/cm.

Tomographic Spatial Resolution **:** The reconstructed tomographic spatial resolution was measured using Tc-99m capillary line sources in air (chapter 2) using both collimator sets and a 20% energy window (3% offset), under both

acquisition modes (step and shoot and continuous). All reconstructions for the estimation of the full width at half and tenth maximum (FWHM and FWTM) tomographic spatial resolution were done using no prefilter, ramp reconstruction filter and no attenuation correction.

Hoffman Brain Phantom Studies : The Hoffman 3-D brain phantom which mimics the normal anatomy of the human brain (chapter 2, figure 2.1) was used in evaluating the effects of the various acquisition parameters on reconstructed image quality and on the reconstructed average grey/white matter ratio. The phantom was carefully filled with uniformly mixed technetium-99m in distilled water (chapter 2). Scans were performed with both collimator sets at 132 mm radius of rotation. All high resolution parallel hole (HR PH) projections were 128 x 128 W matrix; all super high resolution fan beam (SHR FB) projections were acquired as 256 x 256 W matrix but converted to 128 x 128 W matrix, parallel geometry data. Acquisitions were made both in step and shoot and continuous mode. Data were reconstructed using a Butterworth prefilter (order 8, cutoff frequency of 0.6 cycles/cm). The slices thickness was 6.4 mm for high resolution parallel hole (HRPH) collimators (i.e. 2 pixel thick) and 7.0 mm (ie. 4 pixel thick) for super high resolution fan beam (SHR FB) collimators data. Regions of interests of 8.7 x 8.7 mm (corresponding to approximately 1 x FWHM spatial resolution) were used to calculate grey/white matter ratio (chapter 2).

4.2.3. RESULTS

Tomographic Volume Sensitivity: The tomographic volume sensitivity was similar for both types of collimators. The results are shown in table 4.1.

Collimator	Tomographic Volume Sensitivity [kcps/(MBq/ml)/cm]		
	step and shoot	continuous	mean
HR PH	29.4	30.5	30.0
SHR FB	30.4	31.5	30.9

Table 4.1.: Comparison of tomographic volume sensitivity for two sets of collimators, using step and shoot and continuous mode acquisitions. Energy window at 140keV with 3% offset was used. (HR PH= high resolution parallel hole, SHR FB= super high resolution fan beam).

Tomographic Spatial Resolution **:** The tomographic spatial resolution for Tc-99m line sources in air was expressed as Full Width at Half Maximum (FWHM) and Full Width at Tenth Maximum (FWTM) of the line spread function (chapter 2). The comparison of tomographic spatial resolution for both sets of collimators using step and shoot and continuous acquisitions is tabulated in table 4.2.

COLL.	ACQ.	Radial distance 0 mm		Radial distance 40 mm		Radial distance 80 mm	
		FWHM	FWTM	FWHM	FWTM	FWHM	FWTM
HRPH	Step.	10.3	18.6	10.3	18.5	11.1	19.8
	Cont.	10.8	19.0	10.6	19.0	11.3	19.8
SHRFB	Step.	7.9	13.8	8.3	14.4	8.1	14.8
	Cont.	7.9	13.8	8.3	14.4	8.4	14.9

Table 4.2 : Comparison of tomographic spatial resolution between two sets of collimators, using different acquisition modes. These measurements were obtained at minimum radius of rotation (132 mm). (ACQ.=acquisition mode, Step= step and shoot, Cont=continuous, COLL.= collimator, HRPH= high resolution parallel hole, SHRFB= super high resolution fan beam)

Detector	High Resolution Parallel Hole		Super High Resolution Fan Beam	
	FWHM	FWTM	FWHM	FWTM
Detector A	10.5	18.8	8.0	14.6
Detector B	10.4	18.8	8.1	14.7
Detector C	10.7	18.9	8.3	14.6
All	10.5	18.8	8.1	14.7

Table 4.3: Comparison of tomographic spatial resolution between three detectors at the centre of the field of view, with 132 mm radius.

Hoffman Brain SPET : The typical grey/white matter ratio for 4 million count clinical studies was 1.9, whilst in case of a 40 million count study it was increased only to 2.4.

4.2.4. DISCUSSION

The values quoted for the GCA-9300A were calculated using the time period of actual data acquisition, i.e. excluding the time during which the gantry rotates from one step to the next in the step acquisition mode, or the time prior to and after completion of the 120° rotation in the continuous rotation mode; for example, these times were 8, 13 and 22 s for 1, 2 and 5 min scanning times (relevant to dynamic SPET); consequently, the effective volume sensitivity would be reduced. The tomographic volume sensitivity was 30.0 and 30.9 kcps/(MBq/ml)/cm for the HR PH and SHR FB collimators, respectively. For comparison, the tomographic volume sensitivity of the GE/CGR Neurocam (a brain dedicated three detector system) is 28.7 kcps/(MBq/ml)/cm for the HR collimators.

With the cameras set at their minimum radii of rotation (132 mm), the tomographic spatial resolution in air, at the centre of the FOV, was 10.5 and 8.1 mm FWHM with the HR PH and SHR FB collimators respectively (18.8 and 14.7 mm FWTM). These values are in agreement with those of Ichihara et al., (1991): 10.0 and 7.5 mm, respectively. Similar values have been reported by Kouris et al., (1993) as well. For comparison, the FWHM and FWTM tomographic spatial resolution of the IGE Neurocam in air is 9.0 and 15.9 mm for the HR collimators.

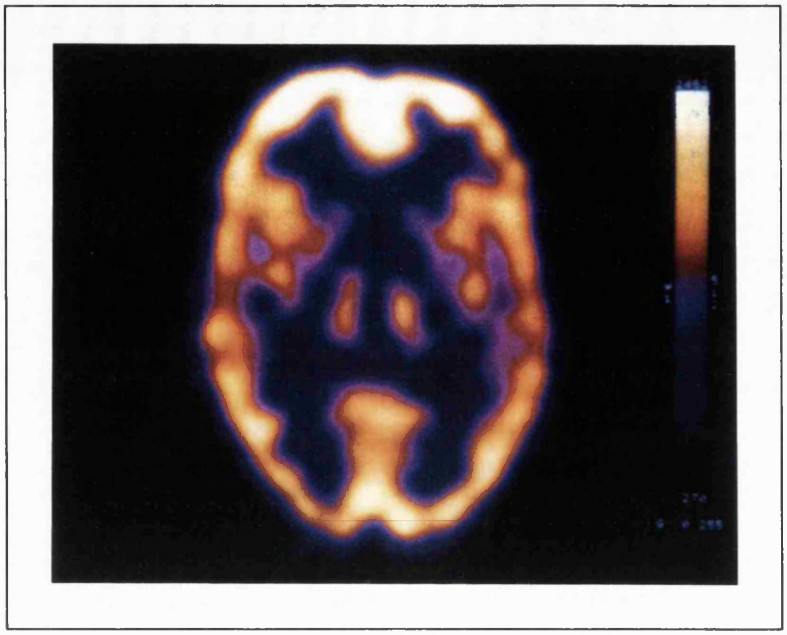

Figure 4.1 demonstrates the excellent image quality achieved by the GCA-9300A in imaging the Hoffman 3-D brain phantom using the SHR FB collimators with 132 mm radius of rotation; the total number of counts in the study was about 40 million counts (Mcnts).

The most serious limitation was a very slow computer but now a new high-speed processor has been introduced. The gantry and detectors are well designed, stable and reliable, and provide sufficiently for patient safety. The speed of rotation between steps should be increased thereby decreasing the "dead time" during scanning.

4.3. Clinical Experience

More than 250 subjects were scanned in a total of more than 600 studies. For a given volunteer or patient more than one SPET study was performed using either different acquisition parameters after a single injection or on separate occasions in order to follow the effects of therapy. Tomographic reconstruction of patient data was performed using the filtered back-projection method. The projection data were prefiltered using the Butterworth filter with power 8 and cut-off frequency depending on the total number of counts (higher for more counts). Backprojection was performed using a Shepp Logan filter. No attenuation correction was used even for brain studies as per Toshiba recommendation.

4.3.1. THALLIUM-201 MYOCARDIAL PERFUSION SPET STUDIES

Thallium -201 myocardial perfusion SPET studies were performed in 57 patients (40 male 17 female, aged 31-72 years). Only patients with documented evidence of coronary artery disease were included in this study. Coronary angiography was known in 23 patients, whilst 40 patients had a past history of myocardial infarction.

Although low energy general purpose collimators are usually used for data acquisition of thallium-201, we decided to utilise high resolution collimators. This was because the tomographic volume sensitivity of the Toshiba GCA-9300A, fitted with high resolution collimators is 30.0 kcps/(MBq/ml)/cm (table 4.1), which is equal to 10.0 kcps/(MBq/ml)/cm for each detector. This compares well with the tomographic volume sensitivity of 12.8 kcps/(MBq/ml)/cm for a typical single detector gamma camera (IGE 400XCT) (Moore et al., 1992). We utilised 360° data acquisition in order to obtain maximum count density.

Typical data acquisition and processing protocols are summarised in table 4.4

Data Acquisition:	
1. Collimator:	Low energy, High resolution
2. Matrix size:	128x128 W
3. Rotation arc:	360°
4. Acquisition mode:	Continuous
5. Acquisition time:	4 rotations of 4 minutes each
6. Corrections:	Energy and linearity on-line Uniformity: before reconstruction
Data Reconstruction:	
1. Data binning:	60 projections
2. Prefiltering:	Butterworth (order 8)
3. Back-projection:	Shepp-Logan filter
4. Slices thickness:	2 pixel
5. Display:	Vertical long axis, horizontal long axis and short axis slices
Redistribution Study: 3 hours post stress.	

Table 4.4: Typical stress/redistribution thallium-201 myocardial perfusion SPET acquisition and processing protocol for Toshiba GCA 9300A.

In a comparative study of 10 patients we compared images obtained by 8, 16 and 32 minutes of acquisition (Mahmood S et al, 1992). The data were reported by two independent observers, unaware of clinical history, time and mode of acquisition. The number of defects reported by each observer in both stress and redistribution studies showed little variation between the 8, 16 and 32 minutes acquisition (Figure 4.2). There was also some variation in the number of defects seen by each observer, with observer 2 reporting a slightly higher number of defects than observer 1. This however was not significant (X^2=2.13, p>0.95).

In conclusion, high resolution thallium-201 images can be obtained using the Toshiba GCA-9300A multi-detector SPET system, even with rather short data acquisition protocols.

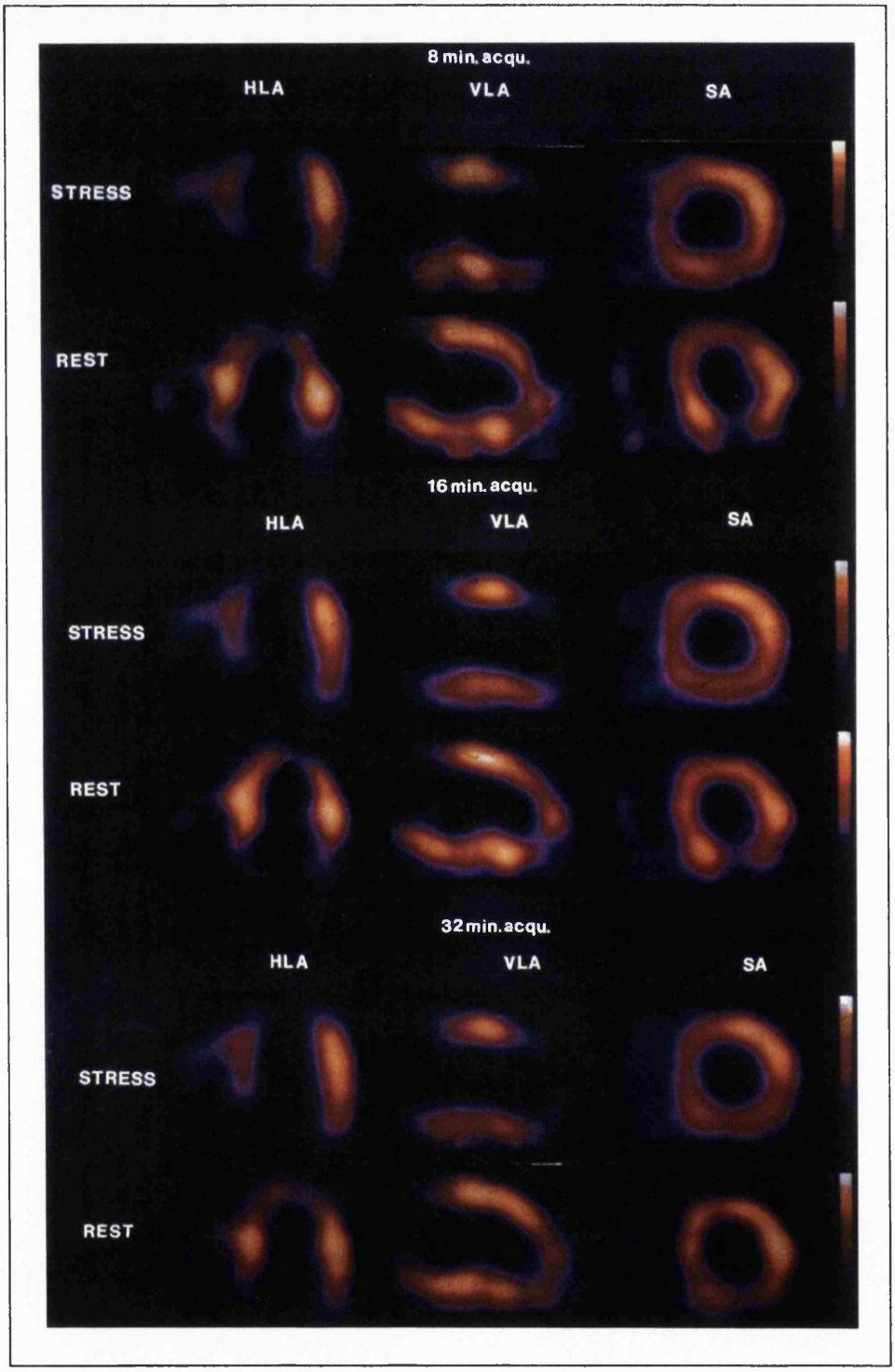

Figure 4.2: Thallium-201 myocardial perfusion SPET slices (stress and rest images). Three studies are displayed: 8, 16 and 32 minutes acquisition. All three demonstrate reversible myocardial ischaemia in the intraventricular septum, apex and apical segment of anterior wall with similar diagnostic accuracy. Stress and redistribution data were acquired for a total of 32 minutes(8 rotations of 4 minutes each). Data were than divided into 3 studies: the first 8, the first 16 and the total 32 minutes for both stress and rest. Data were binned into 60 projections for each study.

4.3.2. SKELETAL SPET STUDIES

Single photon emission tomography (SPET) has been shown to be more sensitive than planar scintigraphy in identifying bony pathology (Onsel et al, 1990, Keogan et al, 1991, Kanmaz et al, 1992). Despite this advantage, the 30 min SPET acquisition time necessary with a conventional single-detector gamma camera, remains a major deterrent to the widespread use of SPET in skeletal scintigraphy.

Using the Toshiba GCA-9300A multidetector system, 85 SPET studies were performed in 81 patients (Table 4.5). Four patients had two different sites imaged. The studies were performed only on patients in which there was a clinical indication for SPET. This was decided after inspection of the planar images. Fifty-three studies were performed for benign disease and the remaining studies were for either primary bone tumour or metastatic bony disease (Table 4.6).

Sites of SPET acquisition	Number of studies
Lumbar spine	38
Thoracic spine	18
Head/neck	7
Lower pelvis/hip	10
Knees	9
Femur	2
Feet	1

Table 4.5 : Sites of SPET imaging in 85 studies.

The typical acquisition/processing protocol recommended from our experience to be used on Toshiba GCA-9300A is tabulated in table 4.7.

Indication	Number of studies	Site imaged	
Mechanical pain	42	32	Lumbar spine
		2	Chest
		4	Pelvis
		4	Head/neck
Primary bone tumour	21	12	Chest
		4	Pelvis
		2	Knees
		2	Femora
		1	Head/neck
Metastatic bone disease	11	5	Lumbar spine
		3	Head/neck
		2	Hips/pelvis
		1	Chest
Trauma	5	5	Knees
Avascular necrosis	4	2	Knees
		1	Feet
		1	Head/neck (Femora)
Osteomyelitis	2	1	Head/neck
		1	Lumbar spine

Table 4.6 : Clinical indications for SPET studies performed on the Toshiba GCA-9300A.

Dose:	550 MBq of Tc-99m MDP
Data Acquisition:	
1. Collimator:	Low energy, High resolution
2. Matrix size:	128x128 W (3.2 mm)
3. Rotation arc:	360°
4. Acquisition mode:	Continuous
5. Acquisition time:	4 rotations of 4 minute each
6. Corrections:	Energy and linearity on-line Uniformity: before reconstruction
Data Reconstruction:	
1. Data binning:	60 projections
2. Prefiltering:	Butterworth (order: 16 for knees, and 15 for spine)
3. Back-projection:	Shepp-Logan filter
4. Slices thickness:	2 pixel
5. Display:	Transaxial, sagittal and coronal slices

Table 4.7 : Recommended acquisition and processing protocol for skeletal single photon emission tomography. MDP=methyldiphosphonate

Comparison of studies with different acquisition times of 8, 16 and 32 minutes revealed similar clinical information. The total number of "hot spots" seen in the 3 studies was the same (Buscombe JR et al., 1993), though there was some differences in the shape and intensity of the abnormalities seen. Comparing image quality, both in terms of definition of normal skeletal structure and lack of distortion, there was some improvement with the 32 min acquisition time compared to the 8 or 16 min acquisition time in the axial skeleton. This was however not significant. Outside the axial skeleton, for example in the knees or femora, where count density was lower the 16 min acquisition protocol demonstrated much better image quality than the 8 min acquisition protocol. It has been noted that activity in the bladder leads to artefacts which may affect imaging of the hip joints. In a previous series of SPET studies of the pelvis 5/25 (20%) studies were not reported due to bladder activity producing artifacts which obscured the hip joints, after tomographic reconstruction (Collier et al 1985). Two groups have described computational methods by

which this problem can be reduced (Gillen et al, 1988, Kouris et al, 1988). One of the main advantages of shorter acquisition, is for SPET of the hip joints and pelvis. In our experience, it was possible to see the hip joints clearly only with the 8 minute acquisition, while in the 16 min and 32 min acquisitions, images were obscured by reconstruction artifacts arising from bladder activity. Generally an 8 min acquisition of the lower pelvis obtained just after the patient had voided, demonstrated the normal bony structure and any pathology clearly.

Comparison with a single-detector gamma camera

Two patients were also imaged using a single detector gamma camera IGE 400ACT Starcam. It was observed that higher counts were obtained in 8 minutes with the Toshiba GCA-9300A, than 32 minutes on the single detector gamma camera (table 4.) for knees. This is because, Toshiba GCA-9300A has a higher tomographic volume sensitivity (section 4.2.) of 10.0 kcps/(MBq/ml)/cm per detector, (30.0 kcps/(MBq/ml)/cm for the complete system) compared to that of the IGE 400ACT Starcam at 7.6 kcps/(MBq/ml)/cm (Moore et al, 1992).

	IGE-400ACT Starcam (64 projections)		**Toshiba GCA-93OOA (60 projections)**					
	K Counts in 32 minutes		**K Counts in 8 minutes**		**K Counts in 16 minutes**		**K Counts in 32 minutes**	
	Total	**per proj.**	**Total**	**per proj.**	**Total**	**per proj.**	**Total**	**per proj.**
Lumbar Spine	1630	25.5	1538	25.6	3167	52.8	6240	102
Knees	862	14.4	918	15.3	1796	29.9	3446	57.5

Table 4. 8 : Comparison of total counts and mean counts per projection between a single detector gamma camera (IGE 400ACT Starcam) and three detector Toshiba GCA-9300A. The counts were calculated using a 400x210 mm region of interest. (Proj.=projection, K = x1000).

In conclusion, high resolution SPET images were obtainable using an 8 minute acquisition protocol for the axial skeleton and a 16 minute protocol for the peripheral skeleton. The shorter acquisition time allows tomographic acquisition of the hip joints and pelvis, without significant contamination from the bladder. The other advantage of shorter acquisition time is that patients can be imaged when there is a clinical indication for SPET without disrupting the routine operation of the department.

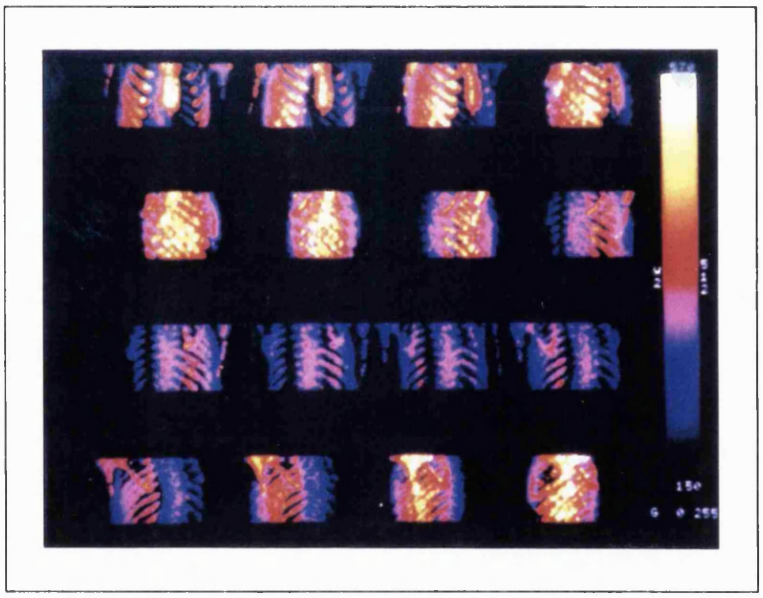

Figure 4.3 : 3-D presentation of the tomograhic images of chest. The study was performed using only 8 minute acquisition.

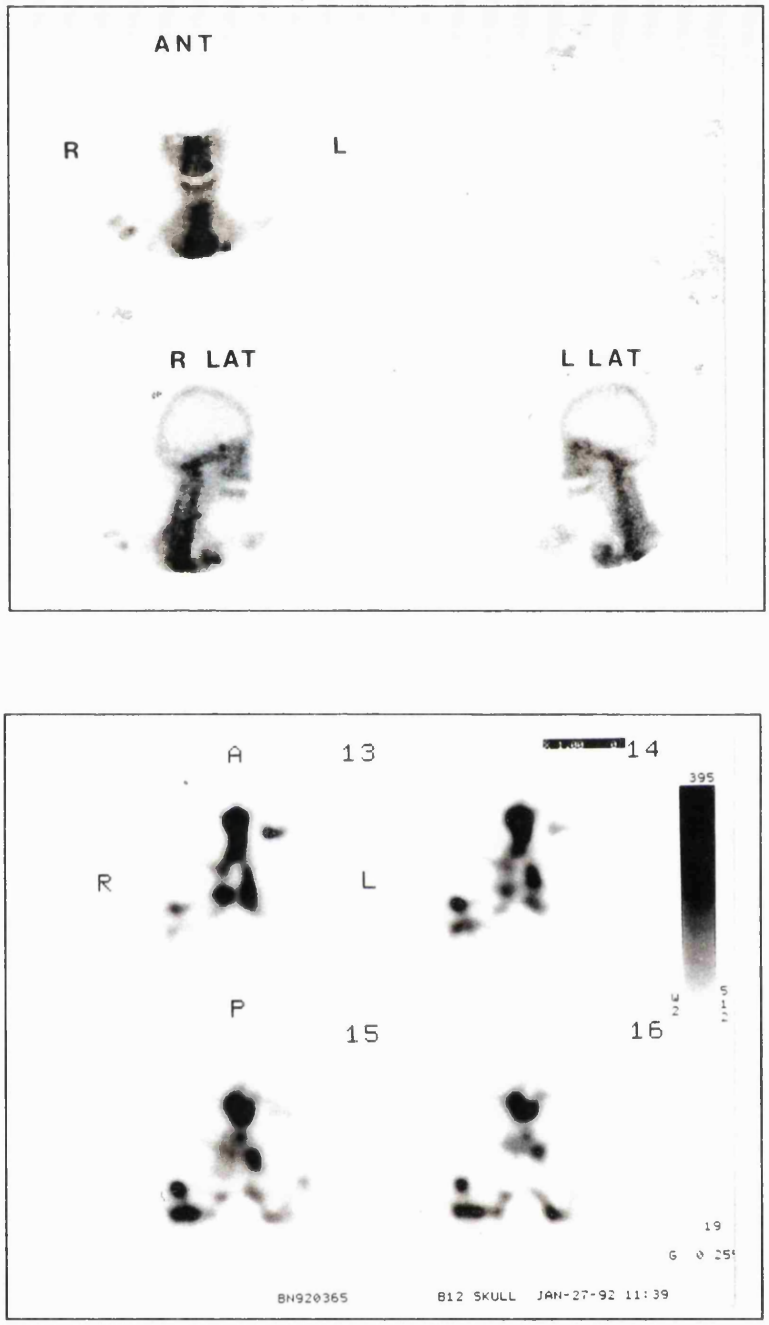

Figure 4.4: Comparison of planar and tomographic images in a patient with suspected osteomyelitis of the right middle ear. Anterior and lateral skull planar Tc-99m MDP images (top) fail to show any abnormality in the area surrounding the right ear canal. Tomographic transaxial slices (bottom) of the skull at the level of the ear canals clearly show increased uptake of tracer in the bone surrounding the right auditory meatus. A labelled white cell study confirmed the presence of infection at this site.

4.3.3. RENAL DMSA SPET STUDIES

Single photon emission tomography (SPET) of the kidneys using Tc-99m labelled dimercaptosuccinic acid (DMSA) has been proposed as a method to improve the sensitivity of static renal scintigraphy (MacDonald et al., 1977, Steyn et al., 1978). SPET allows more defects in the renal cortex to be visualised than can be seen with planar imaging and it gives a better characterisation of the size and extent of a defect (Williams et al., 1986). This may be particularly true in children where the early identification of scars may have a significant effect on subsequent management and morbidity (Saxena et al., 1975). Despite these advantages, the longer acquisition time necessary for acquisition using a single detector gamma camera is the main obstruction in its widespread implementation for clinical routine.

Using the Toshiba GCA-9300A, renal DMSA SPET studies were performed in 73 patients. The recommended acquisition and processing protocol for renal DMSA SPET studies is shown in table 4.9. Although longer acquisition times were used in some patients, it did not enhance the clinical information.

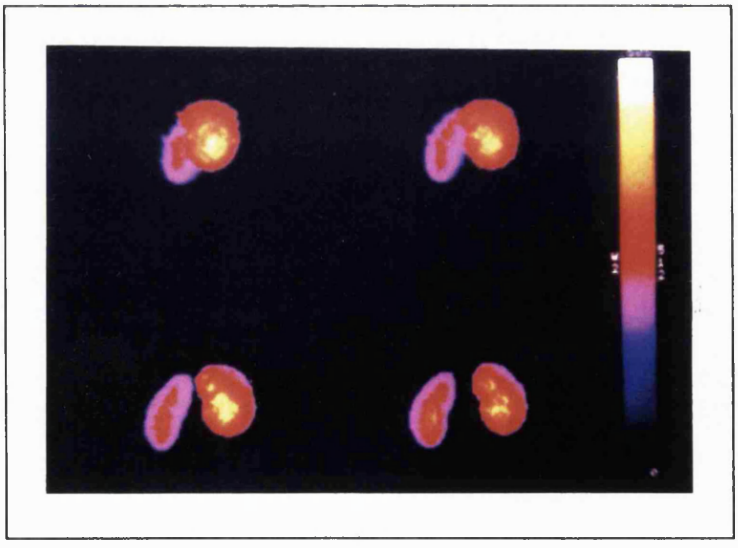

Figure 4.5: Normal 3-D renal DMSA images, using 8 minute SPET acquisition.

Dose:	74 MBq of Tc-99m DMSA
Data Acquisition:	
1. Collimator:	Low energy, High resolution
2. Matrix size:	128x128 W (3.2 mm)
3. Rotation arc:	360°
4. Acquisition mode:	step and shoot, 60 projections
5. Acquisition time:	2 rotations of 4 minute each
6. Corrections:	Energy and linearity on-line Uniformity: before reconstruction
Data Reconstruction:	
1. Prefiltering:	Butterworth, order 15, cut-off frequency 0.6 cycles/cm
2. Back-projection:	Shepp-Logan filter
3. Slices thickness:	3 pixel (6.9 mm)
4. Display:	Transaxial sagittal and coronal slices

Table 4. 9: Recommended acquisition and processing protocol for renal DMSA tomographic studies. (DMSA =dimercaptosuccinic acid)

We also compared 8, 16 and 32 min acquisitions SPET images in 10 patients, in order to determine whether it is possible to produce good quality renal SPET with a short acquisition time. A total of 11 defects seen in the planar images of all 10 patients compared with a total of 16 defects seen in the 8 min acquisition and a total of 15 defects seen in both the 16 and 32 min acquisition SPET images (not significant, X^2=0.75). All but one of the defects seen with the planar imaging were present in the SPET images.

We felt that using a multidetector system such as the Toshiba GCA-9300A, 8 minute acquisition yielded sufficient clinical information. The mean total counts obtained per 8 min acquisition was 2290 Kcounts (range 1269-2902 Kcounts).

It has been previously shown using a 30 minute acquisition on a multidetector gamma camera that the sensitivity of SPET for the detection of renal scars is 35% higher than planar imaging (Tarkington et al., 1990). Unfortunately the long acquisition time meant that when children were imaged sedation was

required. Although a more recent study on a smaller group of children failed to confirm a significant increase in sensitivity in detecting scars with SPET compared with planar imaging, the authors suggested that SPET is still recommended as the extent of scarring was more clearly defined (Mouratidis et al., 1993).

In conclusion, it is possible to obtain high resolution renal DMSA SPET images in 8 minutes using a three-detector SPET system. The ability of a multidetector SPET system to perform high resolution SPET with a short acquisition time will increase the availability and throughput of SPET to patients undergoing studies with Tc-99m DMSA and it may be of particular use in children.

Figure 4.6: (next page) Planar Tc-99m DMSA images (a) of a recent renal transplant showing reduced uptake of tracer in the lower pole. Coronal SPET slices (b) of the same transplanted kidney confirming that there is reduced uptake in the lower pole of the transplant and transaxial slices (c) show that the injury also extends throughout most of the posterior wall. This could not be seen on the planar images (a).

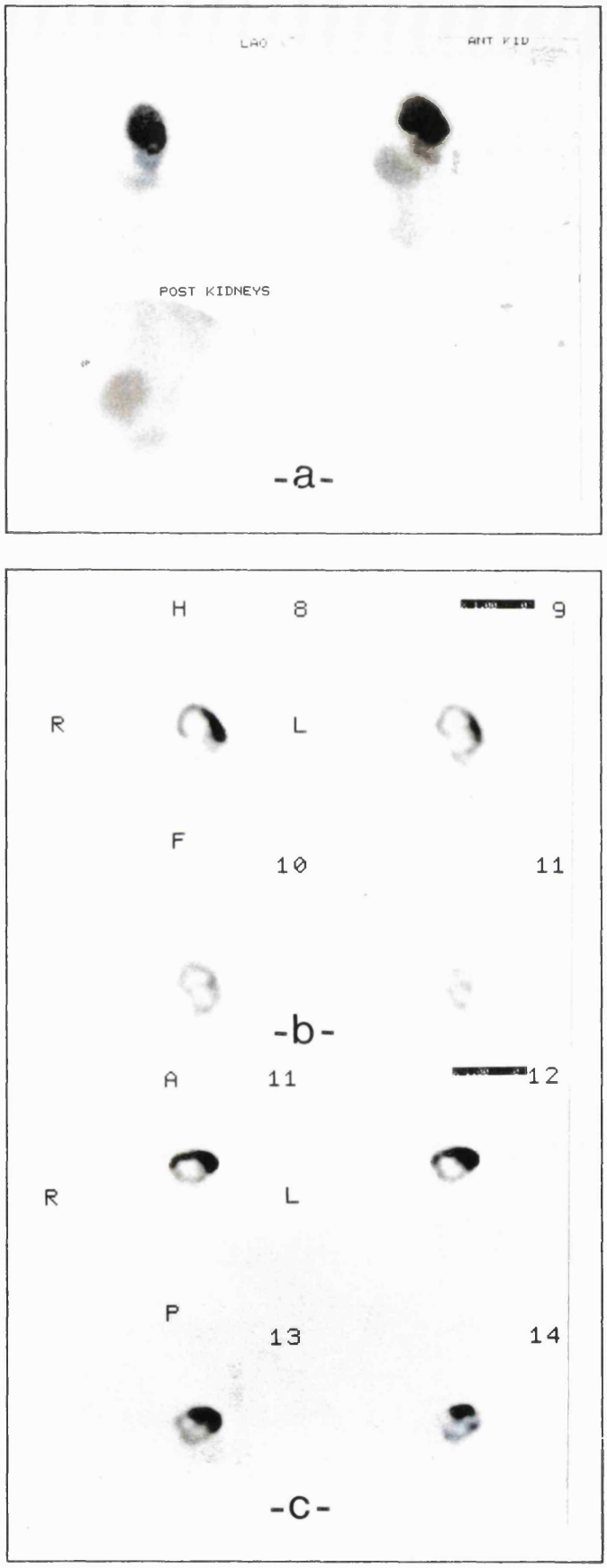

fig. 4.6.

4.3.4 BRAIN SPET STUDIES

The main indications of SPET imaging in brain have already been discussed in chapter 1 (section 1.6).

The Toshiba GCA-9300A instrument has the facility of super high resolution fan-beam collimators for brain SPET imaging. These collimators provide higher tomographic spatial resolution.

Tc-99m HMPAO SPET studies were performed in 20 patients with diagnosis of Wilson's disease (figure 4.9), transient ischaemic attacks (figure 4.8), myeloencephalitis and epilepsy. In addition, thallium-201 brain SPET studies were performed in cases of disruption of blood-brain barrier (figure 4.11). I-123 IBZM studies were performed in two volunteers, in order to demonstrate the ability of the system to perform dynamic SPET (figure 4.10)

Parameters	**IGE 400XCT**	**IGE Neurocam**	**Toshiba GCA-9300A**
Collimator	HR	HR	SHR FB
Number of views	64	128	90 --> 60
Energy window: width, offset	20, 3	20, 3	20, 0
Matrix size	128	64	256->128
Pixel size (mm)	3.2	4.0	1.735
Time per view (seconds)	30-40	20	30
Total time (minutes)	35-45	15	15
Counts per view (KCnts)	50	35	55
Total counts (MCnts)	3.2	4.5	5.1

Table 4.10 : Comparison of acquisition protocols for Tc-99m HMPAO brain perfusion SPET using IGE 400XCT (single detector system), IGE Neurocam (a brain dedicated three detector system) and Toshiba GCA-9300A (whole body/brain three detector SPET system). (HR= high resolution, SHR FB= super high resolution fan beam)

In 4 patients, we compared 8, 16 and 32 minute acquisition times. It was concluded that even an 8 minute of acquisition could give similar clinical data, as a longer acquisition (Figure 4.7).

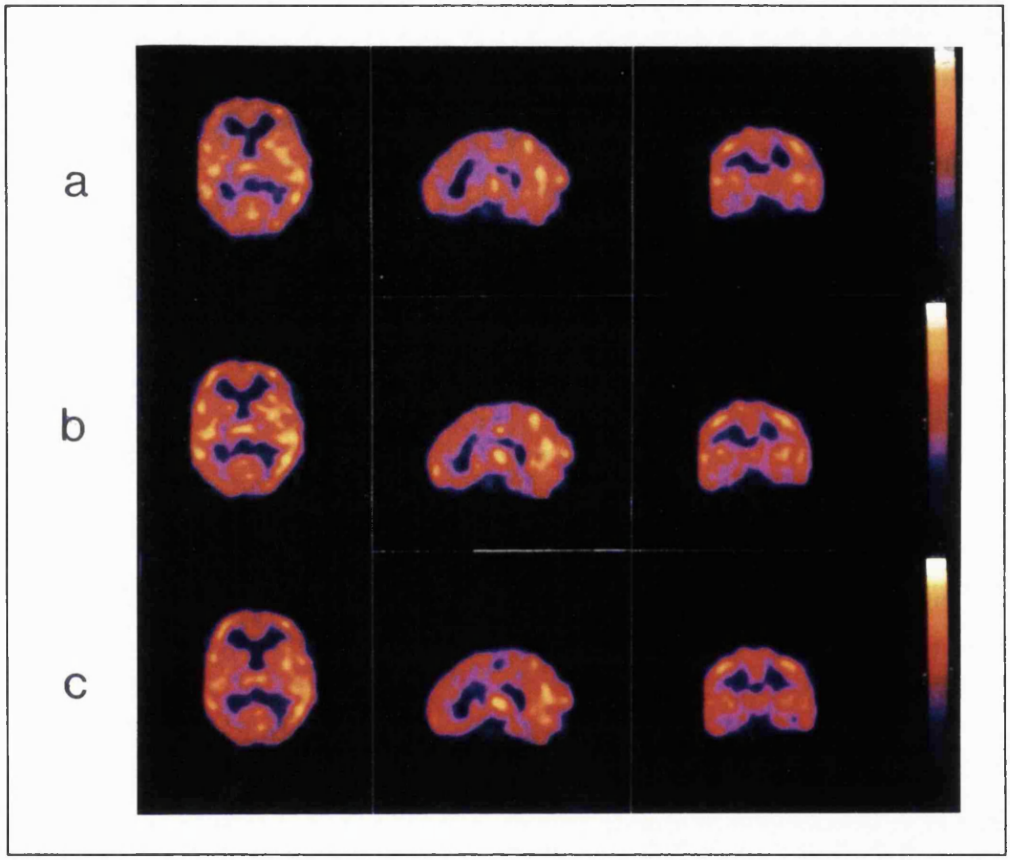

Figure 4.7: Comparison of 8 minute (a), 16 minute (b) and 32 (c) minute Tc-99m HMPAO SPET acquisitions in a normal volunteer.

Figure 4.8: **(Next Page)** Tc-99m HMPAO SPET Study: The three classical slice orientation display is shown with 16 transverse, 16 coronal and 16 sagittal slices for the 3 studies obtained after the rebinning of the data from the 32 minutes continuous acquisition. The 3 studies clearly display an area of significant reduction of perfusion to the right cerebellar hemisphere . In addition, there is a significant widening of the lateral ventricles. The patient suffered bilateral internal carotid artery stenosis and had recently (for the last 6 months) several transitory ischaemic attacks (TIA's).

FIG.4.8.

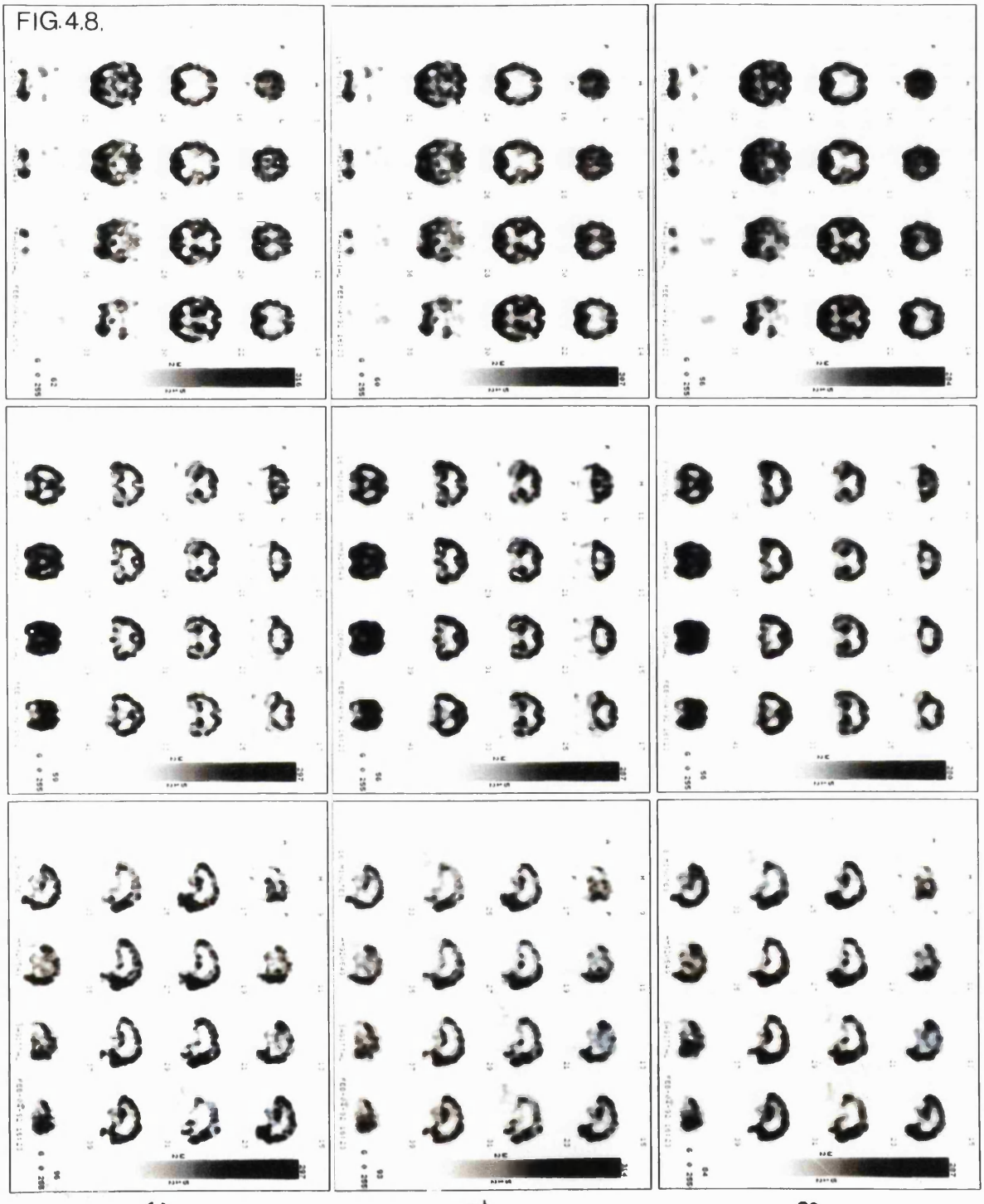

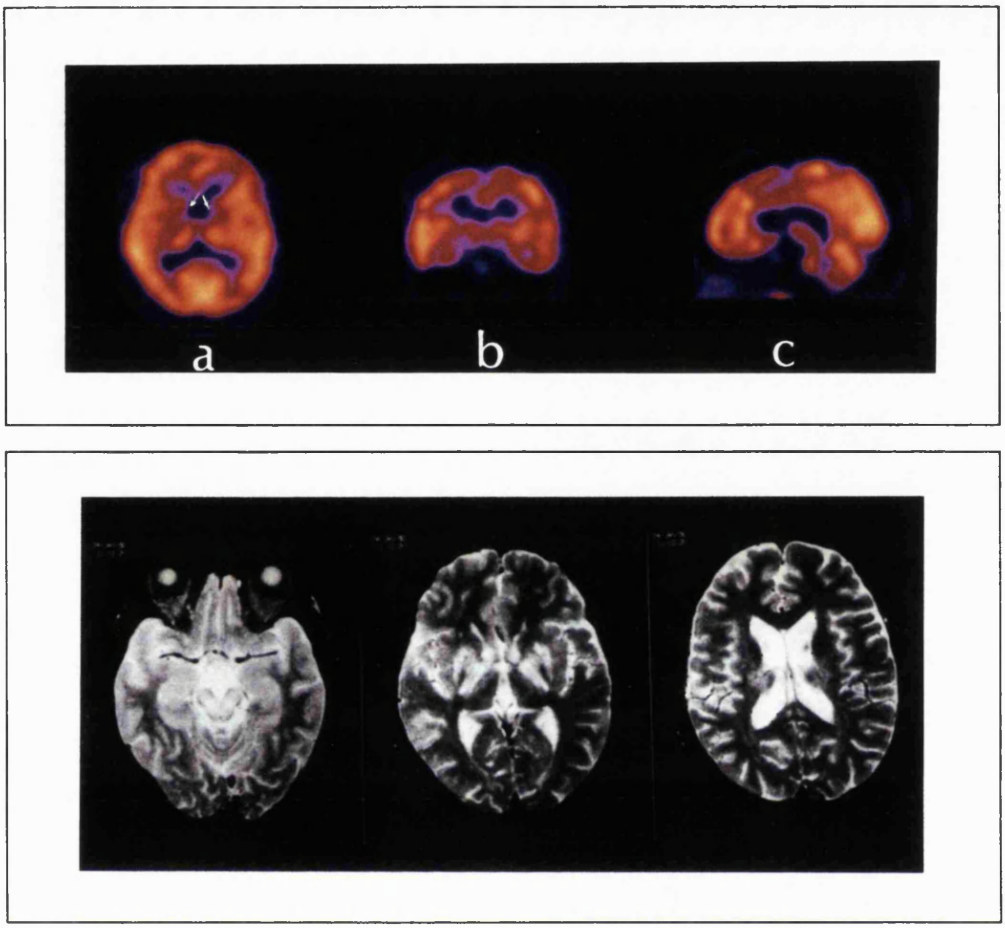

Figure 4.9 : **Upper row**: Tc-99m HMPAO SPET study: transaxial (a), coronal (b), and sagittal (c) slices through the basal ganglia demonstrating low uptake of Tc-99m HMPAO in the basal ganglia. (clinical diagnosis Wilson's Disease)

Lower Row: 3 transverse slices of MRI at the level of brain stem (left), basal ganglia (middle) and bodies of lateral ventricles (right) showing altered signals in pons and basal ganglia of the same patient.

Figure 4.10: (**Next Page**) I-123 IBZM Dynamic SPET Study: Three studies are shown. One(20 minutes p.i. for 10 minutes acquisition time) during the flow /perfusion phase; second at 60 minutes for 10 minutes total acquisition time displaying significant binding of the IBZM to the striatum on both hemispheres and finally the third (at 2 hours p.i. for 30 minutes total acquisition time) at a time when aspecific binding is markedly reduced. This study clearly demonstrates the feasibility of dynamic SPET with a three detector gamma camera. It shows adequate spatial resolution (particularly at 2 hours post injection study) to resolve the head of caudate nucleus from the putamen and globus pallidus as seen in slices 7,8 ,9 and 10 of the later study.

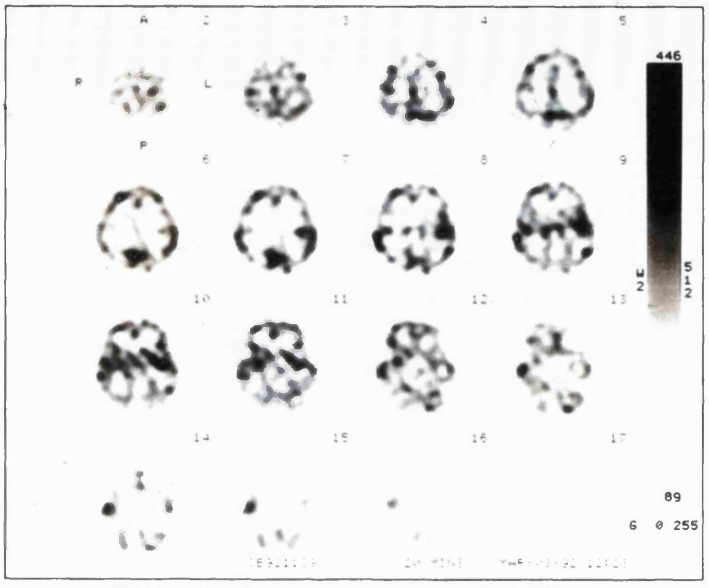

20 minutes p.i.

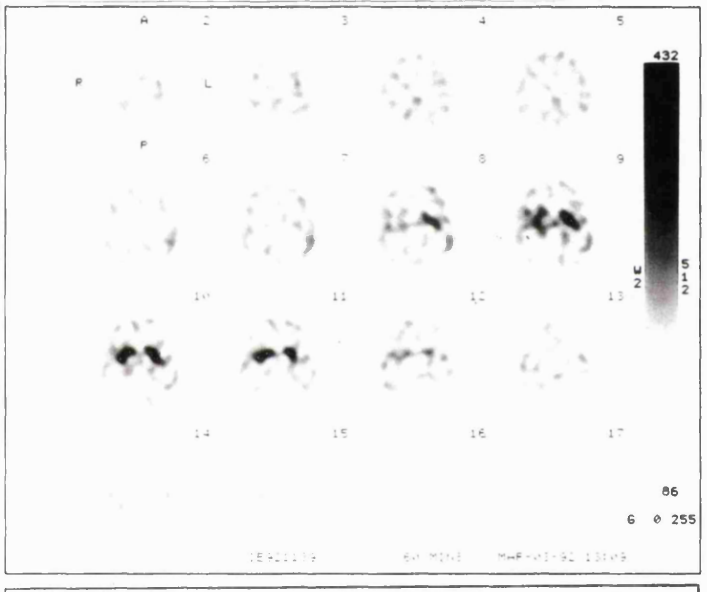

60 minutes p.i.

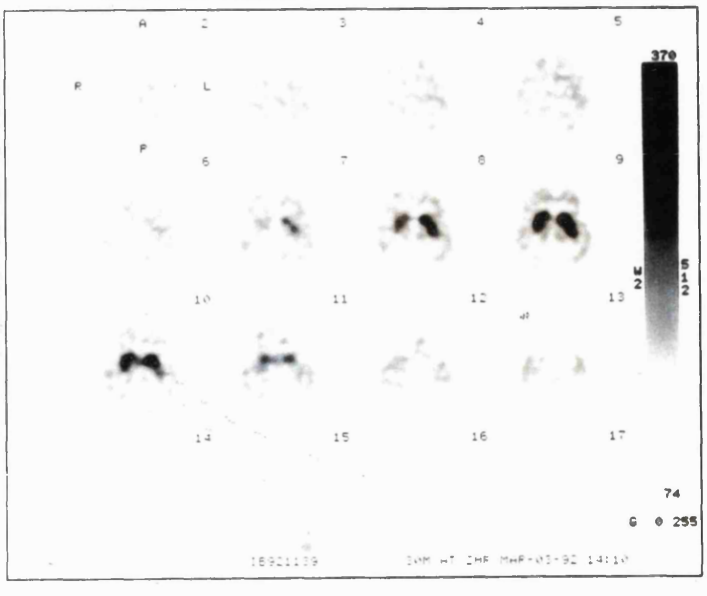

2 hours p.i.

FIGURE:4.10.

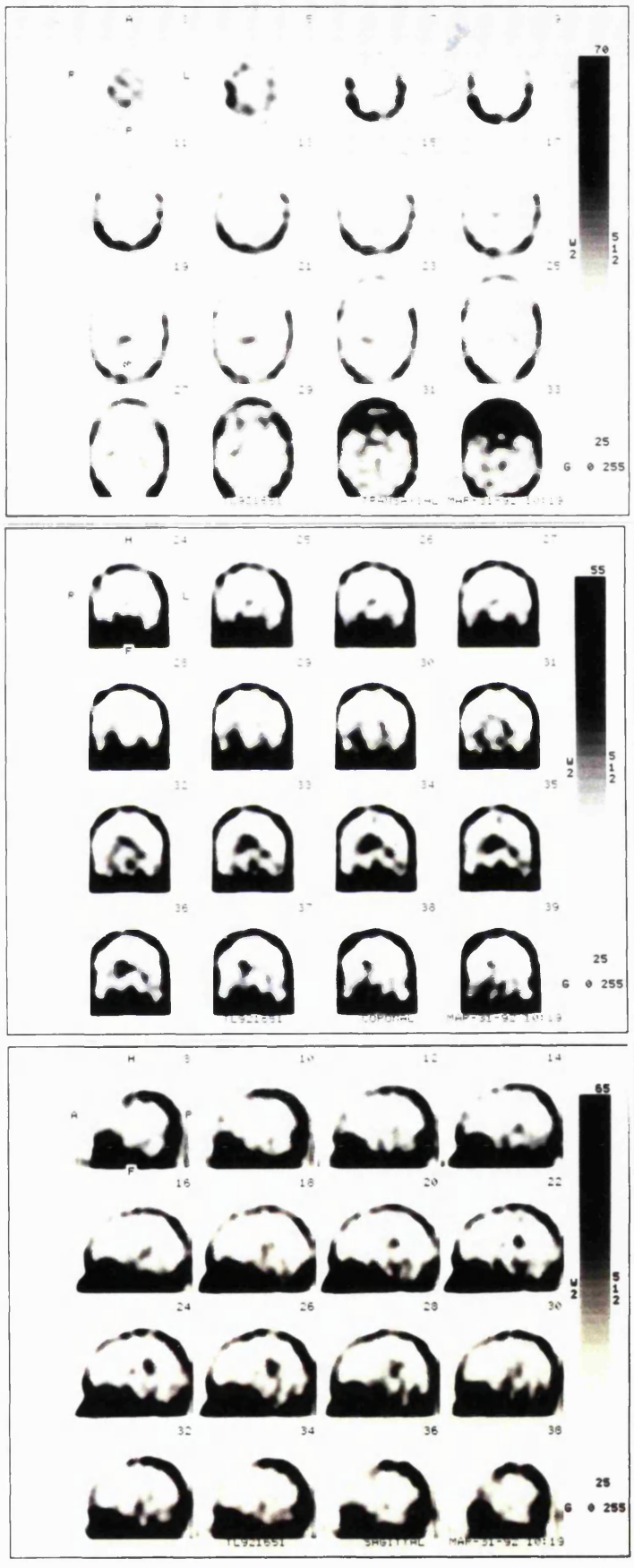

FIGURE: 4.11.

Figure 4.11: (**Page:117**) Thallium-201 blood brain barrier disruption Study. Transverse, coronal and sagittal slices are shown to demonstrate the site of disrupted blood brain barrier. There is one in the right temporal lobe, and a larger site in the para ventricular white matter on the right hemisphere.

It is obvious from the images 4.7-4.11. that high resolution images can be obtained with brain SPET.

4.3.5 CONCLUSIONS

Multidetector SPET instruments such as the Toshiba GCA-9300A, offer a substantial increase in tomographic volume sensitivity compared to a single rotating gamma camera. Depending on collimator type and collimator design parameters, improved tomographic spatial resolution is achievable. In our experience, the Toshiba GCA-9300A triple-headed SPET system achieves both objectives when the SHR FB collimators are used for brain studies and the HR PH collimators for body studies.

Although we did not report on the sensitivity, specificity and accuracy of clinical diagnosis with the GCA-9300A, we have demonstrated its clinical utility under a wide variety of clinical pathologies.

With multi detector systems such as the Toshiba GCA-9300A it is expected that the role of SPET in clinical practice and research will increase. It is important to distinguish routine applications and the solving of clinical problems from research orientated imaging protocols. In many circumstances, specific choices can now be made with different but clearly defined aims.

Chapter 5

IGE Optima
a dual-detector cardiac SPET system

5.1. Description

The IGE Optima (*International General Electric, Milwaukee, WI, USA*) is a dual-detector gamma camera for cardiac imaging. The camera consists of two detectors which are precisely aligned at 90 degrees to each other. These are rigidly housed in an integral gantry of 660 mm diameter. This design ensures the stability of the mechanical rotation of the assembly. The field of view (FOV) is 337x183 mm for each detector. The movement range in the gantry and table is flexible to ensure close proximity to the patient. The radius of rotation is variable between 141.5 and 247.55 mm. Each detector has 37 hexagonal photomultiplier tubes (PMT) coupled to a 6.5 mm thick sodium iodide NaI(Tl) crystal, with shielding for gamma photons up to 170 KeV. The collimators are light and easy to handle/change. The IGE- Optima is basically designed for low energy nuclides, such as Tc-99m and thallium-201. The camera is provided with low energy general purpose, low energy high resolution, low energy high sensitivity and one low energy slant hole collimator. The acquisition is controlled and processed by a Star 4000i computer with a 32 bit processor and 1024 image display monitor. The tomographic data can be acquired either in step and shoot mode or continuous mode. In step and shoot mode the detectors are stationary during data acquisition, whilst no data is acquired during rotation. In the continuous mode, the data are basically acquired in step and shoot mode, with the only difference that data are also acquired during the rotation time and this data is added to preceding projection. The acquired data are saved as two separate files, one for each detector. Data from the two detectors are summed at the time of back-projection. Reconstruction of each detector separately is also possible.

5.2. Tomographic Assessment

5.2.1. DATA ACQUISITION

Relative Sensitivity : It is important to know what response the detector gives from one unit of activity. The relative sensitivity was measured using a Cobalt-57 flood source. The flood source was placed on the detector required for acquisition for 30 minutes. Results of the measurements were expressed as a ratio between two detectors.

Tomographic Volume Sensitivity : A cylinder (200 mm diameter x 300 mm) was filled with an accurately measured amount of Tc-99m, uniformly mixed in water (chapter 2). Tomographic acquisitions were performed in "step and shoot" mode for 64 projection over 360 degrees. A matrix size of 64x64 was used. Data were acquired using both low energy general purpose and high resolution collimators. A 20% energy at 140 keV with 3% offset was used. Using the total counts acquired within the 138 mm length of the FOV, the actual duration of the data acquisition (i.e., excluding the time of rotation) and the activity used (decay corrected), the tomographic volume sensitivity was expressed as kcps/(MBq/ml)/cm.

Tomographic Spatial Resolution : Measurements of the reconstructed spatial resolution were made using Tc-99m capillary line sources in air (chapter 2) using both collimator sets and a wide variety of acquisition conditions. Three line sources were placed horizontally and radially spaced at 0, 40 and 80 mm from the centre of the FOV. 64 and 128 projections data were acquired both in step and shoot and continuous mode. A matrix size of 128 x 128 was used with 20% energy window and 3% offset.

All reconstructions were performed using no prefilter, ramp backprojection filter and no attenuation correction. Using IGE software, horizontal and vertical profiles were analysed and the spatial resolution was expressed as the Full width at Half Maximum (FWHM) and Full Width at Tenth Maximum (FWTM) of the line spread function.

Hoffman Brain Phantom studies **:** The Data spectrum Hoffman 3-D brain phantom (Chapter 2) was utilised for tomographic acquisition. The phantom was placed in the appropriate cylinder and filled with uniformly mixed Tc-99m

in distilled water to which a small quantity of wetting agent was added. The acquisitions were performed using low energy high resolution collimators. A matrix size of 128x128 (pixel size 3mm) was used, with 20% energy window and 3% offset. The data were acquired for 64 and 128 projections, using both step and shoot and continuous mode. The data were acquired for approximately 4 million counts, which is near to a clinical situation for a brain SPET using Tc-99m HMPAO. The data was reconstructed using a Hanning prefilter with a cut off frequency of 1.0 cycles cm^{-1}. This frequency and filter gave adequate resolution. The backprojection filter used was the ramp filter. The images were reconstructed with a slice thickness of two pixels. Attenuation correction was used. The edge of the slice was determined using a threshold of 10% and attenuation coefficient was 0.12 cm^{-1}. Regions of interest (ROI) of 12 x 12 mm were used to obtain an average grey to white matter ratio in the transverse slices (chapter 2, Figure 2.2). At least four samples were obtained from the basal ganglia, the thalamus, visual cortex, cerebellum, frontal-parietal, temporal cortex and white matter separately for each hemisphere. The average counts obtained from the grey matter were then divided by the average counts recorded from the white matter.

5.2.2. RESULTS:

Relative Sensitivity : The relative sensitivity is expressed as the ratio of the counts/second for detector 1: the counts/second for detector 2. The relative sensitivity using high resolution and general purpose collimators was determined to be:

Collimator	Relative Sensitivity
High Resolution	1 : 1.033
General Purpose	1 : 1.028

Table 5.1: Relative sensitivity of two detectors

Tomographic Volume Sensitivity : Results were determined for the high resolution and general purpose collimators and were expressed as kcounts/second/(MBq/ml)/cm.

Detector	Collimator	Volume Sensitivity kcounts/second/(MBq/ml)/cm
1	High Resolution	9.8
	General Purpose	15.1
2	High Resolution	9.4
	General Purpose	15.4

Table 5.2: Tomographic volume sensitivity for each detector.

Tomographic Spatial Resolution : All the data were reconstructed with no pre-filtering, no attenuation correction, a ramp reconstruction filter and a slice thickness of approximately 5 slices. Results were determined by calculating FWHM and FWTM of profiles through the images.

Collimator	Radial Distance 0 mm		Radial Distance 40 mm		Radial Distance 80 mm	
	FWHM	FWTM	FWHM	FWTM	FWHM	FWTM
High Resolution	10.4	19.0	10.6	18.3	10.0	16.9
General Purpose	12.3	24.8	12.5	22.1	9.2	21.1

Table 5.3 a: Tomographic resolution for Tc-99m in air (radius of rotation=141.5 mm)

Acquisition	Radial Distance 0 mm		Radial Distance 40 mm		Radial Distance 80 mm	
	FWHM	FWTM	FWHM	FWTM	FWHM	FWTM
64 proj.	13.2	23.2	13.1	23.2	12.5	22.8
128 proj.	13.1	23.1	13.0	22.6	12.7	22.9
Continuous (128)	13.0	22.9	13.3	23.0	12.8	23.0

Table 5.3 b: Comparison of tomographic resolution for Tc-99m in air, at radius of rotation of 202.5 mm for high resolution collimators.

Acquisition	Radial Distance 0 mm		Radial Distance 40 mm		Radial Distance 80 mm	
	FWHM	FWTM	FWHM	FWTM	FWHM	FWTM
64 proj.	16.1	28.3	12.7	26.6	12.5	26.7
128 proj.	15.7	26.6	15.8	26.9	16.1	27.3
Continuous (128)	15.4	27.0	16.1	28.3	16.0	27.1

Table 5.3c : Comparison of tomographic resolution for Tc-99m in air at radius of rotation of 202.5 mm for general purpose collimators.

Hoffman Brain Phantom Studies : Table 5.4 compares the distribution of radioactivity in different regions of Hoffman brain phantom.

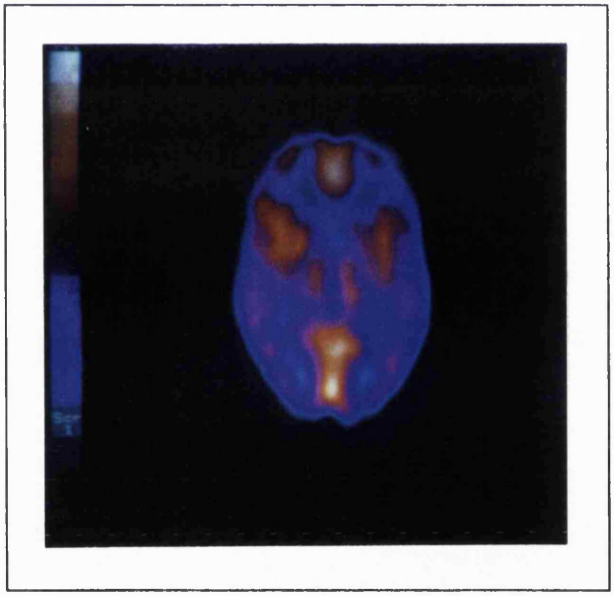

Figure 5.1: Transverse slice of the Hoffman brain phantom at the level of thalami.

Brain regions	IGE Optima (mean ± sd)	IGE Neurocam (mean ± sd)
Visual cortex	0.97 ± 0.013	0.94 ± 0.010
Right visual cortex	0.93 ± 0.010	0.96 ± 0.015
Left visual cortex	0.89 ± 0.016	0.95 ± 0.011
Brain stem	0.93 ± 0.021	0.86 ± 0.050
Right frontal cortex	0.84 ± 0.012	0.78 ± 0.017
Left frontal cortex	0.79 ± 0.024	0.74 ± 0.010
Right parietal cortex	0.71 ± 0.022	0.69 ± 0.015
Left parietal cortex	0.79 ± 0.011	0.77 ± 0.017
Right temporal cortex (lateral)	0.91 ± 0.012	0.83 ± 0.036
Right temporal cortex (medial)	0.82 ± 0.011	0.71 ± 0.020
Left temporal cortex (medial)	0.72 ± 0.017	0.70 ± 0.019
Left temporal cortex (lateral)	0.86 ± 0.011	0.79 ± 0.051
Right thalamus	0.87 ± 0.017	0.82 ± 0.019
Left thalamus	0.89 ± 0.027	0.82 ± 0.028
Right caudate nucleus	0.80 ± 0.018	0.87 ± 0.032
Left caudate nucleus	0.78 ± 0.017	0.76 ± 0.017
Right putamen	0.92 ± 0.021	0.94 ± 0.032
Left putamen	0.88 ± 0.017	0.91 ± 0.029
Right white matter	0.41 ± 0.016	0.48 ± 0.019
Left white matter	0.38 ± 0.012	0.47 ± 0.031

Table 5.4. : Comparison of regional uptake of radioactivity in the Hoffman brain phantom. The activity in each region is corrected to the cerebellum. The distribution is similar to that seen on the IGE Neurocam.

5.2.3. DISCUSSION

In order to obtain artefact free SPET images using a multidetector system, it is important that no misalignment between the detectors occurs, but also that the detector response is similar. The planar and tomographic measurements for sensitivity and spatial resolution suggest that both detectors have similar response.

The dual-detector gamma camera (IGE Optima) has much higher tomographic volume sensitivity even per detector, when compared to a single-detector gamma camera from the same manufacturer. The tomographic volume sensitivity for each detector is about 15.1 kcps/MBq/ml/cm for general purpose collimators and 9.1 kcps/MBq/ml/cm using high resolution collimators. The values for the IGE 400-XCT a single-detector gamma camera, are 11.1 kcps/MBq/ml/cm and 6.6 kcps/MBq/ml/cm for general purpose and high resolution collimators respectively.

The tomographic resolution at the minimum radius of rotation was 10.4 and 12.3 at FWHM for high resolution and general purpose collimator. When the detectors were set to a radius of rotation of 202 mm, there was a slight improvement in the FWHM by increasing the number of projections to 128 or using continuous acquisition mode. This was 13.1 at FWHM in the centre of field of view for the high resolution collimator, using continuous mode acquisition and 15.4 for the general purpose collimator. In comparison, using 64 projections, the tomographic resolution was 13.2 for high resolution and 16.1 for general purpose collimators (table 5.3 b, and 5.3 c). These acquisitions were made at a radius of rotation of 202 mm, as it was not possible to acquire in continuous mode at the minimum radius of rotation.

Using the Hoffman brain phantom, a grey to white matter ratio of 2.4+/-0.023 was achieved. If higher counts were acquired, a ratio of up to 2.6+/-0.019 was achievable. Although the system was basically designed for 180^0 tomography, the Hoffman phantom results suggest that it could be successfully used for brain tomography and good quality images should be achievable.

Recently, during a routine COR analysis study, it was discovered that one of the detectors is not stable. (Figure 5.2).

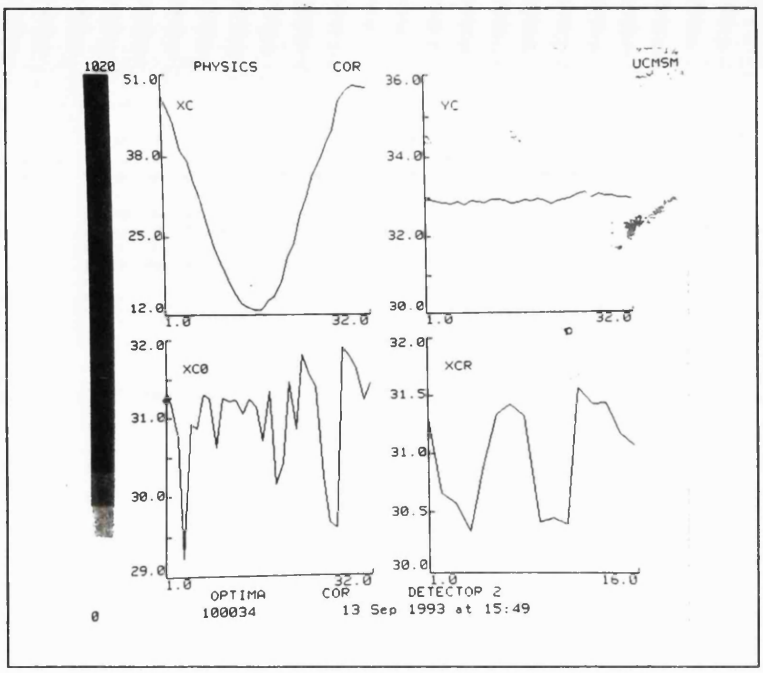

Figure 5.2: COR analysis for detector 2. Marked movement in x-axis is noted.

The system installed at the Institute of Nuclear Medicine, was the first in the Europe, and the manufacturers have taken a keen interest to improve the shortcomings, not only in hardware but also software. It was discovered that the instability was caused by one of the boards. After replacement of this board the detector has been stable. The manufacturers intend to implement further modifications in the system design. One of the most important change which will be implemented in the present system by March 1994 is the installation of line sources for simultaneous transmission/emission scanning. We understand that the manufacturers are also working on the implementation of automatic sensors for patients positioning.

5.3. Cardiac Phantom Studies

Multidetector systems such as Optima, with a fixed geometry were basically designed for 180^0 thallium-201 SPET. However, there is still some controversy about its superiority as compared to a 360^0 data collection (Go et al.,1985, Bice et al.,1987, Knesaurek et al., 1987). Tc-99m compounds are

emerging as an alternative to thallium-201 for the assessment of myocardial perfusion SPET. Since the energy of Tc-99m is higher than thallium-201 it could be hypothesized that for Tc-99m compounds 360^0 mode is preferable to the 180^0 mode. In order to test this hypothesis, both modes were compared using a cardiac phantom.

Cardiac Phantom **:** A specially designed heart lung phantom was used to investigate the change in shape in 180° and 360° SPET studies (chapter 2). The non-uniform attenuations present in the phantom closely match those in the real clinical situation. An activity of 32 MBq of Tc-99m was uniformly distributed in the ventricle wall. The remaining space of the phantom was filled with water and a uniform distribution of 8 MBq of Tc-99m as background.

5.3.1. DATA ACQUISITION

Acquisitions were made using high resolution parallel hole collimators. For 180° SPET using step and shoot mode data were acquired for 32 and 64 projections, whilst another acquisition was made in continuous mode using 64 projections. For 360° acquisition 128 projections were acquired both for step and shoot and continuous mode. Another acquisition of 64 projections over 360° was made in step and shoot mode. Approximately 2 million counts were obtained in each of these acquisitions.

5.3.2. DATA ANALYSIS

The data was prefiltered using a Hanning filter with a cut off frequency of 0.8 cycles/cm. The data were back-projected using a ramp filter. No attenuation or scatter correction was applied. The reconstructed transaxial slices were then reorientated into vertical long axis (VLA), horizontal long axis (HLA) and short axis (SA).

Using midventricular VLA, HLA and SA, regions of interest (ROI) of 12 x 12 pixel were placed over the anterior wall, lateral wall, inferior wall, septum, apex and left ventricular cavity (chapter 2). The image contrast between the apex and left ventricle cavity (LVC), the lateral, anterior and inferior walls and septum and LVC was calculated for 360° and 180° SPET images.

5.3.3. RESULTS

The image contrast calculated for the number and mode of angular sampling is tabulated in tables 5.5 a-c.

No. of projections	180° SPET DATA				360° SPET DATA			
	32 proj.		64 proj.		64 proj.		128 proj.	
Mode of Acq.	ss	cc	ss	cc	ss	cc	ss	cc
Apex/LVC	0.57	0.55	0.60	0.61	0.54	0.53	0.53	0.53
Ant.wall/LVC	0.67	0.66	0.68	0.67	0.56	0.57	0.60	0.57
Inf.wall/LVC	0.64	0.64	0.67	0.67	0.51	0.50	0.52	0.51

Table 5.5.a: Image contrast from reconstructed vertical long axis slices. (ss = step and shoot mode, cc = continuous mode, proj.= projections, Ant.= anterior, Inf.=inferior)

No. of projections	180° SPET DATA				360° SPET DATA			
	32 proj.		64 proj.		64 proj.		128 proj.	
Mode of Acq.	ss	cc	ss	cc	ss	cc	ss	cc
Apex/LVC	0.57	0.56	0.60	0.61	0.52	0.53	0.55	0.54
Lat.wall/LVC	0.68	0.69	0.70	0.69	0.55	0.54	0.57	0.56
Septum/LVC	0.66	0.67	0.68	0.68	0.52	0.52	0.52	0.55

Table 5.5.b: Image contrast from reconstructed horizontal long axis slices.
(ss = step and shoot mode, cc = continuous mode, proj.= projections, Lat.= lateral)

No. of projections	180° SPET DATA				360° SPET DATA			
	32 proj.		64 proj.		64 proj.		128 proj.	
Mode of Acq.	ss	cc	ss	cc	ss	cc	ss	cc
Lat.wall/LVC	0.68	0.68	0.69	0.70	0.55	0.55	0.56	0.56
Septum/LVC	0.67	0.66	0.68	0.69	0.53	0.53	0.54	0.54

Table 5.5.c: Image contrast from reconstructed short axis slices. (ss = step and shoot mode, cc = continuous mode, proj.= projections, Lat.= lateral)

The average lateral wall-to-septum ratio calculated from the horizontal long axis and short axis slices was similar in 180° and 360° data i.e.,1.03 for 180° data and 1.02 for 360° data. The anterior wall-to-inferior wall ratio from the vertical long axis was 1.10 and 1.02 for 360° and 180° data.

5.3.4. DISCUSSION

The quality of reconstructed images in single photon emission tomography (SPET) is affected by attenuation, spatial resolution, scatter, noise, angular and linear sampling as well as the reconstruction method applied.

The results in this study suggest that 360° SPET data has lower count density in the inferior wall, giving a ratio of 1.10 for anterior/inferior wall(figure 5.3). Some of the previous studies have demonstrated that 360° data gives better and more uniform distribution of radioactivity (Knesaurek, 1987, Hoffman, 1982).

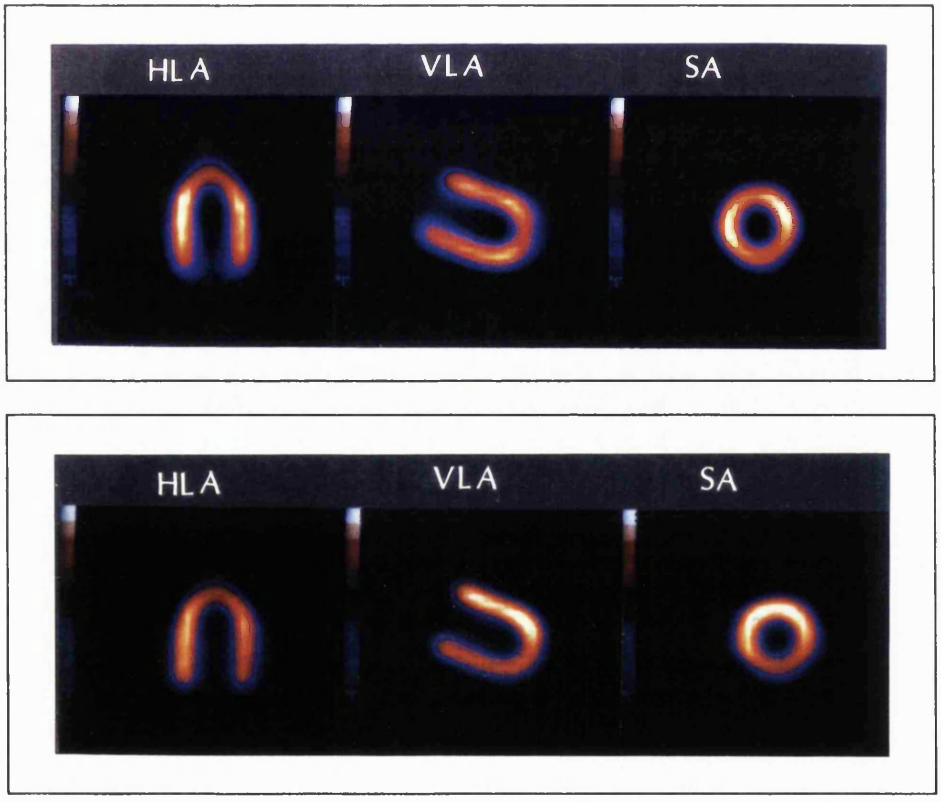

Figure 5.3: Comparison of 180° and 360° SPET images. Upper row demonstrates slices from 180° data, while the images in the bottom row are from 360° SPET data. (HLA=Horizontal long axis, VLA= Vertical long axis, SA= Short axis). It is obvious that there is slightly lower count density in the inferior wall in bottom row, while 180° SPET images demonstrate slightly reduced count density in the apex.

The vertical long axis and horizontal long axis slices demonstrate lower count density in the apex, on the 180° data, suggesting some geometrical distortion. This effect is similar to earlier studies reported by Go et al.(1985).

The debate as to whether to use 360° or 180° angular sampling for myocardial perfusion SPET imaging still exists (Coleman et al., 1982, Tamaki et al. 1982, Hoffman 1982, Clausen et al., 1985, Eisner et el., 1986, Bice et el., 1987, MacIntyre et el. 1988). At present 180° angular sampling is most often used in myocardial SPET perfusion imaging. The 2 main reasons for this are that 180° angular sampling usually provides better image contrast than 360° angular sampling and the duration of acquisition assuming that same time per frame is used, is reduced to half.

In myocardial perfusion SPET studies, projections covering the right side of the body i.e., covering the right anterior oblique-left posterior oblique (RAO-LPO) arc, are significantly contaminated by attenuation and scatter (Larsson SA,1980). Thus, exclusion of these frames that contain much less myocardial signal, reduces scatter and improves the signal to noise ratio. People who believe in 180° angular sampling for myocardial SPET perfusion imaging, go as far as to advocate the deletion of projections covering the RAO-LPO arc in 360° acquisitions performed by three detector systems.

5.3.5. CONCLUSION

This study clearly suggests that 180° should remain the method of choice for myocardial perfusion imaging, even with Tc-99m compounds in order to achieve maximal utility of dual-detector gamma camera, such as the IGE Optima. 180° SPET will continue to be used until routine attenuation and restoration correction techniques designed for myocardial SPET perfusion images become available.

5.4. Clinical Experience

The camera was utilised four days a week for clinical work. This work included mainly thallium-201 myocardial perfusion SPET and radionuclide ventriculography. The camera was also used to evaluate a new radiopharmaceutical (Tc-99m tetrofosmin).

5.4.1. THALLIUM-201 MYOCARDIAL PERFUSION SPET IMAGING

The assessment of myocardial perfusion in patients with coronary artery disease represents a major workloads in a nuclear medicine department. At the Institute of Nuclear Medicine, it constitutes about 30% of the work. One of the major advantages of multidetector SPET technology is to increase the patient through-put in a clinical situation. We have tried to establish the best possible protocols in terms of stress / rest data acquisition using the Optima, in order to increase patient throughput, without affecting diagnostic accuracy of the procedure.

The main indications of thallium-201 myocardial perfusion SPET have already been discussed in chapter 1 (section 1.6).

Patient Population : During a period of 10 months thallium-201 myocardial perfusion SPET imaging was performed in 660 patients (401 male, 259 female, age range 29-78, mean 57±11.5). 82 patients had myocardial infarction. 68 patients were assessed post CABG, while 28 patients were assessed post PTCA. Coronary angiogram results were known in 118 patients. The thallium-201 SPET images detected coronary artery disease in 324 patients (49%).

Stress Test : To evaluate the response of myocardial perfusion, various types of stress can be used. At the Institute of Nuclear Medicine, the standard method is pharmacological stress using adenosine infusion combined with low level dynamic exercise (Mahmood S et al., 1993) (Figure 5.4).

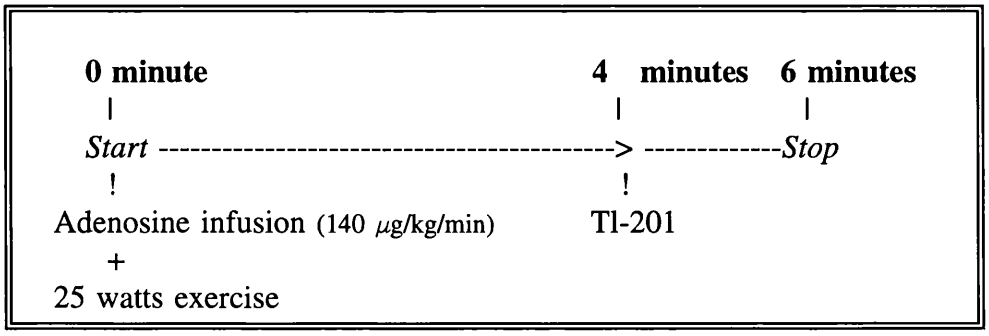

Figure 5.4: Schematic diagram representing the methodology of the stress test, using adenosine combined with low level of exercise.

Data Acquisition and Processing : Typical data acquisition and processing parameters are shown in table 5.6

Data Acquisition:	
1. Collimator:	Low energy general purpose
2. Energy window:	69 keV (20%,no offset)
	170 keV (20%,no offset)
3. Matrix size:	64x64 w
4. Number of projections:	64/180° (32/detector), step/shoot
5. Time per projection:	20 seconds for stress images
	25 seconds for redistribution
Time between stress/redistribution study: 3 hrs.	
Data Processing:	
(Same for stress/redistribution studies)	
1. Pre-processing filter:	Hanning, 0.75 cycles/cm.
2. Back projection Reconstruction: Ramp filter	
3. Trans-axial slices;	1 pixel (6.04 mm)
4. Reorientation into vertical long axis, horizontal long axis and short axis.	

Table 5.6: Table demonstrating the important acquisition and processing parameters for thallium-201 myocardial perfusion SPET.

Results : The results from coronary angiography were known in 118 patients. In this group of patients, thallium-201 SPET had a sensitivity of 91% and a specificity of 81%.

Discussion : It is obvious from table 5.7, that dual detector gamma camera with fixed geometry such as IGE Optima, resulted in a better count density (better image statistics) and therefore, reduced noise in the image. Figure 5.5 demonstrates high quality images obtained from this gamma camera.

Images of good spatial and contrast resolution is ultimate aim of SPET. Theoretically one should increase the angular sampling to improve the resolution and therefore we acquired 64 projections over 180 degrees (Figure 5.6).

	OPTIMA	XCT 400
No. of detectors	2	1
Shape of detectors	Rectangular	Circular
Stress acquisition	11 min	17.6 min.
Redistribution acquisition	14 min	23.0 min
Total acquisition time	25 min	40.0 min
Patient positioning time (average)	2-3 min	5-7 min
Average counts per study: (MCnts) Stress Redistribution	 1.5 1.2	 1.0 0.9

Table 5.7: Comparison between the IGE Optima and XCT gamma cameras, for thallium-201 myocardial perfusion SPET images. (MCnts=million counts)

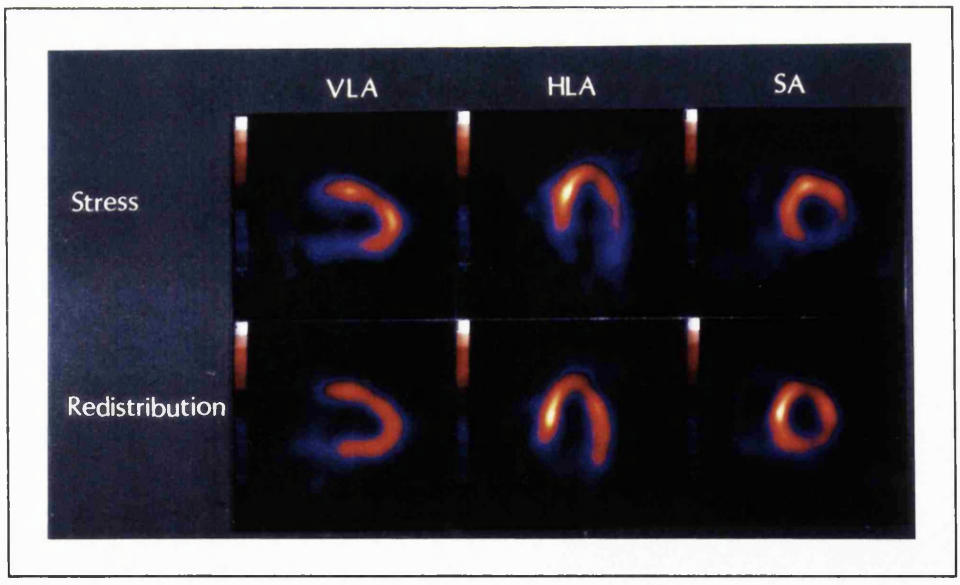

Figure 5.5: Stress and redistribution myocardial perfusion SPET images, demonstrating reversible ischaemia in the lateral wall and basal segment of inferior wall in a patient post-PTCA, suggesting restenosis.(VLA=vertical long axis, HLA=horizontal long axis, SA= short axis)

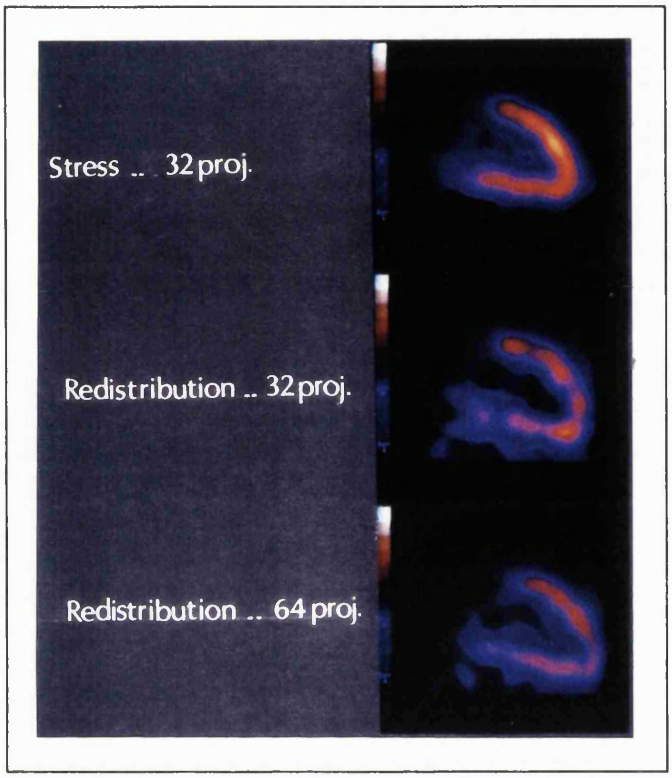

Figure 5.6: Effect of angular sampling on the tomographic images. The vertical long axis slices are displayed. Top slice demonstrate a normal thallium-201 uptake in the myocardium. The data were acquired for 32 frames. Redistribution images demonstrate a washout of thallium-201 from the myocardium, hence leading to a lower count density and marked distortion in the inferior wall. Another acquisition of 64 projections was made immediately (bottom) which demonstrated better resolution for the inferior wall.

Artefacts on SPET imaging : We also assessed at random data from 150 patients, for thallium-201 SPET from a single-detector gamma camera (IGE 400XCT). In this audit it was revealed that the number of difficult to interpret studies was 21 due to poor image quality. The recognisable factors were breast attenuation (3), rapid washout (4), low counts (3), inferior wall attenuation (6) and patient movement (6). In 3 cases the studies needed to be repeated. In comparison, the number of studies from the IGE-Optima which were difficult to interpret was only 26 out of 660 studies. The main recognisable factors in this case were errors in patient positioning (8), error in COR (3), patient movement (5) and to a lesser extent breast/inferior wall attenuation (10) (table 5.9).

Artefacts	IGE 400XCT (n=150)	IGE Optima (n=660)
Breast attenuation	3 (2%)	2 (0.3%)
Inferior wall attenuation	6 (4%)	8 (1.2%)
Low counts	3 (2%)	-
Rapid washout	4 (2.6%)	-
Patient movement	6 (4%)	5 (0.7%)
Patient positioning	1 (0.6%)	8 (1.2%)
Error in COR	-	3 (0.5%)

Table 5.8: Comparison of the artefacts noticed in thallium-201 myocardial perfusion SPET studies.

It is always important to check the planar images in cine mode. The system has a software command, which combines the datasets from each detector to be merged into a single dataset, after correcting for COR values by interpolation. The review of the data will reveal any abnormality of soft tissue attenuation, patient movement, upward creep or mispositioning of the patient. The problem of upward creep hardly exists any more because of pharmacological vasodilation. Two important artefacts which could be worse with a multidetector system are patient movement and COR error. With the longer acquisition times on a single detector gamma camera, the patient movement was inevitable. Although with a two-detector system and shorter acquisition time this problem is less marked, if it occurs the images are distorted (figure 5.7). This is partly because the patient movement is simultaneously detected by the both detectors and hence it will be present in two frames rather than only in one frame.

The other major problem is misalignment of detectors or COR. In dual-detector systems, each detector has its own COR. Therefore, any shift in COR value or misalignment in detector geometry will lead to distortion of the images (figure 5.8). This demands strict quality control.

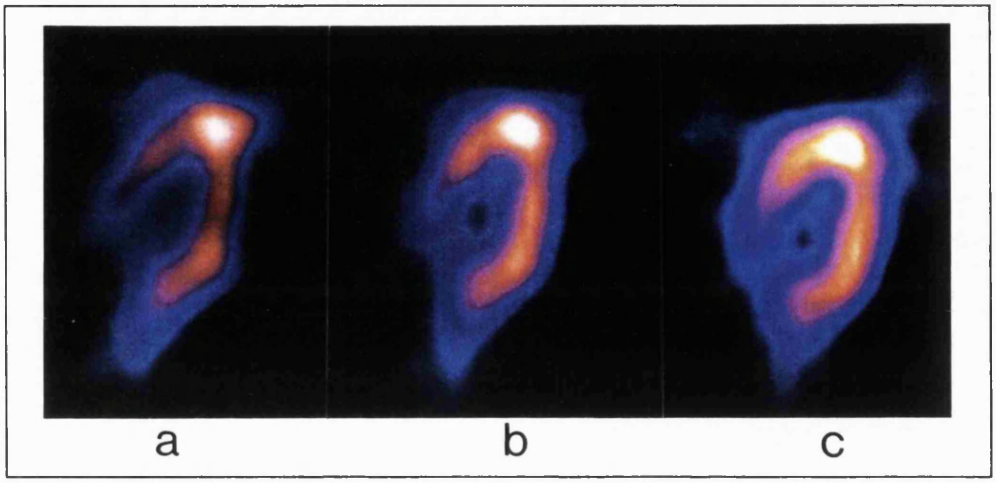

Figure 5.7: Transaxial slices in a patient with movement during SPET acquisition on a dual-detector system. Note the abnormal apical accumulation in the apex (a). After correction (b,c) the abnormality has reduced markedly.

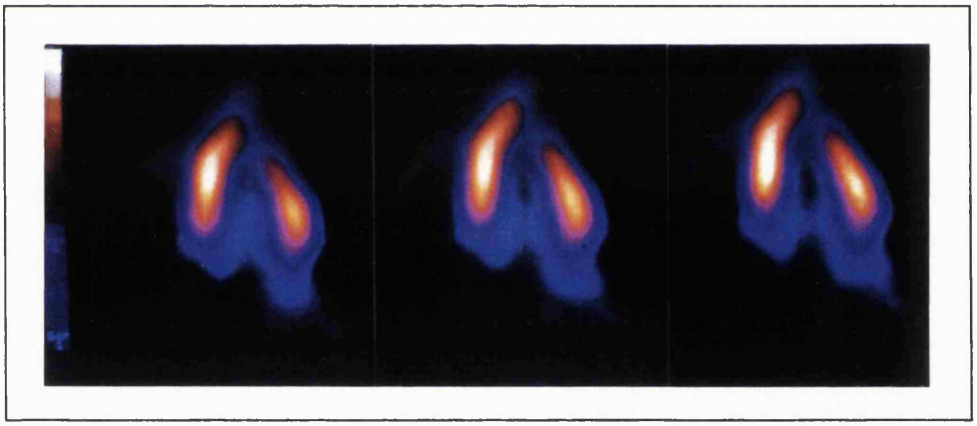

Figure 5.8: Horizontal long axis from a thallium-201 SPET study. Typical distortion in the apex due to a shift in COR is apparent.

The problem of breast attenuation could be solved by compressing the breast tissue, so that the attenuation becomes more uniform. Since applying this method this artefact has markedly reduced and the manufacturers are planning to incorporate a Velcro strap for this purpose in future Optima models.

Conclusion : The multidetector system, Optima, is an excellent system for thallium-201 SPET. Ease of patient positioning and increased throughput with better resolution images are the main advantages.

5.4.2. RADIONUCLIDE VENTRICULOGRAPHY

Electrocardiographic (ECG) gated cardiac blood pool imaging is the most commonly employed technique for assessment of left ventricular function in any nuclear medicine department. One of the most important factors for calculation of the left ventricle function is appropriate positioning. The camera must be positioned to maximize the information from the ventricles, with minimal interference from adjacent areas. A standard low energy general purpose parallel hole collimator is preferred and offers the best compromise between ideal resolution and adequate sensitivity. However attempts to position properly in the left anterior oblique (LAO) view with even a mild caudal tilt may increase the distance from the patient, thus affecting the resolution (Aswegen et al., 1980). Slant hole collimators provide an alternative to overcome this problem. Using a slant hole collimator the distance from the camera face to the heart is minimized, thereby increasing sensitivity and spatial resolution. With the introduction of multidetector gamma camera technology such as IGE Optima, which has two fixed detector geometry of 90 degrees and three-detector gamma cameras (Toshiba GCA 9300A and others such as Triad) there is a primary limitation of caudal tilt for adequate positioning. This problem can be overcome by using a slant hole collimator. Some studies in the past have shown the advantages of slant hole collimators (Parker et al., 1977, Mensforth,1992). However, in these studies the collimators were slanted at 30 degrees from the actual perpendicular to the camera face. For optimal imaging, a 30 degree slant is more than an ideal tilt. IGE has provided us with two new slant hole collimators, one with 15 degree caudal tilt, whilst the other one is 15 degree cephalic tilt, to be used with IGE Optima. The field of view of these collimators were 356 x 196 mm. These collimators contained 19000, 32.3 mm long hexagonal holes of 1.8 mm diameter each with a septal thickness of 0.25 mm.

Aim : The aim of this study was to evaluate the performance of the system for radionuclide ventriculography in a clinical setting, using these collimators. It was also aimed at determining which of these two collimators gave the more reproducible results.

Patients : Group A) Seventy five patients (54 males and 21 females, aged 11-62 years), referred for evaluation of their resting left ventricular function were assessed using the slant hole collimator with 15 degree cephalic tilt.

Group B) Twenty patients (12 males and 8 females, aged 15-57 years), were included in this group. Repeated acquisitions were performed using both collimators i.e., 15^0 cephalic tilt as well as 15^0 caudal tilt

Patient Preparation: Patients were injected with approximately 1 mg of stannous fluoride intravenously. A reconstituted kit containing 4.0 mg stannous fluoride and 6.8 mg of sodium medronate was utilized (Amerscan, *Amersham international plc*). After 20 minutes, depending upon the patients age and weight, 340-740 MBq of Tc-99m pertechnetate was injected.

Data Acquisition: Group A) Using cephalic tilt collimator, 3 acquisitions were performed in the same position in order to assess the reproducibility of the results. The camera head was positioned in the LAO view making sure that the septum was clearly delineated with complete separation of left and right ventricles from the aortic route to the apex. 64x64 W matrix with a zoom of 1.33 was used. The adequacy of ECG gating was assessed prior to the acquisition. A 10 beat heart rate average was calculated and a 15 % non-tracking window was used. For arrythmia rejection, the buffered technique was used. Data were acquired for 20 frames/cardiac cycle and each acquisition was of 4000 KCnts.

Group B) These patients also underwent three acquisitions : one using 15 degrees caudal tilt collimator, and two acquisitions using 15 degrees cephalic tilt collimator. Acquisition parameters were as described above.

Data Analysis: The data were analysed by two independent observers using the manufacturer's semi-automatic software (SAGE). After filtering/smoothing, phase and amplitude images along with the end diastolic (ED) and end systolic (ES) frames were displayed for the purpose of identifying a region of interest (ROI) around the left ventricle (LV). The ROI was always drawn taking into account the phase and amplitude image limits. After ventricular centre determination and edge detection, LV time -activity curves were generated and ejection fractions were calculated.

Statistical Analysis : A correlation coefficient and an equation for the regression line were defined for all the sets of results. Mean ejection fraction of the acquisitions was also calculated and correlation coefficient and regression line were defined.

Results

Group A:

Reproducibility of LVEF : The LVEF values calculated from the three acquisitions were plotted on a graph and the correlation coefficient was calculated between three acquisitions (Figure 5.9 a-c). The LVEF were in a range of 22-79%. A correlation coefficient of 0.98 was found between them ($p < 0.001$). The standard error of estimate (SEE) between the results of the three acquisitions was 2 ($p<0.005$, student *"t"* test).

Inter-observer Variability :The results of analysis from two independent observers at two different times were very similar.(Figure 5.9a-c, 5.10a-c). The mean EF calculated from the three acquisitions for both observers separately showed an excellent correlation.(r=0.99, SEE=1.8) (Figure 5.11).

GROUP B

Caudal vs Cephalic Tilt: The correlation between the two collimators was not excellent. (r=0.88, SEE=5.6) (Figure 5.12).

Reproducibility of LVEF: The LVEF values calculated for the two acquisitions using the caudal tilt collimator demonstrated less reproducible results than the cephalic tilt collimator. (r=0.89, SEE=6) (Figure 5.13)

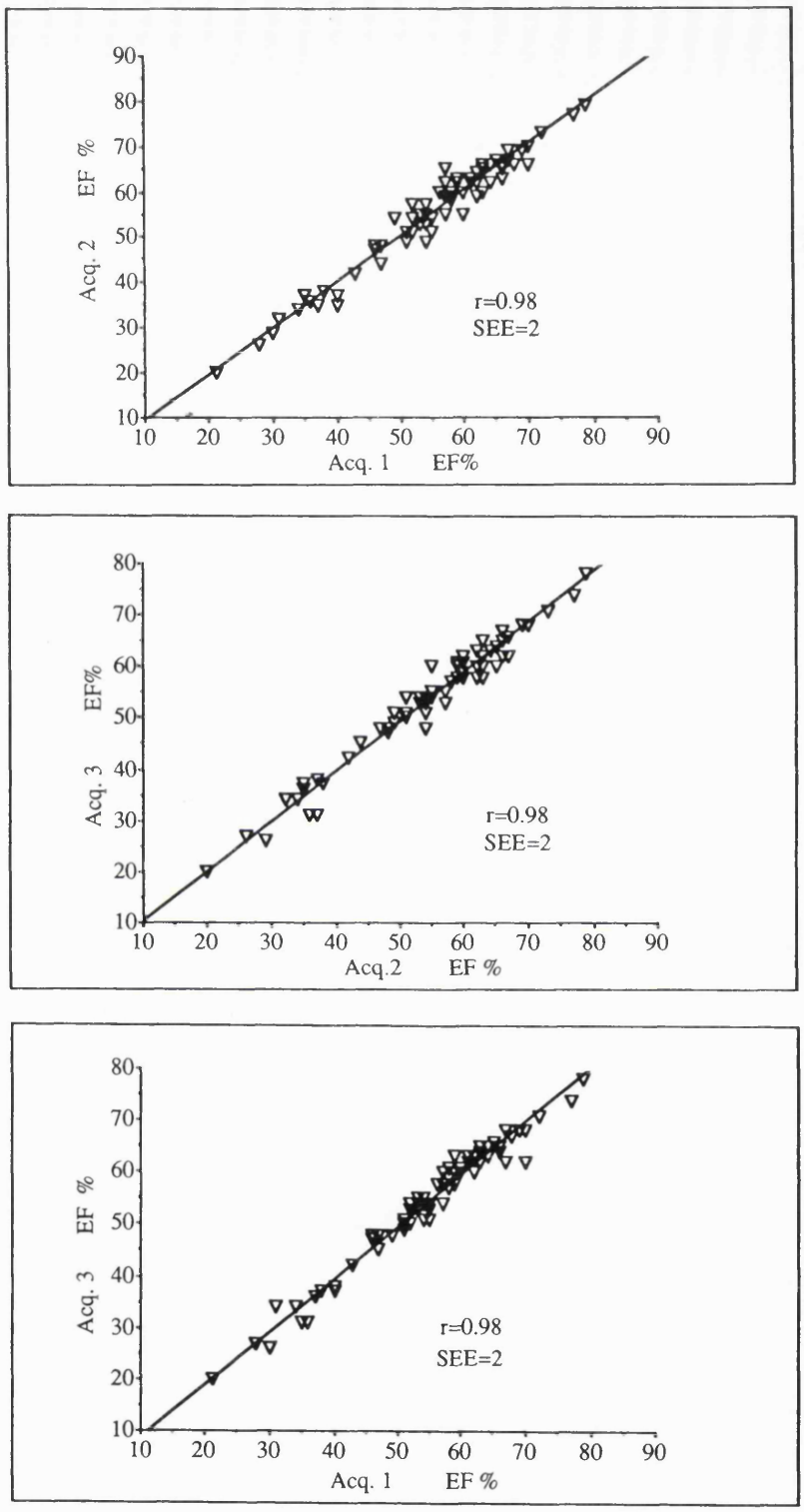

Figure 5.9 a-c: Graphs demonstrating comparisons of three different acquisitions, as analysed by observer 1. (SEE= Standard error of estimate)

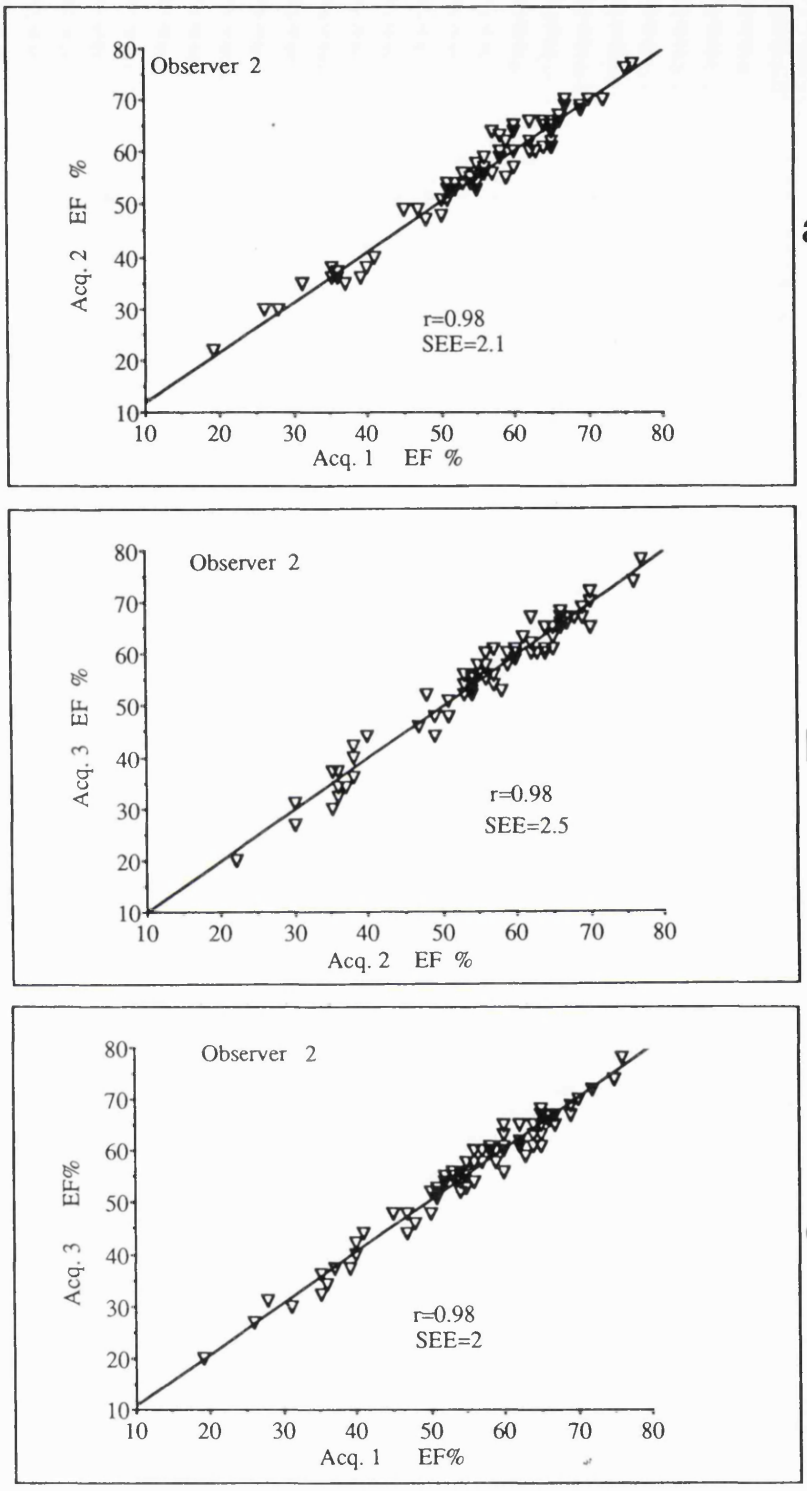

Figure 5.10.a-c: Graphs demonstrating comparisons of three different acquisitions, as analysed by observer 2. (SEE= Standard error of estimate). The results are not very different from figure 5.9 (obsever 1).

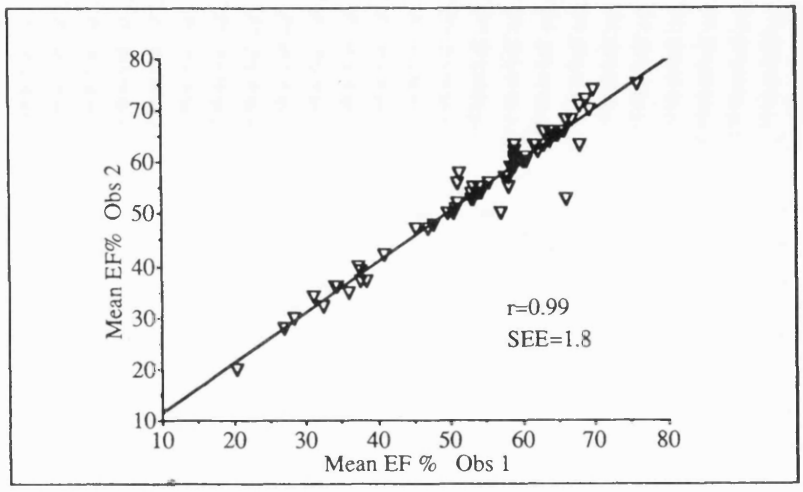

Figure 5.11: Graph demonstrating an excellent correlation between the mean ejection fraction calculated by two different observers. (SEE= Standard error of estimate)

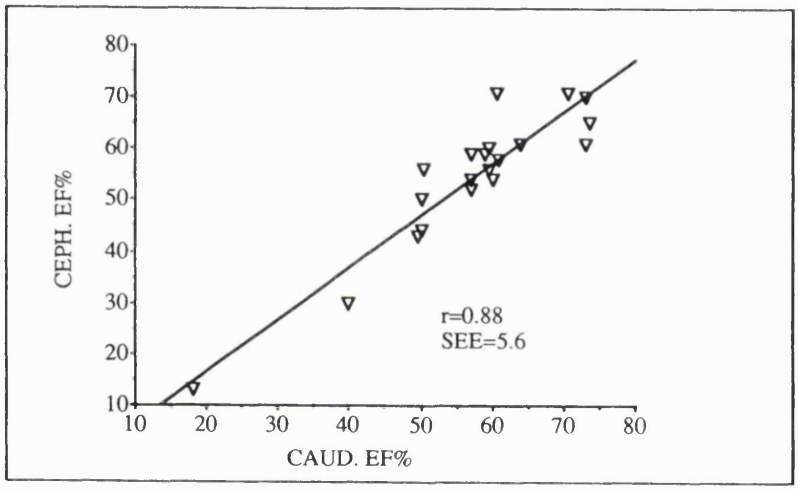

Figure 5.12: Graph demonstrating correlation between the mean ejection fraction calculated using two different collimators. (SEE= Standard error of estimate)

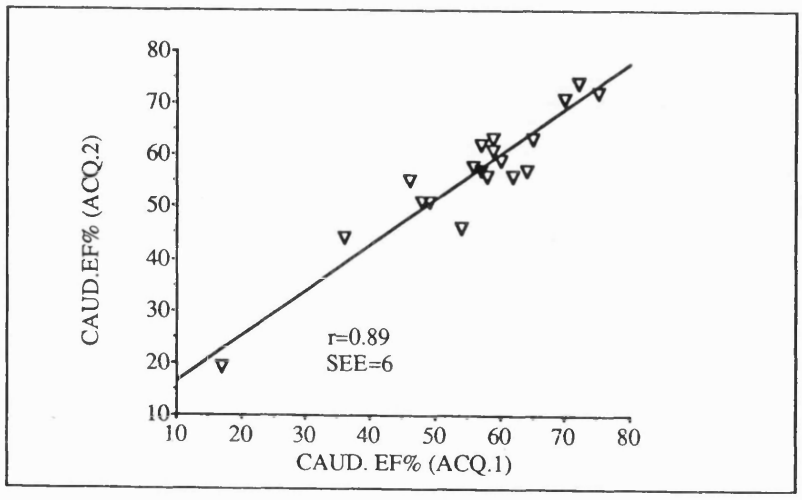

Graph 5.13.: Graph demonstrating the correlation between the ejection fraction calculated using the caudal tilt collimator. (SEE= Standard error of estimate)

Discussion *:* This study compares two entirely different collimator designs. Whilst one collimator was slanted cephalically, the other had a caudal tilt. The cephalic tilt collimator gave highly reproducible results. This is partly due to the fact that the software programme assumes the ventricle to be more of a "doughnut" shape rather than having an elliptical "pear" shape. Using cephalic tilt collimator, comparison of phase and amplitude images reveals that shape of LV is similar to short axis of LV on a SPET study. Overall the collimator with cephalic tilt gave slightly lower values of ejection fraction than one with the caudal tilt. This can be partly explained because of overlap of LV and left atrium (LA) rendering the identification of the mitral valve plane more difficult; this is particularly more marked at end of systole, when the contracted left ventricle is too small and the left atrium (filled because of pulmonary return) is dilated. There is, therefore, a contribution of counts from the LA, which leads to a lower ejection fraction value.

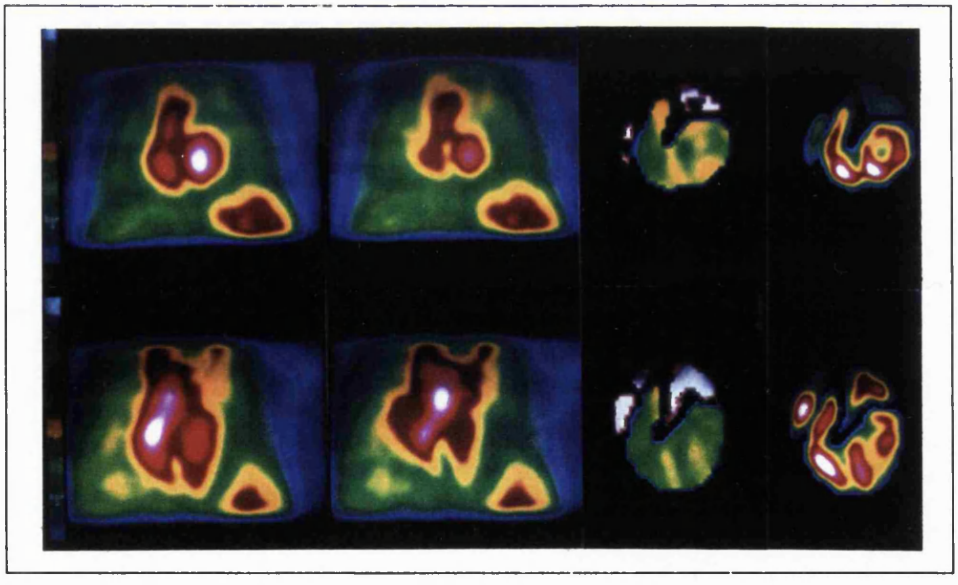

Figure 5.14: Comparison of images between 15 degrees slant hole collimator with cephalic tilt (upper row) and caudal tilt (bottom row). The end diastole and end systolic images along with phase and amplitude images are displayed. The ejection fraction with cephalic tilt was 44% whilst with caudal tilt it was 49%.

We acquired 4000 KCnts to reduce the duration of acquisition and thus were able to obtain three acquisitions comfortably. The result show that variability

was not significant. The results also suggest that with improvement in system resolution, the lower count density is acceptable. We preferred 20 frame/cardiac cycle acquisition instead of 24 frames, in order to further improve statistics in each frame.

A number of studies in the past have shown the usefulness of the slant hole collimation, but none have addressed the question of reproducibility in a clinical setting (Parker et al, 1977, Mensforth,1992). These studies showed good correlation between results using a low energy general purpose collimator and those using a slant hole collimators. However, the slant hole collimators never became popular and even these centres continued using low energy general purpose collimators.

Software : In this study, a semiautomatic method for LV edge detection using a single derivative method was used. The SAGE software has a number of steps in the production of LV regions of interest. The first is production of a limiting ROI outside of which no subsequent region may be drawn. This region helps in determination of subsequent LV regions. The positioning of this region can affect the following edge detection programme. The edge detection programme works in polar coordinates and sub divides the ventricle into five segments: mitral valve plane, lateral wall, apex, interventricular septum, and aortic valve plane. This programme has an automatic ventricular centre determination and also automatically assigns a reference point for the segmentation of the ventricle. The positioning of the segments is initially determined using a derivative algorithm with an option to alter either individual segments or the whole region with a threshold edge finder in each of twenty frames. One limitation of the software is that it allows the maximum count frame to be the end diastolic frame. Although the raw data was filtered/smoothed to find the edge, the ejection fraction was calculated from the raw images/counts. One of the prior assumptions of this programme is that the ventricle is more circular than elliptical. A suitable compromise therefore must be reached so as not to omit LV counts or to include too many background pixels. As mentioned earlier, adequate positioning and the initial limiting ROI position can help to alleviate the extent of this problem and

probably the best solution is to draw a region of interest over the phase and amplitude images. This could be reason for the highly reproducible results using the cephalic tilt collimator. In studies with inadequate count density or in patients with sub-optimal positioning, errors associated with automatic edge detection increase substantially. It is very well known that if the counts in the left ventricle are low, due to either true regional wall motion abnormalities or an exaggerated caudal tilt, the automatic edge-detection technique will frequently exclude the apex from the end systolic ROI, whilst in the manual method, the mitral valve plane and aortic valve plane are frequent sources of error.

Using cardiac phantom, Makler et al., (1985) has reported inter observer variability in the EF determination of 3% when the same studies are processed by computers / software supplied by different manufacturers. In clinically stable patients the physiological variability in EF over a one week period has been reported to be up to 4% (Marshall et al.,1977). Therefore any system giving error of more than +/- 4% should not be used clinically.

Conclusion : The caudal-tilt collimator gave non-reproducible results probably because of inadequate software. The cephalic-tilt slant hole collimator permits highly reproducible results in a clinical setting. This will contribute to an increase in the utility of a multi-detector gamma camera dedicated to cardiac imaging.

5.4.3. SEQUENTIAL TC-99M TETROFOSMIN SPET IMAGING

Thallium-201 myocardial perfusion scintigraphy is a well established method of assessing myocardial perfusion, (Strauss et al.,1977, Kaul, 1989). There are well known disadvantages of thallium-201. These include a low energy emission which results in significant soft tissue attenuation in tissue and a rather long half life, which restricts the amount of dose which can be given safely (ARSAC limits). Efforts have therefore been directed over the past 5 years, towards the development of a suitable technetium-99m based radiophramaceutical which would have ideal imaging characteristics for myocardial perfusion scintigraphy. MIBI and teboroxime have been studied but

there are limitations with these agents as well. There is high hepatic and gut uptake in the case of MIBI (Wackers et al., 1989) and rapid washout in the case of teboroxime (Iskandrian et al.,1991, Beller et al.,1991)

Tc-99m Tetrofosmin (*Myoview, Amersham plc., Buckinghamshire, UK*) is a recently developed cationic diphosphine compound and has shown promising imaging characteristics, displaying rapid accumulation in and slow clearance from the myocardium, with rapid clearance from background organs (Sridhara et al., 1993, Kelly et al.,1993, Highly et al.,1993,Smith et al.,1991).

Aim **:** To evaluate the kinetics of Tc-99m tetrofosmin at rest in order to optimize the imaging protocol and to compare the distribution of resting Tc-99m tetrofosmin with resting thallium-201.

Patients : 5 patients (all males, aged 42-56) were included in this study.

Study Design : All the patients underwent routine stress / redistribution thallium-201 myocardial perfusion SPET. After this the patients were injected with 370 MBq Tc-99m tetrofosmin.

Data Acquisition : Standard stress/redistribution SPET imaging was performed as described in section 5.4.1. of this chapter. Immediately after injection of Tc-99m tetrofosmin, data were acquired on IGE dual-detector gamma camera. A static anterior image was acquired for 300 KCnts. This was followed by a SPET acquisition using a 128x128 W matrix, with 64 projections of 10 second each. Acquisitions were repeated at 20, 40 and 60 minutes post injection, in order to evaluate changes in the accumulation pattern.

Data Analysis : Using the static anterior images, regions of interest were drawn over the myocardium, right lung and liver. The ROI over the liver was placed over the hepatic parenchyma, excluding the biliary tree. The ratios between these regions were calculated.

SPET Image Reconstruction : The acquired data were transformed into a 64x64w matrix before processing. Preprocessing was performed using a Hanning filter with a cut-off frequency of 0.8 cycles/cm. Transaxial images were reconstructed with filtered backprojection using a ramp filter. Short axis and vertical long axis images were generated. Neither attenuation correction nor scatter correction were performed. The same reconstruction parameters

were used as for thallium-201 images.

SPET Image Interpretation: Tomographic myocardial images were divided into nine segments. Eight segments: basal anterior, apical anterior, basal septal, apical septal, basal inferior, apical inferior, basal lateral and apical lateral walls were evaluated using basal and apical short axis slices, as well as vertical long axis and horizontal long axis slices. The ninth segment i.e., apex was evaluated using vertical long axis slices. Both resting thallium-201 and Tc-99m tetrofosmin data were interpreted by a nuclear medicine physician.

RESULTS

Serial changes in Static Images : Serial myocardium-to-lung ratios and myocardium-to-liver ratios determined by planar images are shown in table 5.9. The myocardium-to-lung ratio was high even 5 minutes after injection, and increased gradually with time reaching more than 2.5 at about 20 minutes. Hepatic activity significantly decreased after 40 minutes.

Time (minutes)	**Heart/lung ratio (mean+/-s.d.)**	**Heart/liver ratio (mean+/-s.d.)**
5 min.	2.29+/-0.694	0.40+/-0.18
20 min.	2.58+/-0.98	0.48+/-0.15
40 min.	2.69+/-0.37	1.12+/-0.48
60 min.	2.70+/-0.40	1.79+/-0.51

Table 5.9: Heart/lung and heart/liver ratios of Tc-99m tetrofosmin. The ratios were taken by placing ROIs of 4x4 pixel in 5 patients.

SPET Images : Visual segmental analysis of resting thallium-201 and Tc-99m tetrofosmin scans showed a 100% positive and negative concordance in all 45 segments.

DISCUSSION

Tc-99m tetrofosmin shows no redistribution and is retained by the myocardium (Kelly et al.,1989, Smith et al., 1991). It has shown high myocardial activity and relatively rapid liver clearance, providing a favourable profile for

myocardial imaging (Jain et al.,1992, Rigo et al., 1992, Sridhara et al, Sinusas et al., 1992).

This study demonstrates that a reasonable heart/lung ratio is achieved at 20 minutes post-injection (table 5.9.). However, at this time liver activity is still high, which could interfere with the quality of the data from the inferior wall. A suitable compromise for achieving the best heart/lung and heart/liver ratio would be to image between 20 and 30 minutes post-injection. These results are further supported by Nakajima and co-workers (1993), who have reported similar heart/lung and heart/liver ratios in patients with coronary artery disease. In a more recent study Highley et al (1993) have reported heart to lung ratios which are higher than found in this study (3.1 ± 1.8 at 5 minutes and 7.3 ± 4.4 at 60 minutes). However, these higher ratios are in normal volunteers, which could explain the discrepancy.

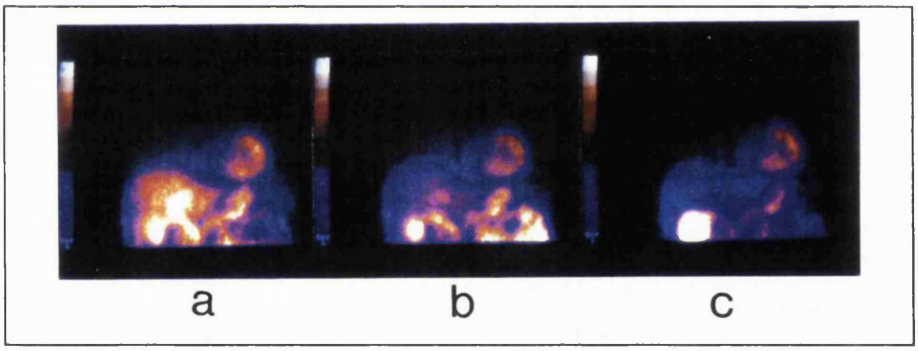

Figure 5.15: Static planar images at 5 minutes (a), 20 minutes (b) and at 60 minutes (c). There is clearance of activity from liver by 20 minutes.

Regarding liver clearance, although hepatic accumulation was initially observed, it did not significantly interfere with the inferior wall of LV. (Figure 5.16).

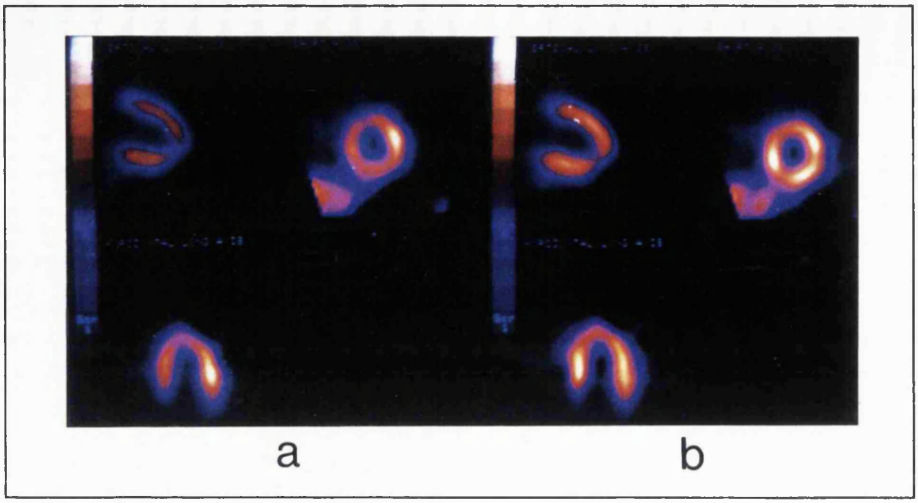

Figure 5.16: Reconstructed SPET images from data acquired 5 minutes(a) and 20 minutes (b) after injection of Tc-99m tetrofosmin.

Comparing this data from Tc-99m tetrofsmin with that from Tc-99m MIBI study (Wackers et al.,1989) resting heart to lung ratios at 5 min, and 60 min post-injection were lower for Tc-99m MIBI (1.9$\pm$0.2 and 2.4$\pm$0.1 respectively). The heart to liver ratios at 5 and 60 minutes for MIBI were 0.5$\pm$0.1 and 0.6$\pm$0.1 respectively. In this study of Tc-99m tetrofosmin the heart seemed to accumulate relatively higher activity and the liver showed relatively lower activity than Weckers' Tc-99m MIBI study, particularly at one hour post-injection.

In this pilot study, resting thallium-201 and resting Tc-99m tetrofosmin images yielded similar clinical information (figure 5.17). This encourages further investigation for the detection of coronary artery disease using Tc-99m tetrofosmin.

CONCLUSION

This study has demonstrated that the optimum imaging time for Tc-99m tetrofosmin is about 20 minutes after injection. This agent shows similar myocardial distribution to thallium-201 at rest.

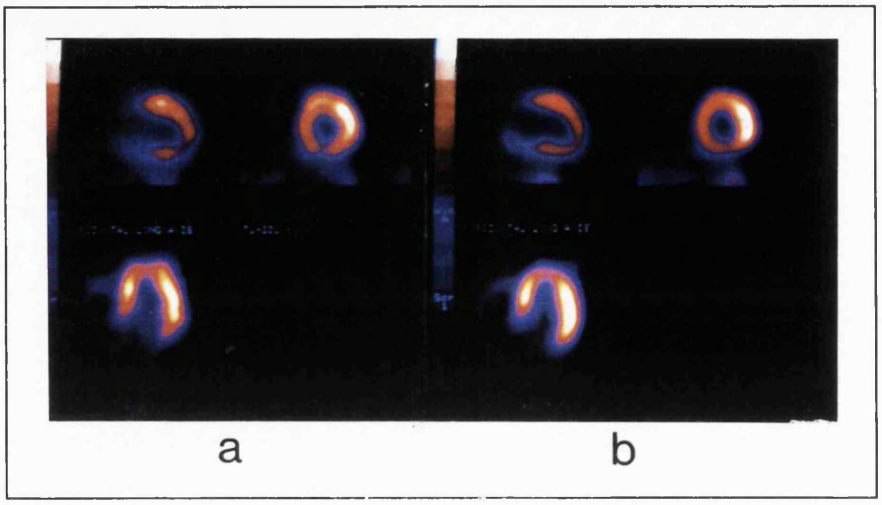

Figure 5.17: Resting thallium-201 (a) and resting Tc-99m tetrofosmin study of the same patient. The vertical long axis, horizontal long axis and short axis slices are displayed.

5.4.4. Resting Thallium-201/Stress Tc-99m Tetrofosmin Myocardial Perfusion SPET

As discussed earlier (section 5.4.3) Tc-99m tetrofosmin (Myoview) is a recently developed compound and has shown promising imaging characteristics. Regarding detection of coronary artery disease, phase I,II and III studies have been performed showing good comparison with Thallium-201 imaging (section 5.4.3., Jain et al., 1993, Sridhara et al., 1992)

Tc-99m tetrofosmin does not display the redistribution characteristics shown by thallium-201, as it is a retention-type agent, and therefore clinical studies conducted have employed separate stress and rest injections, either 4 hours apart or on separate days (Sridhara et al., 1993, Kelly et al., 1993, Nakajima et al., 1993)

Aim : This study looks at the combination of resting images using thallium-201 and post-stress images using Tc-99m tetrofosmin in a protocol of 90 minutes duration and assesses it's role in the detection of coronary artery disease.

Materials and Methods

Patient population: Twenty five patients (23 M, 2 F, aged 36-73) underwent a combined protocol involving rest imaging with Thallium-201, followed by

stress imaging with Tc-99m-tetrofosmin. Patients with obstructive airways disease, unstable angina or second or third degree heart block were excluded from the study. Thirteen had a history of previous myocardial infarction, three complained of atypical chest pain, 22 complained of an anginal pattern of chest pain, and four patients complained of dyspnoea as an additional symptom.

Patient Preparation: Patients were advised to abstain from caffeine containing beverages for at least ten hours prior to the stress protocol. Those patients on beta-blockers were asked to withhold the drug for 48 hours prior to the test and those on dipyridamole were asked to withhold the drug for 72 hours prior to the test. An intravenous cannula was inserted in the right arm, and a three-way stopcock attached and flushed with normal saline.

Thallium-201 administration : 74 MBq of thallium-201 was injected as a bolus and flushed through with normal saline.

Resting Thallium-201 SPET Acquisition : This was conducted twenty minutes after the injection of thallium-201. Single photon emission tomography (SPET) was performed using an IGE dual-detector cardiac dedicated camera, Optima. Data were acquired in a 64 x 64 matrix involving 64 step and shoot projections over 180 degrees beginning at 45 degrees right anterior oblique. Acquisition time was 25 seconds per projection. The camera was equipped with a low energy high resolution collimator and interfaced with an IGE Star 4000i computer. Energy peaks of 72 keV and 169 keV were used with 20 % windows and no offset.

Stress testing and Tc-99m tetrofosmin administration : Following the first data acquisition, the combined adenosine/exercise stress protocol was conducted. Adenosine in normal saline was infused at a rate of 140 ug/kg/min via a volumetric pump, in a concentration of 1mg/ml, for a period of six minutes. Concurrently the patients cycled at a fixed workload of 25 watts on a bicycle ergometer for the six minute period. At four minutes, 370 MBq of Tc-99m tetrofosmin (*Myoview, Amersham Plc, Buckinghamshire, UK*) was injected as a bolus, through the three-way stopcock. The patients' pulse and blood pressure were recorded at rest ,and then every two minutes until the stress protocol was complete. Patients' symptoms and a three lead

electrocardiogram were monitored during the process. Immediately following the completion of the six minutes the patients were provided with chocolate and milk to ingest in order to facilitate rapid clearance from gall bladder.

Tc-99m tetrofosmin acquisition: This was conducted 20 minutes after the stress. Data were acquired in a 64 x 64 matrix, with 64 projections over 180 degrees. An acquisition time of 20 seconds per projection was used. An energy peak of 140 keV was used with a 20 % energy window and no offset.

Protocol Duration : The total duration of the imaging protocol was 90 minutes, including the designated intervals between injection and image acquisition which were to allow for image optimisation.

Data Processing : The data from both the first and second image acquisitions were reconstructed on a Star 4000i computer, utilising a Hanning pre-filter with a cut-off frequency of 0.8 cycles/cm. A ramp filter was applied during reconstruction using a back-projection algorithm. The reconstructed transaxial slices were then reorientated into vertical long, horizontal long, and short axes.

Data Analysis : 3 physicians studied the images produced. Qualitative nine segment analysis was used with the segments being designated as follows: anterior and basal segments of each of the lateral, anterior and inferior walls and septum, and a single segment for the apex. The segments were scored as normal or abnormal (and in the case of the latter the decreased count was scored as fixed or reversible). In the event of disparity, a consensus was reached between the participating observers.

When the image results were analysed in respect of the coronary artery anatomy the segments were assigned as follows:-

Left anterior descending artery - basal and apical anterior wall, basal apical septum, apex

Left circumflex artery - basal and apical lateral wall

Right coronary artery - basal and apical inferior wall

RESULTS

Haemodynamics : Whilst undergoing adenosine plus exercise stress protocol, the mean heart rate of the subjects rose from 63.6 +/- 9.8 to 90.3 +/- 20.4

beats per minute . The mean diastolic blood pressure rose marginally from 82.6 +/- 10.1 to 83.7 +/- 10.1 mm Hg, whilst the change in mean systolic readings was from 133.1+/- 17.4 to 144.1 +/- 17.8 mm Hg . The mean double product rose from 8527+/- 2126 to 13197 +/- 4126 mm/min.

Cardiac Catheterization : Results from coronary angiography of the twenty five patients were analysed . A vessel displaying greater than 50 % stenosis on angiogram was assigned as being diseased. 4 patients had disease of all three coronary vessels, 8 patients had disease of two vessels, 10 patients had single vessel disease, and 3 patients had normal coronary arteries. In terms of the affected vascular territories this comprised 12 lesions of left anterior descending artery (LAD) territory, 10 lesions of left circumflex (LCx)territory, and 16 lesions of the right coronary artery (RCA) territory.

SPET images : The scoring of the segments in terms of the images obtained, i.e. fixed, reversible or normal, was compared with the result of cardiac catheterisation in the designated vascular territories as described above. With regard to the LAD territory, the protocol showed a sensitivity of 85% (34/40 segments) for the detection of a diseased vessel, and the specificity was found to be 70%(59/84). For the RCA, the results were 78% (28/36)and 71% (10/14) respectively, and for the LCx, they were 69 %(9/13) and 70%(26/37) respectively.

The territories of the left circumflex and right coronary artery were then analysed in combination, and the imaging showed specificity of 76% and sensitivity of 70%.

Overall sensitivity was 80% and specificity was 70%.

DISCUSSION

There are reservations amongst nuclear physicians about the use of two different imaging agents in the evaluation of coronary artery disease in a single subject. In the design of this protocol, we attempted to address some of the concerns that might arise

The rationale for stress Tc-99m tetrofosmin imaging being performed after the rest thallium-201 imaging, and not in the reverse order, was to prevent the phenomenon of compton scatter of the 99m-Tc activity into the Tl-201

photopeak, which would affect the thallium images, creating the potential for overestimation of reversible ischaemia. In addition to this, the protocol was designed with emphasis on decreasing patient time in the scanning department. Had the stress study been conducted first, one would have to allow sufficient time for the myocardium to return completely to the resting state before undertaking the rest study, thereby lengthening the patient's stay in the department.

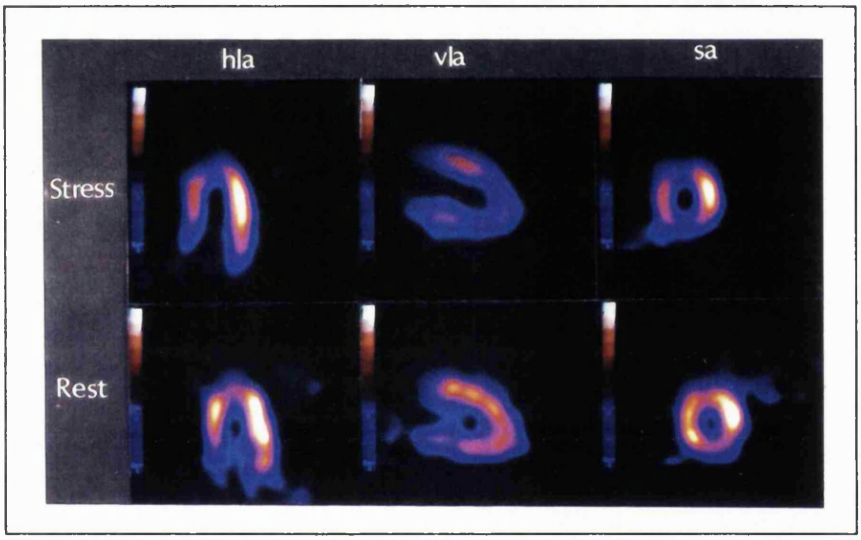

Figure 5.18: Stress/Tc-99m tetrofosmin (upper row) and rest/thallium-201 (lower row) study. Horizontal long axis (hla), Vertical long axis (vla), , and short axis (sa) slices are displayed and demonstrate reversible ischaemia in the anterior and inferior walls. Coronary angiography confirmed disease of LAD and RCA.

Accepting that the physical properties of the two agents differ, data acquisition was adapted to suit the characteristics of each radionuclide. A high resolution collimator was employed, and in the case of thallium-201 rest images, the acquisition time was increased to 25 seconds per projection compared with 20 seconds for Tc-99m tetrofosmin. Appropriate energy windows of 72 keV and 169 keV for Tl-201, and 140 keV for Tetrofosmin, were used.

In previous section,(5.4.3) we have discussed the optimal time for imaging between 20-30 minutes. Higley et al (1993) showed high gall bladder activity of 3.2 +/- 1.9 % of total injected activity at 5 minutes post stress injection which had fallen to 1.0 +/- 0.5% by 60 minutes. In order to expedite clearance from the gall-bladder in this study, we asked patients to ingest 200 mls of milk

and 50 grams of chocolate immediately post exercise. Good quality images were obtained at 20 minutes post stress with low activity recorded in the region of the liver.

Studies conducted thus far, assess the usefulness of two different protocols for rest and stress imaging with Tc-99m tetrofosmin. As tetrofosmin has not been shown to display the characteristic of redistribution (Jain et al., 1992) it is necessary for subjects to receive two separate injections of the radionuclide in the detection for defect reversibility. Therefore the one day protocol employed has involved injection at maximal stress followed 5- 30 minutes later by image acquisition, and 4 hours later reinjection, with imaging after 30 minutes. A separate day protocol involves conducting these two studies more than 24 hours apart. Sridhara et al (1993) in a study of 23 patients found no significant difference in the detection of coronary artery disease between these two methods. In the same study, a favourable comparison emerged in the identification of coronary artery disease, Thallium correctly identifying 83% of abnormal segments, while Tetrofosmin showed 80% and 83% of diseased segments on early and late images respectively.

In a study of 26 patients Nakajima et al (1993) showed concordance of 83% between images obtained with thallium-201 in a rest/redistribution protocol, and with Tc-99m tetrofosmin in a one day protocol in the same subjects. However, the figures for sensitivity of Tc-99m tetrofosmin in the detection of coronary disease were lower ; 60% compared to 72% for thallium-201. Thus the overall sensitivity and specificity figures for this study of a combined protocol of tetrofosmin and thallium, 80% and 70% respectively, are similar to those quoted for the use of tetrofosmin alone, but are somewhat lower than figures obtained with thallium imaging alone, ranging from 72% to 92% for sensitivity and 84% to 100% for specificity (Nakajima et al. 1993, Nguyen et al., 1990, Francisco et al., 1982, Verani et al., 1990)

LIMITATIONS

This study has compared the results of segmental analysis of combined thallium/tetrofosmin protocol images with coronary angiographic data, in order

to obtain figures of sensitivity and specificity for the detection of diseased segments.

Coronary angiography has not been proven to be the "gold standard" in the assignation of definite regions with respect to myocardial perfusion, and results must be interpreted, aware of it's limitation as a frame of reference.

Further studies of this combined protocol could be performed comparing the results with those of thallium imaging alone, or tetrofosmin alone, conducted sequentially in the same subjects. This however raises ethical considerations as the patients would need the stress test to be performed twice.

CONCLUSION

A combined myocardial imaging protocol involving thallium-201 scintigraphy at rest, followed by technetium-99m-tetrofosmin imaging after stress, is a useful method of investigation for the presence of coronary artery disease. Multidetector gamma camera has proven useful for establishing this rapid protocol resulting in high resolution images. The decreased duration of 90 minutes compared to more than 4 hours, confers advantage on this protocol over the use of thallium or tetrofosmin as single agents. The sensitivity and specificity in the detection of coronary artery stenosis as shown on coronary angiography, is similar to that of tetrofosmin alone.

5.4.5. MISCELLANEOUS APPLICATIONS

FIRST PASS ANGIOCARDIOGRAPHY

The system has been provided with two high sensitivity collimators to permit first pass acquisition using both detectors. The two detectors allow simultaneous acquisition in two views.

GATED BLOOD POOL TOMOGRAPHY

Although planar gated blood pool measurements of ejection fraction have excellent agreement with contrast ventriculography, the information regarding wall motion abnormalities could be further enhanced by gated blood pool tomography. It may provide qualitative and quantitative methods of analysis of absolute volumes (Stadius et al.,1985, Gill et al.,1985, Underwood et

al.,1985, Corbett et al., 1985). We have defined a protocol to perform GBPT.

Data Acquisition:
1. Collimator: Low energy general purpose
2. Energy window: 140 keV (20%, no offset)
3. Matrix size: 64x64 w
4. Number of projections: $32/180^0$, step and shoot
5. Cycles per projection: 50
6. Number of frames per cycle: 16
Data Processing:
1. Pre-processing filter: Hanning, 0.75 cycles/cm.
2. Back projection Reconstruction: Ramp filter
3. Trans-axial slices; 1 pixel (6.04 mm)
4. Reorientation into vertical long axis, horizontal long axis and short axis.
5. Addition of short axis slices, vertical long axis and horizontal long axis slices in gated mode.

Table 5.10: Acquisition and Processing protocol for gated blood pool tomography (GBPT)

Assessment of regional wall motion abnormality and function is important in evaluating the presence or consequences of CAD, the effects of interventions (thrombolysis, angioplasty or coronary artery bypass grafting) or efficacy of drug treatment. Gated blood pool tomography gives a truly three dimensional representation allowing optimal evaluation of the LV (Figure 5.19). One of the main reasons that this technique could not develop was an inherent problem of gating because beat rejection lead to longer acquisition times. At the same time there was much development and interest in echocardiographic techniques. With dual-detector systems such as Optima, where the acquisition time can be reduced by half, and development of more powerful computers it is possible that gated blood pool tomography could gain popularity.

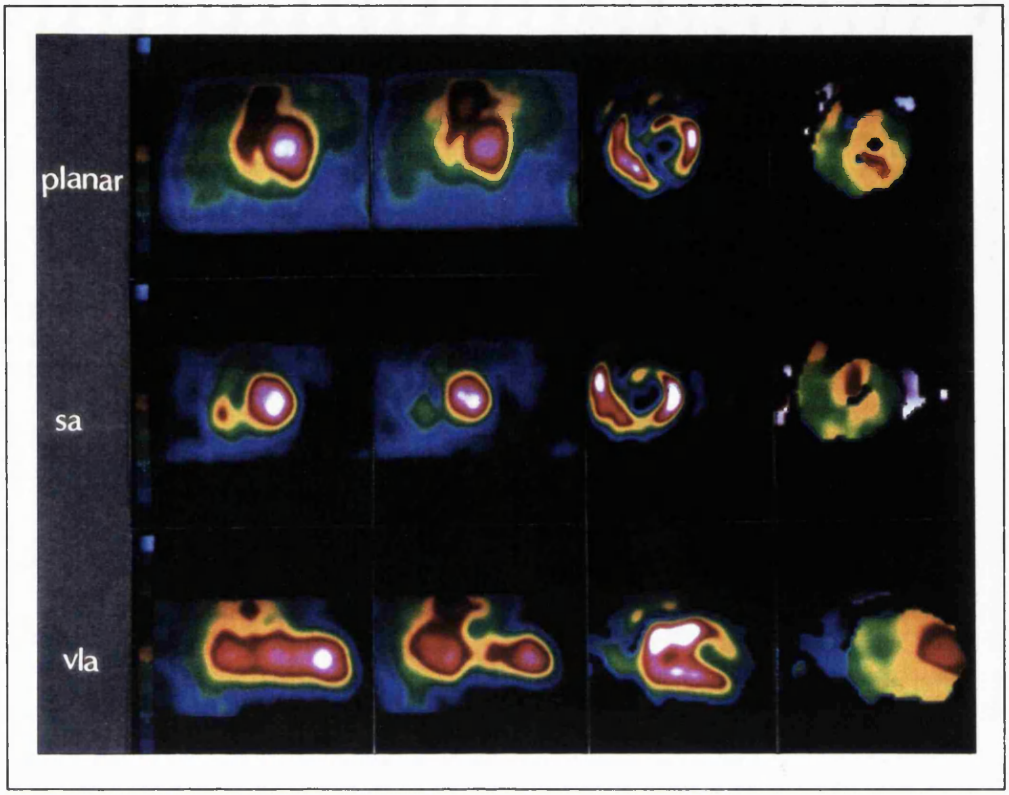

Figure 5.19: Demonstration of improved diagnostic accuracy for regional wall motion abnormality. The upper row displays planar gated blood pool images from a patient, showing regional wall motion abnormality less well marked than the bottom two rows, which display tomographic short axis and vertical long axis slices in end diastole and end systole along with phase and amplitude images. The apical and apico-anterior wall motion abnormality (dyskinesia) is more marked in vertical long axis.

5.4.6. CONCLUSIONS

Although this system is basically designed for 180^0 cardiac SPET imaging, it could be successfully used for radionuclide ventriculography using slant hole collimators. If the caudal tilt collimators are to be used, the software should be altered. High resolution 360^0 SPET is also possible.

Chapter 6

Sopha DST

a dual-detector SPET system

6.1. Description

The Sopha-DST gamma camera (*Sopha medical, Buc Cedex, France*) was evaluated at the Department of Nuclear Medicine, Laperyonie Hospital, Montpellier, Cedex, France.

The Sopha DST is a dual detector, variable angle design gamma camera. Each detector is rectangular (300 x 400 mm) in shape and has a 9.5 mm thick NaI(Tl) crystal coupled to 58 photomultiplier tubes (PMTs), out of which 50 are hexagonal (60 mm) and 8 circular(38 mm). Both detectors are mounted on an axial gantry which is digitally controlled by a built-in microprocessor. Each of the detectors can be positioned at 45 degrees to form a 90° configuration in order to perform 180° cardiac SPET. The detectors can be rotated on their axis to 90° to allow whole body imaging or 360° data acquisition. There is a telescopic movement of the table in order to ensure the closest arc for SPET studies. The SPET data from both detectors are stored in a single dataset. The camera has been provided with low energy general purpose, low energy ultra high resolution parallel hole and a set of low energy convergent collimators. The detectors are fitted with safety pads, in the event of the detector touching the patient, the acquisition stops. The system has a vacuum controlled imaging table, made of low attenuation carbon fibre. The camera is controlled by an acquisition station, whilst a separate 32 bit (Motorola) processing/analysis station is available.

6.2. Tomographic Assessment

6.2.1. METHODS

Tomographic Spatial Resolution **:** The tomographic spatial resolution was assessed using three capillary line sources filled with Tc-99m, and placed at 40 mm distance from each other (chapter 2). The data were reconstructed using a ramp filter, with no pre-filtering or attenuation correction. Horizontal and vertical profiles were run through the reconstructed slices. The values of the line spread function were then calculated using a personal computer and spatial resolution was expressed as Full Width at Half Maximum (FWHM) and Full Width at Tenth Maximum (FWTM).

Hoffman Brain Phantom Studies **:** Tomographic acquisitions were carried out using the Hoffman brain phantom (chapter 2). The acquisitions were performed using the low energy high resolution collimators, a 128 x 128 W matrix. Acquisitions were repeated five times. Approximately 4 million counts (MCnts) were acquired for each acquisition. The data were prefiltered using a Hanning filter, with a cutoff frequency of 0.3 cycles/pixel (pixel size=3.4 mm). A ramp filter was applied during backprojection. 1 pixel (3.4 mm) thick slices were generated. Attenuation correction was not applied, due to software limitations. Regions of interests of 13.6 x 13.6 mm in size were used to obtain cerebrum/cerebellum activity ratios (Chapter 2, Figure 2.2). At least four samples were made for each region, for each acquisition. The average counts obtained from the grey matter were then divided by the average counts recorded from the white matter.

Cardiac Phantom Studies : The heart/lung phantom was used to assess the camera's capability to perform 180° and 360° single photon emission tomography. The various parts of the phantom i.e., ventricular wall, lungs and spine were contained in a perspex cylinder (chapter 2).

Acquisitions were made using ultra high resolution parallel hole collimators. For 180° SPET acquisition, the detectors were angulated at 90° to each other, acquiring 64 frames. For 360° acquisition, 128 projections were acquired with the detectors opposed to each other. Data were acquired in step and shoot mode. The duration of acquisition per frame was 20 seconds for 180° and 10

seconds for 360° data.

The data were prefiltered using a Hanning filter with cut off frequency of 0.25 cycles/ pixel. The data were backprojected using a ramp filter. No attenuation or scatter correction was applied. The reconstructed transaxial slices were then reorientated into vertical long axis (VLA), horizontal long axis (HLA) and short axis (SA) slices.

Using midventricular VLA, HLA and SA slices, region of interests (ROI) of 4x4 pixel (13.6 x 13.6mm) were placed over the anterior wall, lateral wall, inferior wall, septum, apex and the left ventricular cavity.

The image contrast was calculated using standard formula:

$$I = (C1 - C2)/(C1 + C2)$$

where C1 is total number of counts in first ROI, C2 is the total number of counts in the second ROI. The image contrast between the apex and left ventricular cavity (LVC), the lateral, anterior and inferior walls and LVC, and septum and LVC were calculated for 360^0 and 180^0 SPET images.

6.2.2. RESULTS

Tomographic Spatial Resolution : The results of tomographic spatial resolution are shown in table 6.1.

Collimator	**Radial distance 0 mm**		**Radial distance 40 mm**		**Radial distance 80 mm**	
	FWHM	**FWTM**	**FWHM**	**FWTM**	**FWHM**	**FWTM**
LE UHR	10.5	18.7	10.54	19.6	10.8	19.04
LE AP	12.9	23.1	13.06	24.0	13.7	23.9

Table 6.1: Tomographic spatial resolution at a radius of rotation of 140 mm. (LE UHR =low energy ultra high resolution, LEAP = low energy all purpose).

The individual tomographic resolution of each detector could not be calculated, since a single detector could not acquire 360° data independently.

Hoffman Brain Studies : Using the Hoffman data, the mean cerebrum/cerebellum ratios obtained are tabulated in table 6.2.

Brain regions	**Ratios (mean ± sd)**
Visual cortex	0.97 ± 0.013
Right visual cortex	0.92 ± 0.021
Left visual cortex	0.89 ± 0.017
Brain stem	0.93 ± 0.019
Right frontal cortex	1.06 ± 0.012
Left frontal cortex	1.01 ± 0.023
Right parietal cortex	0.86 ± 0.017
Left parietal cortex	0.79 ± 0.020
Right temporal cortex (lateral)	0.91 ± 0.012
Right temporal cortex (medial)	0.76 ± 0.025
Left temporal cortex (medial)	0.72 ± 0.013
Left temporal cortex (lateral)	0.90 ± 0.019
Right thalamus	0.70 ± 0.031
Left thalamus	0.69 ± 0.017
Right caudate nucleus	0.69 ± 0.014
Left caudate nucleus	0.72 ± 0.100
Right putamen	0.69 ± 0.031
Left putamen	0.70 ± 0.018
Right white matter	0.38 ± 0.026
Left white matter	0.39 ± 0.032

Table 6.2.: Comparison of the cerebrum/cerebellum ratios of radioactivity in Hoffman phantom.

The mean grey/white ratios calculated using the five 4 MCnts acquisitions, was 2.6±0.08. The ratio increased to 2.9±0.03 in a study where 40 MCnts were obtained.

Cardiac Phantom Studies : Using 180° and 360° data acquisitions, the image contrast ratios calculated between myocardium/LV cavity are shown in tables 6.3 a-6.3 c.

	180° SPET DATA	360° SPET DATA
Apex/LVC	0.51	0.56
Anterior wall/LVC	0.69	0.58
Inferior wall/LVC	0.64	0.53

Table 6.3.a: Image contrast from reconstructed vertical long axis slices.

	180° SPET DATA	360° SPET DATA
Apex/LVC	0.50	0.56
Lateral wall/LVC	0.71	0.59
Septum/LVC	0.66	0.58

Table 6.3.b: Image contrast from reconstructed horizontal long axis slices.

	180° SPET DATA	360° SPET DATA
Lateral wall/LVC	0.67	0.60
Septum/LVC	0.65	0.59

Table 6.3.c: Image contrast from reconstructed short axis slices.

6.2.3. DISCUSSION

The tomographic spatial resolution (radial) in air was similar to that of the IGE dual detector gamma camera (IGE Optima). (FWHM of 10.5 mm and FWTM of 18.7 mm for Sopha DST versus FWHM of 10.4 mm and FWTM of 19.0 mm for Optima)(chapter 5, Section 5.2.).

Although, the average grey/white matter ratios with this system were better than all other systems (2.6$\pm$0.08 for Sopha DST compared to 2.4$\pm$0.02 for IGE Optima), this may have been to differences between the reconstruction

algorithms. Figure 6.1 demonstrates a transaxial slice of the Hoffman brain phantom. Since no attenuation correction was applied, better grey/white matter ratios were achieved, but the ratios between the different structures within phantom was different i.e., the superficial structures such as frontal cortex exhibited higher ratio, compared to deeper structures e.g., thalami and caudate and putamen nucleus (table 6.2). The SPET reconstruction software was unable to perform attenuation correction.

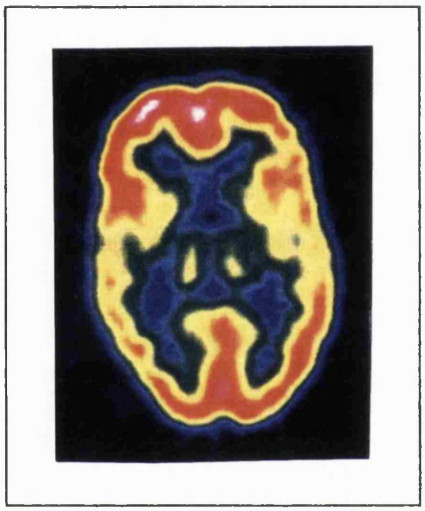

Figure 6.1: Hoffman brain phantom (Transaxial slice at the level of thalami)

The results from the cardiac phantom studies demonstrate a better image contrast using 180° compared to 360° data acquisition. These results were the same as for the other studies (chapter 5, section 5.3). Figure 6.2 compares the 180° and 360° data acquisition images. A markedly reduced apical signal is noted in the 180° data, whilst in the 360° data, the short axis slices appear rather elliptical. This could be either due to a software problem, as it was basically designed to handle and reorientate 180° data only or a marked attenuation and scatter effect as demonstrated earlier in chapter 5, section 5.3.

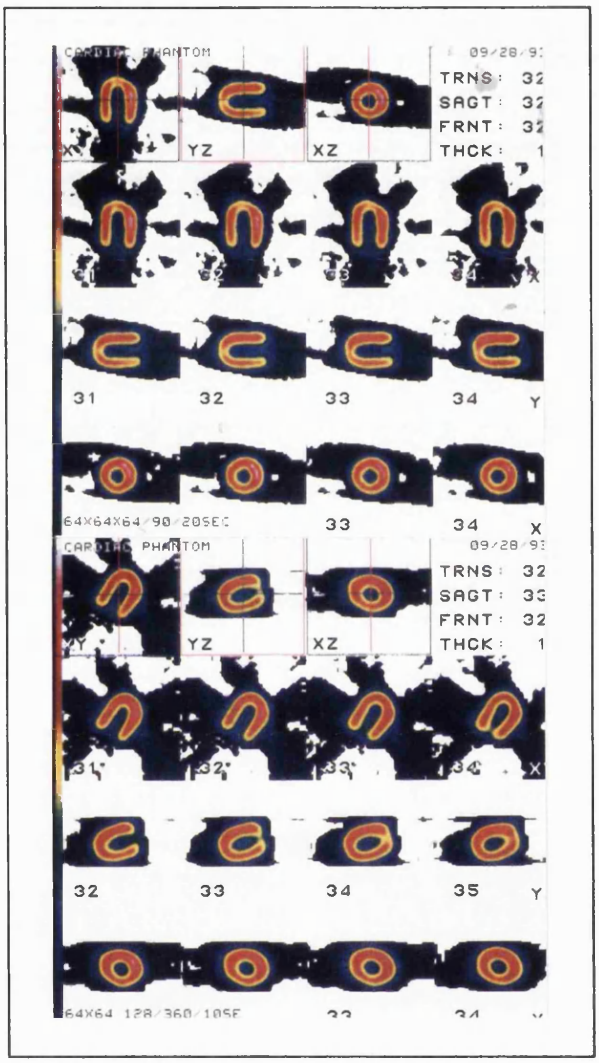

Figure 6.2: Comparison of 180° (upper) and 360° (lower) images. Marked reduced uptake in the apex is noted in the 180° data, whilst the short axis slices of the 360° data demonstrate distortion of the circular shape.

Figure 6.3. : 3-D surface images of the Hoffman brain phantom are displayed in X, Y and Z planes.

6.3. Limitations

The system had following limitations at the time of assessment:

1. The capability for each detector to rotate 360°. This is important for quality control, as it is not possible to assess COR for each head. This would also be useful when there was a failure of one detector. We understand from the manufacturers that such a facility will be available during 1994.

2. Whilst performing 180° SPET, the heads could not be positioned properly at 90° close to each other, and left a dead space between the in-edges. This dead space was much more than with the IGE Optima dual detector SPET system.

3. 180° cardiac SPET is not possible in the prone position with detectors in the 90° configuration.

4. Quality control is very crucial for good quality SPET images and it becomes more important using multidetector SPET systems. It is important to make sure that there is no misalignment between the detectors. The software for quality

assurance of centre of rotation offset was not available but we understand that recently software has been made available although each detector is still not capable of 360° data acquisition.

5. It was observed that the software for the automated reorientation of the cardiac SPET studies was not implemented and therefore the reorientation of the reconstructed slices is operator dependent. Again, we understand that a new version of software has been released, making reorientation easier. The software for 3-D surface image display was found to be best on this system.

6. Attenuation correction was not implemented.

8. Although the acquisition terminal is separate from the processing station, it was noted that whilst trying to reconstruct SPET data during another SPET acquisition the system crashed and needed to be rebooted. The data from the acquisition in progress was lost. This was a frequent problem, particularly when reconstructing 128x128x128 SPET data.

6.4. Clinical Experience

Due to the limitations discussed above it was not possible to assess the system completely.

20 patients had thallium-201 myocardial perfusion SPET during one week. It was noted that patients were being injected 100.0 MBq of thallium-201. This was being done because images obtained were of insufficient resolution (figure 6.4) and diagnostic accuracy. The main reason for this, however, was incorrect patients positioning causing the detectors to be far away from the patient. Whenever an attempt to reduce the radial distance was made the detectors moved away due to automatic prescribed safety reasons. When the closest arc could be obtained the resolution of the images improved (figure 6.5, 6.6).

The advantage of such a system with variable geometry is that it could be used for whole body planar imaging. The system is provided with convergent collimators for this purpose. The images obtained by such collimators contained sufficient clinical information, but were of poor resolution.(Figure 6.8).

6.5. CONCLUSION

Our impression is that this multidetector system is not ready for introduction into clinical practice. Good quality studies were only seen with somewhat higher radiation dose delivered with the given tracer. As mentioned before, hardware and design modifications are still required. Once the system is upgraded, it could be the ideal multidetector system, allowing for rapid 180°, 360° SPET acquisition, as well as multiplane planar imaging.

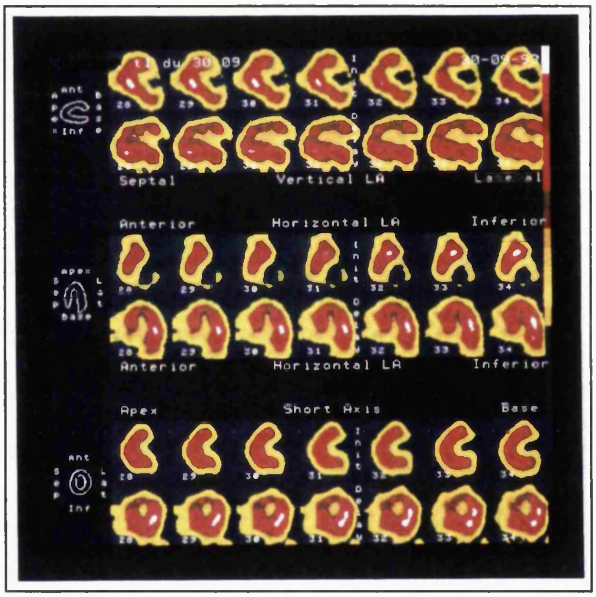

Figure 6.4: Thallium-201 stress/redistribution study of a patient for assessment of his myocardial perfusion status. The images demonstrate reversible ischaemia in anterior and lateral walls. The quality of images is not excellent, despite injecting 100 MBq of thallium-201.

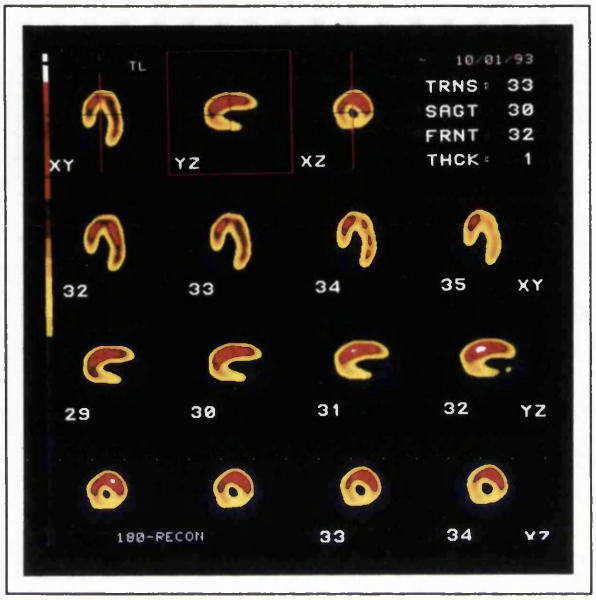

Figure 6.5: Resting thallium-201 study. In comparison to figure 6.4 higher resolution images could be obtained, as it was possible to get the detectors closer to the patient.

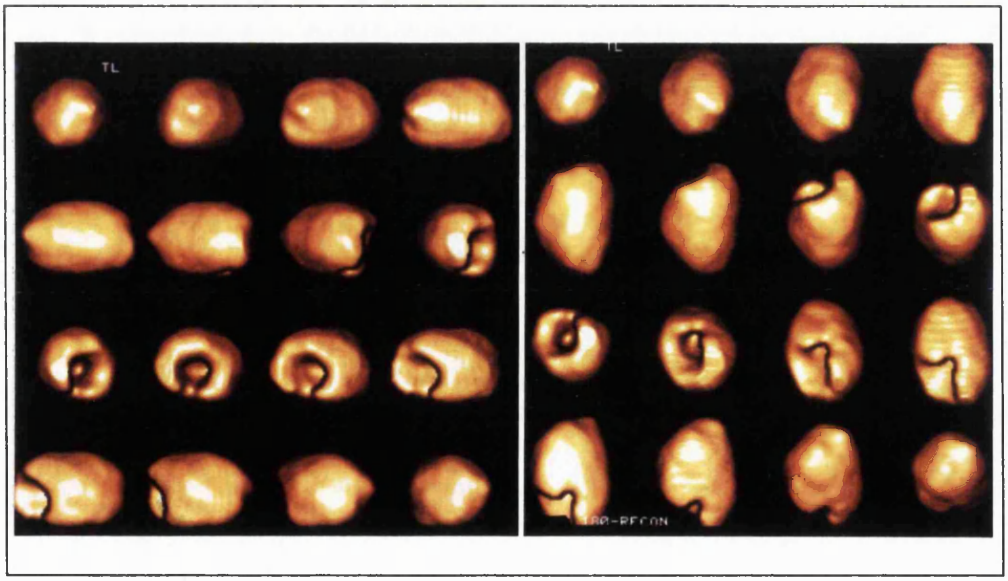

Figure 6.6: 3-D surface display of the thallium-201 resting study, shown in figure 6.5. The images are displayed in x, y and z planes. A small defect in the basal inferior wall is noticed.

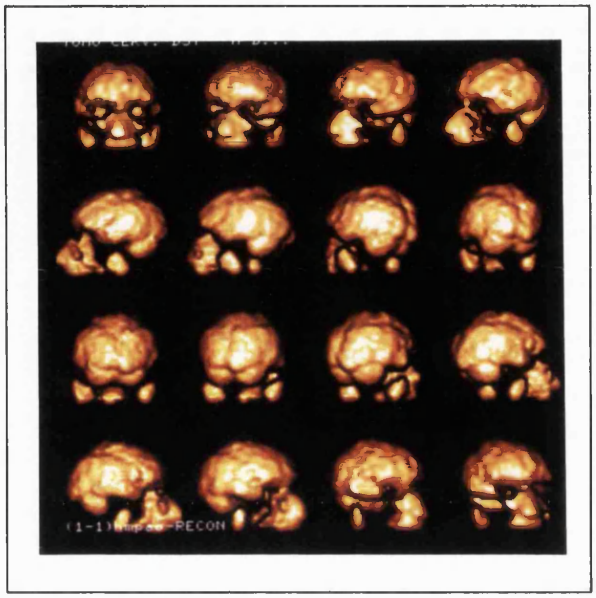

Figure 6. 7: 3-D surface display of a normal Tc-99m HMPAO SPET study.

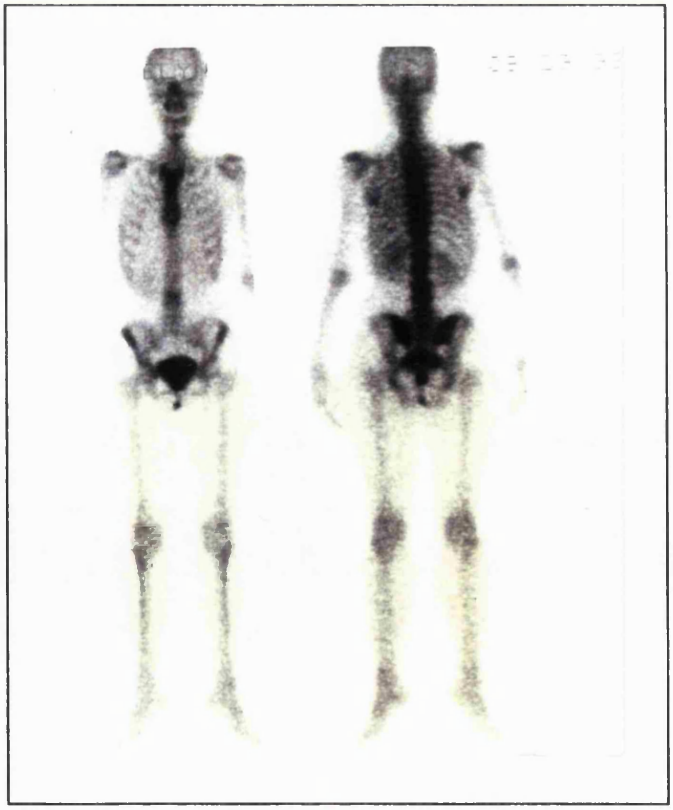

Figure 6.8: Simultaneously acquired whole body bone scan (anterior and posterior views) is displayed. The scan was acquired using the converging collimators.

SECTION C

Discussion

Chapter 7

Discussion

A high performance multidetector SPET systems should have tomographic spatial resolution of the order of 10 mm (FWHM). This study demonstrates that this was achievable by three of the systems investigated. (Table 7.1). For best performance attention must be paid to detector positioning, acquisition arc, acquisition time, collimator selection and reconstruction algorithms. The interplay between these factors determines the final image quality.

Collimator	IGE 400XCT	IGE Neurocam	Toshiba GCA-9300A	IGE Optima	Sopha DST
HR	10.3	9.0	10.2	10.0	-
SHR FB	-	-	9.0	-	-
LE UHR	-	-	-	-	10.5

Table 7.1 : Comparison of tomographic resolution using Tc-99m line souces.

7.1. Improved image quality

The quality of an image can be described by its signal/noise ratio (Shosa et al., 1981). This directly affects diagnostic and quantitative accuracy. For example, it has been shown that Fourier based restoration filtering, which increases an image's signal/noise ratio (King et al., 1984), enhances not only the diagnostic accuracy, as assessed by receiver operating characteristic (ROC) analysis (King et al., 1983) but also quantitative accuracy as assessed by phantom work and animal studies (Links et al., 1991). In essence, an important task for nuclear medicine imaging is to increase the signal/noise ratio of its scanning procedures.

A further goal for all SPET systems is to improve the contrast in an image.

The greater the contrast, the better the signal. Contrast is maintained by avoiding blurring, due to contamination of counts from regions of higher activity into regions of lower activity and vice versa. Therefore, the spatial resolution and contrast are closely related with each other. Inclusion of any scattered photons in the image reduces contrast (Sorenson et al., 1987). The imaging geometry of any SPET system, along with its energy resolution determines the amount of scatter present.

To achieve a high signal/noise ratio, high resolution and high sensitivity are required. In Nuclear Medicine, nevertheless there is always a compromise between resolution and sensitivity. The new multidetector SPET systems have the capability to reduce this problem. Signal/noise ratio may be increased either by **increasing contrast**, through increasing spatial resolution or **decreasing noise** through increasing the sensitivity. In this study, both of these phenomena have been well demonstrated. The Toshiba GCA-9300 three detector system resulted in high resolution SPET images in eight minutes with high resolution collimators (Chapter 4). On the other hand, sensitivity was increased (for thallium-201) using the IGE-Optima dual-detector gamma camera, with general purpose collimator and an acquisition time of 11 minutes for stress data (Chapter 5). For brain imaging, high resolution images were achievable either by using ultra high resolution collimators for the Sopha-DST dual-detector gamma camera, or increasing sensitivity by using the three-detector configuration like IGE-Neurocam or Toshiba-GCA9300.

A)INREASED RESOLUTION: This study suggests that with multidetector SPET systems, high resolution collimators should be used. The benefit of high resolution, even with the loss of sensitivity has also been suggested by others (Mueller et al., 1986, Moore et al., 1992).

To overcome the loss of sensitivity, which occurs with higher resolution collimators, Toshiba has manufactured fan-beam collimators. It has been demonstrated in this study that using such collimators, resolution comparable to parallel hole collimators was achievable, with concurrent higher sensitivity (Chapter 4). The disadvantage of these collimators is the need for special reconstruction algorithms and limited field of view. Therefore, such collimators

may find their place only in brain SPET, whilst for other systems parallel hole, high resolution collimators will remain the best choice.

Effect on Quantification: It is difficult to link increased resolution with diagnostic accuracy directly, but there is a relation in SPET between resolution and quantitative accuracy (Kojima et al., 1989). Table 7.2 gives a comparison of grey to white matter ratios using the Hoffman brain phantom and for different systems. With the new developments in computer technology it is also possible to interlink between different imaging modalities such as SPET/CT/MRI. The high resolution images could be superimposed with images from CT/MRI enhancing the clinical information and future research into clinical practice.

Collimator	IGE Neurocam	Toshiba GCA-9300A	IGE Optima	Sopha DST
HR	2.14	1.9	2.4	-
SHR FB	-	2.4	-	-
LE UHR	-	-	-	2.6

Table 7.2: Comparison of grey/white matter ratio in Hoffman phantom. (Theoretical value=4:1)

B) INCREASED SENSITIVITY: With multidetector systems, the sensitivity goes up by a factor equal to the number of heads: a two-detector system has double the sensitivity, and a three-detector system has three times the sensitivity, of a comparable single detector system. Table 7.3 lists the tomographic volume sensitivities of three different systems in comparison to a single detector system.

Collimator	IGE 400XCT	IGE Neurocam	Toshiba GCA-9300A	IGE Optima
HR	7.6	30.0	33.8	18.5
SHR FB	-		34 .8	-

Table 7.3: Comparison of tomographic volume sensitivity of different systems.

7.2. Influence of acquisition arc on the system choice

Using multidetector systems, it is tempting to trade-off increased sensitivity for even higher spatial resolution, and indeed that will become a standard in future clinical practice (Mahmood S et al., 1992). However, it is important to note that the increase in sensitivity possible with multidetector systems may only be realized for 360° acquisitions. Therefore, an essential issue in the determination of increased sensitivity is the acquisition arc. These relationships are shown in table 7.4.

	360° Acquisition		180° Acquisition	
	Acq. time (min.)	**Relative Sensitivity**	**Acq. time (min.)**	**Relative Sensitivity**
Single detector	30	1	30	1
Double detector (opposed heads)	15	2	30	1
Double detector (heads at 90°)	15	2	15	2
Three detectors	10	3	20	1.5

Table 7.4: Illustration of relative sensitivity as of different detector configurations for 180° and 360° SPET. This assumes that all detectors are of equivalent performance.

Several groups of investigators have convincingly demonstrated the advantages of 180° data acquisition over 360° acquisition for thallium-201 myocardial perfusion SPET (Eisner et al., 1986). Many others have argued that 180° acquisition produces artefacts or a loss in quantification accuracy (Go et al., 1985). In clinical practice most centres utilise 180° for data acquisition. Using a cardiac phantom, it has been demonstrated in chapters 5 and 6, that even with Tc-99m agents, a 180° acquisition protocol leads to images of higher contrast. With 180° acquisition, a three-detector system such as Toshiba GCA-9300A has 1.5 times sensitivity of a single detector system; a two-detector

system which has heads orientated at 180° has no advantage over single detector system (as the sensitivity is similar to that of a single detector system). In this regard the system of choice will be one having either detectors fixed at 90° with respect to each other (IGE Optima) or of variable geometry, which permits the detectors to be orientated at 90° as in Sopha DST. Similar cameras from two other manufacturers are also available in market. Such systems offer twice the sensitivity of a single detector system.

7.3. Clinical impact of increased sensitivity

The improvement in sensitivity of multidetector systems translates into clinical practice in at least two ways.

Firstly there is an improvement in the image quality with an improvement in the signal/noise ratio. Secondly there is an increase in patient throughput.

INCREASED THROUGHPUT: This study has demonstrated that the increased sensitivity achieved results in optimal imaging associated with shorter acquisition times. Such an approach would ***increase the patient throughput.*** (Mahmood et al., 1992, Buscombe et al., 1992, 1993).

In practice, however, many factors influence patient throughput. These include patient set-up time, data processing and patient flow through the department. The emergence of new Tc-99m based compounds such as tetrofosmin with rapid liver clearance may further help to improve the patient throughput (chapter 5).

PATIENT MOTION: One of the potential advantages of a decrease in acquisition time is improvement in image quality by ***reduced patient motion*** over shorter acquisition periods. This will allow the facility of SPET to be extended to ***old aged, severely ill*** and ***paedriatic patients***, who are more prone to motion. The advantage of reducing imaging time in terms of **reducing motion artefacts** has been demonstrated by comparing thallium-201 SPET studies performed on a dual-detector gamma camera to those performed on a single-detector system (chapter 5).

DYNAMIC SPET: A short acquisition time is of great importance in optimum imaging of certain tracers with rapid clearance from the organ of interest, as

epitomized by Tc-99m teboroxime (Stewart et al., 1990). For rapidly clearing radiotracers, very short acquisitions are required to avoid image artefacts and errors in quantification (Bok et al., 1987, Links et al., 1991, O'Connor et al., 1992).

The other advantage of shorter acquisition is that ***repeated acquisitions*** could be performed in the same patient, in order to understand the distribution of new tracers in the organ of interest. We were able to perform repeated acquisition of 10 minutes each in five patients, in order to optimise the imaging time for Tc-99m tetrofosmin (Chapter 5). Similarly, using three detector systems such as Toshiba GCA-9300A and IGE Neurocam, it was possible to perform dynamic / sequential brain SPET studies using I-123 iodobenzamide (IBZM) (Figure 4.10).

DECREASED RADIATION DOSE: The other potential advantage of increased sensitivity is a ***reduction in the administered activity.*** This is helpful in two ways. Whilst using the same standard dose of radiotracer, the dose can be split into two. This **split-dose** protocol has been applied in neuroimaging and neuroactivation studies with acceptable spatial resolution (George MS et al., 1992). The other advantage of reduction in dose is **a reduction in radiation exposure** to patients. The recent recommendations of the International Commission for Radiological Protection (ICRP) may lead to an even stricter set of rules and regulations demanding further reduction in these exposures (IRCP., 1990). This is an important advantage, particularly in the context of studies with significant radiation exposure (e.g. 25 mSv for a standard thallium-201 heart study).

ANTIBODY, RECEPTOR IMAGING: Many nuclear medicine procedures still suffer from poor information density. Many tracers (antibodies, receptor ligands, flow tracers) concentrate in tissue in minute amounts. The multidetector systems allow ***maximisation of information density*** if desired or required. The improvement in image quality is testimony to this improvement.

7.4. Cost Effectiveness

The capital cost of a multidetector SPET system is moderate, when compared to Spiral CT, PET or MRI and of the order of £300,000. Maintenance costs can be estimated at 8-10% of initial purchase price per year, say 30,000 per annum. A multidetector system does not typically require more floor space, nor does it require an additional technologist. The annual salary of a radiographer is approximately 20,000. The running cost (maintenance cost + depreciation / capital cost over 10 years) will be around 80,000 per annum. Using a standard 16 minute acquisition for all SPET studies like heart, brain, kidney and skeletal and allowing 14 minutes set up time for each study, it is possible to perform 14 studies/day in a 7-hour working day. If studies were performed on five days a week for 50 weeks, then 3500 studies could be performed annually, giving a cost of approximately 23.00 per study. At this cost the capital expenditure of such a system would be justified in any department with a high throughput of studies, which use or potentially use SPET. These costs do not include costs of radiopharmaceuticals and other overheads.

Of the systems included in this study, only two have been used to their full potential in clinical and research routine (IGE Neurocam and IGE Optima). The table below describes the total number of studies performed during last five years.

YEAR	Thallium-201 myocardial perfusion SPET	Tc-99m HMPAO SPET
1989	489	71
1990	668	248
1991	552	291
1992	748	360
1993	1172	316

Table 7.5: The number of thallium-201 and Tc-99m HMPAO SPET studies performed during the last five years at the Institute of Nuclear Medicine.

It is obvious from table 7.5, that there has been an increased workload for thallium-201 myocardial perfusion SPET. Before 1993, all the studies were performed on the single-detector systems (IGE 400XCT or IGE 400T). In 1993, all these studies were performed on the IGE Optima. During one year thallium-201 SPET was performed on 1172 patients, which means almost a double number of acquisitions (2344) (in view of the additional redistribution studies). Approximately 15 radionuclide ventriculography studies are also being performed every week, with an average of at least two acquisitions per patient. The camera is also available for small organs SPET (such as renal DMSA) or skeletal / brain SPET, whenever needed. The camera is being used only four days per week. According to the calculations for the cost effectiveness, as discussed earlier this is an economically viable system. This is important, as new changes and reductions in budgets in the health system demand more economical imaging systems.

A dual-detector system with detectors of variable geometry may be a better choice, if there is more need for 360° acquisitions. It is apparent that a department which will use a new system for both planar whole body scanning and a mixture of SPET studies might find that a large field of view gamma camera, with detectors opposed at 180° best meets their needs, whilst a department which will use a new system exclusively for cardiac SPET will find a dual detector 90° (e.g. IGE Optima) system best. A department which will also use the system for brain SPET studies may choose between a dual-detector system with either variable detector geometry (like Sopha DST or ADAC-Vertex) or a three-detector system. There appears to be a trend for two-detector systems rather than single or triple-detector systems (table 7.6).

System type	1991	1992	% change
Single detector	700+	700+	0%
Two detector	90	180	+ 100%
Three detector	80	50	- 38%

Table 7.6: Approximate number of gamma cameras sold in United States (Links JM. 1993)

7.5. Multi-plane planar Imaging

Another benefit of some of the multidetector systems is the ability to acquire multiple planar views simultaneously. This may be helpful in certain clinical studies, where planar imaging is routine. The field of view is an important factor here.

7.5. Quality Control

Although the basic quality control for these multidetector SPET systems is similar as for any other SPET system, it should be carried out more often in order to assess any misalignment and centre of rotation errors and matched detector response. A high performance system should facilitate quality control and calibration procedures. For example, centre of rotation calibration should be performed automatically. Two manufactures (Toshiba and Sopha) do not supply any software for centre of rotation assessment. The manufactures of the Toshiba GCA-9300A assume that there is a single centre of rotation value for all of the detectors. The centre of rotation corrections for Toshiba GCA-9300A are set at the factory and cannot be changed. They argue that a single correction factor used for all positions and all projections is insufficient and that many correction factors should be used; therefore, not allowing on site data acquisition for this purpose. On the contrary, in IGE systems the centre of rotation values are different for each detector and therefore necessitate strict control. It is obvious that any errors can significantly influence the presence of SPET reconstruction artefacts.

Gantry design can significantly affect the ease with which the quality control tests can be performed. It is typically difficult to acquire an intrinsic uniformity flood with a point source on a ring type gantry system like IGE Neurocam, whilst it is easier with IGE Optima.

Chapter 8

Conclusions

---

i). The four mltidetector SPET systems evaluated have a spatial resolution of the order of 10 mm at Full Width at Half Maximum (FWHM).

ii). The multidetector systems also offer increased sensitivity. This relates to the number of detectors, and ranges between 9.2-11.2 kcps/(MBq/ml)cm per detector. Increased sensitivity may be translated into increased patient throughput, by reducing acquisition time. In turn, reduction in acquisition time helps to reduce patient motion artefacts, and also extends the facility of SPET to old, severely ill and paedriatic patients.

iii). Shorter acquisition times also help in repeated SPET acquisitions, which is helpful in the assessment kinetics of new tracers.

iv). The multidetector SPET systems are cost-effective. SPET studies should be performed more frequently in order to obtain the best benefit. For cost effectiveness, a minimum of 14 studies/working day of a five-day work should be performed. This gives a cost of approximately 23.00 per study. At this level the capital expenditure of a multidetector SPET system should be justified. It should be noted that the above cost does not include the cost of the radiopharmaceuticals and other overheads.

v). For myocardial perfusion imaging, 180° SPET acquisition should continue, even for Tc-99m based radiopharmaceuticals.

vi) The study has shown that an 11 minute, 180° SPET acquisition is appropriate for myocardial perfusion studies with thallium-201 (10 minutes of data acquisition for Tc-99m myocardial perfusion agents is sufficient).

vii). For SPET of brain, skeletal system and kidneys a 16 minute, 360° acquisition protocol is appropriate.

viii). The two detector SPET system designed for cardiac imaging could be successfully used for 360° SPET acquisition of other organs.

ix). In this study, I have shown that the technical specifications quoted by the manufacturers are obtained under ideal conditions and do not necessarily give the most useful definition of a camera system performance. Clinical images obtained under routine conditions are much more realistic indicators of a camera system performance and its ease of use, and should be performed as a part of system assessment.

Chapter 9

Future directions and recommendations

9.1. Future directions for multidetector SPET system

9.1.1. Attenuation Correction

Tissue attenuation plays an important role in the diagnostic and quantitative accuracy of SPET. (Manglos et al.,1987). This is often relevant in myocardial perfusion SPET (Depuey et al., 1989) with known differences in the patterns observed in scans of men and women (Eisner et al., 1988). Much work is thus being done on attenuation correction in SPET. Most of these methods rely on a transmission scan, acquired either before or during the emission scan (Ljunberg et al., 1990, Manglos et al., 1991). If this form of attenuation correction is to become a clinical reality, it will require a multidetector system to keep the total imaging time reasonably low. For example, in a three-detector system one of the heads could acquire fan-beam transmission data whilst the other two detectors simultaneously acquire parallel or fan beam emission data (Gulberg et al., 1992). Another example is in a two-detector system like the IGE Optima or Sopha DST, where the detectors have 90° geometry; one of the heads could acquire parallel-beam transmission data from a scanning line source (Bailey et al., 1992), whilst the other detector simultaneously acquires parallel beam emission data. It is still not absolutely clear whether, clinically acceptable methods of attenuation correction will require 360° projection data.

9.1.2. Reconstruction algorithms

Several promising reconstruction algorithms have been proposed which make better use of 360° projection data (Miller et al., 1992). These algorithms are theoretically better as they take into account the varying spatial resolution and photon attenuation due to varying depth. There is, however, hardly any clinical evidence that they are superior to filtered back-projection (Gilland et al., 1992).

If such approaches of reconstruction are implemented, the use of multidetector SPET systems will clearly expand.

9.1.3. PATIENT SETUP

Patient setup in these systems is simplified. One system (Sopha DST) included in this study offered a non-circular orbit. It was felt that in the majority of the patients it was difficult to place the detectors closer to the body (chapter 6), than for circular orbits, thereby decreasing the advantage of increased sensitivity and resolution. It is hoped that in the next generation of these systems these problems will be rectified. We understand that with the advancement of technology, automated patient setup modifications will soon be implemented in some of the instruments, permitting improved body contouring and patient positioning.

9.1.4. SPET USING POSITRON EMITTERS

Metabolic imaging using positron-emitters can provide unique information. This is often applied to the study of the heart, the brain and in oncology. A recent development in SPET is the use of higher energy collimators for the imaging of PET (positron emission tomography) tracers, specially F-18 fluoro-deoxy-glucose (FDG) and Rubidium-18.

9.1.5. DATA-EXCHANGE BETWEEN DIFFERENT MANUFACTURERS

At present, the transfer of data from one manufacture's computer to the computer of another manufacturer (INTER-FILE) is limited. This is basically due to difference in hardware, software and the competition between the manufacturers. Some work has been directed in recent years in this direction. At least one manufacturer included in this study, who offered the facility of data exchange, had under-developed software.

9.2. Recommendations

As a result of this study, several recommendations can be made:

i) All these SPET systems need further development and improvement both in hardware and software.

ii) To provide ease to the clinician, the manufacturers must develop the facility of reliable data transfer between computers of different manufacturers. This

will help a department to operate systems from different manufacturers using a single workstation.

iii) It is also recommended that a body should be constituted at European/UK level, to standardise hard and software from different manufacturers.

iv) It is important that strict quality control is implemented.

v) Manufacturers who have not implemented software for quality control should do so without delay.

vi) 180° SPET should continue to be used for myocardial perfusion imaging, as a clinically useful and cost-effective method for myocardial perfusion scintigraphy.

vii) SPET studies should be performed more often, since patient care will improve from its use.

viii) Manufacturers and users must work together to further streamline this technology for routine clinical use.

ix) Decisions on equipment purchase should also be based on clinical need.

x) A case for the multidetector technology can now be made.

References

AAPM Report No.22 Rotating scintillation camera SPECT acceptance testing and quality control (1987) *American Association of Physicists in Medicine*, New York, USA.

Allen HC, Risser JR, Gree JA (1954) Improvements in outlining of thyroid and localisation of brain tumours by the applications of sodium iodide gamma-rays spectrometry techniques. Proceeding of the 2nd Oxford *Radio-isotope Conference, Oxford*, July 19-23. N.Y. Academic Press Vol 1:76

Almquist H, Palmer J, Ljungberg M, Wollmer P, Strand SE, Jonson B (1990) Quantitative SPECT by attenuation correction of the projection set using transmission data: evaluation of a method *Eur J Nucl Med* 16:587-594

Ancri D, Basset JY, Lonchampt MF, Edward C. (1987) Diagnosis of cerebral lesions by thallium-201. *Radiology* 128:417-422

Anger HO (1958) Scintillation camera *Rev Sci Instum* 29:23

Anger HO, Rosenthall DJ (1959) Scintillation camera and positron camera. *Med. Radioisotope Scanning* IAEA Vienna, Austria p:59

Aswegen A, Alderson PO, Nickoloff EL, Householder DF, Wagner HN (1980) Temporal resolution requirements of left ventricular time-activity curves *Radiology* 135:165-170

Bailey DL, Hutton BF, Walker PJ (1987) Improved SPECT using simultaneous emission and transmission tomography *J Nucl Med* 28:844-851

Baily DL, Eberl S, Tan P, Meikle SR, Fulton RR, Hutton BF.(1992) Implementation of a scanning line source for attenuation correction with simultaneous emission/transmission SPECT (Abstract) *J Nucl Med* 33:901

Beller GA, Watson DD (1991) Physiological basis of myocardial perfusion imaging with the technetium-99m agents *Semin Nucl Med* 21:173-181

Berche C, Mach JP, Lumbroso JD, Langlais C, Aubry F, Bucheger F. (1982) Tumour scintigraphy for detecting gastrointestinal and medullary thyroid cancers: first clinical results using radiolabelled monoclonal antibodies against carcinoembryonic antigen. *Br Med J* 285:1447-1451

Bice AN, Clausen M, Loncaric S, Wagner HN (1987) Comparison of transaxial resolution in 180^0 and 360^0 SPECT with rotating scintillation camera. *Eur J Nuc Med* 13: 7-11

Birnbaum BA, Weinreb JC, Megibow AJ, Sanger JJ, Lubat E, Kanamiller H, Noz ME, Bosniak MA. (1990) Definitive diagnosis of hepatic haemangiomas: MR imaging versus Tc-99m labelled red blood cell SPECT.
Radiology 176:95-101

Black HL, Hawkins RA, Kim KT, Becker DP, lerner C, Marciano D. (1989) Use of thallium-201 SPECT to quantitate malignancy of gliomas.
J Neurosurg. 71:342-346

Blokland KA, Reiber HH, Pauwels EK, (1992) Quantitative analysis in single photon emission tomography (SPET) *Eur J Nucl MED* 19:47-61

Bok BD, Bice AN, Clausen M, Wong DF, Wagner HN. (1987) Artefacts in camera based single photon emission tomography due to time activity variation. *Eur J Nucl Med* 13:439-442

Bonow RO, Dilsizian V, Cuocolo A, Bacharach SL (1991) Identification of viable myocardium in patients with chronic coronary artery disease and left ventricular dysfunction. Comparison of thallium scintigraphy with reinjection and PET imaging with F-18 fluorodeoxyglucose *Circulation* 83:26-37

Bonte FJ, Hom J, Tintner R, Weiner MF. (1991) Single photon tomography in Alzheimer's disease and the dementias. *Semin Nucl Med* 20:303-352

Botvinick EH, Taradesh MR, Shames DM, Parmley WW. (1978)Thallium-201 myocardial perfusion scintigraphy for the clinical classification of normal, abnormal and equivocal electrocardiographic stress tests.
Am J Cardiol 41:43-51

Brown KA (1991) Prognostic value of thallium-201 myocardial perfusion imaging. A diagnostic tool comes of age. *Circulation* 83:363-381

Brownell GL, Sweet WH (1953) Localisation of brain tumours with positron emitters *Nucleonics* 11:40

Buscombe JR, Townsend CE, Clarke G, Kouris K, Ell PJ. (1992) Fast skeletal SPET in the assessment of chest metastases in young patients with primary bone tumours.(Abstract) *Nucl Med Commun* 13: 248.

Buscombe JR, Townsend CE, Kouris K, Clarke G, Mahmood S, Jarritt PH, Ell PJ. (1993) Clinical high resolution skeletal single photon emission tomography using a triple-headed gamma camera. *Brit J Radiol* 66:817-822

Busemann-Sokole E (1987) Measurement of collimator hole angulation and camera head tilt for slant and parallel hole collimators used in SPECT.
J Nucl Med 28:1592-1598

Butler RE, Costa DC, Greco G, Ell PJ, Katona CLE (1992) Diagnosing Alzheimer's disease *BMJ* 304:574-575

Cassen B, Curtis L (1951) The in vivo delineation of thyroid glands with an automatically scanning detector. University of California, Los Angeles Report 130

Cerqueira MD, Matsuoka D, Ritchie JL, Harp GD ((1988) The influence of collimators on SPECT center of rotation measurements. Artefact generation and acceptance testing. *J Nucl Med* 29:1393-1397

Chang LT (1978) A method for attenuation correction in radionuclide computed tomography *IEEE Trans Nucl Sci* NS-25:638-643

Chatal JF, Saccavini JC,, Douillard JY, Fesus SM. (1985) Comparison of SPECT imaging using monoclonal antibodies with computed tomography (CT) and ultrasonography (US) for the detection of recurrence of colorectal carcinoma: a prospective clinical study (Abstract) *J Nucl Med* 26:15

Coleman RE, Jaszczak RJ, Cobb FR (1982) Comparison of 180^0 and 360^0 data collection in thallium-201 imaging using SPECT. *J Nuc Med* 23: 655-660

Collier BD, Hellman RS, Kranow AZ. (1987) Bone SPECT. *Seminars in Nucl Med* 17: 247-266

Collier BD, Carrera GF, Meyer GA. (1983) Internal derangement of temporo-mandibular joint: detection by single photon computed tomography. *Radiology* 149:557-561

Collier BD, Johnson RP, Carrera GF, Meyer GA, Schwab JP, Flatley TJ, Isitman AT, Hellman RS, Zielonka JS, Knobel J. (1985) Painful spondylolysis or spondylolisthesis studied by radiography and single photon emission tomography. *Radiology* 154: 207-211

Collier BD, Carrera GF, Johnson RP, Isitman AT, Hellman RS, Knobel J, Finger WA, Granyo JE, Malloy PJ, (1985) Detection of femoral heads avascular necrosis in adults by SPECT. *J Nucl Med* 26: 979-987

Corbett JR, Jansen DE, Lewis SE (1985) Tomographic gated blood pool radionuclide ventriculography: Analysis of wall motion and left ventricular volumes in patients with coronary artery disease *J Am Coll Cardiol* 6:349-358

Corne RA, Gotsman MS, Weis A. (1979) Thallium-201 scintigraphy in diagnosis of coronary arteriography. *BHJ* 41:575-583

Delaloye B, Bischof-Delaloye A, Grob JP. (1985) SPECT with I-123 labelled F(ab')2 fragments from monoclonal anti-CEA antibodies in colon carcinoma (Abstract). *J Nucl Med* 25:17

Deland FH, Shih WJ. (1984) The status of SPECT in tumour diagnosis. *J Nucl Med* 25:1375-1379.

DePuey EG, Gracia EV. (1989) Optimal specificity of thallium-201 SPECT through recognition of imaging artefacts *J Nucl Med* 30:441-449

Douli V, Brostoff J, Costa DC, Ell PJ (1992) rCBF SPET in patients with Myalgic Encephalomyelitis (Abstract) *Nucl Med Commun* 13:222

Eisner RL, Nowak DJ, Pettigres R, Fajman W (1986) Fundamentals of 180^0 acquisition and reconstruction in SPECT imaging. *J Nucl Med* 27:1717-1728

Eisner RL, Tamas MJ, Cloninger K, Shonkoff D, Oates JA, Gober AM, Dunn DW, Malko JA, Churchwell AL, Patterson RE. (1988) Normal SPECT thallium-201 bull's eye display: gender differences. *J Nucl Med* 29:1901-1909

Ell PJ, Cullum I, Costa DC, Jarritt PH, Hocknell JML, Lui D, Jewekes RF, Nowotnik DP, Pickett RD, Neirinckx RD (1985) A new regional cerebral blood flow mapping with Tc-99m labelled compound *Lancet* ii:50-51

Ell PJ, Costa DC (1992) The role of nuclear medicine in neurology and psychiatry. *Current Opn in Neurol and Neurosurg* 5:863-869

Fawcett HD, Sayle BA. (1989) SPECT versus planar liver scintigraphy: is SPECT worth it ? *J Nucl Med* 30:57-59

Fintel DJ, Links JM, Brinker JA, Frank TL, Parker M, Becker LC. (1989) Improved diagnostic performance of exercise thallium-201 single photon emission tomography over planar imaging in the diagnosis of coronary artery disease: a receiver operating characteristic analysis.
J Am Coll Cardiol 13:600-612

Gates GF (1988) SPECT imaging of lumbo-sacral spine and pelvis.
Clin Nucl Med 13:907-914

Genna S, Smith AP (1988) The development of ASPECT, an annular single crystal brain camera for high efficiency SPECT *IEEE Trans Nucl Sci* 35:654-658

George MS, Ring HA, Costa DC, Ell PJ, Kouris K, Jarritt PH (1991) *Neuroactivation and Neuroimaging with SPET.* Springer-Verlag, London

Gilardi MC, Bettinardi V, Todd-Pokropek A, Milanesi L, Fazio F (1988) Assessment and comparison of three scatter correction techniques in single photon emission tomography. *J Nucl Med* 29:1971-1979

Gill JB, Moore RH, Tamaki N, Miller DD, Barlai-Kovach M, Yasuda T, Boucher CA, Strauss HW. (1986) Multigated blood pool tomography: New method for the assessment of left ventricular function. *J Nucl Med* 27: 1916-1924

Gilland DR, Tsui BMW, Metz CE, Jaszczak RJ, Perry JR. (1992) An evaluation of maximum likelihood expectation maximization reconstruction for SPECT by ROC analysis *J Nucl Med* 33:451-457

Gilland DR, Tsui BMW, McCartney WH, Perry JR, Berg J (1988) Determination of the optimum filter function for SPECT imaging. *J Nucl Med* 29:643-650

Gillen GJ, McKilop JH, Hilditch TE, Davidson JK, Elliott AT. (1988) Digital filtering of the bladder in SPECT bone studies of the pelvis. *J Nucl Med* 29: 1587-1595.

Go RT, MacIntyre WJ, Houser TS, Pantoja M, O'Donnell JK, Feiglin DH, Sufka BJ, Underwood DA, Meaney TF. (1985) Clinical evaluation of 360^0 and 180^0 data sampling techniques for transaxial SPECT thallium-201 myocardial perfusion imaging. *J Nucl Med* 26: 695-706

Gould KL, Noninvasive assessment of coronary stenoses by myocardial perfusion imaging during pharmacologic coronary vasodilation. I. Physiologic basis and experimental validation. *Am J Cardiol* 1978:41:267-278

Graham LS (1986) Automatic tunning of scintillation cameras: a review *J Nucl Med Tech* 14: 105-110

Graham LS (1989) A rotational quality assurance program for SPECT instrumentation *Nucl Med Annua*l, Raven Press Ltd, New York, USA :81-108

Gullberg GT, Zeng GL, Christian PE, Datz FL, Morgan HT (1991) Cone beam tomography of the heart using SPECT *Invest Radiol* 26:681-688

Gullberg GT, Tung CH, Zeng GL, Christian PE, Datz FL, Morgan HT. (1992) Simultaneous transmission and emission computed tomography using a three detector SPECT system (Abstract) *J Nucl Med* 33:901

Hagemeister FB, Fesus SM, Lamaki LM, Haynie TP. (1990) Role of gallium scan in Hodgkin's disease. *Cancer* 65:1090-1096

Halama JR, Henkin MD (1987) Quality assurance in SPECT imaging. *Applied Radiology* 12:41-50

Halama JR, Henkin RE, Friend LE (1988) Gamma camera radionuclide images: Improved contrast with energy-weighted acquisition. *Radiology* 169:533-538

Harper PV, Beck R, Charleston D, Lathrop K (1964) Optimisation of a scanning method using technetium-99m. *Nucleonics* 22:50

Hecht HS, Shaw RE, Bruce TR, Ryan C, Stretzer SH, Myler RK. (1990) Usefulness of tomographic thallium-201 imaging for detection of restenosis after percutaneous transluminal angioplasty. *Am J Cardiol* 66:1314-1318

Hellman RS, Tikofsky RS (1990) An overview of the contribution of regional cerebral blood flow studies in cerebral vascular disease : is there a role for single photon emission tomography? *Semin Nucl Med* 20:325-341

Helms CA, Kaplan P (1990) diagnostic imaging of the temporo-mandibular joint: recommendations for the use various techniques
Am J Roentgenol. 154:319-322

Hevesy G (1923) The absorption and translocation of lead by plants, a contribution to the application of the method of radioactive indicators in the investigation of changes of substances in plants *Biochem J* 17:439

Higley B, Smith FW, Smith T, Gemmell HG, Das Gupta P, Gvozdanovic DV, Graham D, Hinge D, Davidson J, Lahiri A (1991) Technetium-99m-bis[bis(2-ethoxyethyl) phosphino]ethane: human biodistribution, dosimetry and safety of a new myocardial perfusion imaging agent. *J Nucl Med* 34:30-38

Hisada K, (1991) *An atlas of second-generation SPECT*, Maruzen Planning Network Co., Japan.

Hisada K, Tonomi N, Miyamae T, Shanken J (1978) Clinical evaluation of tumour imaging with Tl-201 chloride. *Radiology* 129:497-500

Hoffman EJ, Cutler PD, Digby WM, Mazziota JC. (1990) 3-D phantom to simulate cerebral blood flow and metabolic images for PET.
IEEE Trans Nucl Sci 37:616-621

Hoffman EJ (1982) 180^0 compared with 360^0 sampling in SPECT. *J Nucl Med* 23:745-747

Hoh CK, Khanna S, Harris GC, Chen TT, Black KL, Blecker DP, Maddahi J, Mazziota JC, Marciano DM, Hawkins RA. (1992) Evaluation of brain tumour recurrence with thallium-201 SPECT studies: Correlation with FDG PET and histological results (Abstract) *J Nucl Med* 33:867

Holman BL, Johnson KA, Gerada B, Carvalho PA, Satlin A (1992) The scintigraphic appearance of Alzheimer's disease: prospective study using Tc-99m HMPAO SPECT. *J Nucl Med* 33:181-185

Holman BL, Gerada B, Johnson KA, Mendelson J, Hallgring E, Teoh SK, Worth J, Navia B (1992) comparison of brain perfusion in Cocaine abuse and AIDS dementia complex (Abstract) *J Nucl Med* 33:887

Ichihara T (1990) Development of a high resolution SPECT system. *Toshiba Med Rev* 33:29-35

International Commission on Radiological Protection (ICRP). 1990 Recommendations of the International Commission on Radiological Protection. *ICRP Publication* 60: Pergamon Press, New York: 1991

Ichihara T, Matsudaira M, Yamada M, (1991) Basic development of the Toshiba digital gamma camera, model GCA-9300A In: Hisada K (ed) *An Atlas of Second Generation SPECT.* Marizen Planning Network Co., Chapter III

Iskandrian A, Heo J, Nguyen T, Mercuro J (1991) Myocardial imaging with Tc-99m teboroxime: technique and initial results *Am Heart J* 121:889-894

Jacobson H, Larsson SA, Vesterskold L, Lindvall N. (1984) The application of single photon emission tomography to the daignosis of ankylosing spondylitis of the spine. *Br J Radiol* 57:133-140.

Jain D, Wackers FJ, McMahon, et al. (1992) Is there any redistribution with Tc-99m-tetrofosmin imaging; a quantitative study using serial planar imaging. (Abstract) *Circulation* 86(Suppl. I):I-46

Jain D, Wackers FJ Th, Mattera J, McMahon, Sinusas AJ, Zaret BL (1993) Biokinetics of technetium-99m-tetrofosmin: myocardial perfusion agent: implications for a one day imaging protocol. *J Nucl Med* 34:1254-1259

Jarritt PH, Ell PJ, Myers MJ et al., (1979) A new transverse section brain imager for single gamma emitters *J Nucl Med* 20:319-327

Jaszack R.. Industrial corner, Physical characteristics of SPET systems (1982) *J Comput Assist Tomog* 6:1205-1215

Jaszczak RJ, Greer KL, Floyd CE, Harris CC, Coleman RE. (1984) Improved SPECT quantitation using compensation for scattered photons *J Nucl Med* 25:893-900

Jobst KA, Smith AD, Barker CS, Wear A, King EM, Smith A, Anslow PA, Molyneux AJ, Shepstone BJ, Soper N, Holmes KA, Robinson JR, Hope RA, Oppenheimer C, Brockbank K, McDonald B. (1992) Association of atrophy of the medial temporal lobe with reduced blood flow in posterior parietotemporal cortex in patients with a clinical and pathological diagnosis.
J Neurol Neurosurg Psychiatry 55:190-194

Kanmaz B, Liu Y, Uzman G, Yu L, Uzman F, Uygur G, Akansel G, Gunes I, Krasnow AZ, Hellman RS, Collier BD (1992) SPECT vs planar bone scintigraphy in patients with low back pain. *J Nucl Med* 33:868.

Kaul S (1989) A look at 15 years of planar thallium-201 imaging.
Am Heart J 118:581-601

Kelly JD, Forster AM, Higley B et al. (1993) Technetium-99m-tetrofosmin as a new radiopharmaceutical for myocardial perfusion imaging. *J Nucl Med* 34:222-227

Keogan MT, Wraight EP, Antoun NM, (1991) Basal skull lesions: evaluation by emission tomography (SPECT) and X-ray computed tomography (CT) *Nucl Med Commun* 12: 257.

Keyes JW, Fahey FH, Harkness BA. (1990) Tips for high quality SPECT. *SNM Computer and Instrumentation Council News letter :1990*

Kim KT, Black HL, Marciano DM, Hawkins RA. (1990) Thallium-201 SPECT imaging for brain tumours: methods and results .*J Nucl Med* 31:965-969

Kimura K, Hashikawa K, Etani H, Uehara A, Kozuka T, Moriwaki H, Isaka Y, Matsumoto M, Kamada T, Moriyama H. (1990) A new apparatus for brain imaging: a four-head rotating gamma camera single photon emission tomograph *J Nucl Med* 33:1225-1234

King MA, Doherty PW, Schwinger RB, Jacobs DA, Kidder RE, Miller TR (1983) Fast count dependent digital filtering of Nuclear Medicine images: concise communication. *J Nucl Med* 24:1039-1045

King MA, Schwinger RB, Doherty PW, Penney BC (1984) Two dimensional filtering of SPECT images using the Metz and Wiener filters. *J Nucl Med* 25:1234-1240

King MA, Glick SJ, Penney BC, Schwinger RB, Doherty PW (1987) Interactive visual optimization of SPECT pre-reconstruction filtering. *J Nucl Med* 28:1192-1198

King MA, Hademenos GJ, Glick SJ (1992) A dual photopeak window method for scatter correction. *J Nucl Med* 33:605-612

Knesaurek K (1987) Comparison of 360^0 and 180^0 data collection in SPECT. *Phys Med Biol* 32: 1445-1456

Kodama T, Watanabe K, Hoshi H, Jinnouchi S, Arakawa K, Kusumoto S, Honda H. (1986) Diagnosis of diffuse hepatocellular disease using SPECT. *J Nucl Med* 27:616-619

Kojima A, Matsumoto M, Takahashi M, Hirota Y, Yoshida H. (1989) Effect of spatial resolution on SPECT quantification values. *J Nucl Med* 30:508-514

Kouris K, Musa A, Taha B, Abdel-Dayem H, Collier BD. (1988) Correction of bladder artefact in hip SPECT. *J Nucl Med* 28:868-867

Kouris K, Clarke GA, Jarritt PH, Townsend CE. Thomas SN. (1993) Physical performance evaluation of the Toshiba GCA-9300A triple-headed system. *J Nucl Med* 34:1778-1789

Kouris K, Jarritt PH, Costa DC, Ell PJ (1992) Physical assessment of the GE/CGR Neurocam and comparison with a single rotating gamma camera. *Eur J Nucl Med* 19:236-242

Krasnow AZ, Collier BD, Kneeland JB. (1987) Comparison of high resolution MRI and SPECT bone scintigraphy for non-invasive imaging of the temporo-mandibular joint. *J Nucl Med* 28:1268-1274

Kuhl DE, Edwards RQ (1964) Cylindrical and section radioisotope scanning of liver and brain *Radiology* 83:926

Kung HF, Alavi A, Chang W, Kung MP, Keyes JW, Velchik MG, Billing J, Pan S, Noto R, Rausch A, Reilly J. (1990) In vivo SPECT imaging of CNS D-2 dopamine receptors: Initial studies with iodine-123 IBZM in humans. *J Nucl Med* 31:573-579

Lamaki LM, Patt YZ, Murray LJ, Shanken J. (1990) Superiority of In-111 monoclonal antibody to CT and other conventional imaging studies in the diagnosis of occult recurrence of colorectal cancer (Abstract). *Radiology* 177:258

Lamaki LM, Murray LJ, Patt YZ, Shanken J, Unger MW (1988) Comparison of single photon emission computed tomography (SPECT) and planr imaging in the detection of metastatic colorectal cancer using anti-CEA monoclonal antibody ZCE-025 and its F(ab')2 fragment. (Abstract) *J Nucl Med* 25:886

Larsson SA (1980) Gamma camera emission tomography. Development and proprieties of a multi-sectional emission computed tomography. *Acta Radiol Supp* 363: 1-75

Lewellen TK, Bice AN, Pollard KR, Zhu JB, Plunkett ME (1989) Evaluation of a clinical scintillation camera with pulse tail extrapolation electronics *J Nucl Med* 30:1554-1558

Lim CB, Walker R, Pinkstaff C, et al., (1986) Triangular SPECT system for 3-D total organ volume imaging: performance results and dynamic imaging capability. *IEEE Trans Nucl Sci* 33:501-504

Lim CB, Walker R, Pinkstaff C et al, (1986) Triangular SPECT system for 3-D total organ volume imaging: performance results and dynamic imaging capability *IEEE Trans Nucl Sci* 33:501-504

Links JM. (1993) Multidetector single photon emission tomography: are two (or three or four) heads really better than one? *Eur J Nucl Med* 20:440-447

Links JM, Jeremy RW, Dyer SM, Frank TL, Becker D. (1991) Weiner filtering improves quantification of regional myocardial perfusion with thallium-201 SPECT. *J Nucl Med* 31:1230-1236

Links JM, Frank TL, Becker LC. (1991) Effect of differential tracer washout during SPECT acquisition *J Nucl Med* 32:2253-2257

Ljungberg M, Strand SE. (1990) Attenuation correction in SPECT based on transmission studies and Monte Carlo simulations of build up functions. *J Nucl Med* 31:493-500

Lusins JO, Danielski CF, Goldsmith SJ. (1989) Bone SPECT in patients with posterior back pain after lumber spine surgery. *J Nucl Med* 30:490-496

MacDonald AF, Keyes WI, Mallard JR, Steyn JH (1977). Diagnostic value of computerised isotopic renal scanning. *Eur Urol* 3: 289-191.

MacIntyre WJ, Go RT, O'Donnell JK, Feiglin DHI, Houser TS, Sufka BJ, Saha GB (1988) Thallium-201 and Technetium-99m Pyrophosphate-Single Photon Emission Computed Tomography. In: Gelfand MJ, Thomas SR, eds. *Effective use of computers in Nuclear Medicine*. New York: McGraw-Hill Inc. 109-135

Mahmood S, Buscombe JR, Hall ML, Jarritt PH, Costa DC, Ell PJ (1992) Assessment of myocardial viability with Tl-201 SPET and reinjection technique: a quantitative approach. *Nucl Med Commun* 13:783-789

MahmoodS, Yepes-Mora, Costa DC, Buscombe JR, Ell PJ. (1993) Simulatenous low level dynamic exercise and adenosine infusion in the assessment of myocardial perfusion. (Abstract) *Nucl Med Commun* 14:241

Mahmood S, Townsend CE, Kouris K, Costa DC, Buscombe JR, Ell PJ (1992) Effective myocardial perfusion SPET in 8 minutes utilising a multidetector gamma camera.(Abstract) *Eur J Nucl Med* 19: 671.

Manglos SH, Jaszack RJ, Floyd CE, Hahn LJ, Greer KL, Coleman RE. (1987) Nonisotropic attenuation in SPECT : Phantom tests of quantitative effects and compensation techniques. *J Nucl Med* 28:1584-1591

Manglos SH, Bassano DA, Thomas FD. (1991) Cone-beam transmission computed tomography for nonuniform attenuation compensation of SPECT images. *J Nucl Med* 32:1813-1820

MarshallRC, Berger HJ. (1977) Assessment of cardiac performance with quantitative RN angiocardiography. Sequential LVEF normalised left ventricular ejection rate, and regioal wll motion. *Circulation* 56:820-829

Masdeu CJ, Yudd A, Van Heertum RL, Grundman M, Hriso E, O'Connell RA, Luck D, Camli U, King LN (1991) Single photon emission computed tomography in Human Immunodeficiency Virus Encephalopathy: A preliminary report. *J Nucl Med* 32:1471-1475

Massardo T, Gal RA, Grenier RP, Schidmt DH, Port SC (1990) Left ventricular volume calculation using a count-based ratio method applied to multigated radionuclide angiography. *J Nucl Med* 31:450-456

Makler PT, McCarthy DM, Bergey P, Marshall K, Bourne M, Velchik M, Alavi A. (1985) Multiple hospital survey of ejection fraction variabilty using a cardiac phantom. *J Nucl Med* 26:81-84

Maublant J, Cassagnes J, Jeune JJ, Mestas D, Veyre A, Jallut H, Meyniel G. (1982) A comparison between convential scintigraphy and emission tomography with thallium-201 in the detection of myocardial infarction: concise communication. *J Nucl Med* 23:204-208

Mensforth DJ (1992) Gated blood pool scanning: leap versus slant-hole collimator. *ANZ Nucl Med* March:12-14

Miller TR, Wallis JW. (1992) Clinically important characteristics of maximum likelihood reconstruction. *J Nucl Med* 33:1678-1684

Moore SC, Kouris K., Cullum I. (1992) Collimator design for single photon emission tomography. *Eur J Nucl Med* 19:138-150.

Moore GE (1948) Use of radioactive di-iodofluoresceine in the diagnosis and localisation of brain tumours *Science* 107:569

Mountz JM, Mudell JG, Norman L. (1990) Prognostication of recovery following stroke using the comparison of Tc-99m HMPAO and SPECT. *J Nucl Med* 31:61-66

Mouratidis B, Ash JM, Gilday DL. (1993) Comparison of planar and SPECT Tc-99m DMSA scintigraphy for the detection of renal cortical defects in children. *Nucl Med Commun* 19:82-86.

Muehllehner G (1985) Effect of resolution improvement on required count density in ECT imaging: a computer simulation. *Phys Med Biol* 30:163-173

Mueller SP, Polak JF, Kijewski MF, Holman BL. (1986) Collimator selection for SPECT brain imaging: the advantage of high resolution. *J Nucl Med* 27:1729-1738

Murphy PH (1987) Aceptance testing and quality control of gamma cameras inclding SPECT. *J Nucl Med* 28:1221-1227

Murray IP, Dixon J, Kohan AL, (1990) SPECT for acute knee pain. *Clin Nucl Med* 15:828-840.

Nakajima K, Shuke N, Taki J, Ichihara T, Motomura N, Bunko H, Hoisada KA (1992) Simulation of dynamic SPECT using radiopharmaceuticals with rapid clearance. *J Nucl Med* 33: 1200-1206

Nakajima K, Taki J, Shuke N, Bunko H, Takata S, Hisada K (1993) Myocardial perfusion imaging and dynamic analysis with technetium-99m-tetrofosmin *J Nucl Med* 34:1478-1484

NEMA NU 1 (1986) Performance measurements of scintillation cameras. *National Electrical Manufacturers Association*, Washington DC

Newell RR, Saunders W, Miller E (1952) Multichannel collimators for x-ray scanning with scintillation counters. *Nucleonics* 10:36

Newton MR, Greenwood RJ, Britton KE, Charlesworth M, Nimmon CC, Carroll MJ, Dolke G (1992) A study comparing SPECT with CT and MRI after closed head injury. *J Neurol Neurosurg Psychiatry* 55:92-94

Nguyen T, Heo J, Ogilby JD, Iskandrian AS (1990) Single photon emission computed tomography with thallium-201 during adenosine-induced coronary induced hyperaemia: correlation with coronary arteriography, exercise thallium imaging and two dimension echocardiography.
J Am Coll Cardiol 16:1375-1383

Nishimura S, Mahmarian JJ, Boyce TM, Verani MS (1992) Equivalence between adenosine and exercise thallium-201 myocardial tomography: a multicenter, prospective, crossover trial. *J Am Coll Cardiol* 20:265-275

Nohara R, Kambra H, Suzuki Y, Tamaki S, Kadota K, Kawai C, Tamaki N, Torizuka K. (1984) Stress scintigraphy using single photon emission computed tomography in the evaluation of coronary artery disease.
Am J Cardiol 53:1250-1254

O'Conner MK, Cho DS. (1992) Rapid radiotracer washout from the heart: effect on image quality in SPECT performed with a single headed gamma camera system. *J Nucl Med* 33:1146-1151

Okada RD, Glover D, Gaffeny T, Williams S (1988) Myocardial kinetics of technetium-99m-hexakis-2-methoxypropyl isonitrile. *Circulation* 77:491-498.

Onsel C, Collier BD, Ki M, Larson SJ, Meyer GA, Krasnow AZ, Isitman AT, Hellman RS, Carrera GF (1992). Increased sacroiliac joint uptake after lumbar fusion and/or laminectomy. *Clin Nucl Med.* 17: 283-287

Ourania D. (1993) Single photon emission tomographic studies in patients with Wilson's disease. *M.Sc., Thesis* submitted to University of London.

Parker JA, Uren RJ, Jones AG (1977) Radionuclide left ventriculography with slant hole collimator. *J Nucl Med* 18:848-851

Pilowsky LS, Costa DC, Ell PJ, Murry RM, Verhoeff NPLG, Kerwin RW (1992) Clozapine, single photon emission tomography and the D_2 receptor blockade hypothesis of schizophrenia. *Lancet* 340:199-202

Podoloff DA, Kim EE, Broussard W, Lamaki LM, Haynie TP. (1988) Non uniformity of sulfur clloid distribution on SPECT imaging in patients with Hodgkin disease and non-Hodgkin lymphoma (Abstract) *Radiology* 169:392

Podoloff DA, Kim EE, Haynie TP (1992) SPECT in the evaluation of cancer patients: Not Quo Vadis; Ibi Fere Summus. *Radiology* 183:305-317

Podoloff DA, Broussard W, Kim EE, Lamaki LM. (1989) Diffuse nonuniformity on SPECT liver studies in patients with leukaemia (Abstract) *J Nucl Med* 30:905

Podoloff DA, Kim EE. (1988) Enhanced detection of local colloid uptake with SPECT imaging. *Clin Nucl Med* 13:580-582

Ritchie JL, Williams DL, Harp GD, Stratton JL, Caldwell JH. (1982) Transaxial tomography with thallium-201 for detecting remote myocardial infarction. Comparison with planar imaging. *Am J Cardiol* 50:1236-1241

Rogers WL, Clinthorne NH, Harkness BA, Koral KF, Keyes JW (1982) Field flood requirements for emission computed tomography with an Anger camera *J Nucl Med* 23:162-168

Roper SN, Mena I, King WA, Schweitzwr J, Garret K, Mehringer CM McBride D (1991) An analysis of cerebral blood flow in acute closed-head injury using Tc-99m HMPAO and computed tomography. *J Nucl Med* 32:1684-1687

Rowe CC, Berkovic SF, Austin MC, McKay WJ, Bladin PF (1991) Patterns of post-ictal cerebral blood flow in temporal lobe epilepsy: Qualitative and quantitative analysis. *Neurology* 41:1096-1103

Saxena SR, Laurence BM, Shaw DG. (1975) The justification for early radiological investigation of urinary tract infection in children. *Lancet* ii: 403-404.

Schmitt JM, Ritchie JL, Hamiton GW, Harp GD, Williams DL. (1982) Thallium-201 exercise tomography in the diagnosis of jeopardized myocardium. *Am Heart Assoc. Monogr.* II:149

Schmitz B, Costa DC, Ring H, Moriarty J, Jackson G, Connelly A, Trimble M, Ell PJ (1992) Localization of epileptic foci using HMPAO SPET. *Nucl Med Commun* 13:221

Schwartz RB, Carvalho PA, Alexander E, Loeffler JS, Folkerth R, Holman ML (1992) Radiation necrosis versus high grade recurrent glioma: Differentiation by using dual isotope SPECT with Tl-201 and Tc-99m HMPAO. *AJNR* 12:1187-1192

Simmons GH (1988) On line correction for factors that affect the uniformity and linearity *J Nucl Med Tech* 16(2):82-89

Simon TR, Cowden E, Seastrunk JW, Weiner E, Hickey DC (1991) Chronic fatigue syndrome: Flow and functional abnormalities seen with SPECT *Radiology* 181:173

Smart RC. (1992) Principles of radionuclide imaging: Proceedings of the 5th Asia and Oceania Congress of Nuclear Medicine and Biology, Jakarta. Indonesia

Smith FW, Smith T, Gemmell H. (1991) Phase I study of Tc-99m diphosphine(P53) for myocardial imaging [Abstract] *J Nucl Med* 32:967.

Smith AP, Genna A (1989) Imaging characteristics of ASPECT. A single-crystal ring camera for dedicated brain SPECT. (Abstract) *J Nucl Med* 30:796

Sorenson JA, Phelps ME. (1987) Physics in nuclear medicine, 2nd edition: Grune & Stratton, Orlando

Sridhara BS, Braat S, Itti R, Rigo P, Cload P, Lahiri A (1992) Early and late myocardial imaging with a new technetium-99m diphosphine(PPN1011) in coronary artery disease [Abstract] *J Am Coll Cardiol* 19:202A.

Sridhara BS, Braat S, Rigo P, Itti R, Cload P, Lahiri A (1993) Comparison of myocardial perfusion imaging with technetium-99m tetrofosmin versus thallium-201 in coronary artery disease *Am J Cardiol* 72:1015-1019

Stadius ML, Ritchie JL, (1985) Gated blood pool tomography, in Pohost GM, Higgins CB, Morganroth J, et al.,(eds): *New concepts in cardiac imaging*. Hall Medical Publications , Boston.

Stewart RE, Schwaiger M, Hutchins GD, Chiao PC, Gallagher KP, Nguyen N, Petry NA, Rogers WL. (1991) Myocardial clearance kinetics of technetium-99m SQ30217: a marker of regional blood flow. *J Nucl Med* 31:1183-1190

Steyn JH, MacDonald AF, Keyes WI, Bayliss AP, Towler JM. (1978) An assessment of computerised isotopic renal section scanning.
Br J Urol 50: 437-441.

Stokely EM, Sveinsdottir E, Lassen NA, Rommer P. (1980) A single photon dynamic computed assisted tomograph (DCAT) for imaging brain function in multiple cross sections *J Comput Assist Tomog* 4:23-240

Strauss HW, Pitt B. (1977) Thallium-201 as a myocardial imaging agent. *Semin. Nucl. Med* 7:49-58.

Tamaki N , Mukai T, Ishii Y, Fujita T, Tammamoto K, Minato K, Yonekura Y, Tamaki S, Kambara H, Kawai C, Torizuka K (1982) Comparitive study of thallium emission myocardial tomography with 180^0 and 360^0 data collection.
J Nucl Med 23: 661-666

Tamaki S, Kambara H, Kadota K, Suzuki Y, nohara R, Kawai C, Tamaki N, Torizuka K. (1984) Improved detection of myocardial infarction by emission computed tomography with thallium-201. Relation to infarct size.
Br Heart J 52:621-627

Tarkington MA, Fildes RD, Lewin K, Zeissman H, Harkness B, Gibbons MD. (1990) High resolution single photon emission computerized tomography (SPECT) 99m-technetium-dimercapto-succinic acid renal imaging: A state of the art technique. *J Urol* 144: 598-600.

Tatsch K, Schwarz J, Oertel WH, Kirsch CM (1992) Dopamine-2 Receptor Imaging with I-123 IBZM SPECT to differentiate idiopathic from other Parkinson syndromes (Abstract) *J Nucl Med* 33:917

The Tetrofosmin Study Group. (1992) Comparative myocardial perfusion imaging with Tc-99m-tetrofosmin and thallium-201: results of phase-III international trial. [Abstract] *Circulation* 86(Suppl I):I-506.

Tsui BMW, Gullberg GT, Edgerton ER, Gillnd DR, Perry JR, McCartney WH (1986) Design and clinical utility of a fan-beam collimator for SPECT imaging of the head. *J Nucl Med* 27:810-819

Tumeh SS, Rosenthal DS, Kaplan WD, English RJ, Holman BL. (1987) Lymphoma: evaluation with Ga-67 SPECT. *Radiology* 164:111-114

Underwood SR, Walton S, Ell PJ, Jarritt PH, Emanuel, Swanton RH.(1985) Gated blood pool emission tomography: A new technique for the investigation of cardiac structure and function. *Eur J Nucl Med* 10:332-337

Underwood SR, Walton S, Laming PJ, Jarritt PH, Ell PJ, Emanuel RW, Swanton RH. (1985) Left ventricular volume and ejection fraction determined by gated blood pool emission tomography. *Br Heart J* 53: 216-22

Verani MS, Mahmarian JJ, Hixson JB, Boyce TM, Standacher RA (1990) Diagnosis of coronary artery disease by controlled coronary vasodilation with adenosine and thallium-201 scintigraphy in patients unable to exercise *Circulation* 82:80-87

Verani MS, Marcus ML, Razzak MA, Erhardt JC. (1978) Sensitivity and specificity of thallium-201 perfusion scintigrams under exercise in the diagnosis of coronary artery disease. *J Nucl Med* 19:773-782

Verhoeff NPLG, Brucke T, Podreka I, Bobeldijik M, Angelberger P, Van Royen EA. (1991) Dynamic SPECT in two healthy volunteers to determine the optimal time for in vivo D-2 dopamine receptor imaging with I-123 IBZM using the rotating gamma camera. *Nucl Med Commun* 12:687-697

Verhoeff NPLG, Van Royen EA, Speelman JD, Borm JJ, Kapuco O (1992) Differential diagnosis of Parkinsonism by I-123 IBZM SPECT (Abstract) *J Nucl Med* 33:917

Verma RC, Gan MP, Bennett LR, Mankovich JJ, Go A, Sabbe J, Schiepers C, Jones FD, Mathisen G, Harker J, Yaghmai I (1992) Cerebral perfusion imaging in AIDS (Abstract) *J Nucl Med* 33:827

Wackers FJ Th, Berman DS, Maddahi J, Watson DD, Beller GA, Strauss HW, Boucher CA, Picord H, Holman BL, Fruidrich R, Inglese E, Delaloye B, Bischef-Delaloye A, Camin L, McKusick K (1989) Technetium-99m hexakis 2-methoxyisobutyl isonitrile: human biodistribution, dosimetry, safety and preliminary comparison to thallium-201 for myocardial perfusion imaging. *J Nucl Med* 30:301-311

Williams ED, Parker C, Rankin D, Roy RR. (1986). Multiple section radionuclide tomography of the kidney: A clinical evaluation. *Br J Radiology* 59: 975-983.

Wilson RJ (1988) Collimator technology and advancement. *J Nucl Med* 16:198-203

Young CG, Likos JJ (1972) Medical speciality terminology: x-ray and nuclear medicine. CV Mosby St.Louis, USA

Yudd AP, Van Heertum RL, Vrunetti JC. (1986) Evaluation of liver disease: SPECT versus CAT (Abstract) *J Nucl Med* 27:924

Zimmerman RE (1988) The developing technology of imaging detectors. *J Nucl Med Technol* 16:25-30

Corrections

Page No:	Line No:	Words written as:	To be read as:
23	2	time	times
34	19	now developed	now been developed
42	11	Comparing these	Compare these
56	6	were the first to report on	(repitition)
57	31	application	applications
59	9	HMPO SPET	HMPAO SPET
62	21	other vessel	other vessels
63	27	compares well	compare well
64	30	This sooner	This soon
69	23	180o	180°
77	7	e.,	eg.,
134	10	(table 5.9)	(table 5.8)
149	7	Weckers'	Wackers'
150	15	it's	its
153	22	specificity of 76%	sensitivity of 76%
153	23	sensitivity of 70%	specificity of 70%
156	5	it's	its
164	4	was	were
164	4	as frontal	as the frontal
167	28	convergent	divergent
170	Fig.6.8	converging	diverging
172	4	three	all
173	23	inreased	increased
176	25	paedriatic	paediatric
178	4	30,000	£30,000
178	7	20,000	£20,000

178	8	80,000	£80,000
178	13	23.00	£23.00
178	15	use or potentially use	uses or potentially uses
181	2	mltidetector	multidetector
181	15	23.00	£23.00
197	27-29	Lim CB..et al.,	(repetition)
200	10	19:82-86	14:82-86

List of Publications

---

1. S **Mahmood**, JR Buscombe, K Kouris, G Clarke, CE Townsend, PH Jarritt, DC Costa, PJ Ell, Clinical experience with a multidetector SPET system (Toshiba GCA-9300A) *Nucl Med Comm: (in press)*

2. JR Buscombe, CE Townsend, K Kouris, G Clarke,**S Mahmood**, PH Jarritt, PJ Ell, Clinical high resolution skeletal single photon emission tomography using a multidetector gamma camera
BJR 1993: 66, 817-822

3. JR Buscombe, CE Townsend, K Kouris, G Clarke, **S Mahmood**, PH Jarritt, PJ Ell, Clinical high resolution renal single photon emission tomography in 8 minutes using a multi-detector gamma camera
Clin Nucl Med (in press)

4. **S Mahmood**, M Gunning, J Bomanji, NK Gupta, DC Costa, PH Jarritt, H Swanton, PJ Ell, Combined rest thallium-201/ stress Tc-99m tetrofosmin SPET: A study of feasibility and diagnostic accuracy of a 90 minute protocol. *J Nucl Med: (in press)*

5. S Mahmood, NK Gupta, M Gunning, J Bomanji, PH Jarritt, PJ Ell, Thallium-201 myocardial perfusion SPET: Adenosine Alone or Combined with Dynamic Exercise. *Nucl Med Comm: (in press)*

Nuclear Medicine Communications 1994 : (in press)

Clinical experience with a multidetector SPET system (Toshiba GCA-9300A)

S Mahmood
J R Buscombe
K Kouris
G A Clarke
C E Townsend
P H Jarritt
D C Costa
P J Ell

Institute of Nuclear Medicine,
University College London Medical School,

Address for correspondence:

Institute of Nuclear Medicine,
University College London Medical School,
Mortimer st., London W1N 8AA
Phone:071-380 9421, Fax: 071-387 0578

Introduction

Compared to a conventional single rotating gamma camera, three-headed systems can yield superior image quality (1,2) even at lower patient doses and/or reduced acquisition times (3,4). This is because of the increased tomographic volume sensitivity and improved spatial resolution. With parallel hole collimators, some of the gain in sensitivity can be traded-off for improved resolution using narrower holes and/or increased hole length. Because of the properties of fanbeam collimators, both sensitivity and resolution can improve (5,6,7). Thus, protocols according to which SPET procedures are performed can now be optimised, the pertinent parameters being the amount of administered activity, collimator choice and total data acquisition time.

In this paper, we report our clinical experience with the Toshiba GCA-9300A, a three-headed system for head and body single photon emission tomography (SPET), at the Institute of Nuclear Medicine. Examples are provided of a normal volunteer and selected patients thereby demonstrating the clinical efficacy of this instrument as a multi-slice brain and body imager for both routine and research studies.

Toshiba GCA-9300A

The GCA-9300A (*Toshiba Corporation Medical Systems, Tokyo, Japan*) was the first three-detector single photon emission tomography system for both brain and body imaging (6,8) installed at the Institute of Nuclear Medicine.

The Toshiba GCA-9300A consists of three Anger-type gamma cameras forming a triangular aperture in a rotating gantry. The radius of rotation of each camera can be varied independently between 132 and 307 mm. Each camera has 45 photomultiplier tubes (PMTs) coupled to a 6.5 mm thick sodium iodide (NaI(Tl) crystal and is shielded against gamma and X-rays up to 180 keV. The collimators can be changed using custom trolleys. The collimators available at our institute were the high resolution parallel hole (HR PH) and the super high resolution fan-beam (SHR FB), both cast from lead. The field of view (FOV) is 410 mm x 210 mm (length) with the parallel hole collimators and 220 mm (diameter) x 210 mm (length) with the fanbeam collimators. The fanbeam collimators have a focal length of 397 mm and must be used with the radius of rotation set to 132 mm (the minimum possible value).

Tomographic data can be acquired either in "step and shoot" or "continuous rotation" mode. More than one rotation can be performed in the continuous rotation mode, the data from each rotation being summed for a given angle; the direction of rotation is reversed between rotations. During a continuous rotation acquisition, the radius of rotation of each camera remains fixed but during a step acquisition the cameras can follow an elliptical path ensuring closer patient proximity. Data are energy and linearity corrected on-line, on an event by event basis. Uniformity correction of each projection is done prior to tomographic reconstruction.

Summary

The clinical experience with the Toshiba GCA-9300A single photon emission tomography (SPET) system has been discussed alongwith typical acquisition protocols for various SPET studies. The system was used to perform SPET studies in normals and in a variety of brain and body disorders. Its three Anger-type gamma cameras forming a triangular aperture offer a substantial increase in sensitivity compared to a single rotating gamma camera. This has allowed the routine use of lead fan beam super high resolution collimators (SHR FB) for ^{99m}Tc-HMPAO brain SPET studies and high resolution parallel hole collimators (HR PH) for cardiac and other body studies. The resulting improvement in spatial resolution coupled with the ease of patient positioning and the greater patient throughput compared to a conventional tomographic gamma camera, will enhance the role of brain and body SPET for both routine and research purposes.

using dipyridamole infusion at a rate of 0.56 mg/kg over 4 minutes of time. The patient complained of some central chest discomfort. 74MBq of thallium-201 was injected at peak stress. Stress and redistribution data were acquired using high resolution parallel hole collimators, in a "continuous mode" for a total of 32 minutes (8 rotations of 4 minutes each). 128x128w matrices were used. Data were than divided into 3 studies: the first 8, the first 16 and the total 32 minutes for both stress and rest. Data were binned into 60 projections for each study. The reconstructed tomographic images (Figure 1) demonstrated reversible myocardial ischaemia in the intraventricular septum , apex and apical anterior wall. There was no difference in the clinical information obtained using 8 or 16 minute data acquisition (Figure 1).

SKELETAL SPET STUDIES

Single photon emission tomography (SPET) has been proven to be more sensitive than planar scintigraphy in identifying benign bony pathology (13,14). Unfortunately the 30 min SPET acquisition time necessary with a conventional single-detector gamma camera, remains a major deterrent to the widespread use of SPET in skeletal scintigraphy.

Using the Toshiba GCA-9300A multidetector system, 85 SPET studies were performed in 81 patients (Table 2). Four patients had two different sites imaged. The decision to perform SPET was made after inspection of the planar images, and only if it was clinically indicated.

The typical acquisition/processing protocol recommended from our experience to be used on Toshiba GCA-9300A is tabulated in table 3.

Comparison of studies with different acquisition times of 8, 16 and 32 minutes revealed similar clinical information. The total number of "hot spots" seen in the 3 studies was the same (15), though there was some differences in the shape and intensity of the abnormalities seen. Comparing image quality, both in terms of definition of normal skeletal structure and lack of distortion, there was some improvement with the 32 min acquisition time compared to the 8 or 16 min acquisition time in the thoracolumbar spine. However, in the knees or femora, where count density was lower, the 16 min acquisition protocol demonstrated much better image quality than the 8 min acquisition protocol.

One of the main advantages of shorter acquisition, is for SPET of the hip joints and pelvis. In our experience, it was possible to see the hip joints clearly only with the 8 minute acquisition, while in the 16 min and 32 min acquisitions, images were obscured by reconstruction artefacts arising from bladder activity. Generally an 8 min acquisition of the lower pelvis obtained just after the patient had voided, demonstrated the normal bony structure and any pathology clearly. It has been noted that activity

The physical performance of the GCA-9300A was assessed using standard techniques described by, for example, the National Electrical Manufacturers Association (9), the American Association of Physicists in Medicine (10) and various publications (3). The full results have been reported elsewhere (11).

Clinical Experience

More than 250 subjects were scanned, in a total of more than 600 studies. For a given volunteer or patient more than one SPET study was performed using either different acquisition parameters after a single injection or on separate occasions in order to follow the effects of therapy. Tomographic reconstruction of patient data was performed using the filtered back-projection method. The projection data were prefiltered using the Butterworth filter. Backprojection was performed using a Shepp Logan filter. No attenuation correction was used even for brain studies as per Toshiba recommendation.

THALLIUM-201 MYOCARDIAL PERFUSION SPET STUDIES

Thallium -201 myocardial perfusion SPET studies were performed in 57 patients (40 male 17 female, aged 31-72 years). Only patients with documented evidence of coronary artery disease were included in this study. Coronary angiography was known in 23 patients, whilst 40 patients had a past history of myocardial infarction. Although low energy general purpose collimators are usually used for data acquisition of thallium-201, we decided to utilise high resolution collimators. This was because the tomographic volume sensitivity of the Toshiba GCA-9300A, fitted with high resolution collimators is 30.0 kcps/(MBq/ml)/cm which is equal to 10.0 kcps/(MBq/ml)/cm for each detector (11,12). This compares well with the tomographic volume sensitivity of 12.8 kcps/(MBq/ml)/cm for a typical single detector gamma camera (IGE 400XCT) (7). We utilised 360° data acquisition in order to obtain maximum count density.

Typical data acquisition and processing protocols are summarised in table 1.

In a comparative study of 10 patients we compared images obtained by 8, 16 and 32 minutes of acquisition (4). The data were reported by two independent observers, unaware of clinical history, time and mode of acquisition. The number of defects reported by each observer in both stress and redistribution studies showed little variation between the 8, 16 and 32 minutes acquisition. There was also some variation in the number of defects seen by each observer, with observer 2 reporting a slightly higher number of defects than observer 1. This however was not significant ($X^2=2.13$, $p>0.95$).

Clinical Case Study 1: A 54 years old male was referred to the institute for thallium-201 myocardial perfusion SPET study. The patient was a known diabetic with a history of typical chest pain, but negative EKG stress test. The patient was stressed

function and was removed. A second kidney became available six months later and the patient received this second graft. This time the donor kidney was not perfect and was supplied with two renal arteries and therefore there were two anastomoses into the left iliac artery. Initial function was good but on the 6th day post-transplant urine output fell. A dynamic renogram using ^{99m}Tc diethylene-triaminopenta-acetic acid (DTPA) showed a poorly functioning transplant. It was initially thought that the patient might be experiencing some rejection but in view of the difficult operation an alternative cause of this patients problems could have been a stenosis in one of the arteries supplying the transplant. A ^{99m}Tc Dimercapto succinic acid (DMSA) study was requested to demonstrate if there had been critical ischaemia to part of the transplanted kidney. Static images were performed three hours after the administration of 77MBq of ^{99m}Tc-DMSA. Planar imaging (Fig. 4a) demonstrated reduced uptake of tracer in the lower third of the transplant. Tomographic images (Fig. 4b and c) were able to define more clearly the extent of the damaged area and showed clearly that it involved not only the lower third of the transplant but also the posterior wall. This corresponded to the area supplied by the lower of two arteries and demonstrated clearly that the patient's problems were due to a restricted blood supply from this area.

BRAIN SPET STUDIES

The Toshiba GCA-9300A instrument had the facility of super high resolution fan-beam collimators for brain SPET imaging. These collimators provide higher tomographic spatial resolution in comparison with parallel hole collimators (11,12). Tc-99m HMPAO SPET studies were performed in 20 patients with diagnosis of Wilson's disease, transient ischaemic attacks, myeloencephalitis and epilepsy. In addition, thallium-201 brain SPET studies were performed in cases of disruption of blood-brain barrier. I-123 IBZM studies were performed in two volunteers, in order to demonstrate the ability of the system to perform dynamic SPET.

Table 5 compares the typical acquisition protocols, for Toshiba GCA-9300A, IGE Neurocam (a brain dedicated SPET system) and IGE 400XCT (a single detector gamma camera).

Clinical Case Study 4: A 79 year old male with bilateral internal carotid artery stenosis had recently (for the last 6 months) several transitory ischaemic attacks (TIA's). His medical history revealed long standing diabetes mellitus. He was referred for pre-operative evaluation of his brain perfusion. A ^{99m}Tc- HMPAO SPET study with the Toshiba GCA-9300A was carried out for 32 minutes using a continuous acquisition mode . After rebinning the data into 60 frames, 3 studies were reconstructed: one comprising the first 8 minutes of acquisition, a second including the first 16 minutes of the continuous acquisition and finally the third

in the bladder leads to artefacts which may affect imaging of the hip joints.

Clinical Case Study 2: A 53 year old insulin dependant diabetic who suffered multiple complications of her disease. She had become blind due to cataracts and intra-orbital haemorrhage. She had a peripheral neuropathy which affected her feet. She was admitted to the hospital with a six week history of a pus like discharge from her right ear. Cultures grew Staphylococcus aureus and she was treated with the antibiotics. Despite treatment there was no reduction in the discharge from the right auditory meatus. She did not have any local tenderness suggesting a mastoiditis but osteomyelitis in the bones surrounding the ear canal was suspected. A ^{99m}Tc methyl di-phosphonate (MDP) bone scintigram was requested to look for evidence of an underlying bone infection. Planar and tomographic images were obtained 3 hours after the administration of 550 MBq ^{99m}Tc-MDP. Whilst planar images were unhelpful (Fig. 2a) the transaxial slices clearly show abnormal uptake of tracer in bones surrounding the ear canal (Fig. 2b). A labelled white cell study confirmed the presence of infection and an operation to remove the infected bone was successful.

RENAL DMSA SPET STUDIES

Single photon emission tomography (SPET) of the kidneys using Tc-99m labelled dimercaptosuccinic acid (DMSA) has been proposed as a method to improve the sensitivity of static renal scintigraphy (16, 17) SPET allows more defects in the renal cortex to be visualised than can be seen with planar imaging and it gives a better characterisation of the size and extent of a defect (18,19). This may be particularly true in children where the early identification of scars may have a significant effect on subsequent management and morbidity (20).

Using the Toshiba GCA-9300A, renal DMSA SPET studies were performed in 73 patients. The recommended acquisition and processing protocol for renal DMSA SPET studies is shown in table 4. Although longer acquisition times were used in some patients, it did not enhance the clinical information. Figure 3 demonstrate a 3-D surface display of a normal DMSA SPET study.

We felt that using a multidetector system such as the Toshiba GCA-9300A, 8 minute acquisition yielded sufficient clinical information. The mean total counts obtained per 8 min acquisition was 2290 Kcounts (range 1269-2902 Kcounts).

It has been previously documented that using a 30 minute acquisition, the sensitivity of SPET for the detection of renal scars is 35% higher than planar imaging (21). Unfortunately the long acquisition time meant that when children were imaged sedation was required. Therefore, using a multidetector system an 8 minute acquisition would increase the utility of SPET in children.

Clinical Case Study 3: A 26 year old man with a history of renal failure requiring transplant, received a caderveric transplant. Unfortunately, this transplant failed to

a) Increased throughput: We have shown that rapid imaging protocols can be achieved without significant loss in the detection of abnormalities. In the specific setting of myocardial perfusion scintigraphy we have shown that good quality ^{201}Tl scans can be obtained with imaging times as short as 8 min (4). Similarly, 8 min. SPET bone scans have been recorded for the lumbar spine, with most encouraging results (15,26). A standard tracer dose can therefore be used for significant improvement in patient throughput. The shorter acquisition times for SPET, will be of help in extending the facility to severely ill, old and paedriatic patients.

b) Reduced patient exposure: The permitted radiation exposures to patients vary from country to country. Nevertheless, the recommendations of the International Commission for Radiological Protection (ICRP) may lead to an even more strict set of rules and regulations which may be demanding further reductions in these exposures(27). With the experience obtained so far using the Toshiba GCA-9300A system in brain, myocardium, renal and skeletal imaging, we can now predict that for standard imaging times, a significant reduction in patient exposure can be achieved, without loss of routine levels of information density in the images. This is an important advantage, particularly in the context of studies with significant radiation exposure (e.g. 79 mGy for ^{201}Tl myocardial perfusion SPET being equivalent to 500 chest X-rays), in the context of repeated studies, and in the context of multiple tracer studies (such as perfusion studies, receptor imaging, flow and metabolism studies).

c) Increased information density: Many nuclear medicine procedures (if not most) still suffer from poor information density. Many tracers (antibodies, receptor ligands, flow tracers) concentrate in tissue in minute amounts. The instrumentation we have investigated permits to maximise information density if desired or required. The improvement in image quality is testimony of this improvement.

Conclusion

Multi-detector body and brain SPET systems will have an increasing future and a positive impact on the practice of nuclear medicine. The system investigated by us (the Toshiba GCA-9300A) is a typical example of this new trend in the instrumentation available in nuclear medicine. The figures of merit obtained with this system and the image quality seen in a variety of clinical cases give testimony to the progress achieved in this field.

We hope that the industry will continue its endeavours to offer nuclear medicine practitioners improved instrumentation. Having delivered a new generation of imaging detectors, we hope that it will soon make the next quantum leap, namely that of simultaneous and accurate transmission and emission imaging with SPET.

covering the total acquisition time . The results are displayed in figure 5 .
Clinical Case Study 5:A 32 year old female with no past or present history of neurological or psychiatric disease was studied as a normal volunteer. She received 185 MBq of ^{123}I-iodobenzamide (IBZM) and dynamic single photon emission tomography was performed at 10 minutes intervals from time of injection to 2 hours post injection(figure 6).
Clinical Case Study 6:A 36 year old male , HIV positive for one year, presented with progressive paraparesis of both legs, headache, and mild confusional status. Thallium-201 single photon emission tomography with the Toshiba GCA-9300A was carried out and depicted blood brain barrier disruption on two sites as shown in figure 7.

Discussion

Collimator choice is one of the most important factors that determine image quality in Nuclear Medicine. In agreement with others (22, 23, 24,) we recommend the use of high resolution as opposed to general purpose collimators in SPET. Fanbeam collimators can further improve both resolution and sensitivity (6,7); the apparent system planar resolution improves by the magnification effect. Cone beam collimation gives the highest sensitivity but requires a scanning trajectory that will yield sufficient angular sampling (25).
Multi-headed SPET systems primarily offer a substantial increase in tomographic volume sensitivity compared to a single rotating gamma camera. Depending on collimator type and collimator design parameters, better tomographic spatial resolution is achievable. In our experience, the Toshiba GCA-9300A triple-headed SPET system achieves both objectives when the SHR FB collimators are used for brain studies and the HR PH collimators for body studies. The most serious limitation was a very slow computer but we understand that a new high-speed processor has been introduced. The gantry and detectors are well designed, stable and reliable, and provide sufficiently for patient safety.
Although this paper did not report on the sensitivity, specificity and accuracy of clinical diagnosis with the GCA-9300A, we hope to have demonstrated its clinical utility. A wide variety of clinical pathologies have been studied. In addition, split-dose SPET protocols have been applied in neuroimaging, and neuroactivation studies with acceptable spatial resolution.
With multi-headed systems such as the Toshiba GCA-9300A we expect that the role of SPET in clinical practice and research will increase. It is important to distinguish routine applications and the solving of clinical problems from research oriented imaging protocols. In many circumstances, specific choices can now be made with different but clearly defined aims.

12. Mahmood S. The clinical impact of multidetector SPET technology. M.Phil Thesis, submitted to the University of London. 1994

13. Onsel C, Collier BD, Ki M, Larson SJ, Meyer GA, Krasnow AZ, Isitman AT, Hellman RS, Carrera GF. Increased sacroiliac joint uptake after lumbar fusion and/or laminectomy. *Clin Nucl Med.* 1992; 17: 283-287

14. Kanmaz B, Liu Y, Uzman G, Yu L, Uzman F, Uygur G, Akansel G, Gunes I, Krasnow AZ, Hellman RS, Collier BD. SPECT vs planar bone scintigraphy in patients with low back pain. *J Nucl Med* 1992; 33:868.

15. Buscombe JR, Townsend CE, Kouris K, Clarke G, Mahmood S, Jarritt PH, Ell PJ. Clinical high resolution skeletal single photon emission tomography using a triple-headed gamma camera. Brit J Radiol 1993; 66:817-822

16. MacDonald AF, Keyes WI, Mallard JR, Steyn JH. Diagnostic value of computerised isotopic renal scanning. *Eur Urol* 1977; 3: 289-191.

17. Steyn JH, MacDonald AF, Keyes WI, Bayliss AP, Towler JM. An assessment of computerised isotopic renal section scanning. *Br J Urol* 1978; 50: 437-441.

18. Williams ED, Parker C, Rankin D, Roy RR. Multiple section radionuclide tomography of the kidney: A clinical evaluation. *Br J Radiology* 1986; 59: 975-983.

19. Mouratidis B, Ash JM, Gilday DL. (1993) Comparison of planar and SPECT Tc-99m DMSA scintigraphy for the detection of renal cortical defects in children. *Nucl Med Commun* 1993; 14:82-86.

20. Saxena SR, Laurence BM, Shaw DG. The justification for early radiological investigation of urinary tract infection in children. *Lancet* 1975; ii: 403-404.

21. Tarkington MA, Fildes RD, Lewin K, Zeissman H, Harkness B, Gibbons MD. High resolution single photon emission computerized tomography (SPECT) 99m-technetium-dimercapto-succinic acid renal imaging: A state of the art technique. *J Urol* 1990;144: 598-600.

22. Muehllehner G Effect of resolution improvement on required count density in ECT imaging: a computer simulation. *Phys Med Biol* 1985: 30:163-173

References

1. George MS, Ring HA, Costa DC, Ell PJ, Kouris K, Jarritt PH *Neuroactivation and Neuroimaging with SPET.* Springer-Verlag: 1991

2. Hisada K, (editor) *An atlas of second-generation SPECT*, Maruzen Planning Network Co., Japan: 1991

3. Kouris K, Jarritt PH, Costa DC, Ell PJ Physical assessment of the GE/CGR Neurocam and comparison to a single rotating gamma camera. *Eur J Nucl Med* 1992;19:236-242

4. Mahmood S, Townsend C, Kouris K, Costa DC, Ell PJ Effective myocardial SPET in 8 minutes using a multidetector gamma camera. *Eur J Nucl Med* 1992, 19: 671

5. Lim CB, Walker R, Pinkstaff C, et al., Triangular SPECT system for 3-D total organ volume imaging: performance results and dynamic imaging capability. *IEEE Trans Nucl Sci* 1986; 33:501-504

6. Ichihara T. Development of a high resolution SPECT system. *Toshiba Med Rev*, 1990: 33:29-35

7. Moore SC, Kouris K, Cullum I. Collimator design for single photon emission tomography. *Eur J Nucl Med* 1992: 19:138-150

8. Ichihara T, Matsudaira M, Yamada M, Basic development of the Toshiba digital gamma camera, model GCA-9300A In: Hisada K (ed) *An Atlas of Second Generation SPECT.* Maruzen Planning Network Co., 1991: Chapter III

9.NEMA NU 1 Performance measurements of scintillation cameras. National Electrical Manufacturers Association, Washington DC:1986

10. AAPM Report No.22 Rotating scintillation camera SPECT acceptance testing and quality control. American Association of Physicists in Medicine, New York; 1987

11. Kouris K, Clarke GA, Jarritt PH, Townsend CE. Thomas SN. Physical performance evaluation of the Toshiba GCA-9300A triple-headed system. *J Nucl Med* 1993; 34:1778-1789

Legend for Figures and Tables:

Figure 1: Thallium-201 myocardial perfusion SPET slices (stress and rest images). Two studies are displayed: 8, and 16 minutes acquisition. Both demonstrate reversible myocardial ischaemia in the intraventricular septum, apex and apical segment of the anterior wall with similar diagnostic accuracy. Stress and redistribution data were acquired for a total of 32 minutes(8 rotations of 4 minutes each).

Figure 2 a and 2 b: Comparison of planar and tomographic images in a patient with suspected osteomyelitis of the right middle ear. Anterior and lateral skull planar Tc-99m MDP images (figure 2 a) fail to show any abnormality in the area surrounding the right ear canal. Tomographic transaxial slices (figure 2 b) of the skull at the level of the ear canals clearly show increased uptake of tracer in the bone surrounding the right auditory meatus.

Figure 3: Normal 3-D renal DMSA images, using 8 minute SPET acquisition.

Figure 4 a -c: Planar Tc-99m DMSA images (a) of a recent renal transplant showing reduced uptake of tracer in the lower pole. Coronal SPET slices (b) of the same transplanted kidney confirm that there is reduced uptake in the lower pole of the transplant and transaxial slices (c) show that the injury also extends throughout most of the posterior wall. This could not be seen on the planar images (a).

Figure 5: 99mTc HMPAO SPET study (clinical case study 4): Classical three slice orientation display is shown with 16 transverse, 16 coronal and 16 sagittal slices for the 3 (8 minutes= upper row, 16 minutes=middle row, 32 minutes=lower row) studies obtained after the rebinning of the data from the 32 minutes continuous acquisition. The 3 studies clearly display an area of significant reduction of perfusion to the right cerebellar hemisphere . In addition, there is a significant widening of the lateral ventricles. The patient suffered bilateral internal carotid artery stenosis and had recently several TIAs.

Figure 6 (clinical case study 5): I-123 IBZM Dynamic SPET Study: Three studies are shown. One(20 minutes p.i. for 10 minutes acquisition time) during the flow /perfusion phase; second at 60 minutes for 10 minutes total acquisition time displaying significant binding of the IBZM to the striatum on both hemispheres and finally the third (at 2 hours p.i. for 30 minutes total acquisition time) at a time when aspecific binding is markedly reduced. This study clearly demonstrates the feasibility of dynamic SPET with a three detector gamma camera. It shows

23. Mueller SP, Polak JF, Kijewski MF, et al., Collimator selection for SPECT brain imaging: the advantage of high resolution. *J Nucl Med* 1986 27:1729-1738

24. Keyes JW, Fahey FH, Harkness BA, Tips for high quality SPECT. *SNM Computer and Instrumentation Council News letter* :1990

25. Gullberg GT, Zeng GL, Christian PE, Datz FL, Morgan HT, Cone beam tomography of the heart using SPECT *Invest Radiol* 1991:26:681-688

26. Buscombe JR, Townsend CE, Clarke G, Kouris K, Ell PJ, Fast skeletal SPET in the assessment of chest metastases in young patients with primary bone tumours. *Nucl Med Commun* 1992:13:222

27. International Commission on Radiological Protection (ICRP). 1990 *Recommendations of the International Commission on Radiological Protection.* IRCP Publication 60: Pergamon Press, New York: 1991.

Table1: Typical stress/redistribution thallium-201 myocardial perfusion SPET acquisition and processing protocol for Toshiba GCA 9300A.

Data Acquisition:

1. Collimator:	Low energy, High resolution
2. Matrix size:	128x128 W
3. Rotation arc:	360°
4. Acquisition mode:	Continuous
5. Acquisition time:	4 rotations of 4 minutes each
6. Corrections:	Energy and linearity on-line
	Uniformity: before reconstruction

Data Reconstruction:

1. Data binning:	60 projections
2. Prefiltering:	Butterworth (order 8)
3. Back-projection:	Shepp-Logan filter
4. Slices thickness:	2 pixel
5. Display:	Vertical long axis, horizontal long axis and short axis slices

Redistribution Study: 3 hours post stress.

adequate spatial resolution (particularly at 2 hours post injection study) to resolve the head of caudate nucleus from the putamen and globus pallidus as seen in slices 7,8 ,9 and 10 of the later study.

Figure 7 (clinical case study 6): Thallium-201 blood brain barrier disruption study. Transverse, coronal and sagittal slices are shown to demonstrate the site of disrupted blood brain barrier. There is one in the right temporal lobe, and a larger site in the para-ventricular white matter on the right hemisphere.

Table1: Typical stress/redistribution thallium-201 myocardial perfusion SPET acquisition and processing protocol for Toshiba GCA 9300A.

Table 2: Sites of skeletal SPET imaging in 85 studies.

Table 3: Recommended acquisition and processing protocol for skeletal single photon emission tomography. (MDP=methyldiphosphonate).

Table 4: Recommended acquisition and processing protocol for renal DMSA tomographic studies. (DMSA =dimercaptosuccinic acid).

Table 5: Comparison of acquisition protocols for Tc-99m HMPAO brain perfusion SPET using IGE 400XCT (single detector system), IGE Neurocam (a brain dedicated three detector system) and Toshiba GCA-9300A (whole body/brain three detector SPET system). (HR= high resolution, SHR FB= super high resolution fan beam).

Table 3: Recommended acquisition and processing protocol for skeletal single photon emission tomography. (MDP=methyldiphosphonate)

Dose: 550 MBq of Tc-99m MDP

Data Acquisition:

1. Collimator: Low energy, High resolution

2. Matrix size: 128x128 W (3.2 mm)

3. Rotation arc: 360°

4. Acquisition mode: Continuous

5. Acquisition time: 4 rotations of 4 minute each
(2 rotations of 4 minutes for hips)

6. Corrections: Energy and linearity on-line
Uniformity: before reconstruction

Data Reconstruction:

1. Data binning: 60 projections

2. Prefiltering: Butterworth
(order: 16 for knees, and 15 for spine)

3. Back-projection: Shepp-Logan filter

4. Slices thickness: 2 pixel

5. Display: Transaxial, sagittal and coronal slices

Table 2: Sites of skeletal SPET imaging in 85 studies.

Sites of SPET acquisition	**Number of studies**
Lumbar spine	38
Thoracic spine	18
Head/neck	7
Lower pelvis/hip	10
Knees	9
Femur	2
Feet	1

Table 5: Comparison of acquisition protocols for Tc-99m HMPAO brain perfusion SPET using IGE 400XCT (single detector system), IGE Neurocam (a brain dedicated three detector system) and Toshiba GCA-9300A (whole body/brain three detector SPET system). (HR= high resolution, SHR FB= super high resolution fan beam).

Parameters	IGE 400XCT	IGE Neurocam	Toshiba GCA-9300A
Collimator	HR	HR	SHR FB
Number of views	64	128	90 --> 60
Energy window:			
width, offset	20, 3	20, 3	20, 0
Matrix size	128	64	256->128
Pixel size (mm)	3.2	4.0	1.735
Time per view			
(seconds)	30-40	20	30
Total time			
(minutes)	35-45	15	15
Counts per view			
(KCnts)	50	35	55
Total counts.			
(MCnts)	3.2	4.5	5.2

Table 4: Recommended acquisition and processing protocol for renal DMSA tomographic studies. (DMSA =dimercaptosuccinic acid).

Dose:	74 MBq of Tc-99m DMSA
Data Acquisition:	
1. Collimator:	Low energy, High resolution
2. Matrix size:	128x128 W (3.2 mm)
3. Rotation arc:	360°
4. Acquisition mode:	step and shoot, 60 projections
5. Acquisition time:	8 minutes
6. Corrections:	Energy and linearity on-line
	Uniformity: before reconstruction
Data Reconstruction:	
1. Prefiltering:	Butterworth, order 15,
	cut-off frequency 0.6 cycles/cm
2. Back-projection:	Shepp-Logan filter
3. Slices thickness:	3 pixel (6.9 mm)
4. Display:	Transaxial sagittal and coronal slices

Nuclear Medicine Communications 1994: (in press)

THALLIUM-201 MYOCARDIAL PERFUSION SPET: Adenosine Alone or Combined with Dynamic Exercise

S Mahmood
N K Gupta
M Gunning
J B Bomanji
P H Jarritt
P J Ell

Institute of Nuclear Medicine,
University College London Medical School

Correspondence and Reprints to:

Institute of Nuclear Medicine
University College London Medical School
Mortimer Street, London, UK
Phone:(071)-380 9424 Fax:(071)-637 0578

The use of pharmacological agents as an alternative to dynamic stress test for the assessment of myocardial perfusion is now well established(1-6). Coronary dilatation with adenosine, which has a half life of less than 10 seconds (7) is gaining more acceptance in the performance of routine myocardial perfusion tomographic studies (4, 8-12). The safety of combining a low level of dynamic exercise with adenosine has been reported previously (13). This study examines whether a combination of an infusion of intravenous adenosine and low level dynamic exercise will enhance the detection of coronary artery disease with thallium-201 myocardial perfusion single photon emission tomography (SPET).

MATERIALS AND METHODS

PATIENT POPULATION:

The study involved 90 patients referred for the investigation of myocardial perfusion - cardiac catheterisation data was available in all the cases. Of these, 40 patients (28 males, 12 females, aged 32-78) had undergone myocardial Tl-201 SPET using adenosine only-Group A. Group B-50 patients (32 males, 18 females, aged 30-81) underwent myocardial thallium-201 SPET using adenosine infusion combined with exercise. Significant coronary artery stenoses was considered if at least one of the major coronary arteries demonstrated 50% or more luminal obstruction. Four patients in group A had clinically documented myocardial infarction (MI) whilst eight patients in group B had prior history of MI. A high percentage of the patients in both groups were on medication. (Table 1).

STRESS PROTOCOLS:

Patient Preparation: The patients were advised to abstain from coffee/tea or caffeine containing drinks from the morning of the test. Whenever possible the patients were asked to withhold betablockers for at least 24-48 hours and other medication on the morning of the test. Patients were cannulated using a wide bore (gauge 19-21) i.v. cannula (Vasculon, *Viggo-Spectramed, Helsingborg, Sweden*) attached with a three-way stopcock (Connecta TH, *Viggo-Spectramed, Helsingborg, Sweden)*. The adenosine infusion bag was prepared so as to achieve a concentration of adenosine of 1mg/ml.

Adenosine only: The adenosine was infused at a rate of 140μg.kg^{-1}min^{-1} for a period of six minute, using a volumetric infusion pump (*Flo gard 6200, Baxter SA. NV. Lessines, Belgium*). At fourth minute of the infusion thallium-201 (thallous chloride, *Mallinckrodt Medical b.v. Patten, Holland*) was injected and infusion was continued for another two minutes.

Adenosine combined with Exercise: In patients of Group B, patients were

ABSTRACT

Thallium-201 myocardial perfusion SPET with pharmacological coronary vasodilatation using adenosine is now often used in the investigation of a patient with ischaemic heart disease (IHD). In this study, we present data from two groups of patients. Group A (n=40) experienced thallium-201 SPET with adenosine only as the pharmacological stress test, using an infusion rate of 140μg/kg/min. Group B patients (n=50) had the same test combined with low level dynamic exercise. The side effects were noted for both groups and thallium-201 SPET studies were acquired for stress and redistribution images. There was a lesser degree of non cardiac side effects in patients of group B. There was a significant difference in the haemodynamic parameters between the two groups. There was no significant difference in overall sensitivity (87% vs 90%) and specificity (84% vs 88%) in the detection of IHD between the two groups.

In conclusion, addition of low level of dynamic exercise with adenosine, is to be preferred to adenosine infusion alone, as this protocol is better tolerated and may enhance the detection of RCA disease (sensitivity=82% vs 90%, n.s.).

using a paired 't' test, whilst the mean changes between the two groups were analysed using an unpaired 't' test. The differences between the diagnostic results were analysed using a chi-squared test.

RESULTS:

CORONARY ANGIOGRAPHY:

15 patients in group A and 17 patients in the group B had single vessel disease on angiography. One patient had normal coronary anatomy in group A (Table 2a). The incidence of involvement of at least two coronary arteries was similar in the two groups (19/40 in group A vs 24/50 in group B). The total number of diseased left anterior descending (LAD) arteries was 27/40 (67%) in Group A, whilst it was 35/50 (70 %) in Group B. 57% (23/40) patients had right coronary artery (RCA) involvement in group A, in comparison to 62% (31/50) in group B. The incidence for LCx disease was 18/40 (45%) in group A, while it was 26/50 (52%) in group B.(Table 2b)

STRESS TEST:

Haemodynamic response: The mean heart rate during adenosine infusion changed from 71$\pm$13.3 to 94.4$\pm$18.3 in comparison with adenosine combined with exercise, where it changed from 65$\pm$14.2 at rest to 102$\pm$18.9 at peak stress. The systolic blood pressure changed from 137+20 mm Hg. at rest to 142$\pm$21.3 at peak stress during adenosine infusion, while the change was from 129.9$\pm$22 to 149$\pm$26.3 in patients of group B (adenosine combined with exercise). The diastolic blood pressure changed from 84$\pm$15.1 to 83.4$\pm$15.07 in group A, while it changed from 86$\pm$13.4 to 56$\pm$10.8 in patients of group B. Similarly the double product changed from 9888.79$\pm$2573.2 at rest to 13541.28$\pm$3607.28 at peak stress during adenosine infusion (group A), while in group B (adenosine with exercise) it changed from 8578.5$\pm$3125.54 to 15543.52$\pm$4963.13.

Side effects:Flushing was the commonest side effect noted in the group with Adenosine infusion alone (48%), whilst headache occurred in only 17% of patients in Group A. The incidence of chest pain (typical of angina) was similar in both groups (35% vs 36%) (Table 4). The patients of group B (adenosine combined with exercise) complained less of uneasiness in breathing or shortness of breath (16% vs 32%).

ST segments changes on ECG occurred in similar proportions in both groups (17% vs 20%). One patient in Group B developed marked sinus bradycardia, just after 1 minute of the infusion. Thallium 201 was injected and the test was terminated. The patient recovered spontaneously without any other side effects.

also asked to perform dynamic exercise using a bicycle ergometer, set for 25 watts for six minutes, simultaneous with the adenosine infusion (figure 1). 74 MBq. of thallium-201 was injected at the fourth minute, while adenosine infusion and exercise was continued for another two minutes.

All the patients were monitored with a single standard lead electrocardiogram. Heart rate and blood pressure were measured every two minutes.

DATA ACQUISITION

Single photon emission tomography (SPET) was started within five to ten minutes of the stress procedure. Data was acquired using IGE dual headed cardiac dedicated gamma camera, Optima (*International General Electric, Milwaukee, WI, USA*). The camera was equipped with a low energy, general purpose collimator and interfaced with an IGE Star4000i computer. All patients were imaged supine. For thallium-201 imaging energy peaks of 72 keV and 169 keV were used with 20% windows and no offset. All the acquisitions were performed using a matrix size of 64 x 64 W, 64 step and shoot projections, over 180° commencing at 45° right anterior oblique. The time per projection for stress was 20 seconds and for redistribution imaging the time per projection was 25 seconds. The redistribution imaging was performed at least 3 hours after the stress.

DATA PROCESSING:

The acquired data was reconstructed on a Star 4000i computer using a Hanning pre-filter with a cut off frequency of 0.75 cycles cm^{-1}. A ramp filter was applied during reconstruction using a back-projection algorithm. The reconstructed transaxial slices were then reorientated into vertical long, horizontal long, and short axis.

DATA ANALYSIS:

The data was analysed qualitatively, using vertical long, horizontal long, and short axis. The slices were divided into 9 segments (figure 2) : 1. Apex 2.Apical anterior 3. Basal anterior wall 4. Apical inferior 5. Basal inferior 6.Apical septum 7. Basal septum 8. Apical lateral wall 9. Basal lateral wall. The segments were scored either as normal or abnormal (fixed or reversible). In order to determine the sensitivity and specificity for individual coronary arteries, it was assumed that the anterior wall, apex and septum were supplied by the left anterior descending artery (segments No. 1, 2, 3, 6, and 7). The inferior wall was assigned to the right coronary artery (segments No. 4 and 5) whilst the left circumflex was related to segments No. 8 and 9 (lateral wall).

STATISTICAL ANALYSIS:

The change in haemodynamic parameters in each group was analysed

Overall, both methods of perfusion tomography confirmed the known high sensitivity in the detection of CAD. Although the sensitivity for the LCx was lower than LAD and RCA, with both methodologies, when combining LCx and RCA the sensitivity and specificity increased to 88% and 84% for adenosine only. Combined with exercise, the sensitivity and specificity changed to 90% and 88% respectively. This adds weight to the known concept that angiography does not fulfil the requirements of a gold standard to assign definite regions for detection of myocardial perfusion. Therefore, using the coronary angiogram as a frame of reference in order to determine sensitivity and specificity also has limitations. Figure 3 demonstrates an example, where the patient had single vessel disease of the LCx. The thallium-201 myocardial perfusion SPET images demonstrated reversible ischaemia not only in the lateral wall but also in the inferior wall. If the criteria of determining the sensitivity and specificity is changed, and instead the modified criteria is used, the thallium-201 SPET, by both methods was able to detect at least one abnormal segment for each diseased coronary artery. Our results are similar to those reported by others, using adenosine thallium-201 imaging (8,14-15). Even with adenosine-PET imaging, the sensitivity for the detection of CAD for LAD was 90.6%, for LCx it was 94.4% and for RCA was 96.6%, while the specificity was 93.3%, 96.6% and 94.1% respectively (10).

There was a clear improvement in the detection of RCA disease, when exercise was combined with adenosine, although there was no statistically significant difference (x^2= 1.4,n.s.).

Stress Test: Adenosine alone or combined with exercise changes heart rate and systolic blood pressure significantly. However there was no significant change in the diastolic pressure. There was significant change in the double-product by both methods. The mean change in heart rate with adenosine infusion was 32 ± 20, and it was 60 ± 29 for adenosine combined with exercise ($p<0.0001$)(table 3). The mean percentage change in systolic blood pressure was 4.3 ± 9.3 for adenosine infusion only, while it was 16.1 ± 18.8 for adenosine combined with exercise ($p<0.001$). The mean change in diastolic blood pressure was 0.0 ± 0.09 for group A (adenosine only), while it was 5 ± 9 for group B ($p<0.005$). The double product (mean change) also showed a significant difference by two methods ($p<0.05$).

The commonest side effects were due to the vasodilatory effect of adenosine e.g., flushing, light headedness, headache. However these effects were transient. It is now very well known that a combination of exercise to

One patient felt extremely unwell during adenosine vasodilation.

THALLIUM-201 SPET:

The overall sensitivity and specificity for the detection of CAD was similar in both groups (87% vs 90% and 84% vs 88%, respectively). The overall agreement for the detection of abnormal and normal segments in relation to coronary angiographic results was 91% for group A and 92% for group B. The agreement was 87% and 90% for abnormal segments, whilst the agreement for normal segments was 96% and 94% for both groups respectively. In group A (Adenosine only) out of 360 assigned segments for myocardium in 40 patients 179 segments were abnormal (29 fixed, 150 reversible), which were in agreement with the coronary angiogram. In group B (adenosine combined with exercise out of 450 assigned segments in 50 patients, thallium-201 SPET was able to detect 261 (40 fixed, 221 reversible) abnormal segments correctly in relation to coronary angiographic results (x^2=0.39, n.s.). Table 5 compares sensitivity and specificity for detection of coronary artery disease for individual coronary arteries.

Left Anterior Descending Artery: The sensitivity and specificity for the detection of LAD disease was 90% and 82% for adenosine only, while it was 92% and 84 % for adenosine combined with exercise. Thallium-201 myocardial perfusion SPET detected 161 abnormal segments in agreement with coronary angiogram in group B, while the number was 122 for group A (x^2=0.3, n.s.). 63 segments were declared as completely normal in group A and 72 in group B were detected as normal (concordant with coronary angiogram).

Left Circumflex Artery: The sensitivity for the detection of LCx disease was 80% and 84%, whilst the specificity was 86% and 85% for group A and B respectively. In group A, 36 segments were classified as abnormal based on the coronary angiogram, while thallium-201 myocardial perfusion SPET detected only 28 segments being abnormal. In group B out of 52 abnormal segments assigned for left circumflex disease thallium 201 myocardial SPET detected 44 segments as abnormal.(x^2=3, n.s.).

Right Coronary Artery: For RCA disease detection the sensitivity and specificity was 82% and 80% in group A, whilst it was 90% and 81% in group B. In group A out of 46 diseased segments on the basis of coronary angiogram, adenosine thallium 201 myocardial perfusion SPET detected 36 segments concordant with coronary angiography. In Group B 62 segments were abnormal on the basis of the coronary angiogram, whilst thallium 201 SPET detected 56 segments as abnormal. (x^2=1.4, n.s.).

DISCUSSION:

CONCLUSION:

Pharmacological stress testing facilitates standardization of thallium-201 scintigraphy. Adenosine has been shown to be a useful drug for this purpose. Whilst this study shows that there is no statistically significant difference between using adenosine alone or in combination with exercise for the detection of CAD; there is a some suggestion that adenosine combined with exercise is more sensitive in the detection of lesions in the regions of RCA.

Adenosine with moderate exercise also decreases drug related side effects. We recommend this protocol for routine myocardial perfusion scintigraphy.

adenosine infusion reduces the non-cardiac side effects(13). The incidence of side effects such as prolongation of PR interval, or development of AV block is lower in our study, as compared to results reported by others e.g., 10% by Verani et al., 2-3% (14) and 6.3% by Iskandrian et al.(9). This could be due to the fact that in comparison to others, where an infusion concentration of 2.4mg/ml was used(9) , we used a concentration of 1mg/ml. This allowed the same i.v. line to be used for the injection of thallium-201, with a three way tab. In our experience of more than 1200 patients, we have not encountered any difficulty when injecting the thallium-201 bolus through the same line.

Adenosine vs Dipyridamole: The mechanism of detection of CAD by drugs like adenosine and dipyridamole differs from dynamic exercise.

With dynamic exercise, myocardial oxygen demand is increased which determines the coronary blood flow reserve, the other leads to increased blood flow to segments not supplied by the stenotic coronary artery. The maximal flow in a normal coronary artery must be at least twice than that of the stenotic artery, to detect the defects on thallium-201 imaging (1). The advantage of using a pharmacological test is that it is not dependent upon the physical activity of the patient and the drugs. It is very well established that a sub maximal stress test will reduce the sensitivity of the test(16,17). Although vasodilation using dipyridamole has been studied extensively, and there have been studies suggesting that a combination of dipyridamole with exercise may enhance the detection of CAD (18-20). This could be partly be due to the facts that there is a considerable variation in the subject response to dipyridamole and as well as that it causes lesser degree of vasodilation (21,22). In case of adenosine it is well established that it causes maximal vasodilation (23) and one expects that under maximal coronary vasodilation, further addition of exercise will not increase the oxygen demand. The only advantage of combining exercise with adenosine is to reduce the side effects secondary to its vasodilatory action. It is possible that this maximal dilation of coronary vessels increases the extraction of thallium-201 into the normal myocardium, while it will much less in the abnormal segments and increasing the detection of areas of decreased perfusion.

There is some suggestion from this study that a combination of adenosine with exercise may enhance the detection of CAD in inferior wall because of reduced liver uptake of thallium-201. The average calculated heart to liver ratio in 10 patients was 0.88 ± 0.2 for adenosine alone and 1.06 ± 0.2 for the combined protocol ($p=0.55$, n.s.).

13. Mahmood S, Yepes-Mora S, Costa DC, Buscombe JR, Ell PJ. Simulatenous low level dynamic exercise and adenosine infusion in the assessment of myocardial perfusion. *Nucl Med Commun* 1993;14:241

14. Verani MS, Mahmarian JJ, Hixson JB, Boyce TM, Standacher RA, Diagnosis of CAD by controlled coronary vasodilation with adenosine and thallium-201 scintigraphy in patients unable to exercise. Circulation 1990; 82:80-87

15. Nishimura S, Mahmarian JJ, Boyce TM, Verani MS, Equivalence between adenosine and exercise thallium-201 myocardial tomography: a multicenter, prospective, crossover trial. *J Am Coll Cardiol* 1992;20:265-275

16. Iskandrian AS, Heo J, Kong B, Lyons E, Effect of exercise level on the ability of thallium-201 tomographic imaging in detecting coronary artery disease: analysis of 461 patients. *J Am Coll Cardiol* 1989;14:1477-1486

17. Heller GV, Ahmed I, Tilkermeier PL, Barbour MM, Garber CE, Influence of exercise intensity on the presence, distribution and size of thallium-201 defects. *Am Heart J* 1992:123:909-916

18. Walker PR, James MA, Wilde RPH, Wood CH, Russell R, Dipyridamole combined with exercise for thallium-201 myocardial imaging. *Br Heart J* 1986:55:321-329

19. Penell DJ, Mavrogeni S, Anagnostopoulos C, Ell PJ, Underwood SR, Thallium myocardial perfusion tomography using intravenous dipyridamole combined with maximal dynamic exercise. *Nuc Med Comm* 1993;14:939-945

20. Ignaszewski AP,McCormick LX, Heslip PG, McEwan AJ,Humen DP, Safety and clinical utility of combined intravenous dipyridamole/symptom limited exercise stress test with Thallium-201 imaging in patients with known or suspected coronary artery disease. *J Nucl Med* 1993;34:2053-2061

21. Rossen DJ, Simonetti I, Marcus ML,Winniford MD, Coronary dilation with standard dose of dipyridamole and dipyridamole combined with hand-grip *Circulation* 1989;79:566-572

22. Wilson RF, Laughlin DE, Ackell PH, Chilian WM, Holida MD, Hartley CG, Armstrong ML, Marcus ML, White CW, Transluminal subselective measurement of coronary artery blood flow velocity and vasodilator reserve in man. *Circulation* 1985;72:82-92

23. Wilson RF, Wyche K, Christensen BV, Zimmer s, Laxson DD, Effects of adenosine on human coronary arterial circulation *Circulation* 1990;82:1595-1606

REFERENCES

1. Gould KL, Noninvasive assessment of coronary stenoses by myocardial perfusion imaging during pharmacologic coronary vasodilation. I. Physiologic basis and experimental validation. *Am J Cardiol* 1978:41:267-278

2. Francisco DA, Collins SM, Go RT, Erhardt JC, Vancirck Oc, Marma ML. Tomographic thallium-201 myocardial perfusion scintigrams after maximal coronary vasodilation with intravenous dipyridamole. Comparison of qualitative and quantitative approaches. *Circulation* 1982;66:370-379

3. Leppo J, Boucher CA, Okada RD, Newell JB, Strauss HW, Pohost G. Serial thallium-201 myocardial imaging after dipyridamole infusion: diagnostic utility in detecting coronary stenoses and relationship to regional wall motion. *Circulation* 1982;66:649-657

4. Nguyen T, Heo J, Ogilby D, Iskandrian As. Single photon emission tomography with thallium-201 during adenosine induced coronary hyperaemia: Correlation with coronary arteriography, exercise thallium imaging and two-dimensional echocardiography. *J Am Coll Cardiol* 1990;16:1375-1383

5. Penell DJ, Underwood SR, Swanton RH, Walker J, Ell PJ. Dobutamine thallium myocardial perfusion tomography, *J Am Coll Cardiol* 1991;18:1471-1479

6. Elliott BM, Robinson JG, Zellner JL, Hendrix GH. Dobutamine Tl-201 imaging. Assessing cardiac risks associated with vascular surgery. *Circulation* 1991;84(Suppl III):54-60

7. Moser GH, Schradler J, Deussen A, Turnover of adenosine in plasma of human and dog blood *Am J Physiolog* 1989; 25 (Cell Physiology 25):C799-C806

8. Verani MS, Mahmarian JJ, Myocardial perfusion scintigraphy during maximal coronary artery vasodilation with adenosine. *Am J Cardiol* 1991; 67:12D-17D

9. Iskandrian AS, Single photon emission computed tomographic thallium imaging with adenosine, dipyridamole, and exercise. *Am Heart J* 1991;122:279-284

10. Gupta NC, Esterbrooks D, Mohiuddin S, Hilleman D, Sunderland J, Shiue CY, Frick MP, Adenosine in myocardial perfusion imaging using positron emission tomography. *Am Heart J* 1991;122:293-301

11. Zoghbi WA, Use of adenosine echocardiography for diagnosis of coronary artery disease. *Am Heart J* 1991;122:285-292

12. Coyne EP, Belvedere DA, Van de Streeke PR, Weiland FL, Evans RB, Spaccavento LJ, Thallium-201 scintigraphy after intravenous infusion of adenosine compared with exercise thallium testing in the diagnosis of coronary artery disease. *J Am Coll Cardiol* 1991;17:1289-1294

Table 1: Patients studied.

	Group A	Group B
	Adenosine *(n=40)*	**Adenosine+Exercise** *(n=50)*
Age	32-78(57±11.5)	30-82(56+10.8)
Sex(M/F)	28/12	32/18
Past MI	4	8
Post angioplasty	2	6
Diabetes	2	4
Hypertension	4	6
Valvular heart disease	2	1
Symptoms class:		
a)Typical angina	16	21
b)Atypical chest pain	10	10
c)No chest pain	9	7
d)Exertional dyspnoea	3	6
e)SOB+angina	2	3
Medical Treatment:		
a)Beta blockers only	3	6
b)Calcium blockers only	1	-
c)Nitrates only	5	5
d)Combination of at least two	31	39
Electrocardiogram:		
a)Atrial fibrillation	1	3
b)Ventricular ectopics	2	4
c)LBBB/RBBB	3	-
d)Ist degree A-V block	1	2

(SOB= short of breath, LBBB=left bundle branch block, RBBB=right bundle branch block)

LEGEND:

Table 1: Patterns studied.(SOB= short of breath, LBBB=left bundle branch block, RBBB=right bundle branch block)

Table 2a:Distribution of findings at coronary angiography.

Table 2b:Distribution of diseased coronary arteries amongst the patients of group A and B. There is no significant difference between two groups. (x^2=0.227, n.s.)

Table 3: Haemodynamic Parameters (HR=heart rate, Sys.=systolic, Dia.=diastolic, BP=blood pressure, DP=double product)

Table 4: Side effects observed with adenosine only or in combination with exercise.

Table 5: Sensitivity and Specificity for Thallium-201 SPET using two methodologies. (LAD=left anterior descending artery, LCx=left circumflex artery, RCA=right coronary artery)

Figure 1: Stress protocols

Figure 2: The nine segments of the left ventricle used for qualitative analysis.

Figure 3: Thallium-201 myocardial perfusion SPET of a patient with a lesion of the LCx. The patient underwent a stress protocol of adenosine combined with exercise. Reversible ischaemia is seen in the lateral as well as the inferior walls.

Table 2b: Distribution of diseased coronary arteries amongst patients of groups A and B.

Coronary Artery	*No. of diseased coronary arteries*	
	Adenosine only	*Adenosine + Exercise*
Left anterior descending(LAD)	27	35
Left Circumflex(LCx)	18	26
Right Coronary Artery(RCA)	23	31
Total	68* /120	92* /150

(*, x^2=0.227, n.s.)

Table 2a: Distribution of findings at coronary angiography

Coronary Artery	*Adenosine only (n=40)*	*Adenosine + Exer. (n=50)*
SINGLE VESSEL DISEASE	**15**	**17**
Left anterior descending(LAD)	8	9
Left Circumflex(LCx)	3	1
Right Coronary Artery(RCA)	4	7
TWO VESSEL DISEASE	**19**	**24**
LAD + RCA	9	8
RCA + LCx	5	7
LAD + LCx	5	9
THREE VESSEL DISEASE	**5**	**9**
NORMAL CORONARIES	**1**	-

Table 4: Side effects observed with adenosine only or in combination with exercise.

SIDE EFFECTS	ADENOSINE ONLY	ADENOSINE + EXERCISE
Flushing	19 (48%)	4 (8%)
Headache/light headedness	7 (17%)	2 (4%)
Uneasiness in breathing	13 (32%)	8 (16%)
Abdominal discomfort	4 (10%)	1 (2%)
Chest pain (typical)	14 (35%)	18 (36%)
Pain at other sites	6 (15%)	3 (6%)
Ist degree AV block	2 (5%)	-
ST changes on ECG	7 (17%)	10 (20%)
Ventricular ectopics	6 (15%)	11 (22%)
Sinus bradycardia	-	1 (2%)
Extremely unwell	1 (2.5%)	-

Table 3: Haemodynamic parameters

	Mean change in HR	Mean change in Sys.BP	Mean change in Dia. BP	Mean change in DP
Adenosine only	32±20	4.3±9.3	0.0±0.09	0.019+0.042
Aden.+Exer.	60±29	16.1±18.8	5±9	0.126+0.25
'p'	<0.001	<0.001	<0.005	<0.005

Figure 1: Stress Protocol

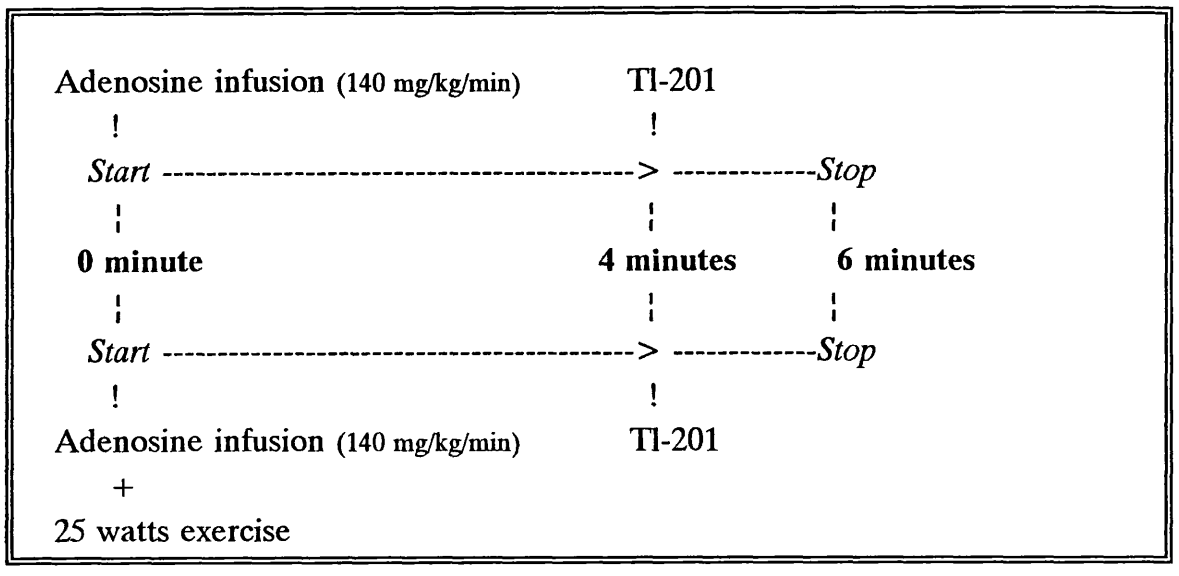

Table 5: Sensitivity and Specificity for Thallium-201 SPET using two methodologies.

Coronary Artery	*Adenosine only (n=40)*		*Adenosine+Exercise (n=50)*	
	Sensitivity	Specificity	Sensitivity	Specificity
LAD	90%	82%	92%	84%
LCx	80%	86%	84%	85%
RCA	82%	86%	90%	81%
Combined LCx+RCA	88%	90%	87.7%	86%
Overall (LAD+LCx+RCA)	**87%**	**84%**	**90%**	**88%**

Clinical Nuclear Med. (in press)

SHORT COMMUNICATION

High resolution renal single photon emission tomography in eight minutes using a multi-detector gamma camera.

John R. Buscombe
Caroline E. Townsend
Kypros Kouris
Gill Clarke
Shahid Mahmood
Peter H. Jarritt
Peter J. Ell

Institute of Nuclear Medicine,
University College London Medical School,
Mortimer Street,
London W1N 8AA, UK.

Address for correspondence: J.R. Buscombe, Institute of Nuclear Medicine, UCLMS, Mortimer Street, London W1N 8AA

Tel +44 71 380 9419

Introduction

Single photon emission tomography (SPET) of the kidneys using ^{99m}Technetium labelled dimercaptosuccinic acid ($^{99}Tc^{m}$ - DMSA) has been proposed as a method to improve the sensitivity of static renal scintigraphy (1,2). SPET allows more defects in the renal cortex to be visualised than can be seen with planar imaging and it gives a better characterisation of the size and extent of a defect (3). This may be particularly true in children where the early identification of scars may have a significant effect on subsequent management and morbidity (4). Despite these advantages, the 30-40 min SPET acquisition time necessary, if a conventional single-headed gamma camera is used, is a major deterrent to the widespread use of SPET.

Multi-detector SPET systems, comprising more than one gamma cameras (typically three) set in a rotating gantry have recently become available. They have been shown to provide better quality images at reduced imaging times compared to a single headed gamma camera in brain, skeletal and cardiac scintigraphy (5-7).

The aim of this study was to use a three headed multi-detector gamma camera (Toshiba GCA-9300A), to determine if it is possible to perform clinical high resolution renal SPET with only an 8 min acquisition.

Abstract

Planar renal scintigraphy with $^{99}Tc^{m}$-DMSA has become established as a standard diagnostic test to determine if a kidney has been scarred by infection. It has been suggested that high resolution single photon emission tomography (SPET) may improve the sensitivity of detection of renal scars. To determine if it is possible to produce good quality renal SPET with a short acquisition time 10 adults were studied on a new multi-detector gamma camera using 8, 16 and 32 min acquisitions. The number of defects seen (n=16) with an 8 min acquisition was not significantly different from the defects (n=15) seen using a 16 and a 32 min acquisition. In adults when imaging with a multi-detector gamma camera there was no clinical advantage in using an acquisition of longer than 8 min.

Key words: Technetium-99m Dimercaptosuccinic acid High

Planar studies were performed following the SPET acquisitions using standard posterior, right posterior oblique and left posterior oblique views with data collected on a 256^2 word matrix, pixel size 1.6mm for 500kcounts per image.

Data processing; Tomographic reconstruction of data from the Toshiba GCA-9300A was done after Butterworth prefiltering of the 60 projections, the parameters of the filter depending on the total counts obtained. A Shepp-Logan backprojection filter was used and no attenuation correction was applied. Tomographic images were displayed as transaxial, coronal and sagittal slices of 3 pixel thickness (9.3mm apart). Images were formatted onto X-ray film using a Kodak Ektascan laser printer (*Kodak limited, Hemel Hampstead, Herts*) and were then reported routinely by a Physician in Nuclear Medicine. An abnormality was defined simply, and qualitatively as a defect seen on the surface of the kidney (except at the site of the renal pelvis, which was considered normal). Planar images were reported positive if defects were seen using the same criteria.

Subjects and methods

Patients; Studies were performed on 10 adults who were referred for clinical static renal scintigraphy and were thought to have a reasonably high risk of renal scarring. This study was limited to adults as the SPET imaging protocol required 32 min. Seven patients were male and the mean age was 35 years (range 18-57 years). To maximise the possibility of finding a reasonable number of renal scars all patients had a history of recurrent proven urinary tract infection and vesico-ureteric reflux.

Instrumentation; Each patient had three studies performed using a Toshiba GCA-9300A three headed gamma camera (*Toshiba Medical Systems Europe BV, Delft, The Netherlands*) consisting of three Anger-type cameras placed 120° apart on a rotating ring gantry in a triangular configuration. For each head the radius of rotation can be adjusted between 132mm and 307mm. Each camera was fitted with a parallel hole high resolution collimator with a 410x210mm field of view (FOV). In addition all 10 patients had planar imaging performed using an IGE 400ACT Starcam single-headed gamma camera/computer (*IGE, Radlett, Berks, U.K.*) fitted with a parallel hole high resolution collimator.

Data acquisition; Each set of SPET studies was performed 3 hours after the administration of 2mCi (74MBq)of $^{99}Tc^{m}$-dimercaptosuccinic acid (DMSA). Data was obtained as 60 projections, 128^2 word matrix, 3.2mm pixel size, over 360°. Since data was acquired continuously for 32 min, it was possible to computationally extract three sets of data for studies

Discussion

The new generation of multi-detector gamma cameras such as the Toshiba GCA-9300A is able to produce high resolution renal SPET images using an 8 min acquisition. Using a dedicated SPET system will allow patients to be imaged when there is a clinical indication for SPET without using valuable time on a conventional camera thereby disrupting the smooth operation of the department. As the patient couch and camera heads are optimised for SPET imaging patient positioning is both quick and simple on a dedicated multi-detector gamma camera system.

The results obtained from an 8 min SPET acquisition are not significantly different from those obtained using longer acquisition times on the same machine. The cortex of the kidney is clearly seen with good definition of the pelvis and calyces.

Good spatial resolution in the images seen using the multidetector gamma camera is due, in part, to the good volumetric sensitivity of the high resolution collimators supplied with the Toshiba GCA-9300A. The Toshiba GCA-9300A has a volume sensitivity of 10.8 kcps/(MBq/ml)/cm per head compared with a volume sensitivity of 7.6 kcps/(MBq/ml)/cm for a high resolution collimator and 12.8 kcps/(MBq/ml)/cm for a general purpose collimator supplied with a standard single headed gamma camera such as the IGE starcam 400AC (8). The tomographic spatial resolution (full width half maximum in air) of the Toshiba GCA-9300A with high resolution collimators was 9.5mm compared with 9.3 mm for the IGE starcam 400AC. Therefore the Toshiba collimator design maintains good spatial resolution but with improved sensitivity.

It has been previously shown using a 30 minute acquisition on

Results

Using the three acquisition times of 8, 16 and 32 min (Table I) the total number of defects, consistent with a renal scar, seen on the 3 studies were almost identical. The images obtained from the multidetector gamma camera were of technically excellent standard with the structure inside the kidney including the calyces being clearly visualised. There was only a slight reduction in the quality of the images obtained using an 8 min acquisition when this was compared with the images produced with 16 and 32 min acquisition times. The site of the lesions seen were identical in all the studies with minimal difference in the size and shape of the defect. (Fig 1). In one patient (D.T.) a small upper pole defect was reported in the 8 min acquisition compared with a normal study seen in the 16 and 32 min acquisitions. This was a small defect and looked less like a scar than some thinning of renal cortex at this site.

There was a total of 11 defects seen in the planar images of all 10 patients compared with a total of 16 defects seen in the 8 min acquisition and a total of 15 defects seen in both the 16 and 32 min acquisition SPET images (not significant, $X^2=0.75$, $0.95>p<0.05$). There was no significant difference in the number of defects seen with 8, 16 and 32 minute SPET acquisition ($X^2=0.42$, $0.95>p<0.05$). All but one of the defects seen with planar imaging were present in the SPET images.

The mean total counts obtaind per 8 min acquisition was 2290 kcounts (range 1269-2902 kcounts). In one patient with chronic renal failure (D.M.) good SPET images were obtained despite a high background activity of $^{99}Tc^m$-DMSA.

SPET. Ensuring that maximum information is obtained from each $^{99}Tc^{m}$-DMSA study.

the detection of renal scars is 35% higher than planar imaging (9). Unfortunately the long acquisition time meant that when children were imaged sedation was required. Though a more recent study on a smaller group of children failed to confirm a significant increase in sensitivity in detecting scars with SPET compared with planar imaging. However the authors suggested that SPET is still recommended as the extent of scarring was more clearly defined with SPET (10).

Though more defects were seen with SPET than planar imaging this was not significant as patient numbers were small. Interestingly one of our patients (D.M.) had an apparent defect seen on planar imaging but a normal SPET. This is probably due to the patient's renal impairment which resulted in a high background level of activity. The improved contrast resolution available from the SPET images therefore enabled the outline of the cortex to be seen more clearly and demonstrated that the apparent scar seen on the planar image was not real.

The ability of a multidetector scanning instrument to perform high resolution SPET with a short acquisition time will increase the availability of SPET to patients undergoing studies with $^{99}Tc^{m}$ DMSA and it may be of particular use in children. The intrument we have used in this study has been able to perform skeletal SPET in children with metastatic disease using a short acquisition time (11).

Conclusion: Many Nuclear Medicine facilities remain resistent to the idea of routine renal SPET with $^{99}Tc^{m}$ DMSA probably because of the difficulties of adding a further 30-35 min acquisition to a tight working schedule. Despite the initial capital outlay for a multi-detector gamma camera, the nuclear medicine department will be able to perform a wid

8) Moore S.C., Kouris K., Cullum I. Collimator design for single photon emission tomography. *Eur J Nucl Med* 1992; 19; 38-150.

9) Tarkington MA, Fildes RD, Lewin K, Zeissman H, Harkness B, Gibbons MD. High resolution single photon emission computerized tomography (SPECT) 99m-technetium-dimercapto-succinic acid renal imaging: A state of the art technique. *J Urol* 1990;144; 598-600.

10) Mouratidis B., Ash J.M., Gilday D.L., Comparison of planar and SPECT $^{99}Tc^{m}$-DMSA scintigraphy for the detection of renal cortical defects in children. *Nucl Med Commun* 1993; 19, 82-86.

11) Buscombe J.R., Townsend C.E., Clarke G., Kouris K., Ell P.J. Fast skeletal SPET in the assessment of chest metastases in young patients with primary bone tumours. *Nuc Med Commun* 1992; 13; 248.

References

1) MacDonald AF, Keyes WI, Mallard JR, Steyn JH. Diagnostic value of computerised isotopic renal scanning. *Eur Urol* 1977; 3; 289-191.

2) Steyn JH, MacDonald AF, Keyes WI., Bayliss AP, Towler J.M. An assessment of computerised isotopic renal section scanning *Br J Urol* 1978; 50; 437-441.

3) Williams ED, Parker C, Rankin D, Roy DD. Multiple section radionuclide tomography of the kidney: A clinical evaluation *Br J Radiology* 1986; 59; 975-983.

4) Saxena SR, Laurence BM, Shaw DG. The justification for early radiological investigation of urinary tract infection in children *Lancet* 1975, ii, 403-404.

5) Kouris K., Costa D.C., Jarritt P.H., Townsend C.E., Ell P.J., Brain SPECT using a multidetector three headed camera system. *J Nucl Med Technol* 1992; 20; 68-72.

6) Buscombe JR, Townsend CE, Kouris K, Clarke G, Jarritt PH, Mahmood, S, Ell PJ. Clinical high resolution skeletal SPET in 8 minutes using a multidetector gamma camera. *Brit J Radiology* 1992; 65; Congress 34.

7) Mahmood S, Townsend CE, Kouris K, Costa DC, Buscombe JR, Ell PJ Effective myocardial perfusion SPET in 8 minutes utilising a multidetector gamma camera. *Eur J Nucl Med* 1992; 19; 871

Legends for figures

Fig 1a-d. Planar image (**a**) of both kidneys of a patient with normal kidneys but some dilataion of the calyces and thinning of the renal cortex at the upper pole seen with 8 (**b**), 16 (**c**) and 32 (**d**) minute acquisitions.

Fig 2a-d. Planar image (**a**) of both kidneys in a patient with two renal scars (arrowed). Coronal SPET slices of the right kidney (the left kidney lies anterior to the right kidney and is only partially visualised) clearly shows three cortical scars (arrowed) and also dilated calyces using 8 (**b**), 16 (**c**) and 32 (**d**) minute acquisitions.

Table I: Comparison of number of lesions seen with 500 kcounts planar, 8, 16 and 32 min SPET acquisitions.

Patient	Number of lesions seen			
	Planar	SPET		
		8min	16min	32min
V.A.	2	3	3	3
A.E.	3	4	4	4
E.B.	0	0	0	0
M.D.	1	2	2	2
D.M.	1	1	1	1
T.G.	0	0	0	0
D.T.	0	1	0	0
D.M.	1	0	0	0
J.A.	3	4	4	4
P.M.	0	1	1	1
Total	**11**	**16**	**15**	**15**

1993, *The British Journal of Radiology*, 66, 817–822

Clinical high resolution skeletal single photon emission tomography using a triple-headed gamma camera

J R BUSCOMBE, MSc, MRCP, C E TOWNSEND, DCR, DNM, K KOURIS, BSc, PhD, G CLARKE, BSc, MSc, S MAHMOOD, MBBS, MSc, P H JARRITT, BSc, PhD and P J ELL, MD, MSc, FRCP, FRCR

Institute of Nuclear Medicine, University College London Medical School, Mortimer Street, London W1N 8AA, UK

Abstract

Planar skeletal scintigraphy has become established as a standard diagnostic test performed within the nuclear medicine department. Since the 1970s good quality images have been produced using an Anger gamma camera and $^{99}Tc^{m}$-labelled diphosphonates. Single photon emission tomography (SPET) has improved the sensitivity of detection and the ability to localize bony pathology, particularly benign bone disease in the spine. Recently multi-detector gamma cameras dedicated to SPET have become available. One such system, the Toshiba GCA-9300A, has been used to perform routine clinical skeletal SPET in 81 patients. Good quality images have been obtained using an 8 min acquisition in the axial skeleton and a 16 min acquisition protocol in the peripheral skeleton. Multiple sites can be tomographed in the same patient during the same examination using two or more 8 min acquisitions. Such a multi-detector gamma camera offers advantages over the standard single-headed rotating camera for skeletal SPET in terms of both imaging time and image quality. A cost analysis was performed which demonstrated that the additional cost of purchasing such a multidetector gamma camera was less than £30.00 per SPET study.

Skeletal single photon emission tomography (SPET) has been shown to be more sensitive than planar scintigraphy in identifying bony pathology (Onsel et al, 1990; Keogan et al, 1991; Kanmaz et al, 1992). Despite this advantage, the 30 min SPET acquisition time necessary if a conventional single-headed gamma camera is used remains a major deterrent to the widespread use of SPET in skeletal scintigraphy.

Multi-detector SPET systems, comprising more than one gamma camera (typically three) set in a rotating gantry, have recently become available. They have been shown to provide better quality images with shorter imaging times than a single-headed gamma camera (Kouris et al, 1992). Some systems have a small field of view and a short radius and are dedicated to imaging the head or possibly small children. Other multi-detector gamma cameras can image any part of the body.

The aim of this study was to use one such new multi-detector gamma camera (Toshiba GCA-9300A) to evaluate the clinical utility of the system in routine skeletal SPET, and particularly to see whether good quality studies can be obtained with a rather shortened 8 min acquisition time.

Subjects and methods

Patients

85 studies on 81 patients were performed over 8 months. Images of the site of interest were acquired in 8 min each for all patients (Table I), and four patients had two different sites imaged. The studies were performed only on patients in whom SPET was clinically indicated. This was decided after inspection of the planar images. 53 studies were performed for benign disease and the rest were for either primary bone tumour or metastatic bony disease (Table II). In all patients whose peripheral skeleton was studied, a 16 min acquisition was performed. Ten patients had a 32 min acquisition from which data for 8 and 16 min were extracted. Two patients also had an additional 32 min SPET acquisition using a single-headed gamma camera for comparison.

Received 3 September 1992 and in revised form 16 February 1993, accepted 22 March 1993.

Instrumentation

All studies were performed using a Toshiba GCA-9300A three-headed gamma camera (Toshiba Medical Systems Europe BV, Delft, The Netherlands) consisting of three Anger type cameras placed 120° apart on a rotating ring gantry in a triangular configuration. For each head the radius of rotation can be adjusted between 132 mm and 307 mm. Each camera was fitted with a parallel hole high resolution collimator with a 410 × 210 mm field of view (FOV). Two patients were also imaged using an IGE 400ACT Starcam single-headed gamma camera (IGE, Radlett, Berks) fitted with a parallel hole high resolution collimator.

Data acquisition

Each study was performed 3 h after the administration of 550 MBq of $^{99}Tc^{m}$-methyl diphosphonate (MDP). Data was obtained as 60 projections, 128^2 word

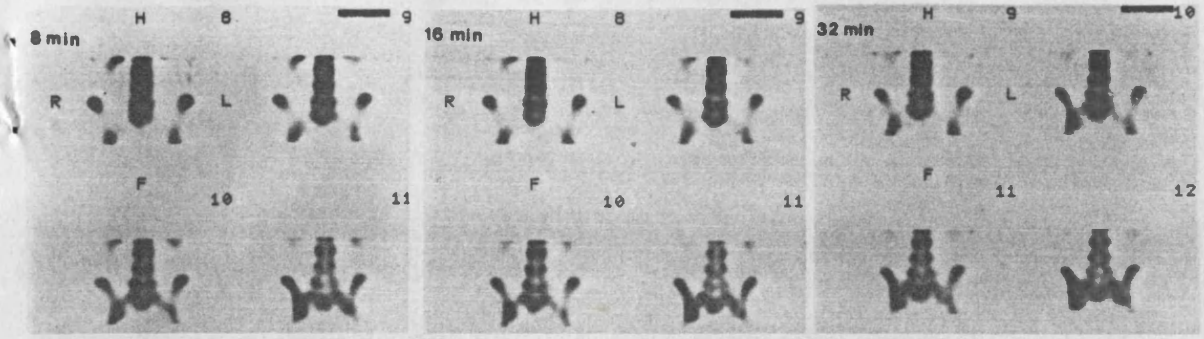

(a) (b) (c)

Figure 1. Coronal SPET slices of the lumbar spine imaged with (a) 8 min, (b) 16 min and (c) 32 min acquisitions. (Acquisition parameters and filter size in Table IVa). *Please note that as data from each acquisition time was reconstructed separately the number assigned to identical slices may not be the same in each image.*

Results

Using the three acquisition times of 8, 16 and 32 min (Table III) the total numbers of "hot spots" seen on the three studies were identical. The sites of the lesions seen were identical in all the studies though there was some difference in the shape and intensity. All the hot spots were in the bone except for one patient (no. 5) where there was uptake in the lung from a soft tissue metastasis originating from an osteosarcoma. This lesion was not visible on the planar images performed before the SPET study.

Comparing image quality, both in definition of normal skeletal structure and lack of distortion, the images with 32 min acquisition time showed some improvement over those with 8 or 16 min acquisition time in the axial skeleton (Figure 1), but this was not significant. In the spine it is possible to see the spinal canal and posterior arch structures clearly on an 8 min acquisition (Figure 2). Outside the axial skeleton, for example in the knees or femora, where count density was lower, the 16 min acquisition produced an image of much better quality than the 8 min acquisition. In a patient whose the pelvis was imaged (no. 10) no hot spots were reported. It was possible to see the hips clearly only with the 8 min acquisition, as in the 16 min and 32 min acquisition images the hips were obscured by reconstruction artefacts arising from bladder activity. Generally an 8 min acquisition of the lower pelvis obtained just after the patient had voided demonstrated the normal bony structure and any pathology clearly (Figure 3).

Comparing the counts obtained from the two patients imaged with both systems (Table IV), it is clear that the total counts obtained with 8 min acquisition using the multi-detector gamma camera are about the same as those from a 32 min acquisition on a single-headed gamma camera, though the image quality of the knee SPET was improved by using a 16 min acquisition (Figure 4).

In 69 out of the remaining 71 patients who underwent either an 8 or 16 min SPET acquisition for a clinical indication, all images were of good quality. Four patients were able to have SPET performed on more than one site using two 8 min acquisitions. Unfortunately two patients had difficulty voiding urine and their SPET studies of the pelvis were unreportable.

Discussion

This study shows that fast high resolution SPET is now possible using the new generation of multi-detector gamma cameras such as the Toshiba GCA-9300A. The advantage of such a system is that patients can be imaged when there is a clinical indication for SPET without using camera time on a conventional camera and thereby disrupting the smooth operation of the department.

Skeletal SPET has become increasingly useful in

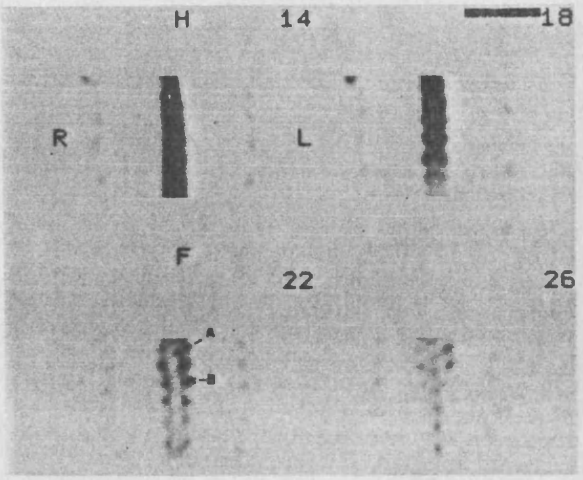

Figure 2. An 8 min acquisition of the spine clearly demonstrating the main features of the skeletal anatomy including (A) the spinal canal and (B) the facet joints. (Total counts 15371 kcounts, Butterworth filter size 18).

Table I. Site of SPET imaging in 85 studies

Site of SPET acquisition	No. of studies performed
Lumbar spine	38
Thoracic spine/chest	18
Head/neck	7
Lower pelvis/hips	10
Knees	9
Femora	2
Feet	1

Table II. Clinical indication for SPET studies and sites imaged

Indication	No. of studies	Site imaged
Mechanical pain	42	32 Lumbar spine 5 Chest 4 Pelvis 1 Head/neck
Primary bone tumour	21	12 Chest 4 Pelvis 2 Knees 2 Femora 1 Head/neck
Metastatic bone disease	11	5 Lumbar spine 3 Head/neck 2 Hips/pelvis 1 Chest
Trauma	5	5 Knees
Avascular necrosis	4	2 Knees 1 Feet 1 Head/neck
Osteomyelitis	2	1 Head/neck 1 Lumbar spine

matrix, 3.2 mm pixel size, over 360°. This was accomplished using the continuous acquisition mode in which each head rotates 120° clockwise and then 120° anticlockwise back to its original position. As each head samples a different 120° sector, a complete 360° of data was collected during each full clockwise/anticlockwise cycle. Each cycle took 4 min so that an 8 min acquisition consisted of two such cycles. If data was acquired continuously for 32 min it was possible to extract multiple data sets for 8 min, 16 min or 32 min of acquisition time. Data from the two patients imaged with the single-headed gamma camera was collected as 64 projections on a 128^2 word matrix using step shoot acquisition mode and 30 s per projection (total acquisition time 32 min).

Data processing

Tomographic reconstruction of data from the Toshiba GCA-9300A was done after Butterworth prefiltering of the 60 projections, the parameters of the filter depending on the total counts obtained. A Shepp-Logan back-projection filter was used. No attenuation correction was applied as the bone tends to be close to the surface and no quantitation was performed on the data. Images were displayed as transaxial, coronal and sagittal slices. Spatial resolution of the reconstructed SPET data was 9.5 mm. Images were formatted onto X-ray film using a Kodak Ektascan laser printer (Kodak Ltd, Hemel Hempstead, Herts) using a 128×128 matrix. The distance between the displayed slices was 6.2 mm. The images were then reported routinely by a consultant in nuclear medicine. An abnormality was defined simply and qualitatively as a "hot spot" within the skeleton, as in the routine interpretation of bone scintigraphy. Tomographic reconstruction of the data from the single-headed gamma camera was performed without attenuation correction using a Hanning pre-filter with 0.8 cycles cm^{-1} cut-off frequency and ramp back-projection filter. Images were displayed in transaxial, coronal and sagittal slices and formatted onto X-ray film. Using a 210×400 mm region of interest (ROI) which corresponded to the area imaged using the Toshiba GCA-9300A, the total counts obtained with each system were compared.

Table III. Number of defects seen in 10 patients imaged for 8, 16 and 32 min

Patient no.	Site imaged	Site of abnormality	Acquisition time (min)		
			8	16	32
1	Knees	Left femoral condyles	5	5	5
2	Knees	Left and right tibial tuberosities and left patella	3	3	3
3	Lumbar spine	L4/5 facet joints	2	2	2
4	Lumbar spine	Bodies L5 and S1	2	2	2
5	Chest	Metastasis left lung	1	1	1
6	Lumbar spine	Bodies L1 and L5 and right L4/5 facet joint	3	3	3
7	Chest	Nil	0	0	0
8	Chest	Bodies T10 and T12	2	2	2
9	Lumbar spine	Body L4, spinuous process L4	2	2	2
10	Pelvis	None seen	0	0[a]	0[a]

[a]In both these studies activity in the bladder led to significant artefacts appearing on the reconstructed image.

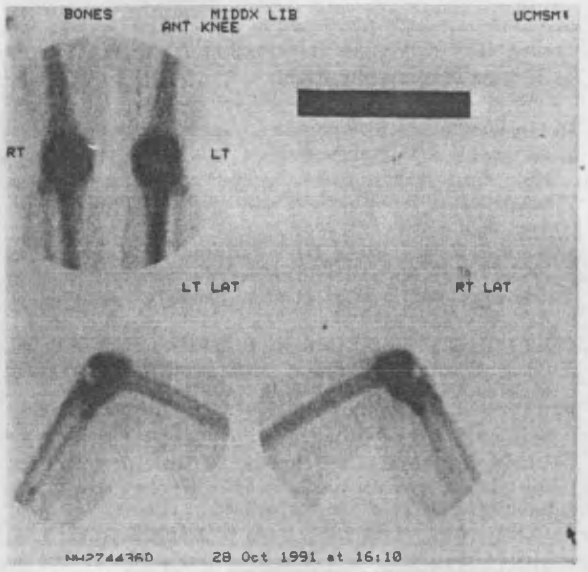

(a)

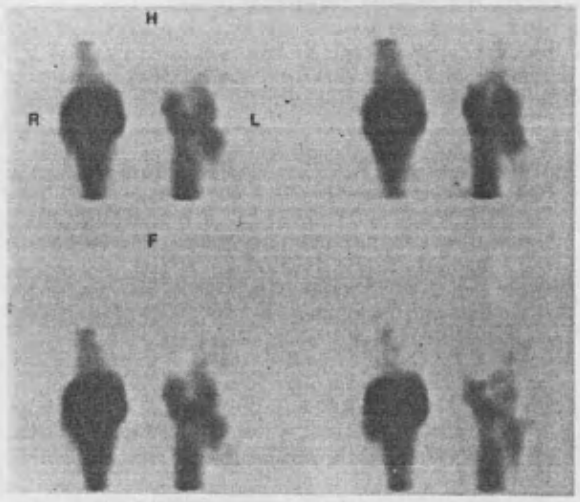

(b)

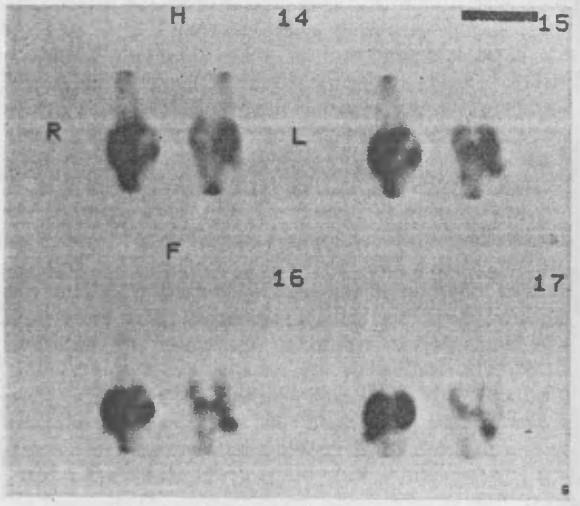

(c)

Figure 4. Skeletal scintigraphy of the knees seen with (a) planar imaging, (b) a 32 min SPET acquisition using a single-headed gamma camera and (c) an 8 min acquisition using the Toshiba GCA-9300A. (Acquisition parameters and filter size in Table IVb).

The two patients imaged using both systems demonstrated that the count obtained in 8 min with the Toshiba GCA-9300A is slightly more than that obtained in 32 minutes on the single-headed camera. This is because the Toshiba GCA-9300A has a higher tomographic volume sensitivity for a single head of 10.8 kcps $(MBq\ ml^{-1})^{-1}\ cm^{-1}$ (32.8 kcps $(MBq\ ml^{-1})^{-1}\ cm^{-1}$ for the complete system) compared with that of the IGE 400ACT Starcam at 7.6 kcps $(MBq\ ml^{-1})^{-1}\ cm^{-1}$ (Moore et al, 1992). The reconstructed spatial resolution (full width half maximum (FWHM) in air) of the single-headed camera was 9.7 mm. This was almost identical to the reconstructed spatial resolution of the Toshiba GCA-9300A which was 9.5 mm. Differences in image quality may be due in part to the higher sensitivity of the three-headed system but may also be due to the different methods of SPET reconstruction and display used on each system.

As the radius of each head can be adjusted independently, it was possible on the multi-detector gamma camera to optimize the position of the heads so that each head was as close to the patient as possible. By using a ring to mount the heads there was no need to use a cumbersome gantry arm which impedes movement of the detectors around the patient. This also made optimum patient positioning simpler.

The ability of the Toshiba GCA-9300A to perform high resolution SPET with a short acquisition time

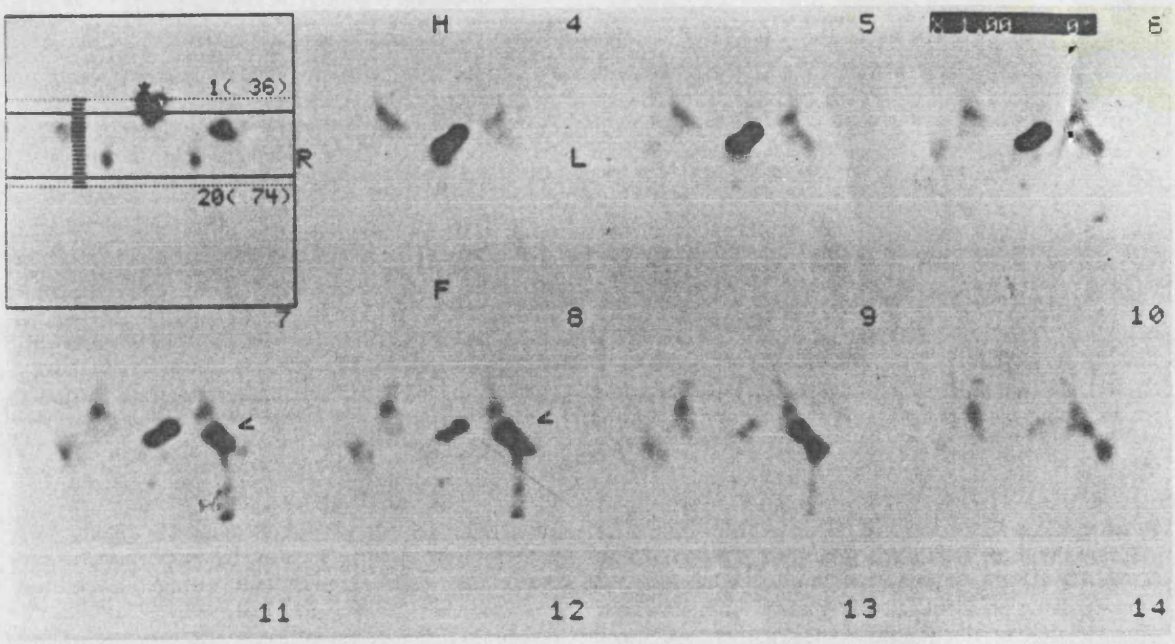

Figure 3. An 8 min acquisition of the pelvis in a patient with fibrous dysplasia (arrowed), demonstrating good imaging of the hips with no interference from activity in the bladder. (Total counts 10011 kcounts, Butterworth 16).

the management of benign bone disease (Jacobson et al, 1984; Collier et al, 1985a; Collier et al, 1987). There is clear evidence, from a series of 1390 patients, that in the lumbar spine at least, the sensitivity can be increased by up to 35%, as compared with planar imaging, by using SPET in finding lesions (Kanmaz et al, 1992). Within the knees it has been shown that SPET increases the accuracy of scintigraphy in identifying the cause of acute knee pain. This is particularly true if it is secondary to a meniscal tear (Murray et al, 1990). In our group of patients the use of the ring gantry enabled the camera to be positioned very close to the knees, ensuring good quality images on the three-headed machine (Figure 4).

Table IV. Comparison of total counts obtained and mean counts per projection in a 400 × 210 mm region of interest using a single-headed rotating gamma camera and a multi-detector system (both machines were fitted with high resolution collimators)

Acquisition parameters	Total counts × 1000	Counts per projection × 1000	Butterworth filter
(a) Lumbar spine			
IGE 400 ACT Starcam, 64 projections			
32 min	1630	25.5	N/A
Toshiba GCA-9300A, 60 projections			
8 min	1538	25.6	14
16 min	3167	52.8	16
32 min	6240	102	18
(b) Knees			
IGE 400 ACT Starcam, 64 projections			
32 min	862	14.4	N/A
Toshiba GCA-9300A, 60 projections			
8 min	918	15.3	13
16 min	1796	29.9	15
32 min	3446	57.5	18

We have shown that by using a dedicated multi-detector SPET camera it is possible to obtain a high resolution SPET image in just 8 min in the axial skeleton and 16 min in peripheral areas such as the knees, with no loss of clinically relevant information. This will therefore enable a department to perform SPET when indicated without disruption to the work schedule.

It has been noted that activity in the bladder leads to artefacts, which affect imaging of the hips. Even with an 8 min acquisition, significant bladder activity affecting SPET reconstruction was seen on 2/10 (20%) of studies of the pelvis. In a previous series of SPET imaging of the pelvis 5/25 (20%) of the studies were not reported due to bladder activity producing artefacts which obscured the hips after tomographic reconstruction (Collier et al, 1985b). Though patients can be catheterized if they have difficulty in voiding, this procedure has a significant level of morbidity. Two groups have described computational methods by which this problem can be reduced (Gillen et al, 1988; Kouris et al, 1988).

made it particularly suitable for use in children with metastatic disease. All 12 children imaged were able to complete the study without patient movement and with minimal discomfort. The ability to perform these studies quickly has been used in children with metastases from primary bone tumours (Buscombe et al, 1992).

Cost

The capital cost of a system such as the Toshiba GCA-9300A is high, of the order of £350 000. If the system has a life of 10 years the annual capital cost is £35 000. Maintenance costs can be estimated at 8% of the initial purchase price per year which is £28 000 per annum. The annual salary of a senior radiographer is of the order of £18 000 per annum at present rates of pay. The running cost would be approximately £81 000 per annum. Using 16 min acquisitions for all forms of SPET including heart, brain and kidney and 14 minute set-up time for each study, it is possible to perform 14 studies in a 7 hour working day. If studies were performed on 5 days a week for 50 weeks then 3500 studies could be performed per annum, giving a cost per study of £23.10 per SPET study. Even allowing for 20% per annum to cover for inflation and depreciation of capital equipment, the cost per study is still less than £30. At this cost the capital expenditure of such a system would be justified in any department with a high throughput of studies which use, or could use, SPET. Naturally these considerations do not include additional costs such as the costs of radiopharmaceuticals etc which may arise because more SPET studies can be performed.

Conclusion

Many nuclear medicine centres remain resistant to the idea of routine skeletal SPET, probably because the addition of a further 30 min acquisition in a tight working schedule results in disruption to the day's work. The multi-detector gamma camera is able to produce high resolution skeletal SPET with short acquisition times. Despite the initial capital outlay of such a machine, it will enable a nuclear medicine department to perform a wide range of clinically useful tests, including fast high resolution skeletal SPET, which will ensure that maximum information is obtained from each bone scintigraphy study.

References

BUSCOMBE, J R, TOWNSEND, C E, CLARKE, G ET AL, 1992. Fast skeletal SPET in the assessment of chest metastases in young patients with primary bone tumours. *Nucl. Med. Comm., 13,* 248.

COLLIER, B D, JOHNSON, R P, CARRERA, G F ET AL, 1985a. Painful spondylolisthesis or spondylolysis studied by radiology and single photon emission tomography. *Radiology, 154,* 207–211.

COLLIER, B D, CARRERA, G F, JOHNSON, R P ET AL, 1985b. Detection of femoral heads avascular necrosis in adults by SPECT. *J. Nucl. Med., 26,* 979–987.

COLLIER, B D, HELLMAN, R S & KRANOW, A Z, 1987. Bone SPECT. *Semin. Nucl. Med., 17,* 247–266.

GILLEN, G J, McKILOP, J H, HILDITCH, T E ET AL, 1988. Digital filtering of the bladder in SPECT bone studies of the pelvis. *J. Nucl. Med., 29,* 1587–1595.

JACOBSON, H, LARSON, S A, VESTERSKOLD, L & LINDVALL, N, 1984. The application of single photon emission tomography to the diagnosis of ankylosing spondylitis of the spine. *B. J. Radiol., 57,* 133–140.

KANMAZ, B, LIU, Y, UZMAN, G, YU, L ET AL, 1992. SPECT vs planar bone scintigraphy in patients with low back pain. *J. Nucl. Med., 33,* 868.

KEOGAN, M T, WRAIGHT, E P & ANTOUN, N M, 1991. Basal skull lesions: evaluation by emission tomography (SPECT) and X-ray computed tomography (CT). *Nucl. Med. Comm., 12,* 257.

KOURIS, K, MUSA, A, TAHA, B ET AL, 1988. Correction of bladder artifact in hip SPECT. *J. Nucl. Med., 29,* 867–868.

KOURIS, K, COSTA, D C, JARRITT, P H ET AL, 1992. Brain SPECT using a multidetector three headed camera system. *J. Nucl. Med. Technol., 20,* 68–72.

MOORE, S C, KOURIS, K & CULLUM, I, 1992. Collimator design for single photon emission tomography. *Eur. J. Nucl. Med., 19,* 138–150.

MURRAY, I P C, DIXON, J & KOHAN, A L, 1990. SPECT for acute knee pain. *Clin. Nucl. Med., 15,* 828–840.

ONSEL, C, COLLIER, B D, KIR, K M ET AL, 1990. Increased sacroiliac joint (SIJ) uptake: A frequent incidental finding in patients undergoing bone scintigraphy for back pain (LBP). *J. Nucl. Med., 31,* 712.

JNM: (in press)

Combined rest thallium-201/ stress Tc-99m tetrofosmin SPET: A study of feasibility and diagnostic accuracy of a 90 minute protocol

S Mahmood[1], M Gunning[1], J B Bomanji[1], N K Gupta[1]
D C Costa[1], P H Jarritt[1], H Swanton[2], P J Ell[1]

[1]Institute of Nuclear Medicine, [2]Department of Cardiology
University College London Medical School

Address for correspondence:

Prof. P J Ell
Institute of Nuclear Medicine,
University College London Medical school,
Mortimer street, London W1N 8AA
Phone: 071-380-9424, Fax: 071-637-0578

INTRODUCTION

Thallium-201 myocardial perfusion scintigraphy is a well established method of assessing myocardial perfusion, (1,2). There are well known disadvantages of thallium-201. These include a low energy emission which results in significant soft tissue attenuation in tissue and a rather long half life, which restricts the amount of dose which can be given safely. Efforts have therefore been directed over the past 5 years, towards the development of a suitable technetium-99m based radiopharmaceutical which would have ideal imaging characteristics for myocardial perfusion scintigraphy. MIBI and teboroxime have been studied but there are limitations with these agents as well. There is high hepatic and gut uptake in the case of MIBI (3,4) and rapid washout in the case of teboroxime (5,6).

Tc-99m tetrofosmin (*Myoview, Amersham plc., Buckinghamshire, UK*) is a recently developed cationic diphosphine compound and has shown promising imaging characteristics, displaying rapid accumulation in and slow clearance from the myocardium, with rapid clearance from background organs (7-10). Regarding detection of coronary artery disease, phase I,II and III studies have been performed showing good comparison with Thallium-201 imaging (10,12,13). Tc-99m tetrofosmin does not display the redistribution characteristics (14) shown by thallium-201, as it is a retention-type agent, and therefore clinical studies conducted have employed separate stress and rest injections, either 4 hours apart or on separate days (7,11,15).

Aim : This study looks at the combination of resting images using thallium-201 and post-stress images using Tc-99m tetrofosmin in a protocol of 90 minutes duration and assesses its role in the detection of coronary artery disease.

MATERIALS AND METHODS

Patient population: Twenty five patients (23 M, 2 F, aged 36-73) underwent a

ABSTRACT

Tc-99m Tetrofosmin is a recently developed compound, with rapid clearance from background organs. Studies have been performed demonstrating a good correlation with thallium-201. The purpose of this study was to assess the feasibility and diagnostic accuracy of a combined protocol involving rest thallium-201 single photon emission tomography (SPET) and stress scintigraphy with Tc-99m Tetrofosmin.

25 patients (23M/2F, aged 36-73 years) with known coronary anatomy underwent the combined protocol. 20 minutes after the resting injection of thallium-201, using LEHR collimators resting SPET data were acquired. Stress test using adenosine infusion combined with low level of dynamic exercise was performed. The stress data were collected 20 minutes later. The reconstructed vertical long axis (VLA), horizontal long axis (HLA) and short axis (SA) slices were analysed qualitatively. Analysis was carried out using nine segments of LV. The segments were reported either as fixed or reversible. The results were compared to the results of coronary angiography.

The sensitivity and specificity for the detection of diseased coronary vessels were 85% and 70% for the left anterior descending territory respectively, 78% and 71% for the right coronary artery, and 69% and 70% for the left circumflex. Overall the sensitivity was 80% and the specificity 70%.

We conclude that the combination of rest thallium-201/stress Tc-99m tetrofosmin SPET provide a protocol of short duration which displays similar diagnostic accuracy to a protocol employing tetrofosmin as a single agent.

ergometer for the six minute period. At four minutes, 370 MBq of Tc-99m tetrofosmin (*Myoview, Amersham Plc, Buckinghamshire, UK*) was injected as a bolus, through the three-way stopcock. The patients' pulse and blood pressure were recorded at rest ,and then every two minutes until the stress protocol was completed. Patients' symptoms and a three lead electrocardiogram were monitored during the process. Immediately following the completion of stress test, the patients were provided with chocolate and milk to ingest in order to facilitate rapid clearance from gall bladder.

Tc-99m tetrofosmin acquisition: This was conducted 20 minutes after the stress. Data were acquired in a 64 x 64 matrix, with 64 projections over 180 degrees. An acquisition time of 20 seconds per projection was used. An energy peak of 140 keV was used with a 20 % energy window and no offset.

Protocol Duration : The total duration of the imaging protocol was 90 minutes, including the designated intervals between injection and image acquisition, which were to allow for image optimisation.

Data Processing : The data from both acquisitions were reconstructed on a Star 4000i computer, utilising a Hanning pre-filter with a cut-off frequency of 0.8 cycles/cm. A ramp filter was applied during back-projection algorithm. The reconstructed transaxial slices were then reorientated into vertical long, horizontal long, and short axes.

Data Analysis : 3 physicians studied the images produced. Qualitative nine segment analysis was used with the segments being designated as follows: anterior and basal segments of each of the lateral, anterior and inferior walls and septum, and a single segment for the apex. The segments were scored as normal or abnormal (and in the case of the latter the decreased count was scored as fixed or reversible). In the event of disparity, a consensus was reached between the participating observers.

When the image results were analysed in respect of the coronary artery anatomy

combined protocol involving rest imaging with Thallium-201, followed by stress imaging with Tc-99m-tetrofosmin. Patients with obstructive airways disease, unstable angina or second or third degree heart block were excluded from the study. Thirteen had a history of previous myocardial infarction, three complained of atypical chest pain, 22 complained of an anginal pattern of chest pain, and four patients complained of dyspnoea as an additional symptom.

Patient Preparation: Patients were advised to abstain from caffeine containing beverages for at least ten hours prior to the stress protocol. Those patients on beta-blockers were asked to withhold the drug for 48 hours prior to the test and those on dipyridamole were asked to withhold the drug for 72 hours prior to the test. An intravenous cannula was inserted in the right arm, and a three-way stopcock attached and flushed with normal saline.

Thallium-201 administration : 74 MBq of thallium-201 was injected as a bolus and flushed through with normal saline.

Resting Thallium-201 SPET Acquisition : This was conducted twenty minutes after the injection of thallium-201. Single photon emission tomography (SPET) was performed using an IGE dual-detector cardiac dedicated camera, Optima (International General Electric, Milwaukee, WI, USA). Data were acquired in a 64 x 64 matrix involving 64 step and shoot projections over 180 degrees beginning at 45 degrees right anterior oblique. Acquisition time was 25 seconds per projection. The camera was equipped with a low energy high resolution collimator and interfaced with an IGE Star 4000i computer. Energy peaks of 72 keV and 169 keV were used with 20 % windows and no offset.

Stress testing and Tc-99m tetrofosmin administration : Following the first data acquisition, the combined adenosine/exercise stress protocol was conducted. Adenosine in normal saline was infused at a rate of 140 ug/kg/min via a volumetric pump, in a concentration of 1mg/ml, for a period of six minutes. Concurrently the patients cycled at a fixed workload of 25 watts on a bicycle

The territories of the left circumflex and right coronary artery were then analysed in combination, and the imaging showed specificity of 76% and sensitivity of 70%. Overall sensitivity was 80% and specificity was 70% (table 1).

DISCUSSION

There are reservations amongst nuclear medicine physicians about the use of two different imaging agents in the evaluation of coronary artery disease in a single subject. In the design of this protocol, we attempted to address some of the concerns that might arise

The rationale for stress Tc-99m tetrofosmin imaging being performed after the rest thallium-201 imaging, and not in the reverse order, was to prevent the phenomenon of compton scatter of the 99m-Tc activity into the Tl-201 photopeak, which would affect the thallium images, creating the potential for overestimation of reversible ischaemia. In addition to this, the protocol was designed with emphasis on decreasing patient time in the scanning department. Had the stress study been conducted first, one would have to allow sufficient time for the myocardium to return completely to the resting state before undertaking the rest study, thereby lengthening the patient's stay in the department.

Accepting that the physical properties of the two agents differ, data acquisition was adapted to suit the characteristics of each radionuclide. A high resolution collimator was employed, and in the case of thallium-201 rest images, the acquisition time was increased to 25 seconds per projection compared with 20 seconds for Tc-99m tetrofosmin. Appropriate energy windows of 72 keV and 169 keV for Tl-201, and 140 keV for Tetrofosmin, were used.

Investigators studying the characteristics of Tc-99m tetrofosmin have concluded that imaging may be performed between 5-30 minutes post injection (7,9,15). In our experience the optimum time is 20-40 minutes p.i. Higley et al (9) showed high gall bladder activity of 3.2 +/- 1.9 % of total injected activity at 5 minutes

the segments were assigned as follows:-

Left anterior descending artery - basal and apical anterior wall, basal apical septum, apex

Left circumflex artery - basal and apical lateral wall

Right coronary artery - basal and apical inferior wall

RESULTS

Haemodynamics : Whilst undergoing adenosine plus exercise stress protocol, the mean heart rate of the subjects rose from 63.6 +/- 9.8 to 90.3 +/- 20.4 beats per minute . The mean diastolic blood pressure did not change significantly; from 82.6 +/- 10.1 at rest to 83.7 +/- 10.1 mm Hg at peak stress. The change in mean systolic readings was from 133.1+/- 17.4 to 144.1 +/- 17.8 mm Hg . The mean double product rose from 8527+/- 2126 to 13197 +/- 4126 mm/min.

Cardiac Catheterization : Results from coronary angiography of the twenty five patients were analysed . A vessel displaying greater than 50 % stenosis on angiogram was assigned as being diseased. 4 patients had disease of all three coronary vessels, 8 patients had disease of two vessels, 10 patients had single vessel disease, and 3 patients had normal coronary arteries. In terms of the affected vascular territories this comprised 12 lesions of left anterior descending artery (LAD) territory, 10 lesions of left circumflex (LCx)territory, and 16 lesions of the right coronary artery (RCA) territory.

SPET images : The scoring of the segments in terms of the images obtained, i.e. fixed, reversible or normal, was compared with the result of cardiac catheterisation in the designated vascular territories as described above. With regard to the LAD territory, the protocol showed a sensitivity of 85% (34/40 segments) for the detection of a diseased vessel, and the specificity was found to be 70%(59/84). For the RCA, the results were 78% (28/36)and 71% (10/14) respectively, and for the LCx, they were 69 %(9/13) and 70%(26/37) respectively.

myocardium, further studies would need to be performed assessing the potential of Tetrofosmin in this regard. Thallium has been established as a useful agent, but in a stress/redistribution protocol alone, will tend to underestimate the presence of ischaemic but viable myocardium[19]. Better results have been obtained by reinjection of Thallium following the standard stress/redistribution imaging, identifying viable or non viable segments in the same regions as positron emission tomography with 18-F-fluorodeoxyglucose[20]. Thus, the current protocol combining Tetrofosmin and Thallium, would probably require reinjection of thallium in order to increase its accuracy in myocardial viability assessment.

LIMITATIONS

This study has compared the results of segmental analysis of combined thallium/tetrofosmin protocol images with coronary angiographic data, in order to obtain figures of sensitivity and specificity for the detection of diseased segments. Coronary angiography has not been proven to be the "gold standard" in the assignation of definite regions with respect to myocardial perfusion, and results must be interpreted, aware of it's limitation as a frame of reference.

Further studies of this combined protocol could be performed comparing the results with those of thallium imaging alone, or tetrofosmin alone, conducted sequentially in the same subjects. This however raises ethical considerations of performing the stress test twice.

CONCLUSION

A combined myocardial imaging protocol involving thallium-201 scintigraphy at rest, followed by technetium-99m-tetrofosmin imaging after stress, is a useful method of investigation for the presence of coronary artery disease. Multidetector gamma camera has proven useful for establishing this rapid protocol resulting in high resolution images. The decreased duration of 90 minutes compared to more than 4 hours, confers advantage on this protocol over the use of thallium or tetrofosmin as single agents. The sensitivity and specificity in the detection of coronary artery stenosis as shown on coronary angiography, is similar to that of tetrofosmin alone.

post stress injection which had fallen to 1.0 +/- 0.5% by 60 minutes. In order to expedite clearance from the gall-bladder in this study, we asked patients to ingest 200 mls of milk and 50 grams of chocolate immediately post exercise. Good quality images were obtained at 20 minutes post stress with low activity recorded in the region of the liver.

Studies conducted thus far, assess the usefulness of two different protocols for rest and stress imaging with Tc-99m tetrofosmin. As tetrofosmin has not been shown to display the characteristic of redistribution (14) it is necessary for subjects to receive two separate injections of the radionuclide in the detection for defect reversibility. Therefore the one day protocol employed has involved injection at maximal stress followed 5- 30 minutes later by image acquisition, and 4 hours later reinjection, with imaging after 30 minutes. A separate day protocol involves conducting these two studies more than 24 hours apart. Sridhara et al (12) in a study of 23 patients found no significant difference in the detection of coronary artery disease between these two methods. In the same study, a favourable comparison emerged in the identification of coronary artery disease, thallium-201 correctly identifying 83% of abnormal segments, while Tc-99m tetrofosmin showed 80% and 83% of diseased segments on early and late images respectively. In a study of 26 patients Nakajima et al (15) showed concordance of 83% between images obtained with thallium-201 in a rest/redistribution protocol, and with Tc-99m tetrofosmin in a one day protocol in the same subjects. However, the figures for sensitivity of Tc-99m tetrofosmin in the detection of coronary disease were lower ; 60% compared to 72% for thallium-201.

Thus the overall sensitivity and specificity figures for this study of a combined protocol of tetrofosmin and thallium, 80% and 70% respectively, are similar to those quoted for the use of tetrofosmin alone, but are somewhat lower than figures obtained with thallium imaging alone, ranging from 72% to 92% for sensitivity and 84% to 100% for specificity (15-19). Figure 1 demonstrates an example of good quality images obtainable.

In order to evaluate the usefulness of this protocol in the detection of viable

9. Higley B, Smith FW, Smith T, Gemmell HG, Das Gupta P, Gvozdanovic DV, Graham D, Hinge D, Davidson J, Lahiri A. Technetium-99m-bis[bis(2-ethoxyethyl) phosphino]ethane: human biodistribution, dosimetry and safety of a new myocardial perfusion imaging agent. *J Nucl Med.* 1993;34:30-38

10. Smith FW, Smith T, Gemmell H, et al. Phase I study of Tc-99m diphosphine(P53) for myocardial imaging [Abstract]. *J Nucl Med.* 1991;32:967.

11. Jain D, Wackers FJ Th, Mattera J, McMahon, Sinusas AJ, Zaret BL. Biokinetics of technetium-99m-tetrofosmin: myocardial perfusion agent: implications for a one day imaging protocol. *J Nucl Med.*1993;34:1254-1259

12. Sridhara BS, Braat S, Itti R, Rigo P, Cload P, Lahiri A. Early and late myocardial imaging with a new technetium-99m diphosphine(PPN1011) in coronary artery disease [Abstract]. *J Am Coll Cardiol.* 1992;19:202A.

13. The Tetrofosmin Study Group. Comparative myocardial perfusion imaging with Tc-99m-tetrofosmin and thallium-201: results of phase-III international trial. [Abstract] *Circulation* 1992;86(Suppl I):I-506.

14. Jain D, Wackers FJ Th, McMahon, et al. Is there any redistribution with Tc-99m-tetrofosmin imaging; a quantitative study using serial planar imaging. (Abstract) *Circulation* 1992;86(Suppl. I):I-46

15. Nakajima K, Taki J, Shuke N, Bunko H, Takata S, Hisada K. Myocardial perfusion imaging and dynamic analysis with technetium-99m-tetrofosmin. *J Nucl Med.* 1993;34:1478-1484

REFERENCES

1. Strauss HW, Pitt B. Thallium-201 as a myocardial imaging agent. *Semin Nucl Med* 1977;7:49-58.

2. Kaul S. A look at 15 years of planar thallium-201 imaging. *Am Heart J.* 1989;118:581-601

3. Okada RD, Glover D, Gaffeny T, Williams S. Myocardial kinetics of technetium-99m-hexakis-2-methoxypropyl isonitrile. *Circulation* 1988;77:491-498.

4. Wackers FJ Th, Berman DS, Maddahi J, Watson DD, Beller GA, Strauss HW, Boucher CA, Picord H, Holman BL, Fruidrich R, Inglese E, Delaloye B, Bischef-Delaloye A, Camin L, McKusick K. Technetium 99m hexakis 2-methoxyisobutyl isonitrile: human biodistribution, dosimetry, safety and preliminary comparison to thallium-201 for myocardial perfusion imaging. *J Nucl Med* 1989;30:301-311

5. Iskandrian A, Heo J, Nguyen T, Mercuro J. Myocardial imaging with Tc-99m teboroxime: technique and initial results. *Am Heart J.* 1991;121:889-894

6. Beller GA, Watson DD. Physiological basis of myocardial perfusion imaging with the technetium-99m agents. *Semin Nucl Med.* 1991;21:173-181

7. Sridhara BS, Braat S, Rigo P, Itti R, Cload P, Lahiri A. Comparison of myocardial perfusion imaging with technetium-99m tetrofosmin versus thallium-201 in coronary artery disease. *Am J Cardiol.* 1993;72:1015-1019

8. Kelly JD, Forster AM, Higley B et al. Technetium-99m-tetrofosmin as a new radiopharmaceutical for myocardial perfusion imaging. *J Nucl Med.* 1993;34:222-227

Table 1: Sensitivity and specificity of combined thallium-201/Tc-99m tetrofosmin protocol in the detection of coronary artery disease.

	Sensitivity	Specificity
LAD	85% (34/40)	70% (59/84)
RCA	78% (28/36)	71% (10/14)
LCx	69% (9/13)	70% (26/37)
Combined LCx+RCA	76% (37/49)	71% (36/51)
Overall	80% (71/89)	70% (95/135)

(figures in brackets represent the number of segments)

16. Nguyen T, Heo J, Ogilby JD, Iskandrian AS. Single photon emission computed tomography with thallium-201 during adenosine-induced coronary induced hyperaemia: correlation with coronary arteriography, exercise thallium imaging and two dimension echocardiography. *J Am Coll Cardiol.* 1990;16:1375-1383

17. Francisco DA, Collins SM, Go RT, Ehrhardt JC, Kirk OC,Marcus ML. Tomographic thallium-201 myocardial perfusion scintigrams after maximal coronary artery vasodilation with intravenous dipyridamole: comparison of qualitative and quantitative approaches. *Circulation* 1982;66:370-379

18. Verani MS, Mahmarian JJ, Hixson JB, Boyce TM, Standacher RA, Diagnosis of coronary artery disease by controlled coronary vasodilation with adenosine and thallium-201 scintigraphy in patients unable to exercise. *Circulation* 1990; 82:80-87

19. Nishimura S, Mahmarian JJ, Boyce TM, Verani MS. Equivalence between adenosine and exercise thallium-201 myocardial tomography: a multicenter, prospective, crossover trial. *J Am Coll Cardiol.* 1992;20:265-275

20. Bonow RO, Dilsizian V, Cuocolo A, Bacharach SL. Identification of viable myocardium in patients with chronic coronary artery disease and left ventricular dysfunction. Comparison of thallium scintigraphy with reinjection and PET imaging with F-18 fluorodeoxyglucose. *Circulation* 1991;83:26-37.

Fig 1

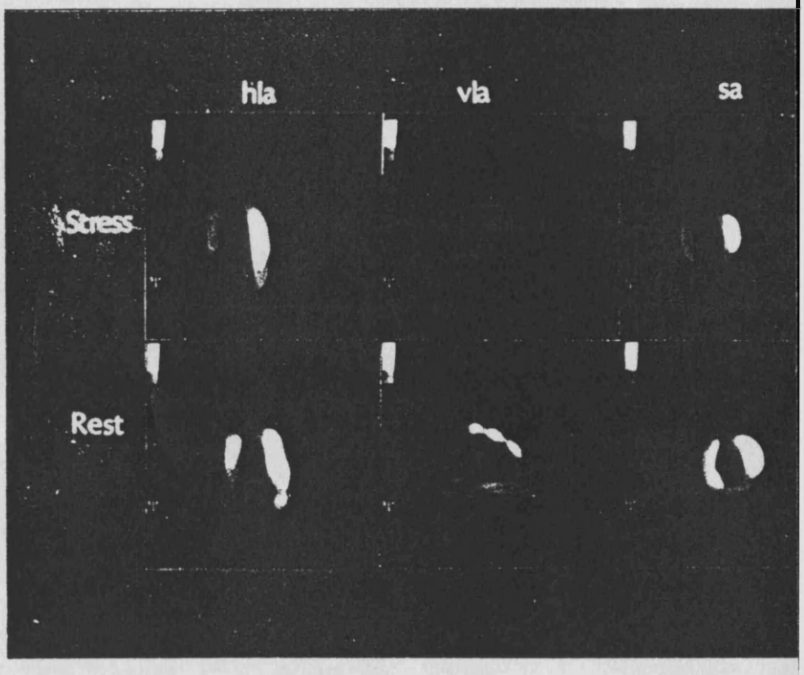

LEGEND:

Table 1: Sensitivity and specificity of combined thallium-201/Tc-99m tetrofosmin protocol in the detection of coronary artery disease. (figures in brackets represent the number of segments)

Figure 1: Stress/Tc-99m tetrofosmin (upper row) and rest/thallium-201 (lower row) study. Horizontal long axis (hla), Vertical long axis (vla), , and short axis (sa) slices are displayed and demonstrate reversible ischaemia in the anterior and inferior walls. Coronary angiography confirmed disease of LAD and RCA.